DEGRADABILITY OF SYNTHETIC DYESTUFF BY ACOUSTIC CAVITATION: IMPACTS OF SYSTEM CONDITIONS AND PHYSICAL/CHEMICAL AGENTS

by

GÖKÇE TEZCANLI GÜYER

B.S. in Environmental Engineering, Yıldız Technical University, 1995

M.S. in Environmental Technology, Boğaziçi University, 1998

Submitted to the Institute of Environmental Sciences in partial fulfillment of the requirements for the degree of

Doctor

of

Philosophy

in

Environmental Technology

Boğaziçi University

2003

ACKNOWLEDGMENTS

This work is not only a product of personal endeavor, but of a common effort. First and foremost I must thank my supervisor, Prof. Nilsun İnce who has dedicated her time and effort to this study, and has been of invaluable help to me over the years I spent at the Institute of Environmental Sciences. Furthermore, she handed the task of teaching me to think like a scientist, and under her guidance I learned that to test a hypothesis one should not only run the proper experiments, but one should also be able to question the hypothesis. I appreciate the efforts she has spent for me both as a scientist and as a person.

I would like to thank financial supports of Boğaziçi University Research Fund and the State Planning Organization of Turkey for funding the project DPT 98K120900, and the Research Council of Turkey (TUBITAK) for a collaborative EUREKA Grant to fund E!2051 "Textefuse" project. Thanks are extended to Dr. Eric Cordemans de Meulenaer for his very precious support in the initiation and follow-up of my trip in sonochemistry and for his kindness in donating the 300 kHz reactor to the laboratory.

I wish to express my special thanks to Prof. Christian Pétrier, who is already an acknowledged expert in the field of sonochemistry, for his cooperation and valuable criticisms, which have been very useful and for his kindness to being a committee member. Further, I wish to acknowledge Prof. Viktorya Aviyente for her supportive comments and enthusiasm throughout my studies. I would like to express my thanks to Prof. Ömer Saygın and Assoc. Prof. Turgut Onay for their critisms and constructive suggestions.

A very heartfelt thanks goes to Işıl Gültekin for her help and kindness. She was always willing and eager to help and was next to me in my laboratory work. I am also thankful to Altan Süphandağ, Rana Kıdak, Yonca Ercümen and Alimet Özen for their encouragement, valuable friendship, and constant willingness to listen to and share my ideas. I would also like to thank Merih Ötker for her help during BOD tests. I am grateful not only to the individuals named here but also to many others who have helped in some way but are not named.

I would also like to recognize Pisa Boya Fabrikası A.Ş., especially Mehmet Ali İnce and İzzet Alaton for their help and technical support on textile dyes and dyeing processes, which were highly essential in the completion of this dissertation.

I want also to express my gratitude to my dear parents Sevgi and İlhan Tezcanlı, my brother Oytun and his wife Güzin, who are always close to me for their endless support, help and love. Thanks a million for everything. My last thanks are for the most precious person in my life, my husband Öncü Güyer. He is the most supportive person in my life with his existence. More than that, his personality, foresight and kindness I will always admire.

ABSTRACT

The use of ultrasound in environmental applications is a novel advanced oxidation process that is currently being investigated as a method to degrade refractory organic wastes, which can not be degraded by conventional wastewater treatment methods such as biological, chemical and combinations thereof. The application of ultrasound to environmental problems relies on the process of acoustic cavitation: the formation, growth, and implosive collapse of micro bubbles in a liquid. The collapse of such bubbles creates hot spots with temperatures as high as 5000 K, and pressures up to 800 atm, and cooling rates in excess of 10^{10} K s^{-1}. These conditions are responsible for a variety of physical and chemical effects. Hydroxyl radicals that are formed during the homolytic cleavage of water molecules upon bubble collapse can be utilized to degrade many compounds including persistent environmental pollutants. In addition, radical formation can be enhanced by coupling of ultrasound with oxidants and/or UV light.

In this dissertation, the degradation of pure and synthetic dyebath solutions of 9 textile dyes were investigated in three ultrasonic systems (System I: 300 kHz, SystemII: 520 kHz, and System III: 3 x 520 kHz frequency), in the presence and absence of chemical oxidants (ozone, hydrogen peroxide, ferrous ion) and/or UV light. The impacts of system conditions, physical/chemical agents, dye properties and dye-bath matrix on sonolytic destruction of textile dyes were studied. The performance of the systems was assessed and compared with each other by monitoring color, organic matter, toxicity, total dissolved solids, total organic carbon, and chemical oxygen demand degradation, and the increase in biochemical oxygen demand.

In case of system comparison, the efficiency of the studied systems with respect to decolorization of the test solutions was such that: System I > System II > System III. System efficiency with respect to the calculated product yield was in the order: System II > System I > System III. Injection of different gasses during ultrasonic irradiation showed that rate of decolorization increased in the sequence: Ar > O_2 > Air, and

maximum decolorization was obtained with an Ar:O_2 gas mixture, at a ratio of 66 per cent Ar to 34 per cent O_2.

It was found that, the decolorization rate of all dyes was more closely related to their structural properties than to the composition of the dye-baths. Anthraquinone dyes bleached faster than azo dyes. The presence of α-substituents around the –N=N– bond accelerated the decolorization rate. Decolorization of dyes with a single OH substituent in *ortho* position to their reactive component was faster than those with a second α-substituent such as SO_3. Decolorization was decelerated by the formation of ionic sites. Decolorization in dyebath effluents was inhibited only in the presence of sufficiently large carbonate and chloride ions.

The abatement in the visible absorption of sonicated dye solutions and dyebaths was always larger than the abatement in their UV absorption. Toxic dyes were detoxified by ultrasound within short contact, but ultrasound was not effective in the overall degradation of the dyes as measured by chemical oxygen demand and total organic carbon of the effluents, unless combined with physical/chemical agents. Sonication of dye solutions in the presence of O_3, Fe^{2+}, H_2O_2, and/or UV irradiation increased degradation yields considerably with respect to those applied individually. The most effective combined scheme was ultrasound/ozone/UV irradiation.

Estimated bimolecular rate coefficient of azo dyes with hydroxyl radicals was calculated as 1.22×10^9 $M^{-1}s^{-1}$. Estimated operational costs of System I, II and III for 45 per cent bleaching of azo dyes were 3.52 USD m^{-3}, 3.37 USD m^{-3}, 9.98 USD m^{-3}, respectively. The cost of O_3/US combination in System III was 2.57 USD m^{-3}, and the operation cost of ozonation was 3.60 USD m^{-3}.

ÖZET

Sesüstü dalgaların çevresel uygulama alanında kullanımı yeni bir ileri oksidasyon prosesidir. Kimyasal veya biyolojik arıtım gibi klasik atıksu arıtım yöntemleriyle ayrışması güç olan organik maddelerin indirgenmesinde kullanımı son zamanlarda araştırılmaktadır. Sesüstü dalgaların çevresel problemlerin çözümünde kullanılması sıvı içerisinde mikro ölçekli vakum kabarcıkların oluşumu, büyümesi ve içeri çökerek patlaması olarak tarif edilen akustik kavitasyon prosesine dayanmaktadır. Patlama sırasında yaklaşık 5000 K sıcaklığında, 800 atm basıncında ve soğuma hızı 10^{10} K sn^{-1} olan sıcak noktalar oluşmaktadır. Bu şartlar sonucu meydana gelen fiziksel ve kimyasal etkiler ile organik maddeler indirgenmektedir. Kabarcığın patlaması sonucu su molekülü parçalanarak hidroksil radikallerini oluşturmakta ve meydana gelen bu radikaller giderimi güç olan bileşikleri içeren çevre kirleticilerini oksitleyerek indirgemektedir. Radikal oluşumu sesüstü dalgaların yükseltgenler ve/veya mor ötesi ışıma ile birlikte kullanılmasıyla arttırılabilir.

Bu doktora çalışmasında, 9 adet tekstil boyarmaddesinin saf ve sentetik boya-kazanı çözeltilerinin 3 farklı sesüstü sisteminde (Sistem I: 300 kHz, Sistem II: 520 kHz, Sistem III: 3 x 520 kHz frekanslı) sesüstü ışıma ile tek başına veya kimyasal oksitleyiciler (ozon, hidrojen peroksit, demir iyonu) ve/veya UV ışıması ile birlikte kullanılarak indirgenmesi araştırılmıştır. Sistem şartlarının, fiziksel/kimyasal ajanların, boyaların kimyasal özelliklerinin ve boya kazanı matrisinin test boyalarının sesüstü dalgalar ile parçalanmasına etkisi incelenmiştir. Sistemlerin performanları renk, organik madde, zehirlilik, toplam çözünmüş katı madde, toplam organik karbon, kimyasal oksijen ihtiyacındaki azalma ve biyolojik oksijen ihtiyacındaki artma izlenip belirlenmiş ve renk ve organik madde giderimi açısından birbirleriyle karşılaştırılmıştır.

Sistemler boya çözeltisindeki renk giderim hızlarına göre karşılaştırıldıklarında Sistem I > Sistem II > Sistem III olduğu, hesaplanan ürün verimlerine göre karşılaştırıldıklarında ise Sistem II > Sistem I > Sistem III olduğu görülmüştür. Sesüstü dalgalar ile ışıma sırasında farklı gazların sisteme beslenmesi sonucu boya çözeltisinde

renk giderimi şu sıradadır: Ar > O_2 > Hava. En yüksek renk giderme verimi Ar:O_2 (% 66 Ar : % 33 O_2) karışımı ile elde edilmiştir.

Kullanılan boyaların tamamında renk giderme hızının boya kazanının içeriğinden çok kimyasal yapı özelliklerine bağlı olduğu saptanmıştır. Antrakinon boyalarda renk gideriminin azo boyalarından daha hızlı olduğu belirlenmiştir. Azo (–N=N–) bağının çevresindeki α-grubun renk ağarmasını hızlandırdığı ve reaktif yapıya orto pozisyonda bulunan tek bir OH yan grubuna sahip boyalarda ağarmanın SO_3 gibi ikinci bir orto yan gruba sahip boyalara nazaran daha hızlı olduğu gözlenmiştir. İyonik yapılar oluştukça ağarmanın yavaşladığı belirlenmiştir. Boya kazanı atık suyunda renk gideriminin sadece yeterince yüksek karbonat ve klorür iyonu konsantrasyonunda engellendiği saptanmıştır.

Sesüsütü ışımaya tabi tutulan boya ve boya kazanı çözeltilerinde görünen dalga boyundaki absorbans azalmasının her durumda UV absorbansındaki azalmadan daha fazla olduğu saptanmıştır. Zehirli boyaların zehirliliklerinin sesüstü ışıma ile kısa sürede giderildiği, fakat sesüstü ışımanın çıkış suyunda kimyasal oksijen ihtiyacı ve toplam organik karbon olarak ölçülen genel boya gideriminde tek başına etkili olamadığı ve fiziksel/kimyasal ajanlar ile birlikte kullanılması gerektiği görülmüştür. Sesüstü ışıması ile O_3, Fe^{2+}, H_2O_2, ve/veya UV ışıması birlikte kullanıldığında, boya giderme veriminin her birinin tek kullanıldığı durumlardan çok daha yüksek olduğu belirlenmiştir. Bu sistemler arasında en etkili sistem sesüstü ışıma/ozon/UV ışımanın beraber kullanıldığı sistemdir.

Azo boyalarının hidroksil radikalleri ile reaksiyonunda tahmini ikinci derece hız katsayısı 1.22×10^9 M^{-1} s^{-1} olarak hesaplanmıştır. Sistem I, II, ve III' ün azo boyalarında sesüstü ışıma ile % 45' lik renk giderimi için tahmini işletme giderleri sırasıyla 3.52 USD m^{-3}, 3.37 USD m^{-3}, 9.98 USD m^{-3} olarak hesaplanmıştır. Sistem III' ün ozon ile birlikte kullanıldığı durumda işletme gideri 2.57 USD m^{-3}, ve ozonun tek başına kullanıldığı sistemin işletme gideri 3.60 USD m^{-3} olarak hesaplanmıştır.

TABLE OF CONTENTS

LIST OF FIGURES

LIST OF TABLES

LIST OF ABBREVIATIONS

A	Absorbance
AB1	C.I. Acid Black 1
AO	Advanced oxidation
AOP	Advanced oxidation processes
AO7	C.I. Acid Orange 7
b	path length
BB3	C.I. Basic Blue 3
BB4	C.I. Basic Brown 4
BB16	C.I. Basic Blue 16
BOD_5	Five-day Biochemical oxygen demand
C	Concentration
C.I.	Color index codes
C_p/C_v	Heat capacity ratio
COD	Chemical oxygen demand
DB1	Dyebath 1
DB2	Dyebath 2
DB3	Dyebath 3
DBE	Dyebath effluents
EC_{50}	Five min Microtox toxicity of the sample
EE/O	Electrical energy requirements per order of pollutant removal
f	Fraction of power deposited to applied generator power
G	Product yield
G'	Actual product yield
GAC	Granulated activated carbon
GP	Generator Power Consumption
I	Intensity
I_0	Incident photon influence rate

I_f	Power intensity at the irradiation frequency
I_{III}	Power intensity at System III
k'	Pseudo-first order decay coefficient
k_{dye}	Second order reaction rate coefficient of the dye with •OH
k_{flH2O2}	Bimolecular reaction rate coefficients of H_2O_2 formation
$k_{norm,f}$	Corrected rate constants at the irradiated frequency
$k_{obs,f}$	Observed rate constants at the irradiated frequency
k_{sH2O2}	bimolecular reaction rate coefficients of H_2O_2 reaction with •OH
K_{fOH}	Zero-order rate coefficient of •OH formation
M	Mass of water
N_L	Avogadro number
$[•OH]_{ss}$	Steady-state hydroxyl radical concentration
OP	Electrical power consumption of ozone generator
P	Ultrasonic power
P_a	Acoustic pressure
P_d	Deposited sonic energy
P_f	Power density at the irradiation frequency
P_v	Vapor pressure of the solution
P_{III}	Power density at System III
PDS	Pure dye solutions
PP	Pump power consumption
RB5	C.I. Reactive Black 5
RB19	C.I. Reactive Blue 19
RH	Organic substrate
RO16	C.I. Reactive Orange 16
RR141	C.I. Reactive Red 141
RTI	Relative toxicity Index
System I	Generator capacity:25W, frequency:300 kHz, volume:150 ml
System II	Generator capacity:100W, frequency:520 kHz, volume:1200 ml
System III	Generator capacity:600W, frequency:520 kHzx3, volume:2000 ml
t_0	Estimated contact time for 1 m^3 wastewater treatment
t_i	Experimental contact volume

T_0	Ambient temperature in bulk liquid
TC	Total operation cost
TC_{s1}	Total cost of System I
TC_{s2}	Total cost of System II
TC_{s3}	Total cost of System III
TDS	Total dissolved solids
TOC	Total organic carbon
TSS	Total suspended solids
UC_E	Unit cost of electricity
UC_{O2}	Unit cost of O_2
US	Ultrasonic irradiation
UV	Ultraviolet irradiation
V_i	Test volume
Vis	Visible
V_{O2}	Volume rate of O_2 consumption
W	Acoustic power
Z	Acoustic impedance
ε	Molar absorptivity
c	Speed of sound
$h\nu$	Radiation
ρ	Density
γ	Polytropic index
ϕ	Quantum yield

CHAPTER 1. INTRODUCTION

Clean and safe water environments are essential not only for growing economies to sustain their developments, but also for modern societies to sustain their life standards. On the other hand, maintaining a clean environment is becoming more and more difficult with the expanding market for synthetic organic chemicals (such as dyestuffs), which are ultimately disposed and/or fed into wastewater treatment plants before discharge into the water environment. Because a great majority of such chemicals are poorly biodegradable, conventional wastewater treatment methods such as biological, chemical and/or combinations thereof are inadequate to maintain clean water, i.e. to meet governments' stricter environmental regulations and societies' growing concern for public health.

Recent developments in "Advanced Oxidation Processes" (AOP) have raised new horizons to the search of innovative and appropriate technologies to deal with this problem. Advanced oxidation is a term to define all those processes that generate powerful and short-lived oxidants such as the hydroxyl radical, which unselectively attacks all organic molecules for partial or complete oxidation. The process involves irradiation of contaminated waters by ultraviolet light or γ-rays during contact with hydrogen peroxide, ozone, titanium dioxide or Fenton's agent. The problem with all these methods is that they are energy and chemical-intensive and thus economically non-feasible.

The use of ultrasonic pressure waves to generate hydroxyl radicals in water thus promoting advanced oxidation of refractory chemicals is a novel approach that requires extensive research and development for technical and economic feasibility. In addition, ultrasound may be ineffective by itself as an advanced oxidation tool, requiring the addition of chemicals and/or ultraviolet light to support radical formation.

This dissertation is devoted to the investigation of three ultrasonic systems and 9 synthetic dyes (common in textile dyeing processes) to assess impacts of system and dye properties on sonolytic degradability of dyestuff. Selection of textile dyes as test chemicals

is due to the fact that textile industry accounts for two thirds of the total dyestuff market, and is recognized with extensive usage of process water, which is ultimately discharged with unfixed dye residuals and dyebath auxiliaries.

The systems and dyes under investigation are specified and identified in terms of their International Color Indices, respectively as:

1. **Systems:**

i) SYSTEM I: Generator capacity=25W, frequency=300 kHz, volume=150 mL.

ii) SYSTEM II: Generator capacity=100W, frequency=520 kHz, volume=1200 mL.

iii) SYSTEM III: Generator capacity=600W, frequency=3 x 520 kHz, volume=2000 mL.

2. **Dyes:**

i) C.I. Acid Black 1

ii) C.I. Acid Orange 7

iii) C.I. Basic Blue 3

iv) C.I. Basic Blue 16

v) C.I. Basic Brown 4

vi) C.I. Reactive Black 5

vii) C.I. Reactive Blue 19

viii) C.I. Reactive Orange 16

ix) C.I. Reactive Red 141

Each system was optimized for power, volume, and input gas flow, based on the rate of color removal in the test dye solution. Systems were also compared with respect to "product yield", a term used to define the change in test chemical concentration in the experiment volume per power of the sonic energy deposited in that volume. System performance was assessed and compared with one another by monitoring effluent properties such as color, organic matter, toxicity and solids content. In some cases, catalysts such as hydrogen peroxide, ozone, ferrous ion and ultraviolet irradiation were added to enhance the rate of dye degradation. The test dyes were either dissolved in

ultrapure deionized water to study the impacts of dye structure, or in tap water spiked with typical dyebath auxiliaries to study combined effects of dye structure and dyebath matrix.

In brief, Chapter 2 presents a theoretical background and literature review of advanced oxidation and textile dyeing/finishing processes. Chapter 3 is an extensive review of ultrasonic processes and their applications in environmental remediation, as discussed in the review article published in *Applied Catalysis B: Environmental* as part of this doctoral study (Ince *et al.*, 2001). Chapter 4 presents the investigation of SYSTEM I, SYSTEM II and SYSTEM III and selection of their operating parameters. Chapter 5 is divided into two sections: the first one is a copy of the article published in *Dyes and Pigments* (Ince and Tezcanli, 2001), where the results of azo dye degradation in SYSTEM II by combined sonolysis and ozonation were reported; the second part presents the impacts of ferrous ion addition on the degradation of the dye in the same system. Chapter 6 is a copy of the article published in *Ultrasonics Sonochemistry* (Tezcanli-Güyer and Ince, 2003), which is an extension of the paper presented in the eighth conference of European Society of Sonochemistry (ESS8), Italy, September, 2002. The article encompasses sonochemical destruction of four textile dyes in SYSTEM II, accompanied by color and toxicity monitoring in the effluents, and a comparative evaluation of results. Chapter 7 is composed of two parts: The first one is a copy of the article published in *Coloration Technology* (Tezcanli-Güyer *et al.*, 2003), where the impact of textile dyebaths (simulated in the laboratory) was studied in SYSTEM I using three different dye classes and dyebath recipes, with emphasis on the effects of dye structure, pH variations and hydrogen peroxide; the second part also deals with SYSTEM I but with a different dye set, all dissolved in tap water and sonicated at acidic and neutral pH. (This section is an extended copy of the poster presented in ColorChem02, Czech Republic, 2002, which was printed in the *Proceedings*). Chapter 8 is also divided into two sections: The first one is made of the study presented in Ultrasonics 03, Spain, July 2003 (manuscript printed in *Proceedings*), and the work recently submitted to *Ultrasonics*, where impacts of pH, carbonate alkalinity and molecular structure of two aryl-azo naphthol dyes dissolved in deionized water were extensively investigated using SYSTEM I; the second part reports the results observed exactly at the same conditions using an other dye set from the same class. Chapter 9 presents a study of ultrasound and its various combinations with ozone and ultraviolet light applied to deionized water solutions of sulphonated aryl-azo-naphthol dyes in SYSTEM

III. Comparative evaluations were made using effluent quality parameters such as color, UV absorption, total organic carbon and Biochemical Oxygen Demand. A part of this work was presented in Ultrasonics 03, Spain, July 2003 (manuscript printed in *Proceedings*) and is recently submitted to *Ultrasonics* after data evaluation. Chapter 10 covers a modeling approach to the kinetics of hydroxyl radical production and consumption reactions in deionized water solutions of sulphonated azo dyes to estimate coefficients of radical generation and bimolecular radical reaction rates with the dyes. Finally, Chapter 11 is a brief summary of all findings, an economic evaluation of the systems and some concluding remarks and suggestions for future work.

CHAPTER 2. THEORETICAL BACKGROUND

2.1. Advanced Oxidation Processes (AOPs)

The second half of the last century has witnessed a rapidly deteriorating environment as the outcome of the extravagant use of complex organic compounds (most of which are non-biodegradable and hazardous) and the discharge of spent or wasted parts into conventionally operated biological wastewater treatment systems. Scientists and engineers, therefore, have been widely challenged in recent years for developing innovative treatment processes and technologies by which to convert complex and toxic organic compounds to less hazardous or more biodegradable forms before they end up in receiving waters or the soil environment (Ince *et al.*, 2000).

Although chemical oxidation reactions are very common in water and wastewater treatment practices, remediation of these waters with conventional oxidants is not always feasible due to very long reaction times (Bircher *et al.*, 1997). A technique that has recently emerged as a promising solution to overcome kinetic limitations is Advanced Oxidation (AO), by which partial and/or complete destruction of even the most complex organic compounds can be rendered without generating any sludge or solids material of hazardous character (Bauman and Stensrom, 1990; Kusakabe *et al.*, 1991; Ince *et al.*, 1997; Ince, 1998). Destruction by AO is based on oxidative degradation by free radical attack, particularly by the hydroxyl radical (•OH), which is far more powerful as an oxidizing agent than all commonly known strong oxidants like oxygen (O_2), hydrogen peroxide (H_2O_2) and ozone (O_3) (Legrini *et al.*, 1993). The efficiency of AO processes, therefore, is directly related to the extent of hydroxyl radical yield within a limited period of time and pre-defined conditions where the rate constants for the reaction of •OH with most organic pollutants are very high as shown in Table 2.1. The hydroxyl radical typically reacts one million to one billion times faster than O_3 and H_2O_2, resulting in greatly reduced treatment costs and system size (Legrini *et al.*, 1993).

Table 2.1. Reaction rate constants (k, in $Lmol^{-1}s^{-1}$) of some organic pollutants with O_3 and •OH (Calgon Carbon Oxidation Technologies, 1996)

Compounds	O_3	•OH
Chlorinated Alkenes	10^{-1} to 10^{3}	10^{9} to 10^{11}
Phenols	10^{3}	10^{9} to 10^{10}
N-containing Organics	10 to 10^{2}	10^{8} to 10^{10}
Aromatics	1 to 10^{2}	10^{8} to 10^{10}
Ketones	1	10^{9} to 10^{10}
Alcohols	10^{-2} to 1	10^{8} to 10^{9}
Alkanes	10^{-2}	10^{6} to 10^{9}

Once •OH is generated, it aggressively attacks all organic compounds and leads to mineralization when the oxidation process is carried out to completion. Depending upon the nature of organic species, two types of •OH reactions are possible: i) hydrogen abstraction (•OH can abstract a hydrogen atom to form water) and ii) addition (Calgon Carbon Oxidation Technologies). Hydroxyl radical can be generated by photochemical and non-photochemical methods as well heterogeneous photocatalysis and they are described below.

2.1.1. Homogeneous AOPs

2.1.1.1. Photochemical Homogeneous AOPs

AOPs involving ultraviolet irradiation in conjunction with an oxidant and/or catalyst are known as UV/Oxidation processes.

2.1.1.1.1. Photolysis of Hydrogen Peroxide

The mechanism most commonly accepted for the photolysis of H_2O_2 is the cleavage of the molecule into hydroxyl radicals and other reactive species that attack the organic molecules (Legrini *et al.*, 1993):

$H_2O_2 + h\nu \rightarrow 2\ {}^{\bullet}OH$ (λ=200 nm radiation) (2.1)

If an excess of H_2O_2 is used, $^{\bullet}OH$ will produce hydroperoxyl radicals, $^{\bullet}OOH$, which are much less reactive. Unfortunately, the molar extinction coefficient of H_2O_2 at 254 nm is only 19.6 $M^{-1}cm^{-1}$, which is significantly lower than that of ozone,3300 $M^{-1}cm^{-1}$. This means that higher concentration of H_2O_2 is needed to yield the same amount of $^{\bullet}OH$ (Glaze *et al.*, 1987).

2.1.1.1.2. Photolysis of Ozone

The O_3 / UV process seems at present to be the most frequently applied AOP for a wide range of compounds. This is due to the fact that ozonation is a well-known procedure for water and wastewater technology. For the photolytic oxidation by ultraviolet light combined with ozone, hydroxyl radicals are generated as active species.

$O_3 + h\nu \rightarrow O_2 + O(^1D)$ (λ=254 nm radiation) (2.2)

$O(^1D) + H_2O \rightarrow {}^{\bullet}OH + {}^{\bullet}OH$ (2.3)

$O_3 + H_2O \rightarrow \rightarrow H_2O_2 + O_2$ (2.4)

Hydrogen peroxide is produced after photolysis of ozone, and that is photolyzed to $^{\bullet}OH$ radical.

2.1.1.1.3. O_3/H_2O_2/UV Process

Addition of hydrogen peroxide results in a net enhancement due to the dominant production of $^{\bullet}OH$ radicals.

$H_2O_2 \leftrightarrow HOO^- + H^+$ (2.5)

$O_3 + HOO^- \rightarrow {}^{\bullet}OH + O_2^{\bullet-} + O_2$ (2.6)

$$O_3 + O_2^{\cdot-} \rightarrow O_3^{\cdot-} + O_2 \quad (2.7)$$

$$O_3^{\cdot-} + H_2O \rightarrow {}^{\bullet}OH + HO^- + O_2 \quad (2.8)$$

2.1.1.1.4. The Photo-Fenton's Reaction ($Fe^{2+}/H_2O_2/UV$)

The reaction is based on the catalytic effect of the ferrous ions on the decomposition of H_2O_2 (Ruppert *et al.*, 1993):

$$Fe^{2+} + H_2O_2 \rightarrow Fe^{3+} + OH^- + {}^{\bullet}OH \quad (2.9)$$

The primary step is oxidation of ferrous ions to ferric ones (Equation (2.9)) and the formation of ${}^{\bullet}OH$. In the dark, the reaction is retarted after complete conversion of Fe^{2+} to Fe^{3+}. After the complete disappearance of the oxidant, no more Fe(II) can be consumed. In the presence of UV or near-UV light, ferric ions are photo-reduced and ferrous iron can be regenerated and feedback reaction takes place. The following reaction occurs at acidic conditions, especially at pH 3-5 (Tezcanli, 1998).

$$Fe^{3+} + H_2O_2 + h\nu \rightarrow Fe^{2+} + {}^{\bullet}OH + H^+ \ (\lambda > 300 \text{ nm}) \quad (2.10)$$

2.1.1.2. Non-Photochemical Homogeneous AOPs

Generation of ${}^{\bullet}OH$ can also be achieved in the absence of UV light by a number of AOPs. Some well-known methods are described below.

2.1.1.2.1. Ozone at High pH

In an aqueous solution, ozone reacts with various organic compounds via two different pathways namely direct molecular and indirect radical chain type reaction depending upon pH of water. Molecular O_3 is the major oxidant at acidic pH and reacts directly by electrophilic attack, where as less selective and faster radical reaction oxidation (mainly ${}^{\bullet}OH$) becomes predominant at pH>7 as a consequence of OH^- accelerated O_3

decomposition (Glaze *et al.*, 1987). The net reaction of ozone with OH^- ions is given below (Calgon Carbon Oxidation Technologies, 1996):

$$2O_3 + H_2O \xrightarrow{OH^-} {}^{\bullet}OH + 2O_2 + HO_2 \qquad (2.11)$$

Staehelin and Hoigné (1982) showed that the mechanism of reaction of ozone with another substrate M may involve both direct reaction of ozone and indirect $^{\bullet}OH$ chain type reaction with M, even at neutral pH the relative proportions of which will depend on various contaminants present or added. It was also reported that at pH > 10.3 where carbonate ion is a more prevalent species than bicarbonate ion, its scavenging effect is 20 times greater than that of bicarbonate ion.

2.1.1.2.2. Ozone and Hydrogen Peroxide

Hydrogen peroxide is a weak acid and depending upon the pH of the medium it partially dissociates into hydroperoxide ion, which easily reacts with ozone than hydrogen peroxide and results in $^{\bullet}OH$ formation (Glaze *et al.*, 1987).

$$H_2O_2 + H_2O \leftrightarrow HO_2^- + H^+ \qquad pK = 11.8 \qquad (2.12)$$

$$HO_2^- + O_3 \rightarrow {}^{\bullet}O_2H + O_3^- \qquad k_1 = 2.8 \times 10^6\ M^{-1}s^{-1} \qquad (2.13)$$

$$H_2O_2 + {}^{\bullet}OH \rightarrow O_2^- + H_2O + H^+ \qquad k_2 = 2.7 \times 10^7\ M^{-1}s^{-1} \qquad (2.14)$$

$$HO_2^- + {}^{\bullet}OH \rightarrow OH^- + {}^{\bullet}O_2H \qquad k_3 = 7.5 \times 10^9\ M^{-1}s^{-1} \qquad (2.15)$$

The overall reaction for HO_2^- initiated O_3 decomposition is as follows:

$$2O_3 + H_2O_2 \rightarrow 2{}^{\bullet}OH + 3O_2 \qquad (2.16)$$

The concentration of H_2O_2 added is an important control parameter, for the fact that excess amounts induced an inhibitory effect due to the increased competition for hydroxyl radicals (Ince and Gönenc, 1997).

2.1.1.2.3. The Fenton's Reaction

If H_2O_2 is added to an aqueous medium containing organic compounds and excess ferrous ions (Fe^{2+}) at acidic conditions ($2 < pH < 5$), the following complex redox reaction will occur [13]:

$$Fe^{2+} + H_2O_2 \rightarrow Fe^{3+} + {}^{\bullet}OH + HO^- \qquad k_1=76\ M^{-1}s^{-1} \qquad (2.17)$$

$$^{\bullet}OH + Fe^{2+} \rightarrow Fe^{3+} + OH^- \qquad k_2=3\times10^{8}\ M^{-1}s^{-1} \qquad (2.18)$$

The generated $^{\bullet}OH$ radicals attack the organic substrate RH resulting in the formation of new organic radicals;

$$RH + {}^{\bullet}OH \rightarrow {}^{\bullet}R + H_2O \qquad k_2=10^{7}\text{-}10^{10}\ M^{-1}s^{-1} \qquad (2.19)$$

Three reaction alternatives are possible:

$$^{\bullet}R + Fe^{3+} \rightarrow Fe^{2+} + \text{product} \qquad \text{(Oxidation)}$$

or

$$^{\bullet}R + {}^{\bullet}R \rightarrow R\text{-}R \qquad \text{(Dimerization)}$$

or

$$^{\bullet}R + Fe^{2+} \rightarrow Fe^{3+} + RH \qquad \text{(Reduction)}$$

The main advantage of this system to the more popular homogenous AOP UV/H_2O_2 oxidation is that the process and reactor configuration is not limited by UV-irradiation. However, the main disadvantage is the formation of ferric ion precipitation after pH adjustment as well as acidic conditions ($pH < 5$) necessary for this treatment process (Majcen-Le *et al.*, 1997).

2.1.1.2.4. Ionizing Radiation

It is based on the chemical changes produced by the absorption of radiation of sufficiently high energy to produce ionization (Cooper *et al*., 1998). The most widely used commercial radiation sources in use at present time are cobalt-60 for γ-irradiation, and electron accelerators for electron-beam irradiation.

2.1.1.2.5. Ultrasonically-Induced Cavitation

Ultrasonically-induced cavitation is being investigated as an AOP, and chemical effects of ultrasound are due to the phenomenon of acoustic cavitation. It is the formation, growth and violent collapse of bubbles formed by coupling the pressure waves of ultrasound with a liquid (Hua and Hoffmann, 1996; Mason,1990). Upon ultrasonic irradiation , organic compounds in water are degraded via several mechanisms, due to the extreme conditions. Three main pathways of pollutant degradation are •OH oxidation, pyrolytic degradation, and the existence of supercritical water oxidation. In Chapter 3, more detailed information about ultrasonic irradiation is given.

2.1.2. Heterogeneous Photocatalysis

Overall process can be summarized by the following reaction:

$$\text{Organic Pollutant} + O_2 \xrightarrow[h\nu \geq E_{bg}]{\text{Semiconductor}} CO_2 + H_2O + \text{mineral acids}$$

When TiO_2 particles are irradiated by UV photons, photon energy matching or exceeding the band gap energy excites an electron on the TiO_2 surface from the valence band to the conduction band, leaving a positive hole in the valance band. If electron donors such as OH^- and H_2O are available, hydroxyl radicals can be generated by electron transfer from the electron donors to positive holes. Organic compounds then are destroyed either by hydroxyl radicals or by positive holes directly.

2.2. Overview of Textile Industry

2.2.1. Textile Industry Wastewater Quality

Textile dyeing/finishing is one of the largest industrial producers of wastewater with intense color, chemical oxygen demand (COD), total suspended solids (TSS), total dissolved solids (TDS), unstable levels of pH, and toxic substances. The variability arises both from the diversity in the types of industrial processes employed and the huge amount of chemicals and materials involved. The individual processes involved in the textile industry, the chemicals used, and the pollutants associated with each process are summarized in Table 2.2. (EPA., 1996; Nemerow, 1978).

Table 2.2. Textile processes and their contribution to the pollution load (EPA, 1996)

Process	Applied Chemicals	Wastewater Characteristics
Sizing	starch, modified starch, cellulose, polyvinyl acetate, polyacrylate and gums	low in volume, high levels of BOD, COD and TSS
Desizing	enzymes, acids or alkali	very high BOD and total solids (TS) incase of starch consumption
Scouring	hot caustic soda solution, herbicides and fungicides	greatest contributor to effluent pollution load for cotton and woolen fabrics
Bleaching	H_2O_2, NaOCl, H_2SO_4, HCL, Na_2CO_3,surfactants,chelating agents	high TS, low BOD
Mercerizing	Caustic soda and inorganic acids	low BOD and TS, high alkalinity
Milling	H_2SO_4 and Na_2CO_3 solution in the presence of detergents and soaps	high BOD
Dying	Dyes and dye auxiliary chemicals	Strong color, high COD, pH and TDS, low BOD and TSS, variable in composition, sometimes toxic
Finishing	Pentachlorophenols, ethylchlorophosphates, chlorinated rubbers, resins	variable in composition, sometimes toxic, low in volume

Conventional methods (biological, chemical or combinations thereof) for treating textile wastewaters are insufficient because of non-biodegradable, potentially toxic dyestuffs, and a variety of other chemicals (Lin and Peng, 1996). If organic substances such as dyes, starches and detergents in textile effluent are improperly processed they not only deteriorate the aesthetics of receiving waters, but also threaten aquatic life forms via hydrolysis and reduction reactions of some dyes to form toxic and carcinogenic end products.

High concentrations of soluble inorganic salts may make the receiving body unsuitable for industrial and municipal use and may have corrosive effect. Metals such as chromium, copper, and zinc originate from the dyes themselves and are toxic to aquatic life and hence should be removed prior to discharge. Some carrier chemicals used in dyeing, such as phenol, may be toxic and add odors. Management of such waters, therefore, requires the incorporation of innovative technologies into conventional treatment plants, while fulfilling the discharge standards.

2.2.2. Pollutants Associated with Dyeing

Dyebath effluents are very difficult to treat via conventional methods. The wastewater characteristics from a dyehouse are highly variable from day to day, and even from hour to hour, depending on the type of the dye, the type of fabric, and concentration of chemical auxiliaries added. The contribution to pollution load of dyeing together with washing and rinsing operations may not be more than 20 per cent - 40 per cent, but the spent volume is considerably large, usually not less than 50 per cent of the total (Correia *et al.*, 1994).

Pollutants associated with dyeing may originate from the dyes themselves (e.g., toxicity, metals, color) or derive from auxiliary chemicals used during the dyeing process (e.g., salt, surfactants, levellers, lubricants, and alkalinity). Dyeing contributes essentially all of the salt and color in effluent from textiles operations (EPA; 1996). Color removal remains a very difficult environmental problem for textile industry since most of the dyes are non-biodegradable and sometimes toxic. Dyes are the principle source of color because of their low fixation capacities. In typical dyeing processes, 50 to 100 per cent of the color

is fixed on the fiber as can be in Table 2.3., and the remainder is discarded in the form of spent dyebaths or in wastewater from subsequent textile-washing operations (EPA, 1996). Reactive dyes are widely used because of their bright and highly saturated color, but unfortunately fall in the lower range of the fixation scale. In the following section, more detailed information of dyestuffs is given.

Table 2.3. Typical exhaustion/fixation rates for dyes of various classes (EPA, 1996)

Dye Classes	Typical Fixation (%)	Fibers Typically Applied to
Acid	80 to 93	wool, nylon
Basic	97 to 98	acrylic
Direct	70 to 95	cellulose
Disperse	80 to 92	synthetic
Reactive	50 to 80	cellulose
Vat	80 to 95	cellulose

High concentrations of salt are another environmental problem that textile industry faces. Salt addition enhances dyebath exhaustion by increasing dye affinity for cellulose fibers. It is added to the dye solution to displace the dye to the fibre. Among the other dyestuffs, reactive dyes require the maximum amount of salt, up to 100 g L^{-1} to maximize dye fixation.

Alkalinity of dyeing effluents is a further environmental concern. Preparation processes are generally carried out in a range of neutral pH conditions to highly alkaline conditions. Alkali is introduced to cause the reaction between the dye and the fibre, and any reaction between the dye and the alkalinity in the water before the dyeing process will result in significant loss of dyestuff.

2.2.3. Textile Dyestuffs

Textiles are dyed using many different colorants, which may be classified in several ways (e.g. according to chemical constitutions, dyeing property, solubility). The primary classification of dyes is based on the fibers to which they can be applied, and the chemical

nature of each dye determines the fibers for which the dye has affinity. Table 2.4. lists the major dye classes and the types of fibers for which they have an affinity.

Table 2.4. Dye classes and their associated fibers (EPA, 1996)

Dye Class	Fibers
Acid	Wool and nylon(polyamide)
Basic	Acrylic, certain polyesters
Direct	Cotton, rayon and other cellulosic
Disperse	Polyester, acetate, and other synthetics
Fiber reactive	Cotton and other cellulosic, wool
Mordant	Natural fibers
Vat	Cotton and other cellulosic

Despite their low fixing capacity, reactive dyes have the greatest consumption in dyeing process due to their bright and wide color spectra. Acid dyes are commonly used in dyeing of fibers other than cotton. Basic dyes are not as popular as reactive and acid dyes, because of their toxic nature. They should be applied properly to minimize discharge of unfixed dye residuals. In this study, a variety of acid, basic and reactive dyes have been used as model compounds.

Most of the model dyes in this study were made of azo groups containing at least one azo-(N=N), and one or more alkyl sulfonate reactive groups (Ganesh *et al.*, 1994). In general, azo dyes are recognized with their bright and dark shades of yellow, orange, red, maroon, navy blue, brown, and black colors. In addition, an anthraquinone dye was used as a model compound to study impacts of dye structure. Benzoquinone component between two benzene rings represents the anthraquinone dye chromophore. They usually have bright blue colors.

2.2.3.1. Acid Dyes

Acid dyes are water soluble anionic compounds applied to nylon, wool, silk, and some modified acrylic textiles in an acidic medium. They exhibit little affinity for

cellulosic or polyester fiber. Colors are generally bright, and the material exhibits good to excellent fastness properties. Fastness of dyes is a term referring to its relative resistance to chemical and physical breakdown or removal when in use. Acid dyes have one or more sulfonic or carboxylic acid groups in their molecular structure. The dye-fiber affinity is the result of ionic bonds between the sulfonic acid part of the dye and the basic amino groups in wool, silk, and nylon fibers (U.S. EPA, 1996).

2.2.3.2. Basic Dyes

Basic dyes are cationic compounds and have limited water solubility and are applied in weakly acidic dyebaths. Ionic bonds are formed between the cation in the dye and the anionic site on the fiber. They have unlimited color range and good fastness properties. Although most textile dyes do not have aquatic toxicity, cationic (basic) dyes generally are moderately toxic due to metal content. Most of the basic dyes include metals as an integral part of the dye molecule. Fortunately, cationic dyes exhaust essentially 97-98 per cent in batch dyeing operations (see Table 2.3.) (EPA, 1996). The metals most commonly found in basic dyes are zinc and copper, but this does not imply that all basic dyes contain metals.

2.2.3.3. Reactive Dyes

Reactive dyes are water soluble, anionic dyes that are mainly used for dyeing cellulosic fibers such as cotton and rayon. Reactive dyes have the largest dye class in commercial value. They have bright shades, particularly orange, scarlet, and turquoise (EPA, 1996). Fiber reactive dyes form covalent chemical bonds with the fiber and become part of the fiber, giving excellent fastness properties. To exhaust the dyes, however large amounts of salt are generally necessary and substantial amounts of dye can remain unfixed at the end of the process. After dyeing, the fabric is washed with an anionic surfactant to remove unreacted dye. The characteristic structural features of a reactive dye are shown in Figure 2.1. (Bird and Boston, 1975).

RG : reactive group
B : bridge link
F : chromogen
W : water-solubilising group

Figure 2.1. Characteristic structural features of a reactive dye.

Reactive Groups: All reactive groups are based on the fact that cellulose, protein and nylon fibres contain groups that are able to react as nucleophilic substrates, i.e. hydroxyl, amino groups.

Bridge Link: Generally the reactive system is attached to the chromogen by a bridging group. The reactivity and other dyeing characteristics of a reactive dye are influenced by the bridging group, and still more, by other substituents attached to the reactive system. It influences a) the reactivity of the reactive system since dissociation of reactive groups can lead to lower fixation, b) the degree of fixation; some isomeric forms of the dyes have lower selectivity towards cellulose, c) the stability of reactive dyeing.

Chromogen: The colored part of a reactive dye, usually an azo, metal-complex azo, or anthraquinone residue. Fastness to light and to chemical treatments are largely determined by the stability of the chromogen.

Water-Solubilising Groups. Water solubility is generally conferred by sulphonic acid groups attached to the chromogen and/or, occasionally to the reactive system.

2.2.4. Degradation of Textile Dyes by AOP: Literature Review

2.2.4.1. H_2O_2/UV Process

There are many studies for the treatment of azo-dyes with UV/H_2O_2. Neither UV (without H_2O_2) nor H_2O_2 (without UV) treatments were found to be efficient to decompose azo dyes significantly (Shu *et al.*, 1994). The two non-biodegradable azo-dyes C.I. Acid Red 1 and C.I. Acid Yellow 23 were degraded efficiently under UV/H_2O_2, using a low pressure mercury lamp. The high reaction was due to the generation of radicals from the

UV irradiation of hydrogen peroxide at acidic pH. Total organic carbon removal was found to be slow at the beginning of reaction as the •OH was used for decolorization reaction and after the color was removed, the •OH was then spent on the degradation of TOC compounds.

Ince and Gonenc (1997) studied the H_2O_2/UV oxidation of C.I. Reactive Black 5 in aqueous solution. Effects of the initial H_2O_2 concentration, initial dye concentration and alkalinity at neutral pH was tested by calculating pseudo-first order reaction rate constants ,and electrical energy requirements per order of pollutant removal (EE/O) were calculated.

Ince *et al.*, (1997) studied the degradation and toxicity reduction of C.I. Reactive Black 5 under H_2O_2/UV process, using a medium pressure mercury lamp. Complete color degradation was accompanied with 44 per cent mineralization and 68 per cent toxicity reduction under the experimental conditions employed.

Majcen-Le *et al.*, (1997) described the decolorization of the monochlorotriazine dye C.I. Reactive Red 120 in the absence and presence of dyebath constituents. It was found that dye auxiliaries reduced the efficiency of the decolorization process significantly. The decolorization rate was proportional to the UV output of the light source.

Colonna *et al.*, (1999) studied the photodegradation of some azo and anthraquinone dyes in the presence of hydrogen peroxide. They observed that at least 90 per cent mineralization was obtained in no more than 3 hours. It was observed that color removal and TOC decay followed first-order-kinetics. They studied the effect of H_2O_2 concentration on dye degradation and found that faster dye degradation occurred until a $[H_2O_2]$/[dye] ratio of 400 and it was observed that at higher ratios, the degradation process became slower.

Namboodri and Walsh (1996) investigated the H_2O_2/UV treatment of simulated reactive dye-bath wastewater (hydrolyzed Reactive Blue 21 and Reactive Red 195 solutions) by using both batch operation and continuous circulation methods. A pilot plant study was also conducted using a high intensity reactor. For both reactive dyes under similar dye concentration, radiation dosage and H_2O_2 concentration levels, the continuous

circulation method gave higher rates of decolorization. Though compared to the low intensity lamp experiments in lab scale, the high intensity lamps required a higher energy input per volume of wastewater, they were more compact and the number of bulbs were fewer that becomes an important criteria for full scale application.

Ince *et al.*, (2002) studied the treatability of textile dyebath effluents by two simultaneously operated processes comprising adsorption and advanced oxidation using Everzol Black-GSP. The method was performed by contacting dye solutions with H_2O_2 and granulated activated carbon (GAC) during UV irradiation. Each individual processes were run separately as control experiments. In combined scheme color was principally removed by oxidative degradation while adsorption contributed to the longer process of dye mineralization. Economic evaluation (for total color and 50 per cent TOC reduction) showed that the combined scheme provided 25 per cent and 35 per cent reduction in H_2O_2 and energy consumption relative to the UV/H_2O_2 system.

2.2.4.2. Ozone and UV/Ozone Processes

Wu and Wang (2001) studied the ozonation of Reactive Black 5 in a semi-batch reactor. The pseudo-first-order decolorization rate constant was found to increase with increasing applied ozone dose and increasing temperature, but decreased with initial dye concentration. They further observed that ozonation reduced COD and enhanced the biodegradability of the solution.

Arslan and Balcioglu (1999) investigated ozonation, hydrogen peroxide coupled with ozone, and UV irradiated processes for the treatment of synthetic dyebath effluents containing six reactive dyestuffs and their assisting chemicals. They observed rapid and complete decolorization for all systems with optimum H_2O_2 dose and reaction pH. The increase in pH from acidic conditions to basic conditions yielded 41 per cent enhancement in ozone absorption rate. Total decolorization of synthetic dyebath effluent was achieved after 20 minutes of ozonation (33 mg O_3) at pH=11.5.

Warren *et al.*, (1999) reported the ozonation and biological treatability of composite textile wastewater and two spent dyebaths. They achieved an increase in biological

treatability of dye wastewater. The decrease in the toxicity of the spent dyebath was carried out with *Ceriodaphnia dubia*.

Huang and Shu (1994) assessed the decolorization and mineralization of textile wastewater containing the direct dyes Black 22 and Blue 199 by the sequential application of O_3 and H_2O_2/UV. The effects of pH and H_2O_2 dose were also investigated. Fastest decolorization was achieved at neutral pH and an initial optimum concentration of 1 per cent w/w H_2O_2.

Lin and Lin (1993) investigated the treatment of low, medium and high strength textile waste effluents by ozonation and chemical coagulation. It was observed that ozone is highly effective in removing color of these effluents but relatively ineffective in reducing the COD especially for the high and medium strength effluents. The COD reduction was improved to a maximum of 70 per cent after a proceeding chemical coagulation.

Wu *et al.*, (1998) evaluated membrane filtration coupled with ozonation of a simulated textile wastewater representing an exhausted dyebath. The membrane filtration process generated a permeate with over 99 per cent of color and copper removal and reusable quality, whereas the retentate was subjected to an ozonation stage for its decolorization. The pseudo-first order decolorization rate constant decreased with increasing initial dye concentration.

Law *et al.*, (1996) studied the treatment of simulated cotton dyehouse wastewater with ozonation. The presence of NaCl had no significant effect upon decolorization removal rate. Ozonation of the NaCl free reactive and acid dyes had no significant effect on treatment performance nut increased the toxicity towards the nematode *Caernorhabditis elegans*, respectively.

2.2.4.3. Fenton and Photo-Fenton Process

Ince and Tezcanli (1999) reported the treatability of Reactive Red 141 by photo-Fenton oxidation. Complete color and 79 per cent TOC removal was achieved with a H_2O_2/Fe(II) molar ratio of 20:1, and at pH 3.

Namboodri and Walsh (1995) conducted a study for decolorizing spent dyebaths using small amount of hydrogen peroxide in the absence of ultraviolet light, at neutral pH, and a temperature close to the boiling point of water. Small amounts of ferrous or ferric ions (ferric ion gave a higher rate of decolorization) as catalyst with peroxide at pH 7, and at 95-98 °C decolorized the resistant azo direct dye.

Herrera *et al.*, (1999) studied the decolorization of anthraquinone dyes, Remazol Brilliant Blue and Remazol Uniblue in the presence of H_2O_2/Fe (III) under various UV lights. Electron transfer between the excited dye and Fe(III) was reported as initiating step and the photoreduction of Fe(III) to Fe(II) was pointed for the acceleration during the initiation of radical chain reactions.

Lin and Peng (1995) used a continuous process of combined chemical coagulation, Fenton's reagent, and activated sludge for the full treatment of textile wastewater. Optimum Fe^{2+}, H_2O_2 dose and pH conditions were explored to determine their respective effects on COD removal efficiency. Economic evaluation of the continuous Fenton's treatment method indicated that the combined system was highly competitive with conventional treatment methods practiced in the textile finishing industry.

Kuo (1992) investigated the decolorization of simulated dye wastewater by the Fenton's reagent. Treatment efficiency was examined in terms of both color and COD removal. The effect of temperature, pH, H_2O_2 and Fe^{2+} dose was discussed. The treatment yield of Fenton's reagent depended upon the type of the dye.

2.2.4.4. Ultrasonic Processes

Vinodgobal *et al.*, (1998) have investigated the ultrasonic mineralization of a textile dye, Remazol Black B at 640 kHz under a stream of O_2 gas. They reported that the destruction of the dye starts by the rupture of the azo-bond by •OH attack in the solution bulk, and complete decolorization was accompanied by total mineralization, provided that sufficient contact was allowed. The authors concluded that ultrasonic remediation should be considered as a solution alternative to the reuse and/or recycle of textile dyeing mill effluents as process water.

In another study by Vindgopal and Kamat (1998), the authors have reported the results of three hydroxyl radical medicated oxidation reactions (photocatalysis, γ-radiolysis and sonolysis) for the degradation of the dye Acid Orange 7 under oxygen-saturated conditions. They noted the similarity of reaction pathways in all three processes, as made evident from the single identifiable intermediate produced in all experiments, and concluded that textile azo-dyes can be effectively destroyed by advanced oxidation processes, or any hydroxyl radical medicated reaction pathways.

Joseph *et al.*, (2000) studied the effect of Fenton's reaction on the sonochemical degradation of azobenzene and some related azo dyes at 500 kHz. As in the previous work of Vinodgopal *et al.*, (1998), they also reported that the first step in the reaction scheme was the cleavage of the azo-double bond upon hydroxyl radical attack. Fenton's reaction at optimal Fe(II) concentrations was found to induce a three fold increase in the reaction rates. They also reported that saturating the solution with Ar increased the efficiency by 10 per cent thereof with saturation by O_2.

Ince and Tezcanli (2001) studied the degradation of Remazol Black B by combined sonolysis (520 kHz) and ozonation. They found that color removal in 15 minutes with the combined system was twice as faster than that of ozone, while no significant removal was observed by ultrasound alone. The lack of color degradation by ultrasound was attributed to the shortness of the contact period. They observed that total mineralization over 1 hour in ultrasound alone, ozone alone and in the combined scheme were 2, 50 and 76 per cent, respectively. They concluded that longer contact time was necessary for appreciable conversion of organic carbon to CO_2 by ultrasonic treatment alone.

Ince and Tezcanli (2003) studied the degradability and toxicity reduction of Reactive Red141, Reactive Black5, Basic Brown4 and Basic Blue3 in deionized water solutions during 520 kHz ultrasonic irradiation. The destruction of aromatic content in azo dyes was slower than that of color. Toxicity analysis of the initial dye solutions revealed that reactive dyes were non-toxic, and basic dyes were toxic at the test concentrations employed. Significant degrees of toxicity reduction were achieved by ultrasonic irradiation.

Lorimer *et al.*, (2000) studied the decolorization of Sandolan Yellow with sonolysis, electrolysis and sonoelectrolysis. They observed a synergism in dye decolorization rate with the combined system, while no decolorization was obtained with ultrasound alone (20 kHz). Platinum electrodes were used for the electrolysis.

CHAPTER 3. INTRODUCTION TO SONOCHEMISTRY

Section 3.2 of this chapter is the review entitled "Ultrasound as a Catalyzer of Aqueous Reaction Systems: The State of the Art and Environmental Applications," which was published in Applied catalysis B: Environmental, 29, 167-176, 2001.

3.1. Fundamental Principles

Sonochemistry is an emerging field of science that uses ultrasound to promote chemical reactions. The history of sonochemistry begins in the late 1800s. During field tests of the first high-speed torpedo boats in 1894, Sir John I. Thornycroft and Sydney W. Barnaby discovered severe vibrations from and rapid erosion of the ship's propeller. They observed the formation of large bubbles (or cavities) formed on the spinning propeller and postulated that the formation and collapse of these bubbles were the source of their problems. By increasing the propeller size and reducing its rate of rotation, they could minimize this difficulty of "cavitation". As ship speeds increased, however, this became a serious concern and the Royal Navy commissioned Lord Rayleigh to investigate. He confirmed that the effects were due to the enormous turbulence, heat, and pressure produced when cavitation bubbles imploded on the propeller surface.

This phenomenon of cavitation occurs in liquids not only during turbulent flow but also under high-intensity ultrasonic irradiation. It is responsible for both propeller erosion and for the chemical consequences of ultrasound. Alfred L. Loomis noticed the first chemical effects of ultrasound in 1927, but the field of sonochemistry lay fallow for nearly 60 years. The renaissance of sonochemistry occurred in the 1980's, soon after the advent of inexpensive and reliable laboratory generators of high-intensity ultrasound. Scientists now know that the chemical effects of ultrasound are diverse and include substantial improvements in both stoichiometric and catalytic chemical reactions. In some cases, ultrasonic irradiation can increase reactivities by nearly a million fold (Suslick, 1994).

3.1.1. Ultrasound

Sound can be viewed as a wave of energy transmitted through a medium by vibrating molecules. The vibrating molecules at one end of the medium propagate their vibrational motion to the other end of the medium through minute pressure differences. Pressure differences occur in cycles, forming pressure waves that can be viewed in two distinct portions: compression and rarefaction (expansion).

Ultrasound is defined as any sound of a frequency above that to which the human ear has no response (i.e. above 16 kHz). In practice, three ranges of frequencies are reported for three distinct uses of ultrasound (Mason and Cordemans, 1998): i) high frequency, or diagnostic ultrasound (2-10 MHz); ii) low frequency or conventional power ultrasound (20-100 kHz); and low-to-medium-frequency, or "sonochemical-effects" ultrasound (20-1000 kHz). It is this latter range, where chemical reaction processes are uniquely catalyzed through very "extreme" temperatures and pressures generated by the formation, growth and collapse of cavitational bubbles. The use of power ultrasound has been well known for many years in fields such as medical, flow detections, emulsification, solvent degassing, cleaning, cutting, welding; however chemical applications of ultrasound, "sonochemistry", in environmental processing is an emerging field. The chemical effects of ultrasound in liquids are largely linked to the formation of free radicals.

3.1.2. Ultrasonically-Induced Cavitation

The chemical effects of ultrasound are due to the phenomenon of a "cold boiling" termed acoustic cavitation, which is the production of microbubbles in a liquid when a large local negative pressure is applied. When a liquid is exposed to an acoustic field, the pressure waves of the sonic vibrations create a time and frequency dependent acoustic pressure, consisting of alternating compression and rarefaction cycles (Mason, 1990). If the applied pressure is equal to the negative pressure developed in the rarefaction cycle of the wave such that the distance between the molecules of the fluid exceeds the critical molecular distance to hold it together, the liquid breaks apart to form acoustic cavities, made of vapor and gas-filled microbubbles (Mason, 1990; Dahlem *et al.*, 1998). The phenomenon called "acoustic cavitation" consists of at least three distinct and successive

stages: *nucleation*, *bubble growth* (expansion), and under proper conditions *implosive collapse* (Suslick, 1990). Development and collapse of cavitation bubbles can be seen in Figure 3.1. (Suslick, 1994).

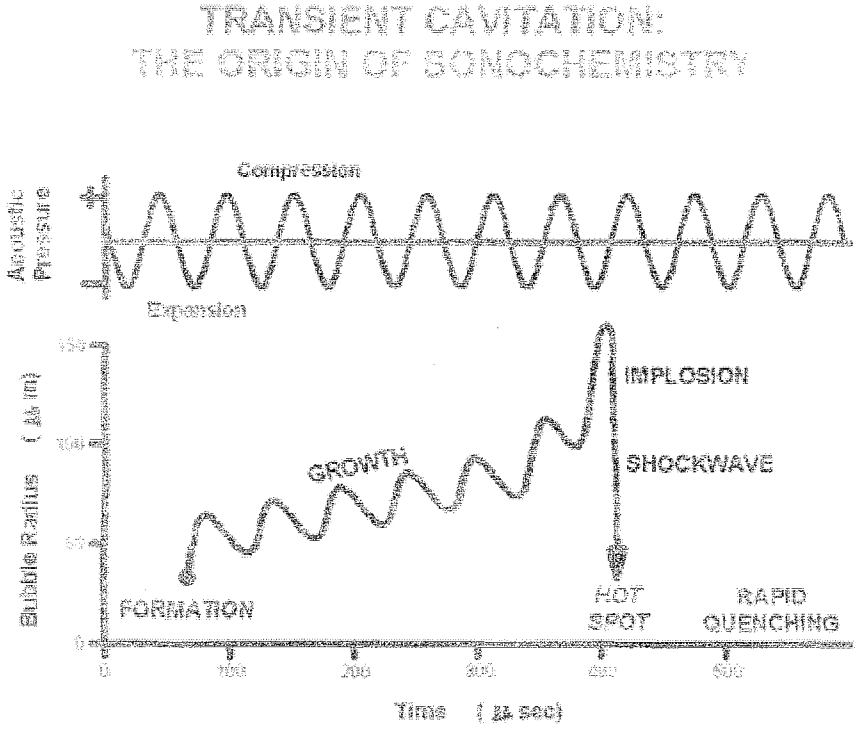

Figure 3.1. Development and collapse of cavitation bubbles (Suslick, 1994).

The first stage, also known, as "cavity formation" is a nucleated process, by which cavitational nuclei are generated from microbubbles trapped in micro crevices of suspended particles within the liquid (Suslick, 1990; Reisse, 1995). In the second stage, the bubbles grow and expand in a manner restricted by the intensity of the applied sound wave. With high-intensity ultrasound, a small cavity grows rapidly through inertial effects, whereas at lower intensities the growth occurs through "rectified diffusion", proceeding in a much slower rate, and lasting many more acoustic cycles before expansion (Suslick, 1990). The third stage of cavitation occurs only if the intensity of the ultrasound wave exceeds that of the "acoustic cavitational threshold" (typically a few watts/cm^2 for ordinary liquids exposed to 20 kHz). At this condition, the microbubbles overgrow to the extent where they can no longer efficiently absorb energy from the sound environment to sustain

themselves, and implode violently, therefore, in a so called "catastrophic collapse" (Ince *et al.*, 2001; Mason, 1990; Suslick *et al.*, 1990).

It is reported that during this collapse stage, such extremes of temperatures and pressures are released that the entrapped gases undergo molecular fragmentation- the underlying phenomenon in homogenous sonochemistry (Hung and Hoffmann, 1998). Furthermore, it has been observed that just before the catastrophic collapse of compressed gas-filled cavities in water, the bubbles produce a flash of light called "sonoluminescence", as detected by a peak at 310 nm and a broad continuum throughout the visible(Ince *et al.*, 2001; Crum, 1994; Verrall *et al.*, 1988). Sonoluminescence from a high ultrasonic horn can be seen in Figure 3.2. and it can be used as a spectroscopic probe of cavitation (Suslick,1996). The spectrum of sonoluminescent water was associated with the formation of high-energy species (e.g. excited hydroxyl radicals) from molecular fragmentation of compressed gases, rather than with black body radiation (Suslick *et al.*, 1990; Crum, 1994; Lepoint-Mullie *et al.*, 1996)]. Hence, like photochemistry, sonochemistry involves the introduction of very large amounts of energy in a short period of time, but the type of molecular excitation is thermal, unlike the electronic excitation felt by molecules in photochemical processes (Suslick, 1990). It is further reported that sonochemistry lies in between "high-energy" and "molecular" physics, requiring therefore, the use of microscopic description of matter (Reisse, 1995).

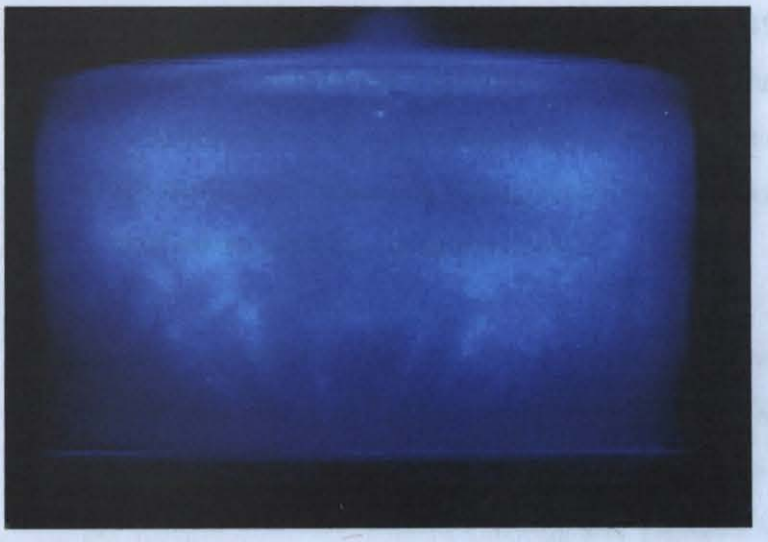

Figure 3.2. Sonoluminescence generated by a high frequency ultrasound (Suslick, 1994).

As mentioned until now, the violent collapse of a bubble due to acoustic stress can produce a large amount of energy and this produced energy drives sonochemistry. There are several theories as to how this energy is developed.

The most highly favored explanation is that given by the "Hot Spot Theory", which suggests that the collapse is so rapid that the compression of the gas and vapor inside the bubble is adiabatic (Rayleigh, 1917; Noltingk and Neppiras, 1950). Consequently, the temperatures and pressures within a collapsing microbubble can reach values as high as 4200-5000 K and 200-500 atm, respectively just before fragmentation (Dahlem *et al.*, 1998; Suslick, 1990). It is also reported that the localized "hot spot" generated by the rapid collapse of acoustic cavities is very short-lived (less than 10 μs), implying the existence of extremely high heating and cooling rates in the vicinities of 10^{10} K s^{-1} (Mason, 1998; Suslick, 1990). Substituents trapped inside or around a collapsing bubble are also subjected to these extremes.

The second most accepted, "Electrical Theory" by Margulis (Margulis, 1992; Margulis, 1995) suggests that during bubble formation and collapse, enormous electrical field gradients are generated and these are sufficiently high to cause bond breakage and chemical activity.

The "Plasma Theory" by Lepoint and Mullie (1994) also suggests the extreme conditions associated with the fragmentative collapse is due to intense electrical fields and seems not to involve a true implosion. They compared the origin of cavitation chemistry to corona-like discharges caused by a fragmentation process and supported and indicated the formation of micro plasmas inside the bubble.

"The Supercritical Theory" recently proposed by Hoffmann (Hua *et al.*, 1995) suggests the existence of a layer in the bubble-solution interface where temperature and pressure may be beyond the critical conditions of water (647 K, 22.1 MPa) and showed that supercritical water is obtained during the collapse of cavitation bubbles generated sonolytically.

3.2. Literature Review on Principles and Environmental Application of Ultrasound

The below section is the extension of review" Ultrasound as a Catalyzer of Aqueous Reaction Systems: The State of the Art and Environmental Applications," published in Applied catalysis B: Environmental, 29, 167-176, 2001.

A great majority of sonochemical systems, having potential industrial applications involve heterogeneous reactions, where enhancement of chemical reactivity is associated with the physical effects of ultrasound such as heat and mass transfer, surface activation, and phase mixing (Suslick, 1990; Reisse, 1995; Leighton, 1994; Serpone *et al.*, 1994). Sonocatalysis of liquid-liquid heterogeneous reactions is based on the mixing effect of acoustic streaming, which promotes the emulsification of non-miscible liquids by enhancing reaction rates upon increased interfaces (Reisse, 1995). When the heterogeneous system is made of a solid-liquid biphasic medium, catalysis of reactions is a consequence of the disruption of the solid by the jetting phenomenon associated with the collapse of cavitation bubbles. It is important to note that many of such effects are observed when the heterogeneous medium is irradiated with low frequency, or power ultrasound at the 20-100 kHz range (Ince *et al.*, 2001).

On the other hand, homogenous sonochemistry induced by ultrasonic irradiation of homogenous fluids is a direct outcome of the extreme conditions generated in collapsing microbubbles (Ince *et al.*, 2001; Reisse, 1995). Such extremes are reported to produce very unique catalytic effects, arising from inherent advantages of the system such as: (i) the ability to generate high-energy species and (ii) the mimicry of autoclave reaction conditions (i.e. high temperatures and pressures) on a microscopic scale (Ince *et al.*, 2001; Suslick, 1990). These catalytic effects start in the "microreactors" (cavities), which are made of microbubbles filled with vapor of the liquid medium and/or dissolved volatile solutes and gases diffused into them (Mason and Cordemans, 1998). During the collapse of these cavities in pure aqueous systems, gaseous water molecules entrapped in expanded microbubbles are fragmented as in pyrolysis to generate highly reactive radical species such as hydroxyl radicals and hydrogen atoms (Riesz and Mason, 1991). The formation of these radicals in sonicated water has been demonstrated in various laboratories, using

combined spin trapping and EPR techniques; the Weissler reaction; fluorescence measurements from 2-hydroxy-terephthalate produced by hydroxylation of aqueous terephthalate ion; DMPO trapping; and sonoluminescence measurements based on the oxidative degradation of luminol to aminophtalate under the action of sonochemically produced hydroxyl radicals (Pétrier *et al.*, 1992; Mason *et al.*, 1994; Weissler *et al.*, 1920; Negishi, 1961; Hart and Henglein, 1985; Riesz *et al.*, 1990). In non-aqueous organic solvents or aqueous media containing volatile organic gases and solutes, cavitational collapse not only results in hydroxyl and hydrogen radicals, but also in organic radical species, as confirmed by experimental studies with ESR spectroscopy (Seghal *et al.*, 1982).

3.2.1. Possible Reaction Sites in the Cavitation Process

Experiences in homogenous sonochemistry have shown that there are three reaction sites in ultrasonically irradiated liquids (Weavers *et al.*, 1998), as illustrated in Figure 3.3., i) the cavitation bubble itself; ii) the interfacial sheath between the gaseous bubble and the surrounding liquid; and iii) the solution bulk.

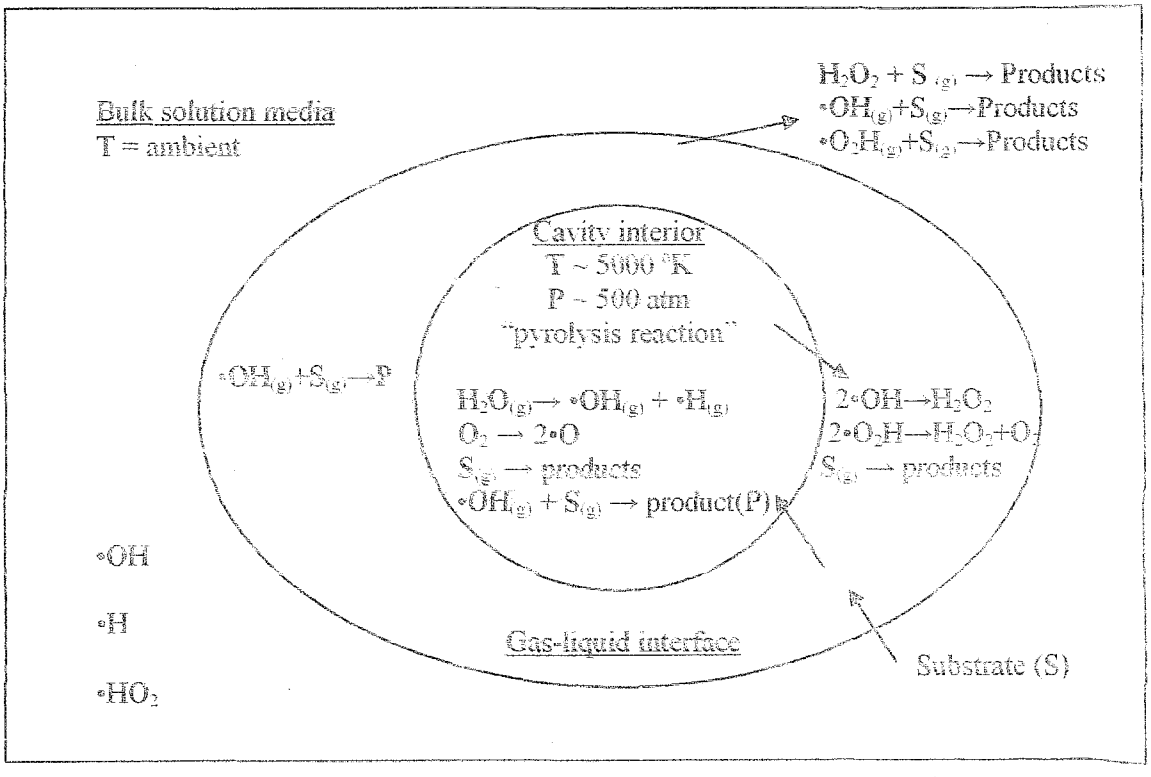

Figure 3.3. Possible sites of chemical reactions in homogeneous reaction media (Adewuyi, 2001).

The hydroxyl radicals generated by water sonolysis may either react in the gas phase or recombine at the cooler gas-liquid interface and/or in the solution bulk during cavity collapse to produce hydrogen peroxide and water as (Ince *et al.*, 2001; Riesz, 1991; Fischer *et al.*, 1986):

$$H_2O \rightarrow))) {}^{\bullet}OH + {}^{\bullet}H \qquad \text{(pyrolysis)} \qquad (3.1)$$

$$^{\bullet}OH + {}^{\bullet}H \rightarrow H_2O \qquad (3.2)$$

$$2\ {}^{\bullet}OH \rightarrow H_2O \qquad (3.3)$$

$$2\ {}^{\bullet}OH \rightarrow H_2O_2 \qquad (3.4)$$

$$2\ {}^{\bullet}H \rightarrow H_2 \qquad (3.5.)$$

If the solution is saturated with oxygen, peroxyl and additional hydroxyl radicals are formed in the gas phase (due to the decomposition of molecular oxygen), and the recombination of the former at the cooler sites (interface or the solution bulk) produces more hydrogen peroxide, as shown (Ince *et al.*, 2001; Makkino *et al.*, 1982; Pétrier *et al.*, 1994):

$$O_2 + {}^{\bullet}H \rightarrow {}^{\bullet}O_2H \qquad (3.6)$$

$$O_2 \rightarrow))) O + O \qquad (3.7)$$

$$O + H_2O \rightarrow {}^{\bullet}OH + {}^{\bullet}OH \qquad (3.8)$$

$$^{\bullet}O_2H + {}^{\bullet}O_2H \rightarrow H_2O_2 + O_2 \qquad (3.9)$$

In water and wastewater treatment practices, organic pollutants may be destroyed either at the first two sites upon combined effects of pyrolytic decomposition and hydroxylation, or in the solution bulk via oxidative degradation by hydroxyl radicals and

hydrogen peroxide. The extend of oxidation in the latter site is limited by the quantity of uncombined hydroxyl radicals available in solution.

3.2.2. Parameters Affecting Sonochemical Reactions

The main concern of scientists and engineers working with ultrasonic systems is to accomplish maximum reaction yields and/or maximum pollutant destruction at optimal conditions. Research and development in sonochemical systems exposed the significance of two basic strategies for maximizing reaction efficiencies: i) optimization of power and reactor configuration and/or ii) enhancement of cavitation. The first strategy requires a mechanistic approach with features like: (a) selection of the transducer (piezoelectric or magnetic material that converts electrical impulses to mechanical vibrations) and generator (probe types for low frequency, and plate types for high frequency effects), (b) configuration and dimensioning of the reaction cell, and (c) optimization of the power efficiency (i.e. the effective power density delivered to the reaction medium). The effect of frequency, applied pressure, power intensity and bulk solution temperature for the optimization of power and reactor configuration are explained. The effect of physicochemical properties of the pollutant and the solute, bubbled gas, and the solid addition to enhance cavitation, and therefore maximize chemical reactions are explained (Ince *et al.*, 2001).

3.2.2.1. Frequency

The more important cavity effects are reported to occur when the frequency of the ultrasonic wave is equal to the resonating frequency of the bubbles. The resonance radius of a bubble excited by low frequency waves is reported to be ~170 μm (at 20 kHz), and the cavities entrapping such bubbles are said to be "stable" or long-lived, with average life times of ~10 μs (Mason, 1990; Pétrier *et al.*, 1994). In this kind of cavitation, the collapse stage is delayed till after the elapse of a number of compression and rarefaction cycles, during which sufficient volumes of volatile solutes and solvent vapors within the liquid may flow into the gas phase (Mason, 1990). The delayed growth and long collapse duration of gas-filled bubbles allow radical scavenging and recombination reactions at the

interfacial sheath (as shown by equations 3.2, 3.3, 3.4, 3.5 and 3.9), thus inhibiting the mass transfer of hydroxyl radicals into the solution bulk (Barbier *et al.*, 1996).

On the contrary, the resonance radii of bubbles excited by medium frequency (300-1000 kHz) ultrasound waves are extremely small (4.6 μm at 500 kHz), giving rise to very short-lived (0.4 μs on the average) and mainly void or vapor-filled "transient" cavitations (Ince *et al.*, 2001; Mason, 1999). Furthermore, such cavitations are so short-lived and the collapse is so rapid that the time for appreciable degree of radical scavenging reactions in the hot bubble or at the interfacial region is insufficient. As a consequence, medium frequency waves are highly effective for oxidation reactions in the liquid bulk, due to the highly probable ejection of uncombined hydroxyl radicals into the surrounding liquid during collapse (Ince *et al.*, 2001; Mason *et al.*, 1994; Barbier *et al.*, 1996).

It should be remembered that, lower frequency ultrasound produces more violent collapse, leading to higher localized temperatures and pressures. However, current research indicates that higher frequencies lead to higher oxidation reaction rates. Beckett and Hua (2001) have postulated that the degree of heat generated upon collapse would be most intense at lower frequencies but there would be more cavitation events and thus more opportunities for the free radicals to be produced and diffuse into the bulk media with increasing frequency. Thus, there should be an optimum frequency where the competing effects balance.

3.2.2.2. Bulk Solution Temperature

Lowering the bulk solution temperature has been shown to actually increase the effect of sonication (Beckett and Hua, 2001). This is due to a decrease in the vapor pressure of the solvent, which leads to an increase in the intensity of the bubble. At low vapor pressure, less vapor has an opportunity to diffuse into the bubble which favors the more violent collapse. Also, as liquid temperature decreases, the amount of gas dissolved increases and the vapor pressure of the liquid decreases. Very volatile solvents lead to relatively high pressures in the bubble and also "cushion" the collapse (Adewuyi, 2001).

3.2.2.3. Applied Pressure

Increase in the pressure of the system will give rise to a larger intensity of cavitational collapse and consequently an enhanced sonochemical effect (Mason, 1999). Too much pressure reduces the rate of reaction by decreasing the frequency or efficiency of bubble formations.

3.2.2.4. Power Intensity

The intensity of sonication (in W m^{-2}) is directly proportional to the square of the amplitude of vibration of the ultrasonic source (Eqn 3.10). By increasing the amplitude, the power is increased, and in most cases, as the power is increased, the reaction rate also increases. It is important to remember that, as in the other cases, sonochemical activity rises with increasing intensity to an optimum at which efficiency falls. When a large amount of ultrasonic power enters a system, a great number of cavitation bubbles are generated in the solution. Many of these will come together to form larger and more longer lived bubbles. These will certainly act as a barrier to the transfer of acoustic energy through the liquid (Mason, 1990).

$$I = \frac{P_a^2}{2\rho c} \qquad (3.10)$$

where ρ is the density of the fluid (e.g., water) and c is the speed of sound in fluid (1500 m s^{-1} in water). The acoustic power (W) represents the intensity emitted by a given surface. The term ρc represents the acoustic impedance (Z) of the medium. Values of Z for air, water, benzene and ethanol are 400, 1.5×10^6, 1.1×10^6, and 0.95×10^6, kg $m^{-2}s^{-1}$, respectively (Luche, 1998).

3.2.2.5. Physicochemical Properties of the Pollutant

The physicochemical properties of the contaminating species, such as vapor pressure (or Henry's constant), solubility and octanol-water partition coefficient can have dramatic effects on the cavitational collapse.

Hydrophobic chemicals with high vapor pressures have a strong tendency to diffuse into the gaseous bubble interior, so that the most effective reaction site for their destruction is the bubble-liquid interface and/or the gaseous bubble itself (Kontronarou, *et al.*, 1991; Drijivers *et al.*, 1999). Hence, irradiation of aqueous solutions contaminated with volatile pollutants by power ultrasound at 20-100 kHz (whereby long-lived "stable" cavities are generated) is a very effective decontamination method, owing to its potential to render pyrolytic destruction of the solutes in the gas and gas-liquid phase (Ince *et al.*, 2001; Kontronarou, *et al.*, 1991).

In contrast, hydrophilic compounds with low vapor pressures and low concentrations tend to remain in the bulk liquid during irradiation, due to the repulsive forces exerted to-and-from the slightly hydrophobic bubble surfaces. The major reaction site for these chemicals, therefore, is the liquid medium, where they may be destroyed by oxidative degradation, provided that sufficient quantities of hydroxyl radicals are ejected into the solution during cavitational collapse. As pointed out previously, maximum radical transfer into the bulk medium occurs when the collapse is "transient", or when sonication is carried out via medium frequency ultrasound waves (Ince *et al.*, 2001; Drijvers *et al.*, 1999). Thermal decomposition of non-volatile solutes is also possible at the interfacial bubble sheath, at which solutes may accumulate via adsorptive processes during the formation and growth of acoustic cavities, but is not as effective as hydroxylation in the bulk medium.

3.2.2.6. Physicochemical Properties of the Solute

Cavities are more readily formed when using solvents with high vapor pressure, low viscosity, and low surface tension; however, the intensity of cavitation is benefited by using solvents of opposite characteristics. The intermolecular forces in the liquid must be overcome in order to form the bubbles. Thus, solvents with high densities, surface tensions, and viscosities generally have higher threshold for cavitation but more harsh conditions once cavitation begins (Young, 1989).

3.2.2.7. Dissolved Gases

Dissolved gas bubbles serve as nuclei for cavitation. However, since the first effect of cavitation is degassing, the solution will rapidly be free of dissolved gases if gas introduction is ceased during sonication (Mason, 1999). Therefore, the liquid is bubbled continuously with a gas throughout the sonication to maintain a constant gas flow into the bubbles so as to sustain the "extreme" conditions of collapse (Ince *et al.*, 2001).

The selection of the gas is also of significance, because the final temperature of a collapsing bubble is closely related to specific heat (heat released upon gas compression), thermal conductivity (heat dissipation to the surrounding environment), and the solubility of the sparge gas. The higher the heat capacity ratio (C_p/C_v) or polytrophic ratio (γ) of the gas in the bubble, the higher the final temperature produced in an adiabatic compression, and the cause of reaction (Hua and Hoffmann, 1997). Assuming adiabatic bubble collapse, the maximum temperatures and pressures within the collapsed cavitation bubbles are predicted by Noltingk and Neppriás from approximate solutions of Rayleigh-Plesset equations as follows (Noltingk and Neppiras, 1950; Neppiras, 1980):

$$T_{max} = T_0 \left[\frac{P_a(\gamma - 1)}{P_v} \right] \tag{3.11}$$

$$P_{max} = P_v \left\{ \frac{P_a(\gamma - 1)}{P_v} \right\}^{\left[\gamma/\gamma-1\right]} \tag{3.12}$$

where T_0 = ambient (experimental) temperature in the bulk, P_v = pressure in the bubble at its maximum size or the vapor pressure of the solution, P_a = pressure in the bubble at the moment of transient collapse (acoustic pressure), γ = polytropic index. As can be seen from these equations, higher temperatures and pressures are generated with monatomic gases with higher γ than those with polyatomic gases with lower γ (Riesz *et al.*, 1990). Another parameter that affects cavitational collapse is the thermal conductivity of the gas. Although compression is adiabatic in the sonochemical process, still small amounts of heat are transferred to the bulk liquid. A gas with low thermal conductivity reduces heat dissipation

from cavitation site following adiabatic collapse and should favor higher collapse temperature. Thermal conductivity of rare gases decreases in the order: Xe < Kr < Ar < Ne < He. Despite the equal γ ratios of Ar and Helium, much higher yields of pyrolysis products were detected with Ar by Colarusso and Serpone (1996), as attributed to its 10-fold lower thermal conductivity. Gas solubility is also an important aspect, the more soluble the gas, the more likely it is to diffuse into the cavitation bubble. Hence, larger number of cavitation nuclei will form and will lead to an extensive bubble collapse (Kontronarou *et al.*, 1991). The reactions that occur and the radicals that can be formed upon bubble under sparge gases Ar and O_2 can be found in Section 3.2.1.

3.2.2.8. Addition of Solids

The addition of solid catalysts, such as glass beads, ceramic disks, SiO_2, Al_2O_3 and talc into the reaction medium is another common method for enhancing cavitation effects. Furthermore, the presence of such material is reported to be especially useful for micronization of species (in ultrasonic cell disruption), and for the abrasion, activation and alteration of the chemical properties of catalyst surfaces during ultrasonic irradiation of liquid media (Serpone *et al.*, 1994).

3.2.3. Applications in Environmental Remediation

The use of sonochemical technologies in environmental remediation practices render pollutant destruction either directly via activating thermal decomposition reactions, or indirectly by increasing the hydroxyl radical yield in advanced oxidation treatment processes. Many of such studies are focused on parametric and kinetic analyses of contaminant degradations, and comparison of reaction efficiencies with those conducted in the absence of ultrasound. The input concentrations in almost all of the published work are low (in the order of 10^{-6} to 10^{-3} moles per liter), as typical of refractory organics found in industrial effluents. The chemicals studied range from phenol and its (nitro-, chloro-) derivatives to benzene, toluene, chlorinated solvents, herbicides, substituted ethers, natural organic matter, surfactants, textile dyestuff and chlorofluorocarbons. A brief summary of some of the reported work is given below (Ince *et al.*, 2001).

Destruction of phenol by sonolysis at low and high frequency irradiation has shown that reactions are much faster at high frequency (487 kHz), the pathway being advanced oxidation, as verified by the presence of oxidation intermediates such as hydroquinone, cathecol and benzoquinone, and the lack of pyrolysis products such as acetylene and methane (Pétrier *et al.*, 1992). In another study by Drijvers *et al.*, (1999) the decomposition of phenol and trichloroethylene (TCE) was investigated under the combined effect of sonolysis (at 520 kHz) and chemical oxidation with hydrogen peroxide, using solid catalysts such as Al_2O_3, ZnO, Ni_2O_3 and CuO. The authors reported that while TCE degradation was not at all effected by the addition of H_2O_2 and solid catalysts, the degradation of phenol was largely enhanced by the presence of H_2O_2/CuO. They attributed this different behavior to the difference in the hydrophobicity of the two compounds.

A study involving the sonochemical decomposition of p-Nitrophenol (p-NP) in the presence and absence of strong scavengers of hydroxyl radicals such as humic acid has shown that the rate of degradation was not significantly affected by the concentration of hydroxyl scavengers below a threshold value (Cost *et al.*, 1993). This suggested that pyrolysis is the main reaction channel for the sonochemical decay of this compound. The result was consistent with previous work showing that p-NP decays via first-order reaction kinetics near the hot interface of cavity bubbles due to its thermal instability at temperatures over 160°C (Kontronarou *et al.*, 1991). The reported decrease in the rate of degradation upon increased concentrations of phosphate and bicarbonate ions in this study has under laid the pH sensitivity of the reactions. It was claimed that at pH values higher than pKa of p-NP, the molecule becomes negatively charged and is repulsed by bubble surfaces, thus being displaced away from the interfacial region where the main •OH decomposition reactions are expected to occur (Kontronarou *et al.*, 1991).

Serpone *et al.*, (1994) have studied the kinetics of 2-, 3-, and 4-Chlorophenol decomposition in air equilibrated media by low frequency ultrasound irradiation. They reported that reaction products and kinetics were parallel to those observed in heterocatalytic oxidation of these compounds with semiconductor particles.

Sonochemical treatment of wastewaters contaminated with benzene and toluene in a "parallel plate near field acoustic processor" was shown by Thoma *et al.* (1998) to be

highly effective for the destruction of both compounds within reasonable energy requirements. The authors further found that the degradation of parent molecules followed first order reaction kinetics, and the rate constants in each case were inversely proportional to the initial concentration of the compound.

Pétrier *et al.*, (1992) have studied the degradation of pentachlorophenate in argon, air and oxygen saturated aqueous solutions under 20 and 530 kHz ultrasonic irradiation. They reported that the process was more effective at the higher frequency, and the degradation was faster when the solution was bubbled with argon than when it was bubbled either with O_2 or air.

Kang and Hoffmann (1998) have studied the kinetics and mechanism of sonolytic destruction of Methyl tert-Butyl Ether (MTBE) under the effect of ozone gas and ultrasonic irradiation at 205 kHz. They reported that ozone accelerates the first order degradation rate of MTBE by sonolysis at decreasing initial concentrations of the compound. They have also observed that the presence of carbonate and bicarbonate ions in solution as potential competitive reagents for hydroxyl radicals did not lower the rate of MTBE degradation, concluding that the degradation occurred at the interface of the cavitation bubble, not in the liquid bulk.

David *et al.*, (1998) have shown that the systematic herbicides chlorpropham and 3-chloroaniline can be destroyed more effectively at 482 kHz than at 20 kHz. Chemical analyses of effluent samples have shown that while the mechanism of destruction for chlorpropham was pyrolytic decomposition inside the gaseous bubble, 3-chloroaniline was destroyed mainly by radical mechanisms and oxidative degradation in the solution bulk.

The degradation of fulvic acid (as a representative of natural organic matter) under the combined effect of ultrasonic irradiation at low frequency and ozonolysis was studied by monitoring the time rate of change in total organic carbon content of the solution during contact (Olson and Barbier, 1994). The combination was reported to provide a significant advantage as total mineralization of organic carbon, which could be achieved neither by ozone nor ultrasound alone. It was concluded that the ultrasound/ozone process extends the

application of sonochemical techniques to the catalysis of advanced oxidation processes for the removal of refractory organic electrolytes in natural water.

Alegria *et al.*, (1989) have studied the mechanism and site of degradation of some selected non-volatile surfactants by ultrasonic irradiation at 50 kHz, using argon as the saturating gas. They reported that surfactants orient themselves radially in the interfacial region, with their polar head groups pointing to the bulk solution. This was verified by the detection of pyrolysis products and high rate of hydrogen peroxide uptake in the solution during irradiation.

Cheung and Kurup (1994) have studied the sonochemical destruction of two chlorofluorocarbons, CFC11 and CFC113 in dilute aqueous solutions under the effect of power ultrasound at 20 kHz. They observed that the reactions were governed by first order kinetics, and the observed rate constants for both compounds were found to decline slightly with an increase in solution temperature from 5 to 10°C. The result being in agreement with temperature effects observed with other chlorinated hydrocarbons (Bhatnagar and Cheung, 1994) was attributed to the decrease in the cavitation intensity with an increase in solvent vapor pressure. The authors further reported that the rapid rate of degradation was not affected by the very slight degree of parent compound volatilization (5%) during the experiments.

Gonze *et al.*, (1990) have studied the effect of ultrasonic irradiation (500 kHz) as a pre-treatment operation to reduce the toxicity of untreated effluents or to increase their biodegradability prior to secondary treatment. Experiments were carried out with synthetic effluents contaminated with sodium pentachlorophenate, and acute toxicity tests were conducted using *Vibrio fischeri* and *Daphnia magna* as test organisms. The authors reported that ultrasound is a highly effective pretreatment method, owing to its potential for toxicity reduction and rapid enhancement of the biodegradability of the solution. Finally, there is supportive evidence that power ultrasound provides ultimate bacterial destruction in infected waters, and the rate of the process increases with solids addition into the reaction medium (Ince and Belen, 2001).

CHAPTER 4. EXPERIMENTAL SYSTEM CONFIGURATIONS AND SELECTION OF SYSTEM PARAMETERS

4.1. Determination of the Ultrasonic Power in a Reaction Medium

In sonochemical systems, optimization of input power and the reactor configuration is the most important strategy to achieve maximum reaction yields. An ultrasonic system transforms electrical power into vibrational energy, i.e. mechanical energy, which is then transmitted into the sonicated reaction medium. Part of it is lost to produce heat, and another part produces cavitation, but not all of the cavitational energy produces chemical and physical effects. Some energy is reflected and some is consumed in sound re-emission (Mason, 1999). Hence, there can be significant differences between the power supplied from the generator and that delivered into the reactor. In a pure liquid, one might assume that almost all the mechanical energy (acoustic energy) is transformed to heat by absorption. Of the methods available to measure the amount of ultrasonic power entering a sonochemical reaction medium, the most common and easiest is calorimetry, which involves a measurement of the initial rate of heating produced when a system is irradiated by ultrasound (Mason, 1999). The method involves the measurement of the temperature rise T against time t for about 30 seconds, using a thermocouple placed in the reaction vessel. From T versus t data, the temperature rise at zero time, dT/dt, can be estimated either by curve-fitting the data to a polynomial in t, or by constructing a tangent to the curve at time zero. The ultrasonic power (P) actually entering the system can then be calculated by substituting the value of dT/dt into Equation 4.1. (Mason, 1999; Mason and Cordemans, 1998; Mason *et al.*, 1992):

$$\text{Power} = (dT/dt).C_p.M \qquad (4.1)$$

where C_p= heat capacity of water (~4.1840-4.1790 J $g^{-1}.°C^{-1}$), (dT/dt)= the temperature rise at zero time, and M= total mass of water in the reaction vessel (g).

After calculating the power in the reaction medium, the efficiency of the system can be determined either by calculating the ultrasonic intensity which is equal to total

(determined) power per unit emitting area (W cm^{-2}), or by ultrasonic density (W mL^{-1}), i.e. total power per total mass of the solvent (water) in the reactor.

In general, the generator power should not automatically be turned to a maximum, because a relatively small amount of energy is often sufficient. In most cases, the increase in power leads to the creation of more bubbles in the bulk liquid, which lowers the effective reaction yield by absorbing the acoustic energy. Decoupling can also result from a reduction of the area of the emitter surface due to the greater number of bubbles.

4.2. Identification and Optimization of Experimental Systems and System Parameters

Three experimental systems were used in this study; namely SYSTEM I, SYSTEM II, and SYSTEM III, which are defined in Sections 4.2.1, 4.2.2, and 4.2.3., individually. The following parameters were determined and fixed for each experimental system:

i) *Reaction Volume*: Calorimetry was performed at various solution volumes to select the optimum volume.

ii) *Optimum Power*: Optimum power setting was determined by dye decolorization kinetic study. Pre-aerated solutions of 20 mg L^{-1} C.I. Acid Orange 7 was used for kinetic studies. Rates of dye decolorization were estimated at various power settings to select the optimum power.

iii) *Injected Gas Type and Flow Rate*: The selection of injected gas and flow rate was based on dye decolorization kinetic studies at various gas flow rates.

4.2.1. System I (300 kHz / 150 mL Reactor)

The reactor is made of a 150 mL glass cell surrounded by a water-cooling jacket to keep its contents at constant temperature (20±0.5 °C); a plate type piezoelectric transducer emitting ultrasonic waves at 300 kHz, and a 25 W generator to convert electrical power

input into mechanical energy (Undatim Ultrasonics, Belgium). The active acoustical vibrational area of the transducer is 22 cm^2. A photograph of the system is given below:

Figure 4.1. Photographic view of SYSTEM I: 300 kHz-150 mL reactor.

i) Reaction Volume

The study of volume optimization covered the examination of power/volume ratios and estimation of the power density by calorimetry in tap water. The optimum volume was selected by estimating the power density at various power outputs of the generator and at constant solution volume. The measurements were repeated at three distinct volumes, namely 100, 125, and 150 mL of tap water. No cooling and gas injection was applied during these experiments, and the temperature rise (T) at every 30 seconds was recorded using an Ikamag RCT Basic thermocouple during 5 minutes. The rate of temperature increase (dT/dt) was estimated by fitting the data to a polynomial in t.

The ultrasonic power entering the system was then calculated by substituting the value of dT/dt into Equation 4.1., where M was 100, 125, and 150 g, respectively. Since heat capacity of water is related to temperature, the average of C_p values between t=0 and t=10 min irradiation were substituted in Equation (4.1) (Weast and Astle, 1983). Power

densities in 100, 125 and 150 mL of tap water were calculated by dividing P by 100, 125 and 150, respectively. The results of the study are presented in Table 4.2.

Sample calculation for generator P = 25 W, and V= 100 ml is as follows:

The temperature rise (T) against time (t) for 30 seconds was recorded during 5 minutes sonication of 100 ml of tap water, and the data are given in Table 4.1.

Table 4.1. Temperature rise in 100 mL tap water during sonication at 25 W generator output in System I

t (min)	0	0.5	1	1.5	2	2.5	3	3.5	4	4.5	5
T (°C)	16	17.6	18.7	20	21	22.1	23	24	24.9	25.7	26.7

From T versus t data plotted in Figure 4.2., the temperature rise at zero time, (dT/dt), was estimated by curve-fitting the data to a polynomial in t.

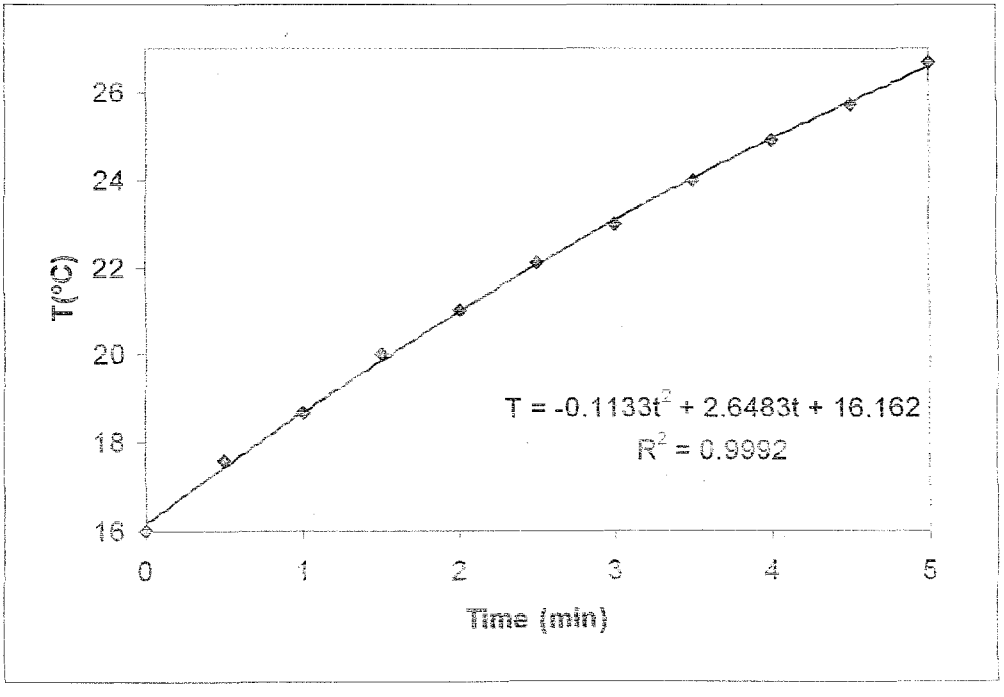

Figure 4.2. Temperature rise during sonication at 25 W power output (tap water volume 100 mL, System I).

The ultrasonic power (P) actually entering the system was calculated by substituting the value of dT/dt into Equation 4.1, using :

C_p = 4.182 J g^{-1} $°C^{-1}$ (average of the heat capacity of water in between 16 – 27 °C) (Weast and Astle, 1983), M = 100 g, dT/dt= (2.6483/60) = 0.044 °C sec^{-1}

Thus, Power = 0.044 (°C sec^{-1}) × 4.182 (J g^{-1} $°C^{-1}$) × 100 (g) = 18.44 W

Power Density is calculated as 0.184 W mL^{-1} (18.44 W / 100 mL),

Ultrasonic Intensity is calculated as 0.836 W cm^{-2} (18.44 W / 22cm^2).

Table 4.2. Calorimetric measurements of power input and power densities at various generator outputs and reaction volumes in System I

Generator Power (W)	V (100 mL)		V (125 mL)		V (150 mL)	
	Power Input (W)	Power Density (WmL^{-1})	Power Input (W)	Power Density (WmL^{-1})	Power Input (W)	Power Density (WmL^{-1})
5.0	1	0.010	-	-	2	0.011
10.0	7	0.070	4	0.034	4	0.027
15.0	9	0.087	7	0.056	6	0.040
17.5	12	0.115	-	-	-	-
20.0	12	0.115	13	0.104	11	0.071
22.5	14	0.136	-	-	-	-
25.0	18	0.184	14	0.118	12	0.078

It is observed that for any given generator power, the power density diminished as the volume of the reaction mixture was increased. Therefore, the volume of the solution should be considered in optimizing the power dissipated into the system. Consequently, because the reaction volume is an important parameter, the power in solution must be preferably reported in terms of total power per unit volume.

Literature points out that in most cases, too much power reduces the sonochemical activity (Lorimer and Mason, 1987), but it was found that the power density for test volumes was enhanced by increases in the electrical output of the generator. These results can point out the lack of decoupling effect and the lack of excess bubbles, which might act as barriers to the transfer of acoustic energy.

As a result, the optimum value of liquid volume was selected as 100 mL at which the power density was a maximum at a generator power of 25 W.

ii) Optimum Power

100 mL of pre-aerated solutions of 20 mg L^{-1} C.I. Acid Orange7 (AO7) were irradiated at various generator powers for 1 h to monitor decolorization by absorption abatements at the UV_{484} band. The degradation of color was found to follow pseudo-first order kinetics with respect to the absorption maximum of the dye in the visible band as:

$$\frac{dA}{dt} = -kA \qquad (4.2)$$

where A is the maximum absorbance of the solution in the visible band at time t and k is the pseudo-first order absorbance decay coefficient (min^{-1}).The relation between k (min^{-1}) and generator power (W) and the results of calorimetry are illustrated in Figure 4.3.

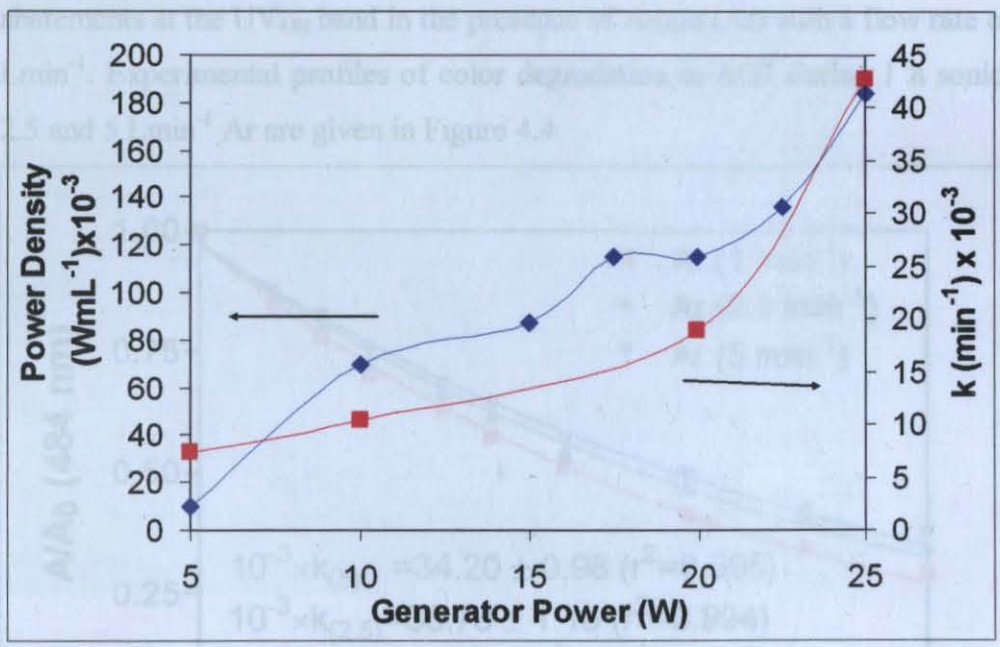

Figure 4.3. Power density in tap water at various power outputs and profiles of color degradation rate constants in 20 mg L^{-1} AO7 (volume =100 mL, System I).

The rate of color decay was accelerated by increases in the electrical power output of the generator, and a similar trend was observed for power density-generator power data. The sonicated volume for each experiment was 100 mL and the maximum power dissipation into the solution was 0.184 WmL^{-1} at a power output of 25 W.

iii) Injected Gas Type and Flow Rate

If the main cause of sonochemical effect is cavitational collapse, then sonochemical efficiency must be linked directly to the generation of cavitation bubbles in the chemical reaction. For reproducible results, gas is bubbled to generate large numbers of nucleation sites for cavitation and provide bubbles of uniform energy of collapse. Most effective gases for such processes are the monoatomic gases such as Argon (Ar), diatomics such as oxygen next (Mason, 1999). As discussed in Section 3.2.2.7., the highest specific heat of the gases gives the greatest cavitational effects. Therefore, after the correct choice of generator power output via calorimetric method, the next step of the optimization of the sonochemical system should be cavitation enhancement by appropriate gas introduction.

100 mL of pre-aerated solutions of 20 mg L^{-1} C.I. Acid Orange7 (AO7) were irradiated at 0.184 W mL^{-1} (optimum power density) for 1 h to monitor absorption abatements at the UV_{484} band in the presence of Argon (Ar) with a flow rate of 1, 2.5 and 5 $Lmin^{-1}$. Experimental profiles of color degradation in AO7 during 1 h sonication with 1, 2.5 and 5 $Lmin^{-1}$ Ar are given in Figure 4.4.

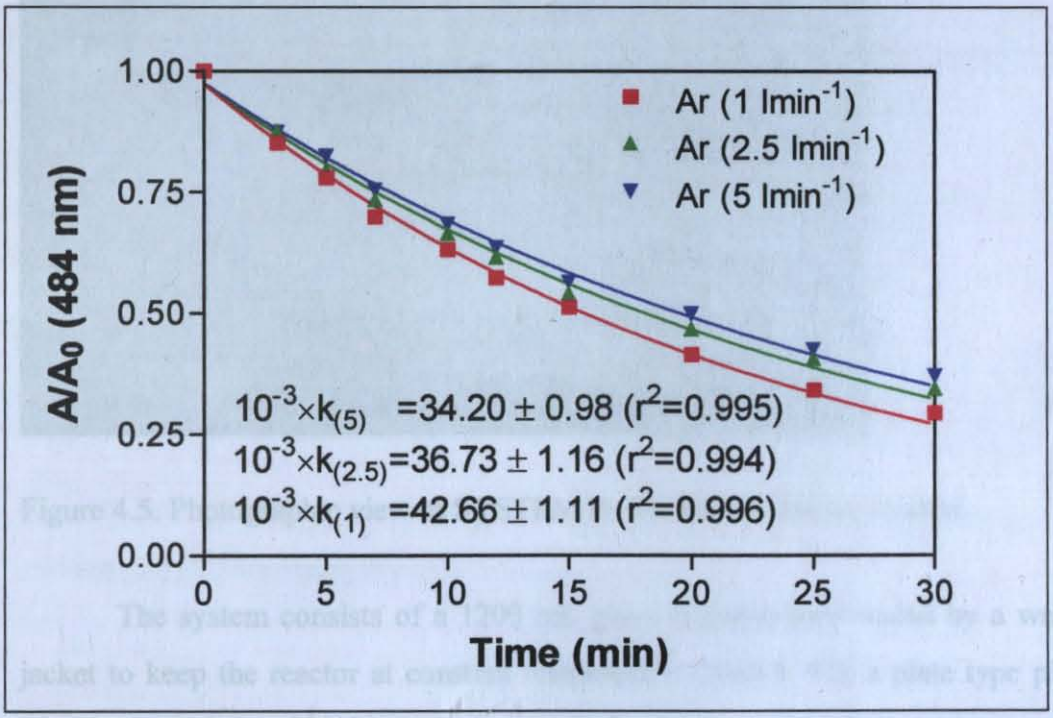

Figure 4.4. Experimental profiles of color degradation in AO7 during 1 h sonication with various gas sparge ratios in System I (Subscripts 1, 2.5, and 5 refer to Ar flow rates, $Lmin^{-1}$).

The highest rate of color degradation was observed during Ar injection at 1 L min^{-1}, and the rate decreased with higher flow rates. Although sonication of the solution in the presence of Ar provides maximum decolorization rate, high gas content in the medium reduces the power of the collapse. As a result, Ar flow rate was selected as 1 L min^{-1} for the rest of the studies with System I.

4.2.2. System II (520 kHz / 1200 mLReactor)

The design and dimensioning of the ultrasonic reactor was made after preliminary studies and long-time collaboration with ultrasound (US) equipment and system manufacturers. A photograph of the system is given below:

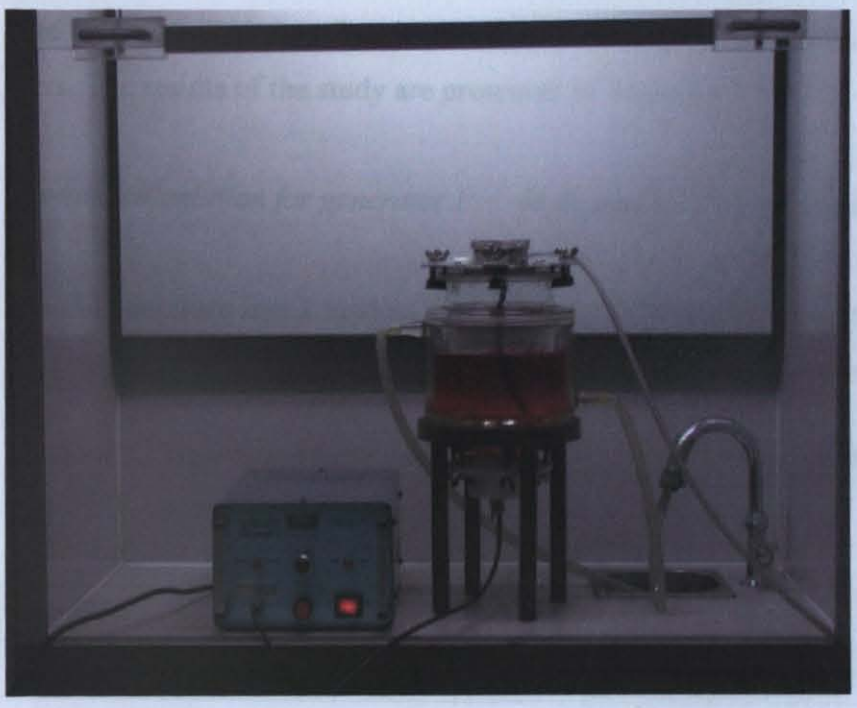

Figure 4.5. Photographic view of SYSTEM II: 520 kHz-1200 mL reactor.

The system consists of a 1200 mL glass chamber surrounded by a water cooling jacket to keep the reactor at constant temperature (20±0.5 °C); a plate type piezoelectric transducer emitting 520 kHz of ultrasound frequency, a stainless steel top cover, and a generator operating at 100 W to convert electrical power input to mechanical energy (Undatim Ultrasonics, Belgium). The generator can operate either at 25 W for 300 kHz

frequency studies or at 100 W for 520 kHz ultrasonic frequency studies by a switch in front of it. The active acoustical vibrational area of the transducer is 22 cm^2.

i) Reaction Volume

As described in Section 4.2.1., the power density in solution was measured calorimetrically by estimating the power density at various power outputs of the generator and at constant solution volume. The measurements were performed at four different volumes, namely 300, 600, 900 and 1200 mL of tap water. No cooling and gas injection was applied during these experiments. The temperature rise (T) at every 30 seconds was recorded during 5 minutes, and the rate of temperature increase dT/dt was estimated by fitting the data to a polynomial in t. The power in the system was calculated by substituting the value of dT/dt into Equation 4.1., where M were 300, 600, 900 and 1200 g for each sets. The results of the study are presented in Table 4.4.

Sample calculation for generator P = 40 W, and V= 300 mL is as follows:

The temperature rise T against time t for about 30 seconds was recorded during 5 minutes sonication of 300 mL of tap water, and the data are given in Table 4.3.

Table 4.3. Temperature rise in 300 mL of tap water in System II during sonication at 100 W generator output

t (min)	0	0.5	1	1.5	2	2.5	3	3.5	4	4.5	5
T (°C)	26.6	27.6	28.4	29.1	30.0	31.0	31.7	32.5	33.3	33.8	34.7

From T versus t data plotted in Figure 4.6., the temperature rise at zero time, (dT/dt), was estimated by curve-fitting the data to a polynomial in t.

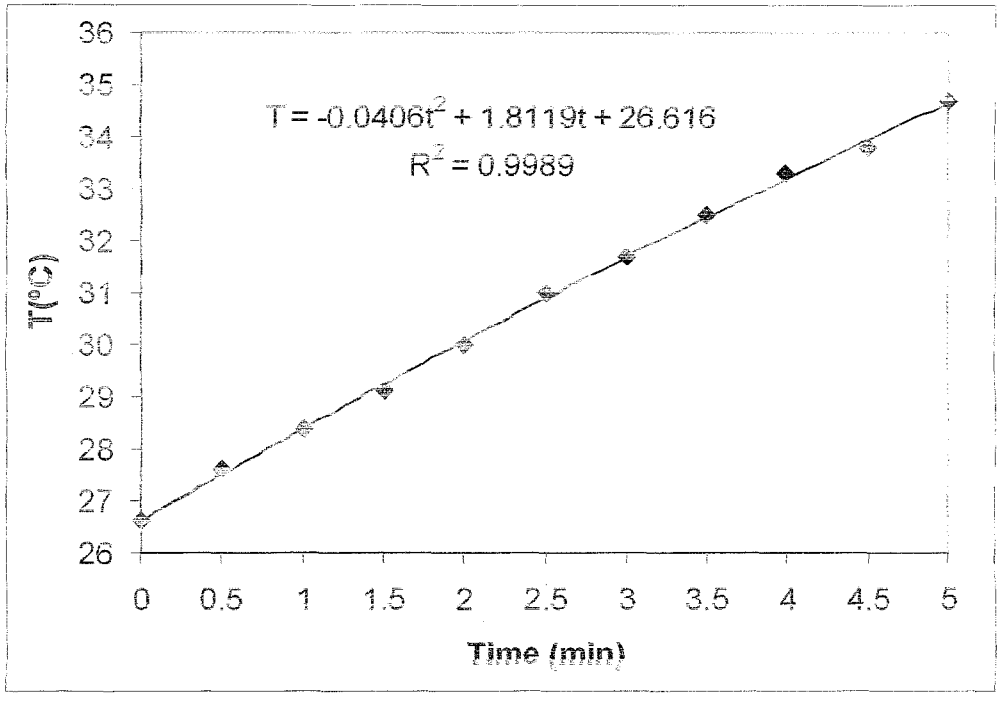

Figure 4.6. Temperature rise during sonication at 100 W power output (tap water volume in System II=300 mL).

The power input is calculated by substituting the value of dT/dt into Equation (4.1), using :

C_p = 4.179 J g^{-1} $°C^{-1}$ (average of the heat capacity of water in between 26 – 35 °C) (Weast and Astle, 1983).

M = 300 g,

dT/dt= (1.8119/60) = 0.030 °C sec^{-1}

Thus, Power = 0.030 (°C sec^{-1}) × 4.179 (J g^{-1} $°C^{-1}$) × 300 (g) = 37.95 W

Table 4.4. Calorimetric measurements of power input and power densities at various generator outputs and reaction volumes in System II

Generator Power (W)	V= 300 mL		V= 600 mL		V= 900 mL		V= 1200 mL	
	Power Input (W)	Power Density (WmL^{-1})	Power Input (W)	Power Density (WmL^{-1})	Power Input (W)	Power Density (WmL^{-1})	Power Input (W)	Power Density (WmL^{-1})
10	23.13	0.077	-	-	-	-	-	-
20	31.44	0.105	-	-	28.220	0.031	39.100	0.028
30	31.74	0.106	-	-	-	-	-	-
40	37.95	0.126	35.86	0.060	32.460	0.036	36.610	0.026
50	27.39	0.091	-	-	-	-	-	-
60	25.08	0.084	29.56	0.049	31.260	0.035	35.490	0.025
70	23.94	0.080	-	-	-	-	-	-
80	21.12	0.070	-	-	26.850	0.030	34.140	0.024
100	20.73	0.069	17.53	0.029	-	-	-	-

The maximum power density was obtained when the solution volume was 300 mL. It was found that the power dissipation increased in the electrical power output of the generator within 10-40 W, but decreased as the power was further increased. For the studied generator outputs, the power density diminished as the volume of the tap water was increased. The increase in acoustic power increases the maximum radius of the cavity bubble, as well as increases its time of collapse (Luche, 1998). When too much power is applied to the solution, excess number of bubbles can be formed, and then they coalesce forming larger and more longer lived bubbles and act as a barrier to the transfer of acoustic energy through the liquid. Decoupling effect can be the other reason for the loss in efficiency of transfer of power from the source to the medium by the formation of large numbers of cavitation bubbles at or near the emitting surface of the transducer (Mason, 1999).

As a result, the power density reduced as the volume of water was increased. The working solution volume for each set of experiments was selected as 300 mL at 40 W generator output.

ii) Optimum Power

300 mL of pre-aerated dye solutions of 20 mg L^{-1} C.I. Acid Orange7 (AO7) were irradiated at various generator outputs for 1 h to monitor absorption abatements at the UV_{484} band. It was found that the pseudo-first order color decay rate was accelerated by increases in the electrical power output of the generator within 10-40 W, but decelerated as the power was further increased. Thus, it is very important to drive a sonochemical reaction in an optimum power in order to avoid unnecessary supply of energy. Variations in the estimated values of k at 10, 20, 40, 60, 80 and 100 W applications of electrical power to 300 mL dye solutions is presented in Figure 4.7.

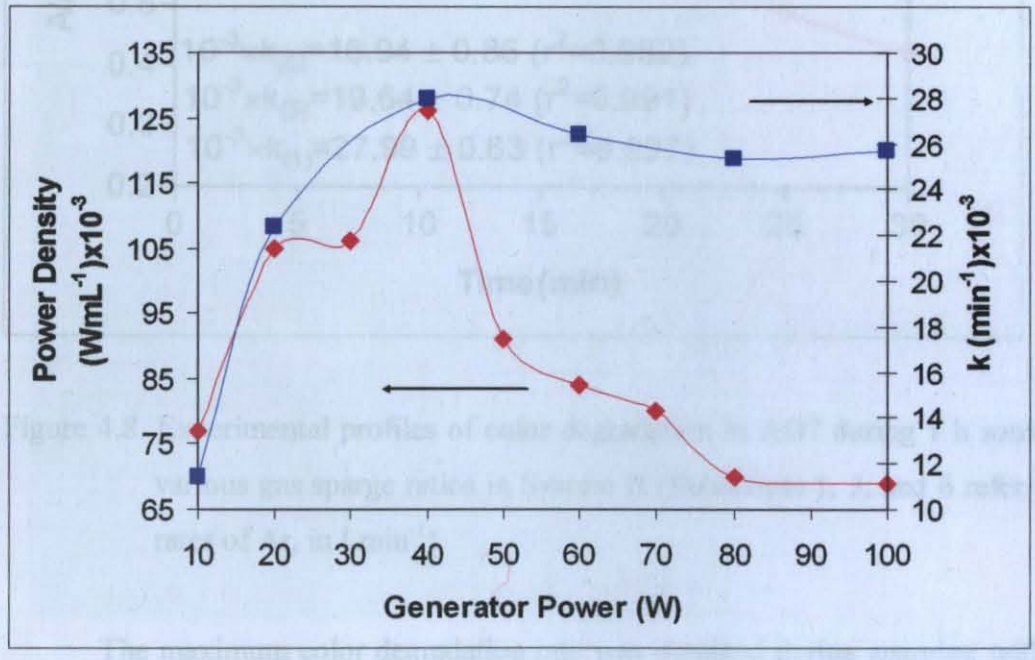

Figure 4.7. Calorimetric measurements of power density and profiles of color decay in 20 mgL^{-1} AO7 at various power outputs in System II (V= 300 mL).

Maximum degradation of color was shown to occur at a generator output of 40 W, at which the power dissipated into the solution was 0.126 W mL^{-1}.

iii) Injected Gas Type and Flow rate

300 mL of pre-aerated dye solutions of 20 mg L^{-1} AO7 were irradiated at 0.126 W m L^{-1} (optimum power density) for 1 h to monitor absorption decay at the UV_{484} band in

the presence of Argon (Ar) with a flow rate of 1, 3 and 6 l min^{-1}. Pseudo-first order color degradation rates for AO7 in 1 h sonication with various Ar flow rates are given in Figure 4.8.

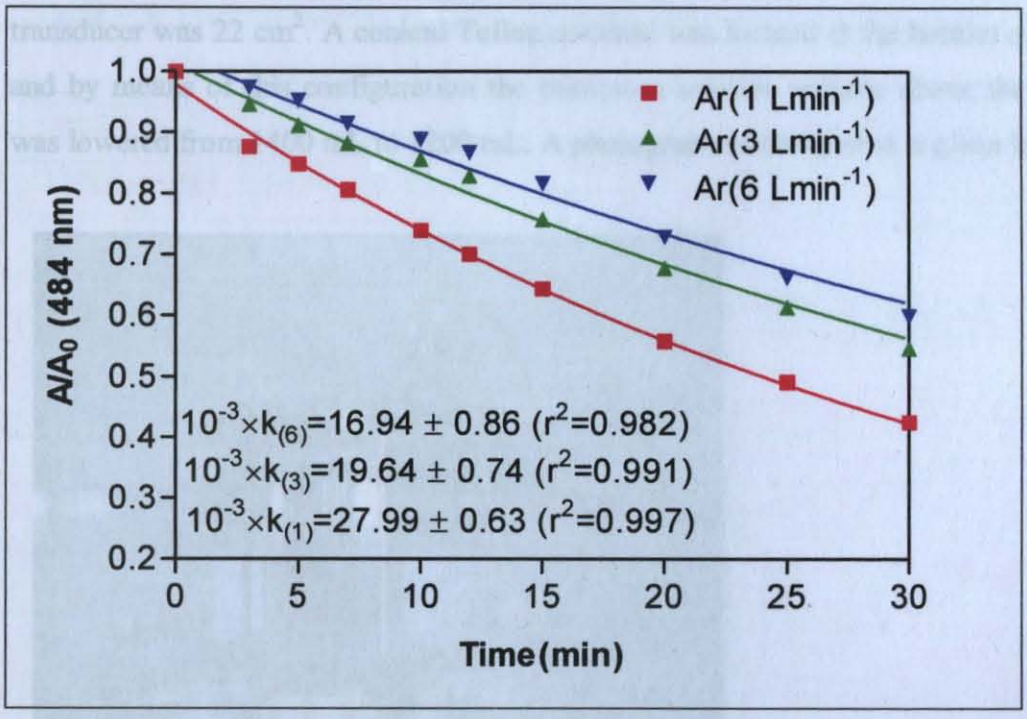

Figure 4.8. Experimental profiles of color degradation in AO7 during 1 h sonication with various gas sparge ratios in System II (Subscripts 1, 3, and 6 refer to the flow rates of Ar, in $Lmin^{-1}$).

The maximum color degradation rate was obtained during sparging with 1 L min^{-1} Ar, and decreased with further increase in flow rates. Ar flow rate was selected as 1 L min^{-1} for each set of experiments conducted using the System II.

4.2.3. System III (3 x 520 kHz / 2000 mL Reactor)

The system consists of a 2 L stainless-steel hexagonal reactor and a generator operating at 600 W (maximum) (Undatim Ultrasonics, Belgium). Three piezoelectric transducers each emitting at 520 kHz frequency are mounted on the lateral walls of the reactor. Quartz windows are located on the other three walls, in which UV lamps (253.7 nm, Philips, PL-L 18W TUV) are mounted in front of each quartz panels outside the

reactor. Each of the UV light sources consists of two UV lamps and cooled by air circulation. The temperature is kept constant at 25 ± 1°C by water running through the stainless-steel pipe located inside the reactor. Four ports are located on the reactor cover for gas bubbling, sampling and gas outlet. The active acoustical vibrational area of each transducer was 22 cm^2. A conical Teflon material was located at the bottom of the reactor and by means of this configuration the minimum solution volume above the transducers was lowered from 1400 mL to 1200 mL. A photograph of the system is given below:

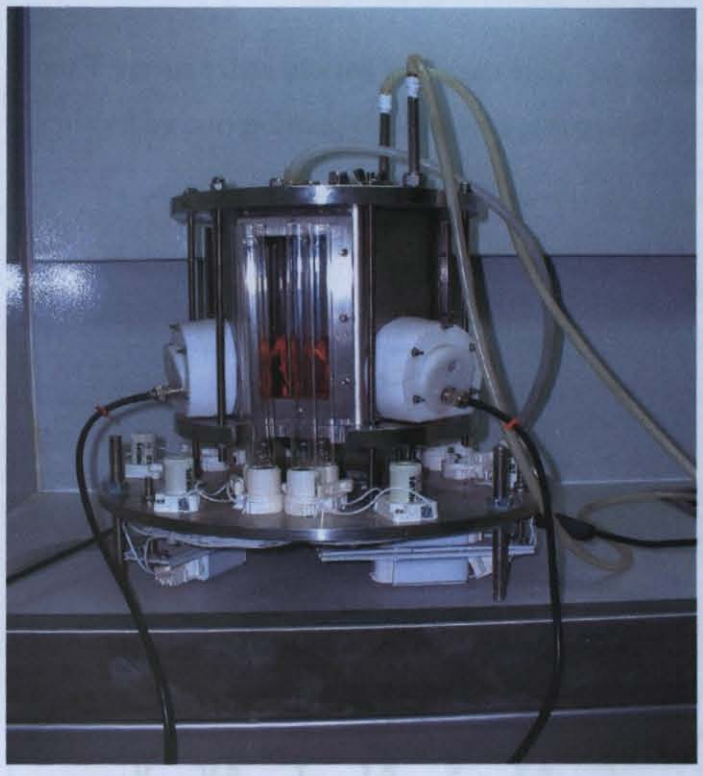

Figure 4.9. Photographic view of SYSTEM III: 3 x 520 kHz-2000 mL reactor.

i) Reaction Volume

Calorimetric tests were performed at various power settings during 5 min sonication of 1200 and 1600 mL of tap water. The minimum water level above the transducers was 1200 mL, therefore calorimetric and kinetic tests could not be performed in lower solution volumes. The power input was calculated from the change in temperature, and the results of calorimetry are presented in Table 4.6.

Sample calculation for generator P = 390 W, and V= 1200 mL is as follows:

The increase in temperature T against time t for 30 seconds was recorded during 5 minutes ultrasonic irradiation of 1200 mL of tap water, and the data are given in Table 4.5.

Table 4.5. Temperature rise in 1200 mL of tap water in System III during sonication at 390 W generator output

t (min)	0	0.5	1	1.5	2	2.5	3	3.5	4	4.5	5
T (°C)	19.1	19.9	20.4	20.9	21.2	21.5	21.9	22.5	22.8	23.0	23.4

From T versus t data plotted in Figure 4.10., the temperature rise at zero time, (dT/dt), was calculated by curve-fitting the data to a polynomial in t.

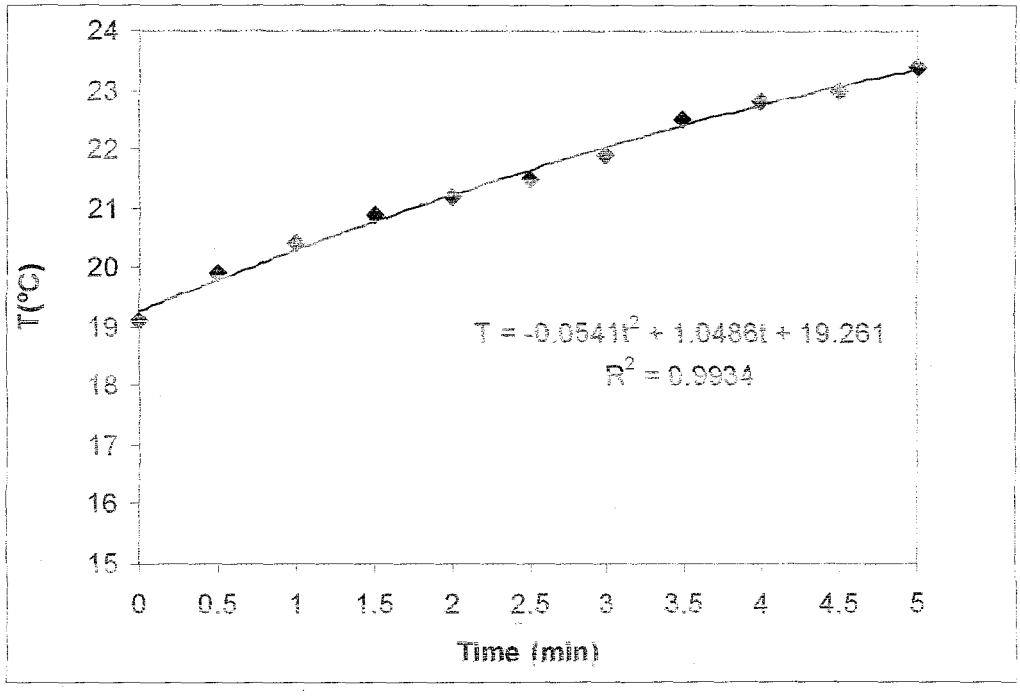

Figure 4.10. Temperature rise during ultrasonic irradiation at 390 W generator output (tap water volume in System III =1200 mL).

The power input is calculated by substituting the value of dT/dt into Equation 4.1. using :

C_p = 4.178 J g^{-1} $°C^{-1}$(average of the heat capacity of water in between 19 – 23 °C) (Weast and Astle, 1983).

M = 1200 g,

dT/dt= (1.0486/60) = 0.0174 °C sec^{-1}

Thus, Power = 0.0174 (°C sec^{-1}) × 4.178 (J g^{-1} °C^{-1}) × 1200 (g) = 87 W and the corresponding power density value is 0.073 (87/1200) W mL^{-1}.

Table 4.6. Calorimetric measurements of power densities at various generator output and reaction volumes in System III

Generator Power (W)	V = 1200 mL		Generator Power (W)	V = 1600 mL	
	Power Input (W)	Power Density (WmL^{-1})		Power Input (W)	Power Density (WmL^{-1})
240	60	0.050	240	55	0.034
300	67	0.056	260	61	0.038
320	78	0.065	320	99	0.062
340	74	0.062	360	82	0.051
350	76	0.063	370	64	0.040
360	80	0.067	390	90	0.056
370	79	0.066	420	88	0.055
390	87	0.073	450	70	0.044
400	91	0.076			
450	110	0.092			

The power density decreased with increasing volume of the tap water, optimum solution volume was selected as 1200 mL.

ii) Optimum Power

The optimum power to be applied was based on the rate of bleaching (by plotting rate vs. applied power). 1200 mL of 20 mg L^{-1} AO7 solution was irradiated at various power settings. The relation between pseudo-first order color decay and generator output with the results of calorimetry are presented in Figure 4.11.

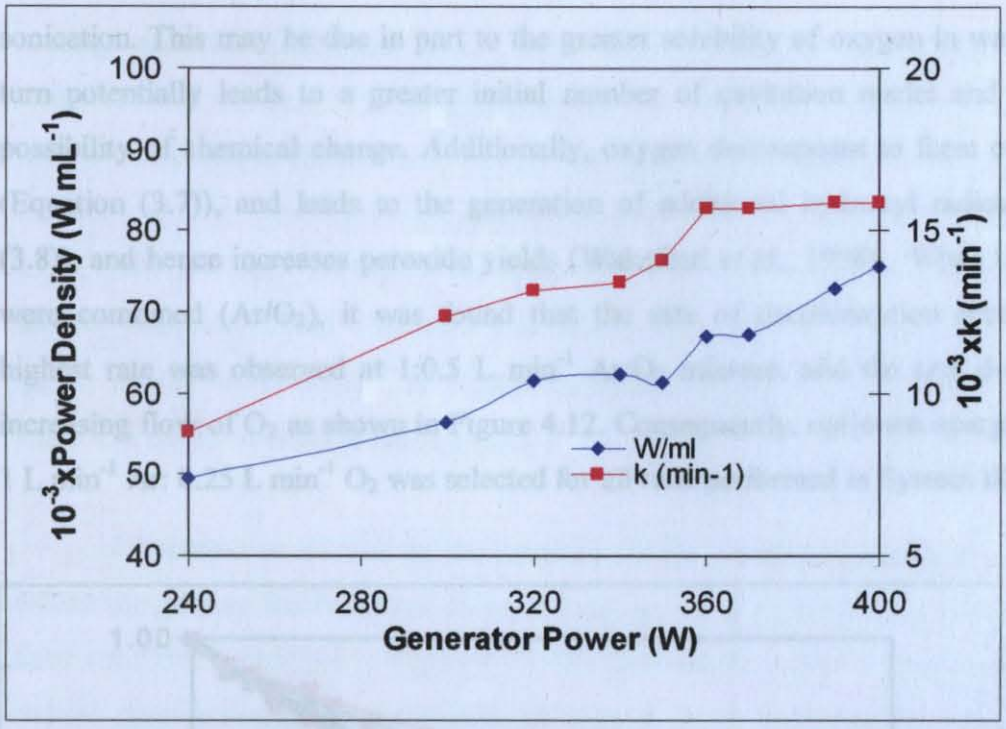

Figure 4.11. Power density in tap water at various power outputs and profiles of color degradation rate constants in 20 mg L^{-1} AO7 (irradiated volume=1200 mL).

The figure shows that, maximum color decay was observed at an output of 390 and 400 W. Decolorization rates were the same between 390-400 W, and the power density values of the two were close. Therefore, 390 W was selected as the optimum value, at which the power density in solution was 0.073 W mL^{-1}.

iii) Injected Gas Type and Flow Rate

1200 mL of air-saturated 20 mg L^{-1} of AO7 solutions were irradiated at 0.073 W mL^{-1} power density in the presence of Ar, O_2 and various combinations of the two. Samples were collected within short intervals for spectrophotometric analyses to monitor the absorbance abatement in the visible region for AO7 degradation. Decolorization rate with respect to gas injection decreased in the sequence: Ar > O_2 > Air. Argon is a monatomic gas having the highest γ value (1.66), and therefore provides rapid reaction rates by high temperature and pressure generation on cavitational collapse. Oxygen and air (considered to be predominantly a nitrogen/oxygen mixture) are diatomic gases having similar γ values (1.41 and 1.40, respectively), and sonication in the presence of oxygen yielded a decolorization rate that was 20 per cent larger than the rate for air injected

sonication. This may be due in part to the greater solubility of oxygen in water, which in turn potentially leads to a greater initial number of cavitation nuclei and increase the possibility of chemical change. Additionally, oxygen decomposes to form oxygen atoms (Equation (3.7)), and leads to the generation of additional hydroxyl radicals (Equation (3.8)), and hence increases peroxide yields (Wakeford *et al.*, 1998). When the two gases were combined (Ar/O_2), it was found that the rate of decolorization accelerated. The highest rate was observed at 1:0.5 L min^{-1} $Ar:O_2$ mixture, and the rate decreased with increasing flow of O_2 as shown in Figure 4.12. Consequently, optimum sparge gas ratio of 1 L min^{-1} Ar: 0.25 L min^{-1} O_2 was selected for all runs performed in System III.

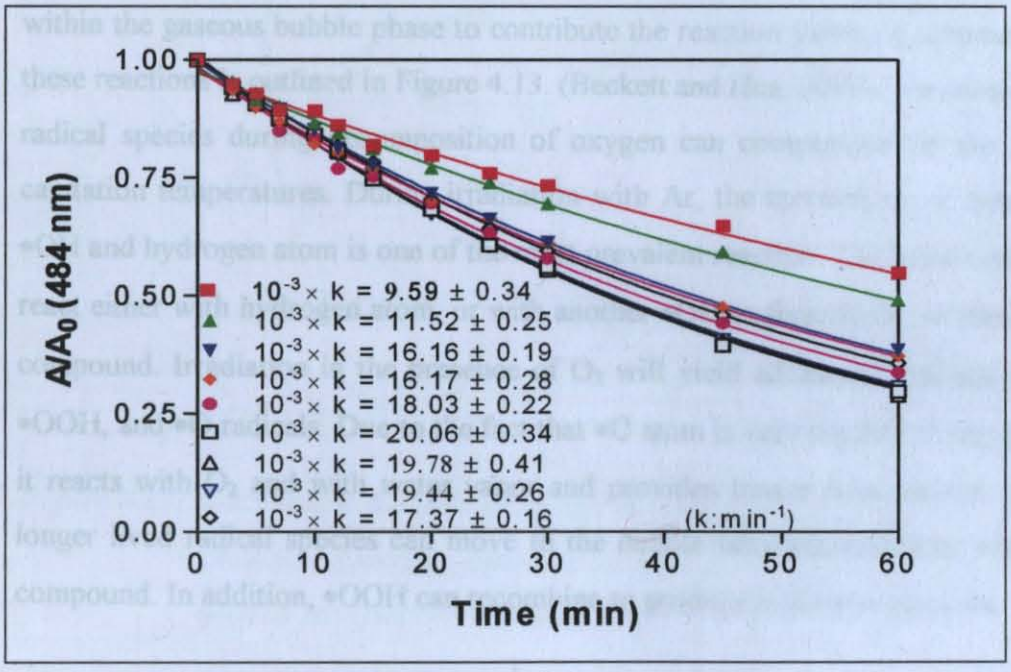

Figure 4.12. Experimental profiles of color degradation in AO7 during 1 h irradiation with various gas sparge ratios in System III (gas flow rates are given in lmin^{-1}; ■ Air 1, ▲ O_2 1, ▼ Ar 1, ♦ $Ar:O_2$ (1:1), ● $Ar:O_2$ (1:0.75), □ $Ar:O_2$ (1:0.5), Δ $Ar:O_2$ (1:0.25), ∇ $Ar:O_2$ (1:0.125), ◊ $Ar:O_2$ (1:0.0625), all $R^2 > 0.98$).

Increased color degradation rates by gas combination can be explained by series reactions that may occur within the cavitation bubble during sonolysis.

Gases with higher polytrophic index, γ, (heat released upon gas compression) and lower thermal conductivity (heat dissipation to the surrounding environment) promote more extreme conditions within the collapsing bubbles as discussed in Section 3.2.2.7.

During acoustic cavitation, gases with high polytropic indices and low thermal conductivities will lead to more intense conditions within a collapsing bubble because less heat is dissipated to the surrounding aqueous environment during the rapid implosion (see Equation (3.11)). γ is higher for Ar (1.66) than for O_2 (1.41), and the thermal conductivity of O_2 (48.1 mW mK^{-1}) is higher than that of Ar (30.6 mW mK^{-1}) (Beckett and Hua, 2000; Beckett and Hua, 2001). Therefore, the bubble implosion in the presence of Ar favors a higher overall temperature. The higher collapse temperature increases the •OH rate and leads to a higher formation rate for H_2O_2.

Ultrasonic irradiation in the presence of O_2 generates additional chain reactions within the gaseous bubble phase to contribute the reaction yields. A schematic diagram of these reactions is outlined in Figure 4.13. (Beckett and Hua, 2001). The production of these radical species during decomposition of oxygen can compensate for the lower internal cavitation temperatures. During irradiation with Ar, the thermolysis of water to generate •OH and hydrogen atom is one of the most prevalent reaction. The generated •OH radicals react either with hydrogen atom, or with another •OH to form H_2O_2, or react with organic compound. Irradiation in the presence of O_2 will yield additional radicals, such as •OH, •OOH, and •O radicals. Due to the fact that •O atom is very reactive in the gaseous phase, it reacts with O_2 and with water vapor and provides longer lived radical species. These longer lived radical species can move to the bubble interface and react with the organic compound. In addition, •OOH can recombine to produce hydrogen peroxide.

To summarize, increased dye degradation by combination of Ar and O_2 is due to a synergy of the gas properties: while Ar induces higher collapse temperatures by its relatively higher polytrophic gas ratio and lower thermal conductivity, O_2 promotes the formation of additional radicals upon thermal fragmentation within the gas phase. Deceleration of the rate upon increased O_2 flow above the selected value is due to the offset of its benefits by domination of its poorer gas properties, i.e. lower polytrophic gas ratio and higher thermal conductivity. Therefore, one should be very careful in selecting the optimum Ar:O_2 combinations to obtain the highest sonochemical yield.

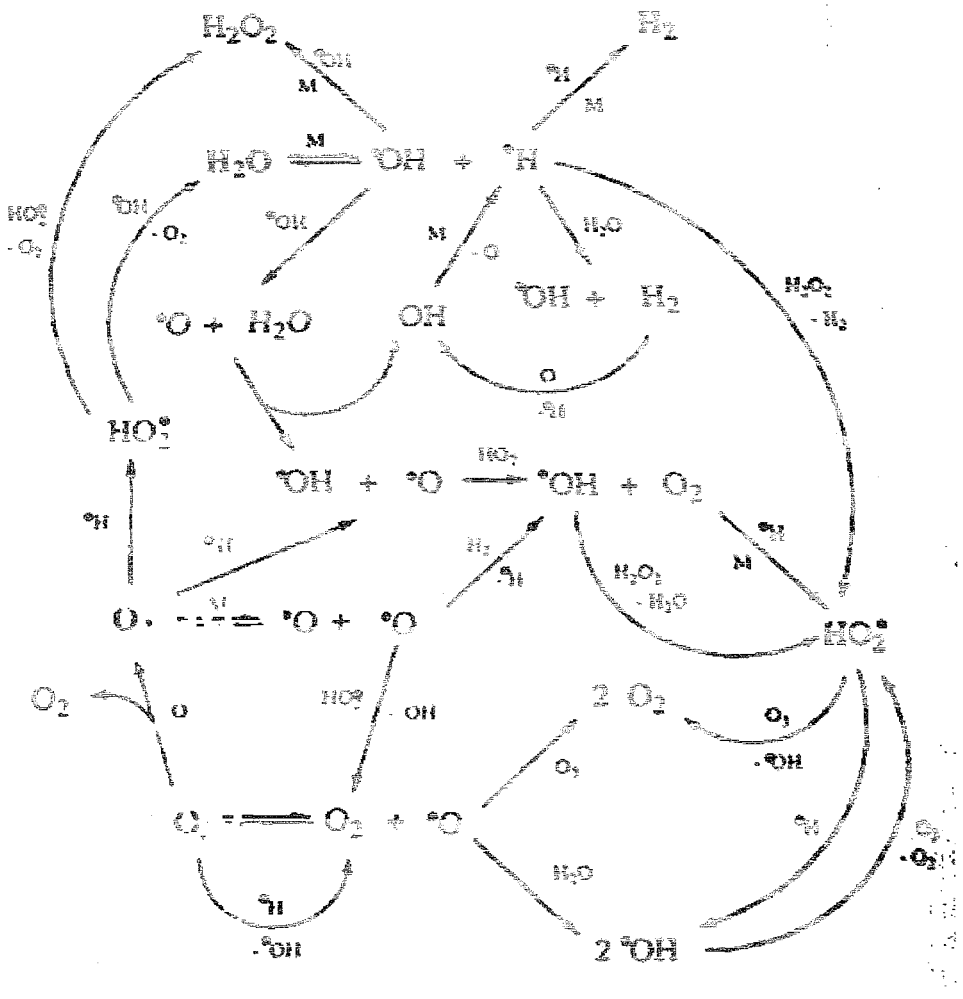

Figure 4.13. A schematic diagram of chemical reactions during acoustic cavitation in the presence of oxygen, ozone, or an inert gas (M). (M is an inert third molecule such as Ar) (Beckett and Hua, 2001).

As a consequence, the highest sonochemical efficiency occurs at an optimum balance between the higher temperatures generated during acoustic cavitation from Ar and the generation of additional active radical species from O_2.

4.3. System Comparison at Optimized and Equivalent Power Densities

4.3.1. Rate of Color Removal at Optimized Conditions

Pre-aerated 20 mg L^{-1} C.I. Acid Orange7 (AO7) solutions were irradiated at the optimum generator powers of each system for 30 minutes to monitor absorption abatements at the UV_{484} band. Plots of comparable profiles of color decay versus time for each system are shown in Figure 4.14.

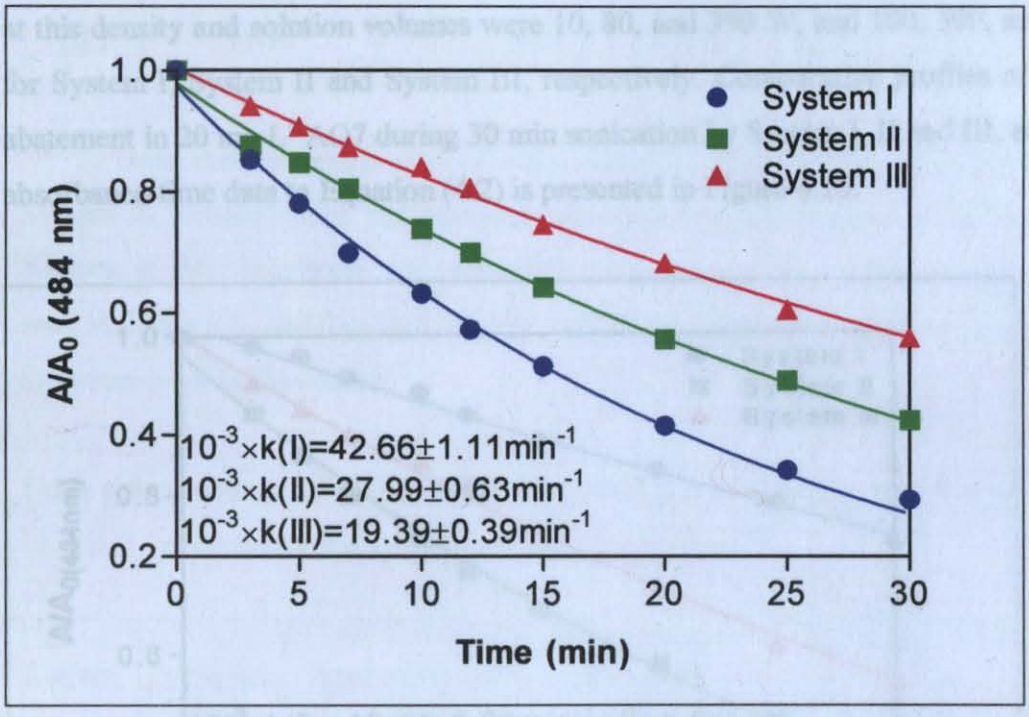

Figure 4.14. Comparative rates of color degradation in 20 mg L^{-1} AO7 during sonication by System I, System II and System III at optimized conditions (subscripts I, II, and III refer to the system I, system II, and system III, respectively).

Per cent color removals after 30 minutes were 70.59 per cent, 57.52 per cent, and 44.54 per cent for the systems I, II, and III, respectively. This result can be attributed to the higher power density value obtained in System I. The results indicate that, whatever the frequency is (system I, II or III), the total sum of ultrasonic energy (power density) delivered to the system is important.

4.3.2. Rate of Color Removal at Equivalent Power Densities

Sonolysis of C.I.Acid Orange7 (AO7) was studied in all systems at equivalent power densities and the systems were compared for their performance in the rates of total color removal. Reaerated solutions of 20 mg L^{-1} AO7 were irradiated for 30 minutes at 0.070 W mL^{-1} of power densities in System I and II, and at 0.073 W mL^{-1} in System III to monitor absorption abatements at the UV_{484} band. Because the maximum possible density was 0.073 W mL^{-1} in System III, the other two systems were also adjusted approximately to this value to compare system performances at similar conditions. The generator outputs at this density and solution volumes were 10, 80, and 390 W, and 100, 300, and 1200 mL for System I, System II and System III, respectively. Comparative profiles of absorption abatement in 20 mg L^{-1}AO7 during 30 min sonication by System I, II and III, and the fit of absorbance-time data to Equation (4.2) is presented in Figure 4.15.

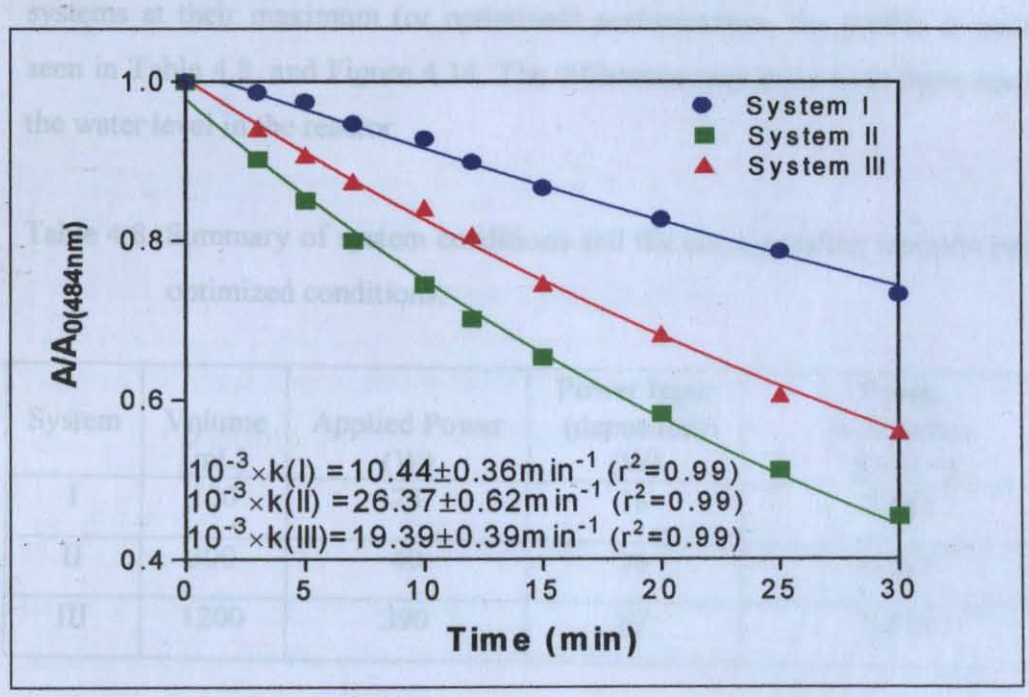

Figure 4.15. Comparative rates of color degradation in 20 mg L^{-1} AO7 during sonication by System I, System II and System III at equivalent ultrasonic densities (subscripts I, II, and III refer to the system I, system II, and system III, respectively. Power density of each system was 0.070-0.073 W mL^{-1}).

A summary of system conditions with the corresponding color degradation coefficients is listed in Table 4.7.

Table 4.7. Summary of system conditions and the corresponding reaction performances at equivalent power densities

System	Volume (ml)	Applied Power (W)	Power in Solution (WmL^{-1})	Yield, k x 10^{-3} (min^{-1})
I	100	10	0.070	10.44 ± 0.36
II	300	80	0.070	26.37 ± 0.62
III	1200	390	0.073	19.39 ± 0.39

Note that maximum rate of color decay at these conditions is accomplished by System II, although it is not operated at its maximum performance. If we compare all systems at their maximum (or optimized) performances, the profile is quite different as seen in Table 4.8. and Figure 4.14. The difference may arise both from reactor shape and the water level in the reactor.

Table 4.8. Summary of system conditions and the corresponding reaction performances at optimized conditions.

System	Volume (mL)	Applied Power (W)	Power Input (deposited) (W)	Power in Solution (WmL^{-1})	Yield, k x10^{-3} (min^{-1})
I	100	25	18	0.184	42.66 ± 1.11
II	300	40	38	0.127	27.99 ± 0.63
III	1200	390	87	0.073	19.39 ± 0.39

With respect to the pseudo-first order decolorization rates for each system at equivalent power densities, the rate of color degradation was in the order: System II > System III > System I. Systems I (520 kHz) and II (520 kHz x 3) had significantly higher decolorization rates than System I (300 kHz). Although the systems have different reactor geometry, which may affect the cavitation efficiency, this result can still be attributed to the increased mass transfer of •OH radicals into the surrounding medium at 520 kHz frequency. As the frequency increases, the flux of active radical species toward the

cavitation bubble interface accelerates. Higher decolorization rates obtained by System II than System III may be due to observation of more pronounced standing waves in System III. The presence of standing wave zones which were observed to be more prominent in System III may have reduced the overall decolorization efficiency by not allowing the unstable conditions necessary for bubble growth and collapse. Power densities versus decolorization rate for each system are plotted in Figure 4.16.

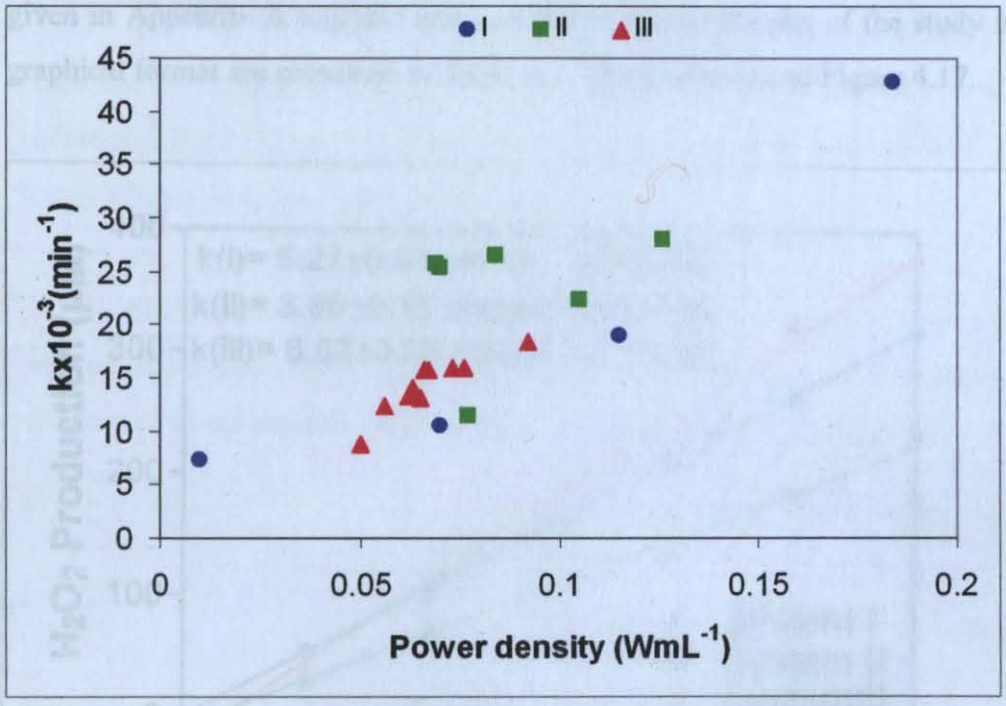

Figure 4.16. Variations of decolorization rate coefficients with ultrasonic power density in System I, System II, and System III.

The figure shows that, the efficiency of System I is highly related to the applied power and it also implies that higher efficiencies can be obtained by higher powers. The same is not true for the other two systems because of their sensitivity to the geometry and configuration of the reactor cells.

4.3.3. Rate of Hydrogen Peroxide Production

In an attempt to determine correlation between system performance in terms of chemical effects, the production of hydrogen peroxide was monitored in dye-free deionized water as an indirect indicator of free radical production (Hydrogen peroxide is produced

during the sonolysis of water by the recombination of •OH at the cooler bubble interface as $•OH + •OH \rightarrow H_2O_2$).

Pre-aerated deionized water was sonicated for 1 h at optimized conditions (maximum conditions) of System I, II and III and samples were withdrawn from the reactors at 10 minute intervals to analyze hydrogen peroxide concentration in the effluents. The analysis was made by the triiodide method (Klassen *et al.*, 1994), details of which are given in Appendix A together with calibration curve. Results of the study in tabular and graphical format are presented in Table A.1. (Appendix A) and Figure 4.17.

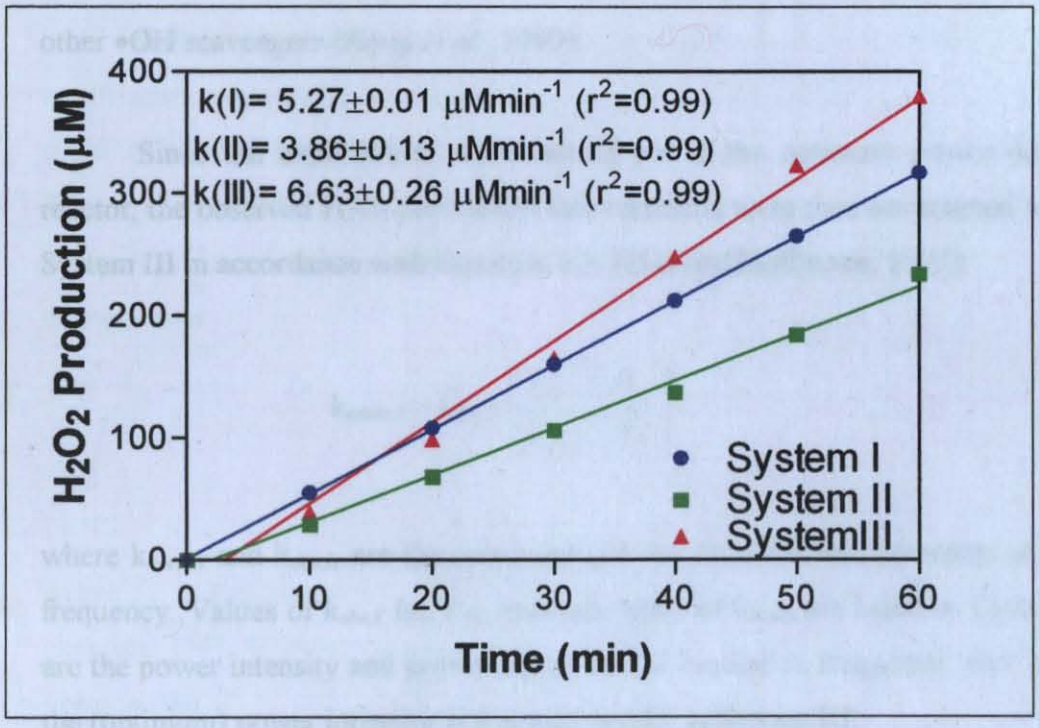

Figure 4.17. Comparable profiles of hydrogen peroxide production with increased contact time each operated at optimized conditions in System I, II, and III.

Note that the net rate of hydrogen peroxide production is linear (R^2=0.99) in all systems to be attributed the relative insignificance of hydrogen peroxide by scavenging (Equation (4.4)) and/or dissociation reactions.

$$•OH + H_2O_2 \rightarrow •O_2H + H_2O \qquad (4.4)$$

The zero-order rates of H_2O_2 production were in the order of: System III > System I > System II. The highest H_2O_2 production rate in System III may be due to reactor configuration. However, when the systems (at their optimum power densities) were compared (Figure 4.14.) with respect to color removal rates, the order was: System I > System II > System III. Hence, the rate of H_2O_2 production is not a direct indicator of the reaction yield, or the rate of color removal. This may be attributed to the •OH scavenging potential of H_2O_2 to lower the steady state [•OH] in the bulk solution (Hua and Hoffmann, 1997), and the witness of unreactivity of most color components (particularly azo chromophores) with molecular H_2O_2, or its dissociation products ($•O_2H$, $•O_2^-$). It should be noted that H_2O_2 is a powerful •OH scavenger ($k_{•OH,H2O2}=2.7x10^7\ M^{-1}\ s^{-1}$) in the absence of other •OH scavengers (Kang *et al.*, 1999).

Since the experiments were carried out at the optimum power density of each reactor, the observed H_2O_2 production rate constants were then normalized with respect to System III in accordance with Equation 4.5. (Hua and Hoffmann, 1997):

$$k_{norm,f} = k_{obs,f}\left(\frac{I_{III}}{I_f}\right)\left(\frac{P_{III}}{P_f}\right) \qquad (4.5)$$

where $k_{norm,f}$ and $k_{obs,f}$, are the corrected and the observed rate constants at the irradiated frequency. Values of $k_{obs,f}$, I_{III}, P_{III}, and estimation of k_{norm} are listed in Table 4.9. I_f and P_f are the power intensity and power density at the irradiation frequency; and I_{III} and P_{III} are the (optimum) power intensity and power density at System III.

Table 4.9. Optimum power intensity and power density of System I, II, and III.

System	Power Input (W)	Transducer Area (cm^{-2})	Volume (mL)	I (Wcm^{-2})	P (WmL^{-1})	$k_{H2O2obs}$ $\mu Mmin^{-1}$	$k_{H2O2norm}$ $\mu Mmin^{-1}$
I	18	22	100	0.82	0.18	5.27	3.44
II	38	22	300	1.73	0.13	3.86	1.41
III	87	22 x 3	1200	1.32	0.07	6.63	6.63

The table shows that, the order of H_2O_2 production is the same in normalized conditions (at equivalent power densities); i.e. System III > System I > System II. This

result can be explained that, at higher frequencies, more hydroxyl radicals are ejected out of the bubble before they can recombine at the gas phase, because the collapse time at higher frequency is shorter. As it was noted previously, H_2O_2 is the most likely •OH scavenger in the absence of other •OH scavengers (Equation (4.4)). The H_2O_2 production was higher in System III and the scavenging of •OH with those higher amounts of H_2O_2 is more probable. Therefore, less •OH will be available for dye decolorization and this will lead to lower degradation efficiencies in System III than in System II.

4.3.4. System Comparison with Respect to Product Yield

Comparison of systems reported so far was focused on decolorization reaction rate coefficients, whereas in the present section systems are compared on the basis of "product yield". This parameter has already been defined and explored by Mark *et al.*, (1998) and Tauber *et al.*, (2000). Product yield is defined as the change in test chemical concentration in the experiment volume per power of the sonic energy deposited in that volume, and is expressed as:

$$G = \frac{\Delta C \times V}{P_d} \qquad (4.6)$$

where G is product yield (mol W^{-1}), ΔC is change in molar concentration of the test chemical (M), V is sonicated volume (l), and P_d is sonic energy deposited in a given volume (W).

The parameter ΔC was calculated by using the visible absorbance data presented in Figure 4.3.1.1 Dye concentrations were calculated by using Beers Law as represented by Equation (4.7).

$$A = \varepsilon \times C \times b \qquad (4.7)$$

where A is the absorbance, ε is the molar absorptivity (M^{-1} cm^{-1}) when the concentration of C is expressed in terms of moles per liter, and b is the pathlength given in centimeters.

Molar absorptivity coefficient (ε_{max}) of AO7 was calculated by using Equation (4.7) (for λ = 484 nm) as 23471 $M^{-1}cm^{-1}$. Deposited powers in all systems were determined by calorimetry and presented in Table 4.8. Product yield or sonochemical yield in the present section has been defined as the amount of AO7 removed per ultrasonic energy deposited in the reaction volume. Figure 4.18. depicts the increase in *G* with irradiation time.

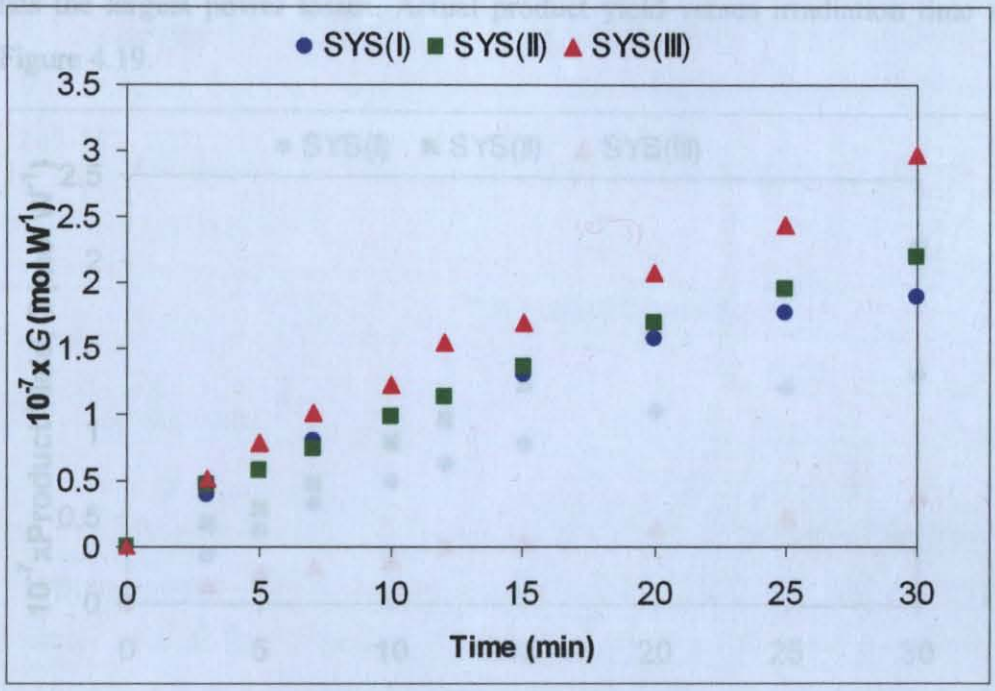

Figure 4.18. Product yields of 20 mg L^{-1}AO7 during ultrasonic irradiation by System I, II and III at their optimized power densities.

As presented in Figure 4.18., the increase in *G* is in the order : System III > System II > System I. It should however be noted that the above results were obtained by considering only the power deposited in solution. However, each system had its own deficiency in terms of total energy loss, as determined by the difference between applied and deposited powers. This is why, the power efficiency must be considered in determination of the actual product yield. This was accomplished by including a new term "f" into Equation (4.6):

$$G' = \mathrm{f} \times \frac{\Delta C \times V}{P_d} \qquad (4.8)$$

where G' is the actual product yield (mol W^{-1}), f is the ratio of the power deposited in a given volume to the power applied.

The fractions of power deposited to applied power were calculated by using the data presented in Table 4.8. The f values were calculated as 0.72, 0.95 and 0.22 for System I, II and III, respectively. The lowest f value found for System III means that this system has the largest power losses. Actual product yield versus irradiation time are plotted in Figure 4.19.

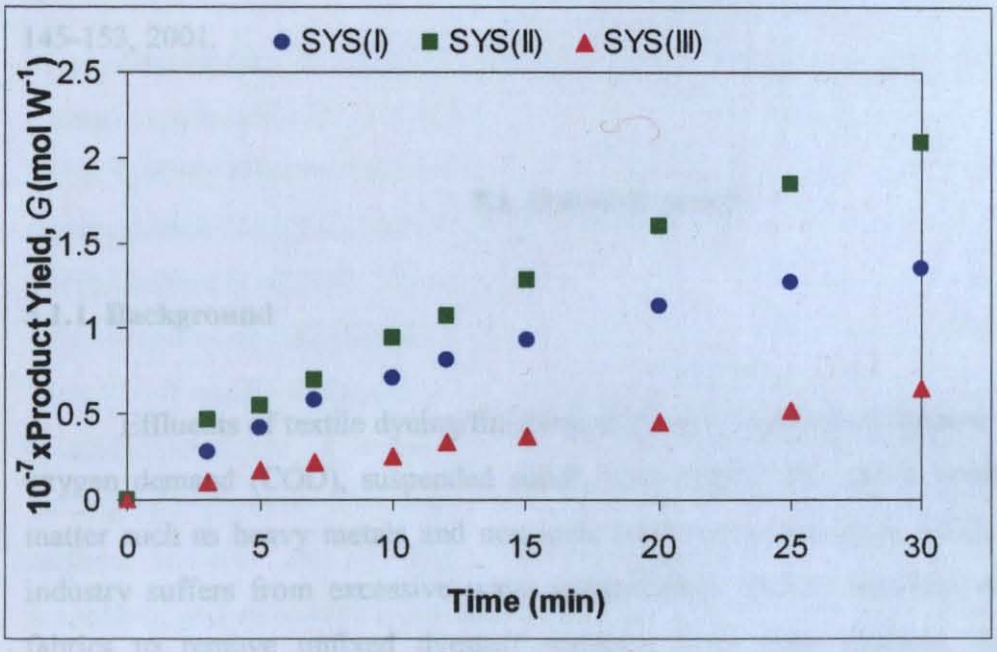

Figure 4.19. Actual product yields of 20 mg L^{-1}AO7 during ultrasonic irradiation by System I, II and III.

With respect to the calculated G' for each system, it was concluded that system efficiency was in the order: System II > System I > System III. Note that although System III appeared to be the most efficient in Figure 4.18., it was the least efficient in Figure 4.19. due to its inefficiency in energy transfer.

CHAPTER 5. REACTIVE DYESTUFF DEGRADABILITY BY OZONE/ULTRASOUND AND FENTON/ULTRASOUND: APPLICATIONS IN SYSTEM II

Section 5.1. of this Chapter is the paper entitled " Reactive Dyestuff Degradation by Combined Sonolysis and Ozonation", which was published in *Dyes and Pigments*, 49, 145-153, 2001.

5.1. Ozone-Sonolysis

5.1.1. Background

Effluents of textile dyeing/finishing mills are complex with intense color, chemical oxygen demand (COD), suspended solids, temperature, pH, and a variety of refractory matter such as heavy metals and non-ionic surfactants (Gurnham, 1965). Moreover, the industry suffers from excessive water consumption, due to manifold washing of dyed fabrics to remove unfixed dyestuff residuals from their surfaces. Accordingly, the management of dyehouse effluents requires an integrated approach to the solution of "effluent treatment" and "water consumption" problems by developing suitable treatment schemes that produce harmless effluents and recyclable water.

The expanded use of reactive dyes during the last decade has turned conventional methods inadequate for treating dyehouse effluents, due to poor biodegradation of such dyes (especially those containing azo-groups) under aerobic conditions (Boeniger,1980). Furthermore, some precursors of azo-reactive dyes are toxic and carcinogenic, requiring separation and advanced treatment of dyebath effluents before discharge into conventional systems or publicly owned wastewater treatment works (Boeniger, 1980; Brown and De Vito, 1993).

Recent developments in advanced oxidation processes (AOP), which are recognized with their potential to generate free radicals, have shown that under proper operation they render complete color removal, detoxification and mineralization in the effluents of textile dyeing mills (Ince *et al.*, 1997; Gregor, 1992; Gouldm and Groff, 1987; Ince and Tezcanli, 1999). The advantage of AOP over conventional oxidation processes is due to the reactivity of free radical species, especially that of the hydroxyl radical (•OH), which, unlike molecular oxidants is non-selective and far more powerful than all (Glaze *et al.*, 1987).

One of the most common methods of free radical production in AOP practices is ozonation (coupled with or without a source of ultraviolet light), and lab-scale treatment of textile dyebath effluents with ozone has been found effective for color removal and partial mineralization (Gregor, 1992; Gouldm and Groff, 1987; Bahorsky, 1997; Arslan *et al.*, 1999; Carriere *et al.*, 1991; Snider and Porter, 1974). The attractiveness of ozonation over other chemical oxidation methods is that it provides two possible degradation routes: i) at basic pH, it rapidly decomposes to yield hydroxyl and other radical species in solution; ii) at acidic conditions, it is stable and may react directly with organic substrates as an electrophile (Gouldm and Groff, 1987; Glaze *et al.*, 1987). The shortcomings of the method, however, are its energy intenseness (due to onsite generation of ozone), pH sensitivity, and selectivity of O_3 for organic substrates and the increased level of turbidity in effluents (Bahorsky, 1997). Hence, ozonation requires further research and development for applicability in large-scale operations as part of an environmental management system.

Free radical formation in water by ultrasonic irradiation (US) is a much less popular technique, despite the very "extreme" conditions provided by sonic vibrations in liquids for "high energy chemistry" (Suslick, 1990). Research studies on dyestuff degradation by ultrasonic irradiation is rare, except for a couple of investigations with reactive dyes, reporting complete decolorization and partial mineralization after sufficiently long exposure (Vinodgopal *et al.*, 1998; Joseph *et al.*, 2000).

When a liquid is sonicated, the pressure waves are transmitted through the medium by acoustic cavitations, which are made of microbubbles entrapping dissolved gases and vapors of the surrounding medium (Suslick, 1990; Mason, 1990). These bubbles grow and

expand within the rarefaction and compression cycles of the pressure until they reach a critical size, at which further compression leads to their implosive collapse, with temperature releases of 2000-5000 K (Suslick *et al.*, 1990). During this collapse stage, water molecules and volatile organic solutes entrapped in bubble interiors undergo pyrolytic fragmentation to dissociate into hydroxyl, hydrogen and organic radicals, respectively (Serpone *et al.*, 1994; Hung and Hoffmann, 1998).

When a water body is ozonated simultaneously during ultrasonic irradiation (US), the increase in hydroxyl radical production is synergistic due to an additional pathway that involves thermal decomposition of O_3 (Kang and Hoffmann, 1998; Weavers *et al.*, 1998). A further advantage of such a combination is enhanced O_3 transfer in solution, resulting from larger gas diffusion coefficients in the presence of sonic vibrations than in non-irradiated solutions (Weavers and Hoffmann, 1998). A simplified reaction scheme for •OH generation during US/O_3 treatment of water is as follows (Serpone *et al.*, Kang and Hoffmann, 1998; Weavers *et al.*, 1998; Hart and Henglein, 1986):

$$O_3 + H_2O \rightarrow 2HOO\bullet \quad (5.1)$$

$$O_3 + HOO\bullet \rightarrow \bullet OH + 2O_2 \quad (5.2)$$

$$H_2O +))) \rightarrow \bullet H + \bullet OH \quad (5.3)$$

$$O_3 +))) \rightarrow O_2(g) + O(^3P)(g) \quad (5.4)$$

$$O(^3P)(g) + H_2O(g) \rightarrow 2\bullet OH \quad (5.5)$$

Some of the hydroxyl radicals recombine at the cooler bubble-liquid interface to yield water and hydrogen peroxide, others react with gaseous substrates within the collapsing bubbles, and under proper conditions some diffuse into the bulk liquid to activate aqueous phase oxidation reactions (Serpone *et al.*, 1994; Kang and Hoffmann, 1998; Weavers *et al.*, 1998). Depending on their solubility and vapor pressures, organic solutes during combined ozonation and US treatment may be destroyed by direct thermal decomposition, •OH-mediated advanced oxidation in the bulk liquid, chemical oxidation with ozone and hydrogen peroxide, and/or a combination of all (Weavers and Hoffmann, 1998).

The purpose of this study was to investigate the effectiveness of combining ultrasonic irradiation (US) with ozone in treating textile dyebath effluents contaminated with reactive dyestuff. The degradation process was expected to occur in the bulk solution by hydroxylation and direct reactions of the dyestuff (and the reaction intermediates) with molecular ozone and hydrogen peroxide. Pyrolytic destruction was not an expected pathway because of the hydrophilic nature of reactive dyes, which inhibits their partitioning between aqueous and gaseous phases (Serpone *et al.*, 1994; Weavers *et al.*, 1998).

The method of study involved: i) preparing synthetic dyebath solutions with C.I. Reactive Black5 (RB5), which owing to its high consumption records was selected as a model compound to represent azo-dyes; ii) monitoring the degradation of the dye by means of the decay in its absorbance at the UV-visible band and the reduction in its total organic carbon (TOC); and iii) estimating the rate of dye degradation by regression analysis of the absorbance-time data.

5.1.2. Materials and Methods

5.1.2.1. Dye

Remazol Black-B (MW=991.8 g mol^{-1}) was obtained from Dystar Hoechst (Istanbul) in 80-85 per cent purity. The chemical structure and characteristics of the dye is given in Figure 5.1. Ozone was generated onsite by electricity using dry pure oxygen.

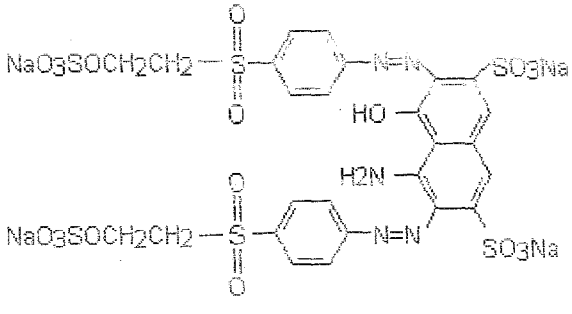

Figure 5.1. The chemical structure of C.I. Reactive Black5 (RB5).

Sodium Hydroxide and Sulfuric Acid

Reagent grade NaOH (Merck) and H_2SO_4 (96 %, Merck) at various concentrations were used for pH adjustments.

5.1.2.2. Optimized System Parameters

The optimized system parameters used for the studies in this chapter are summarized in Table 5.1.

Table 5.1. Optimized parameters of system II

System	Transducer Frequency	Reaction Volume (mL)	Power Density ($W\ mL^{-1}$)	Type of Gas and Flow Rate
II	520 kHz	600 mL	0.060	Ar ($1\ L min^{-1}$)

During ozonation and ultrasound coupled ozonation experiments, ozone was supplied into the system through a Fischer OZ-500 model generator at a rate of 50 L h^{-1}, yielding (in non-irradiated water) 3.36 g L^{-1} O_3, as determined by iodometry (Arslan, 2000). The reactor was bubbled mildly with a stream of air throughout contact to enhance cavitation events.

5.1.2.3. Preparation of the Dye Solutions

A 300 μM stock solution was prepared by dissolving 0.363 g of RB5 in 1 L deionized water, followed by heating to 80 °C and adjusting to pH=11 with dilute NaOH (1 N). The solution was kept in these conditions for 6 h to allow complete hydrolysis of the dye and to simulate dyebath effluents from batch dyeing processes with reactive dyes (Mason *et al.*, 1992). Test samples of various concentrations prepared from the stock (stored in the dark at 4 °C) by appropriate dilutions were aerated for 2 h to lower their cavitational threshold and to allow rapid bubble formation during initial contact with US. The solutions were readjusted to neutral pH before experimentation.

5.1.2.4. Laboratory Equipment and Analytical

The optical absorption spectra (200-800 nm) and the reduction in UV/visible absorption of the dye solutions were recorded by a Unicam, Helios Alpha/Beta double beam spectrophotometer through a 1 cm path length.

The removal of organic carbon via mineralization was monitored by a Fisons 480 TOC analyzer. The instrument was calibrated by standard solutions of phenol (1-30 ppm), and calibration curves were established by linear regression.

The stock solution was heated to 80 °C by using Ikamag RCT Basic Temperature Controlled Stirrer. WTW 100 model pH meter was used for pH adjustments.

5.1.2.5. Procedure

The test concentrations as 10, 20, 40, 50 and 60 μM of C.I. Reactive Black5 were selected in accordance with typical dye residuals found in dyebath effluents of batch processes after rinse (Pisa Corp., 2000). Six-hundred milliliters of air-saturated test solutions were ozonated simultaneously with ultrasonic irradiation for 20 min, and samples were collected within short intervals for spectrophotometric analyses at the UV-visible region. Exposure was periodically extended to 1 h or more to allow time for mineralization, which was monitored by periodic TOC analysis in effluent samples.

Control experiments with ozone and ultrasound alone were performed on air-saturated dye solutions to compare rates of decolorization, oxidation and total mineralization with those accomplished in the simultaneous scheme, and to assess synergistic effects.

5.1.3. Results and Discussion

5.1.3.1. Decay of the UV-Visible Absorption Bands

C.I. Reactive Black5 is a strongly absorbing dye in the UV-visible range with a distinct band in the near-UV region (λ=312 nm) and another one in the visible (λ= 596 nm). The latter is responsible for the dark blue color arising from aromatic rings connected by azo groups, and the former is associated with "benzene-like" structures in the molecule (Ince *et al.*, 1997). The absorption spectrum of 20 μM air-saturated RB5 before and during exposure to US/O_3 is presented in Figure 5.2.

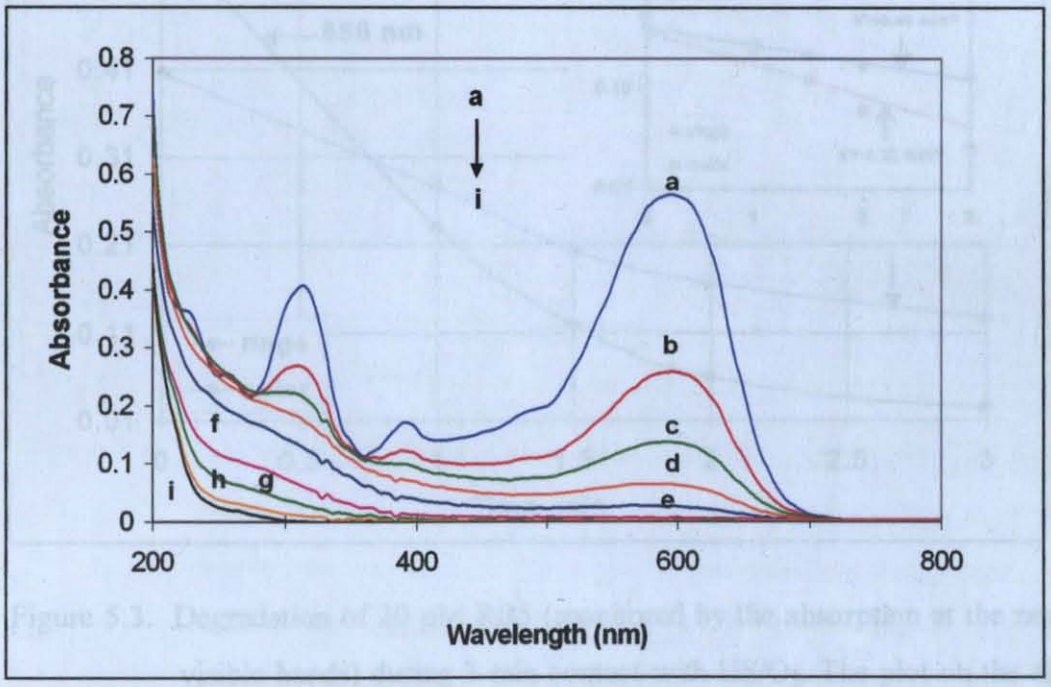

Figure 5.2. Changes in the absorption spectra of 20 μM pre-aerated RB5 during 20 min irradiation with US in the presence of O_3. (The legends a, b, c, d, e, f, g, h, i refer to contact times as 0, 1, 1.5, 2, 3, 5, 8, 12 and 15, respectively. Reactor conditions as power density, O_3 input and volume were 0.060 Wm L^{-1}; 50 L h^{-1}; and 600 mL, respectively).

The disappearance of the visible band within the first few minutes is due to the fragmentation of the azo links by immediate •OH attack (hydroxylation), which is

proposed as the first step in the degradation of azo dyes (Joseph *et al.*, 2000). Further to this rapid bleaching effect, the decay of the absorbance at 312 nm was the evidence of aromatic fragment degradation in the dye molecule and its intermediates. The time rate of abatement in the two absorption bands and comparison of their first order rate constants are presented in Figure 5.3. The significantly faster rate of decay in the visible band is due to the priority of hydroxylation of the azo-links in the oxidation process, resulting in the rapid disappearance of color chromophores in the dye structure (Vinodgopal *et al.*, 1998; Joseph *et al.*, 2000).

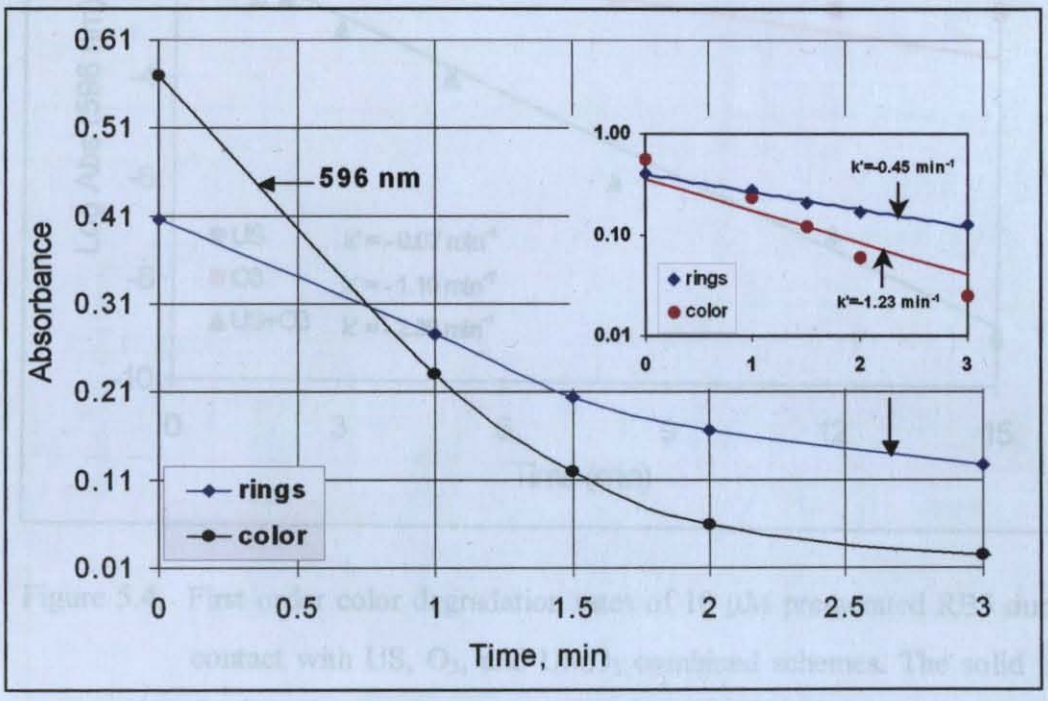

Figure 5.3. Degradation of 20 μM RB5 (monitored by the absorption at the near-UV and visible bands) during 3-min contact with US/O_3. The plot on the right corner shows the graphical estimation of first-order absorption decay rate by log-linear regression analysis of absorbance-time data.

The rate of decolorization of RB5 upon exposure to the combined scheme was compared with the rates observed in the control sets using O_3 and US individually. The degradation in all schemes as monitored by the decay of absorbance at 596 nm was found to follow pseudo-first order kinetics. Under the same conditions and for identical contact times, color removal with US/O_3 was twice as fast than that with ozone alone, while no

significant removal was observed in the control experiments with ultrasound alone. The data are presented in Figure 5.4. The lack of decolorization by US alone can be attributed to the relative shortness of the contact period, which is consistent with the literature, where minimum contact for appreciable degradation of color in 33 μM RB5 under similar conditions was reported as 2 hours (Vinodgopal *et al.*, 1998).

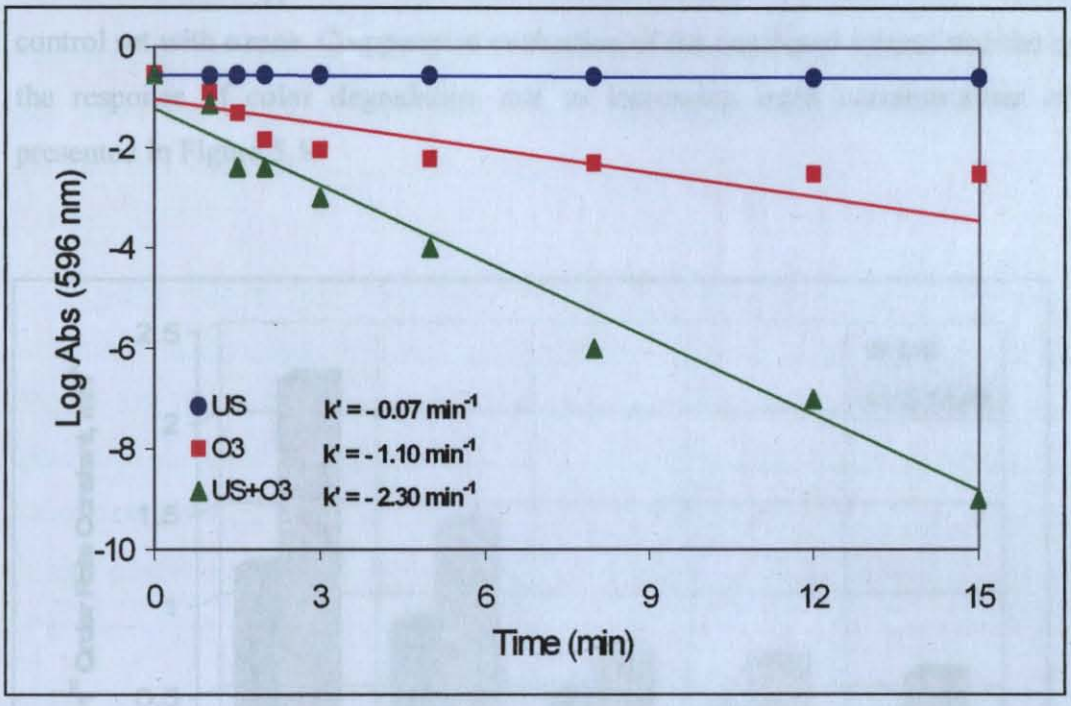

Figure 5.4. First order color degradation rates of 10 μM pre-aerated RB5 during 15-min contact with US, O_3, and US/O_3 combined schemes. The solid lines and k′ denote the regression fits and the pseudo-first order rate coefficients, respectively. Reactor conditions as power density, ozone flow and volume were same as listed in the caption of Fig. 5.2.

Despite the insignificancy of decolorization by US in 20 min however, the coefficient of degradation in combinative treatment was much larger than the sum of the coefficients of the two control sets, signifying a remarkable synergistic effect. The synergy, however, must principally emerge from enhanced ozone dissolution, resulting in excess decomposition reactions (in aqueous and gas phases) for enhanced rate of radical and peroxide production.

5.1.3.2. Effect of Dye Concentration

The impact of initial dye concentration on color degradation was studied by comparing absorbance decay rates in a variety of concentrations of RB5. It was found that the coefficient of decay decreased with subsequent increases in the input dye concentration, as typical of first order reaction kinetics. The tests were repeated in the control set with ozone. Comparative evaluation of the combined system and the control for the response of color degradation rate to increasing input concentrations of RB5 is presented in Figure 5.5.

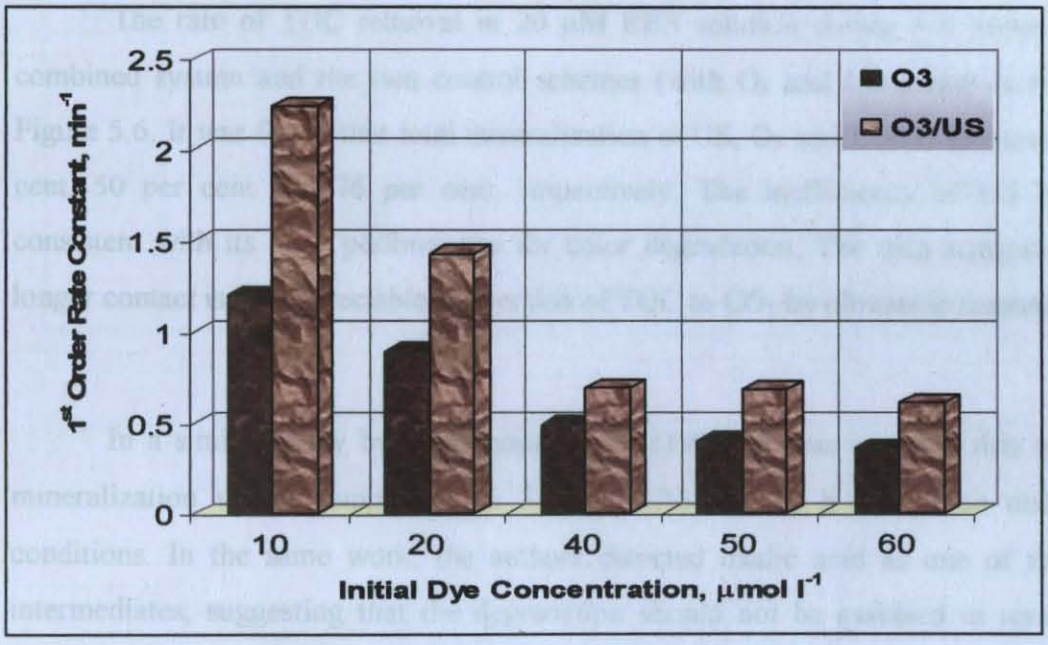

Figure 5.5. The response of pseudo-first order color degradation rate coefficient to the initial dye input.

It was found that, in both cases, degradation slowed down with increasing dye concentrations, while the kinetics remained unchanged. However, the combined system was less responsive to an increase in dye concentration in the higher range (beyond 40 µM), suggesting that perhaps thermal degradation reactions occurred at high dye concentrations. This is in agreement with the results of other researchers, who showed that at appreciable concentrations, hydrophilic solutes might slightly move away from solution and adsorb on the bubble-liquid interface to undergo thermal decomposition (Serpone *et al.*, 1994).

5.1.3.3. Carbon Mineralization

Oxidative degradation processes produce organic intermediates, which may be more harmful than the parent molecule if released into the environment without further treatment. Bleaching of a dye solution produces intermediates, which compete with the parent dye for •OH, O_3 and H_2O_2. Consequently, the destruction of the dye should be evaluated as an overall degradation process, involving the ultimate mineralization of both the parent dye and its intermediates. The most practical means of estimating this overall process is to monitor the reduction of total organic carbon (TOC).

The rate of TOC removal in 20 μM RB5 solution during 1 h contact with the combined system and the two control schemes (with O_3 and US alone) is presented in Figure 5.6. It was found that total mineralization in US, O_3 and US/O_3 schemes was 2 per cent, 50 per cent and 76 per cent, respectively. The inefficiency of US by itself is consistent with its poor performance for color degradation. The data suggest that much longer contact is for appreciable conversion of TOC to CO_2 by ultrasonic treatment alone.

In a similar study by Vinodgopal *et al.* (1998), it was reported that 60 per cent mineralization was accomplished in 33 μM RB5 after 6 h irradiation under similar conditions. In the same work, the authors detected oxalic acid as one of the reaction intermediates, suggesting that the degradation should not be assessed in terms of total mineralization alone, because some of the organic carbon may be converted to stable and environmentally acceptable products other than carbon dioxide.

Ozonation alone was relatively more effective than US for total mineralization, but combination of the two resulted in a synergistic increase in the overall process rate. The synergy suggests that cavitation events accelerate degradation of the ozone-induced intermediates of RB5. This is particularly obvious from the lack of TOC reduction between 15 and 30 min in both of the control sets (US and O_3 alone), as opposed to the linear reduction in TOC in the combined scheme. (Note that total mineralization with ozonation, and ozonation combined with US in 30 min were 14.4 per cent and 59.7 per cent,

respectively.) Hence, despite its insufficiency when used alone, ultrasound when combined with ozonation was extremely effective for accelerating the mineralization of the dye.

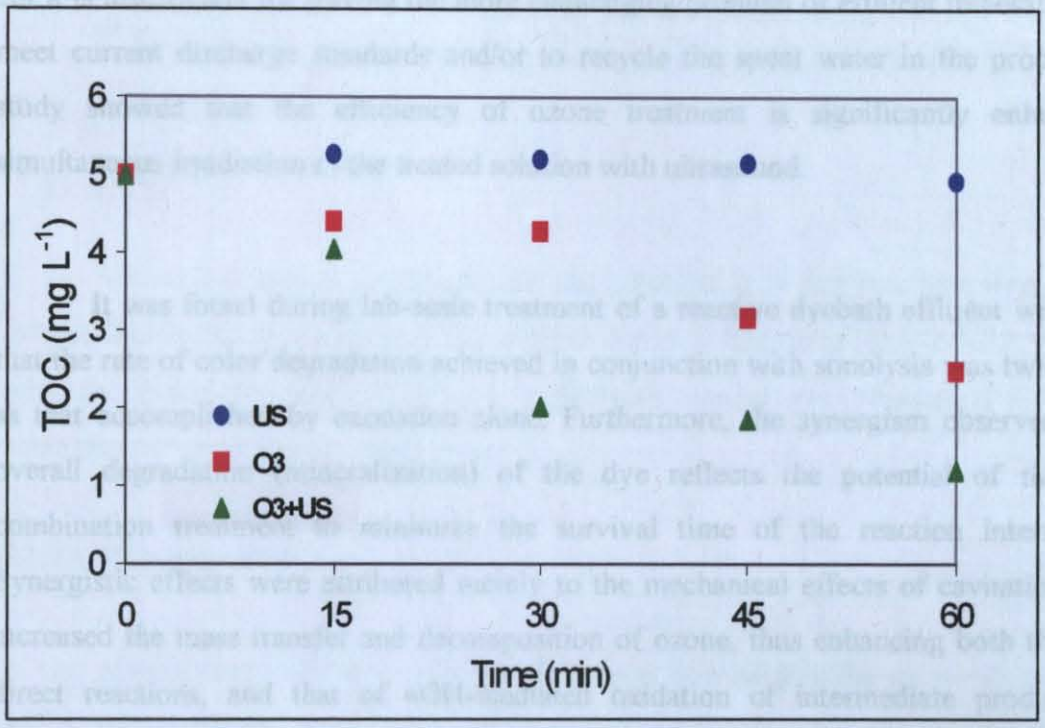

Figure 5.6. Comparison of US/O_3 combined scheme with the two control sets for rates of total organic carbon removal (mineralization) in 20 μM pre-aerated RB5.

It is most likely that during simultaneous operation, the early oxidation reactions resulting in dye bleaching are governed by ozone and its decomposition products, whereas the destruction of oxidation intermediates in achieved by the joint action of US and O_3. It is likely that the observed synergism involves factors such as: i) enhanced efficiency of ozone dissolution induced by the mechanical effects of ultrasound; ii) larger decomposition of ozone in water by additional pathways such as chain reactions (involving the production of peroxy and superoxide radicals); iii) reduced competition for •OH, O_3 and H_2O_2 by thermal decomposition of some intermediates; and iv) increased quantity of oxidizing species in solution upon migration of some relatively stable thermolysis products from collapsing cavities into the solution bulk.

5.1.4. Conclusions

Ozonation is a widely practiced method of color degradation in dyehouse effluents, but it is insufficient for solving the more challenging problem of effluent mineralization to meet current discharge standards and/or to recycle the spent water in the process. This study showed that the efficiency of ozone treatment is significantly enhanced by simultaneous irradiation of the treated solution with ultrasound.

It was found during lab-scale treatment of a reactive dyebath effluent with ozone, that the rate of color degradation achieved in conjunction with sonolysis was twice as fast as that accomplished by ozonation alone. Furthermore, the synergism observed for the overall degradation (mineralization) of the dye reflects the potential of the US/O_3 combination treatment to minimize the survival time of the reaction intermediates. Synergistic effects were attributed mainly to the mechanical effects of cavitation, which increased the mass transfer and decomposition of ozone, thus enhancing both the rate of direct reactions, and that of •OH-mediated oxidation of intermediate products. The proposed combination may be applicable in the management of dyehouse effluents, particularly in the search of new alternatives to achieve recycling of spent waters in dyeing process.

5.2. Fenton - Sonolysis

Section 5.2. of this chapter examined the effect of ferrous ion addition to System II on the rate of color and TOC removal of 20 μM C.I. Reactive Black5.

5.2.1. Background

As mentioned in Section 5.1., during ultrasonic irradiation of water, •OH formed by thermolytic reactions recombine to form hydrogen peroxide that tends to accumulate in the solution, without significant impacts on aqueous phase oxidation of organic matter. However, upon $FeSO_4$ addition the decomposition of sonochemically produced H_2O_2 (Eqn 3.4 and 3.9) is accelerated through Fenton's reaction (Eqn 5.6), and thus additional •OH

radicals are produced. As a consequence, non-reactive H_2O_2 is made reactive by ferrous ions, resulting in enhanced yields upon excess •OH formation (Joseph *et al.*, 2000; Petrier *et al.*, 2002; Beckett and Hua 2003).

$$Fe^{2+}\ (aq) + H_2O_2\ (aq) \rightarrow Fe^{3+}\ (aq) + {\bullet}OH\ (aq) + OH^-\ (aq) \qquad k_1 = 76\ M^{-1}s^{-1} \qquad (5.6)$$

5.2.2. Materials and Methods

System parameters, dye properties and preparation of dye solutions were the same as specified in the first section of the chapter. Fresh solutions of 20 µM RB5 were made using the hydrolyzed stock (0.363 g L^{-1}). Fenton's reagent was prepared as 5 g L^{-1} Fe^{2+}, using reagent grade $FeSO_4.7H_2O$ (Merck).

5.2.2.1. Experimental

Air-saturated solutions of 20 µM RB5 were sonicated in the presence of 0.01, 0.1, 0.5, 1, and 5 mM Fe^{2+} for 30 min, and samples were collected within short intervals for spectrophotometric analysis. The optimum Fe^{2+} concentration was determined by monitoring the rate of color decay at each level. Control experiments were run in the same test samples without Fe^{2+}, and the degradation of the dye for color and total organic carbon were monitored to assess the impact of Fe^{2+}.

Dye mineralization was monitored during 1 h ultrasonic irradiation of the test dye in the absence and presence of Fe^{2+} (0.1 mM).

5.2.3. Results and Discussion

5.2.3.1. Selection of Ferrous Ion Concentration

No hydrogen peroxide or buffering agents were added, and the initial pH of the samples was 5.5 in each run. Profiles of decolorization as a function of Fe^{2+} concentration is presented in Figure 5.7. The rate constants were pseudo-first order in all cases and all

coefficients were estimated by fitting the absorption data (at 596 nm) to Equation (4.2) and the results are given in Table 5.2.

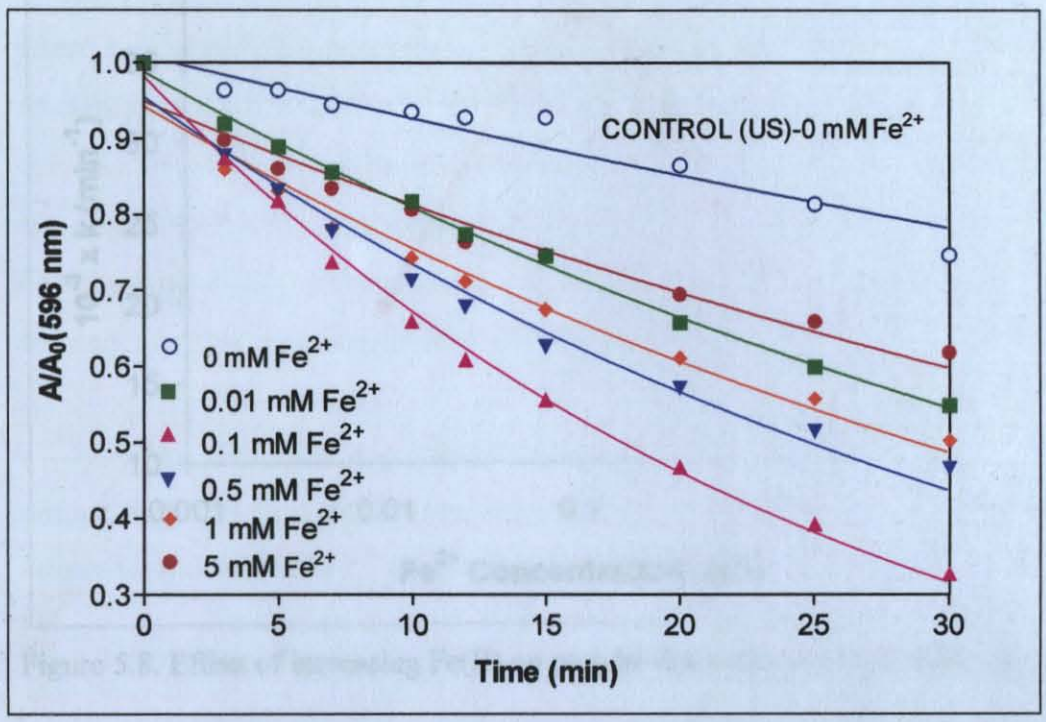

Figure 5.7. Rate of color degradation as a function of Fe^{2+} (solid lines represent the fit of related data set to Equation (4.2)).

All spectrophotometric measurements were performed in the absence of $Fe(OH)_3$ precipitate and the maximum decolorization efficiency was observed when 0.1 mM of Fe^{2+} was present in solution. Sequential increase in decolorization rate constant from 0 to 0.1 mM can be attributed to the production of excess •OH (Equation 5.6) through Fenton's reaction.

However, further increases in Fe^{2+} resulted in the reduction of decolorization rate constant (Figure 5.8.). The adverse effect of excess Fe^{2+} must be due to •OH scavenging of Fe^{2+} at high concentration via the following reaction (Tezcanli, 1998):

$$Fe^{2+}(aq) + \bullet OH \rightarrow Fe^{3+}(aq) + OH^{-}(aq) \qquad k_2 = 3 \times 10^8\ M^{-1} s^{-1} \qquad (5.7)$$

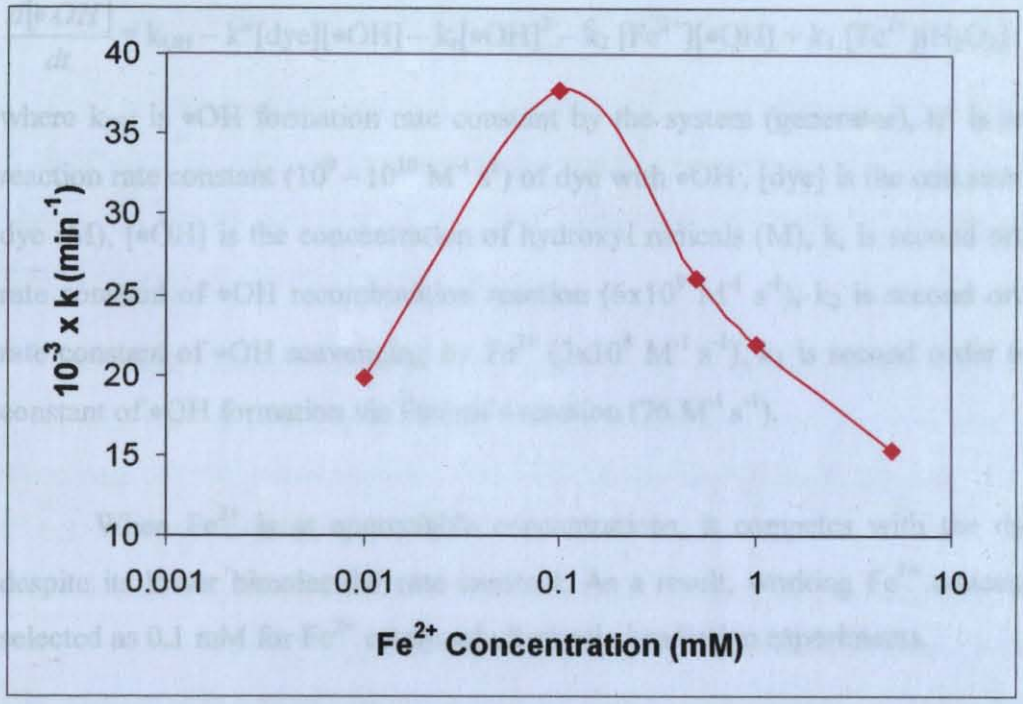

Figure 5.8. Effect of increasing Fe(II) on pseudo-first order decolorization rate coefficient.

Table 5.2. Pseudo-first order decolorization rate constants of RB5 sonication in the absence and presence of Fe^{2+}.

Fe^{2+} (mM)	10^{-3} x k (min^{-1})	R^2
0.00	8.47 ± 0.86	0.99
0.01	19.78 ± 0.41	0.99
0.10	37.74 ± 0.82	0.98
0.50	26.04 ± 1.35	0.97
1.00	22.00 ± 1.35	0.98
5.00	15.39 ± 1.10	0.99

The following model (Equation (5.8)) may explain the importance of •OH scavenging of Fe(II) for the steady-state hydroxyl radical concentration in the bulk liquid. In this model formation and utilization of •OH in bulk liquid by the dye, combination reactions of •OH, and scavenging of hydroxyl radical by Fe^{2+} are considered. Hydroxyl radical attack on dye intermediates and scavenging of •OH by H_2O_2 is not considered.

$$\frac{d[\bullet OH]}{dt} = k_{OH} - k''[dye][\bullet OH] - k_r[\bullet OH]^2 - k_2[Fe^{2+}][\bullet OH] + k_1[Fe^{2+}][H_2O_2] \quad (5.8)$$

where k_{OH} is •OH formation rate constant by the system (generator), k″ is second order reaction rate constant ($10^9 - 10^{10}$ M^{-1} s^{-1}) of dye with •OH, [dye] is the concentration of the dye (M), [•OH] is the concentration of hydroxyl radicals (M), k_r is second order reaction rate constant of •OH recombination reaction ($6x10^9$ M^{-1} s^{-1}), k_2 is second order reaction rate constant of •OH scavenging by Fe^{2+} ($3x10^8$ M^{-1} s^{-1}), k_1 is second order reaction rate constant of •OH formation via Fenton's reaction (76 M^{-1} s^{-1}).

When Fe^{2+} is at appreciable concentrations, it competes with the dye for •OH despite its lower bimolecular rate constant. As a result, working Fe^{2+} concentration was selected as 0.1 mM for Fe^{2+} catalyzed ultrasonic irradiation experiments.

5.2.3.2. Contribution of Fe^{2+} to Color Degradation

Figure 5.9. shows the improvement in decolorization of RB5 with the addition of 0.1 mM Fe^{2+}. The observed rate enhancement (nearly 5 fold) is again due to increased •OH formation. Hence, Fe^{2+} addition provides the same efficiency (40 per cent) as that of US in 1/6 times less contact.

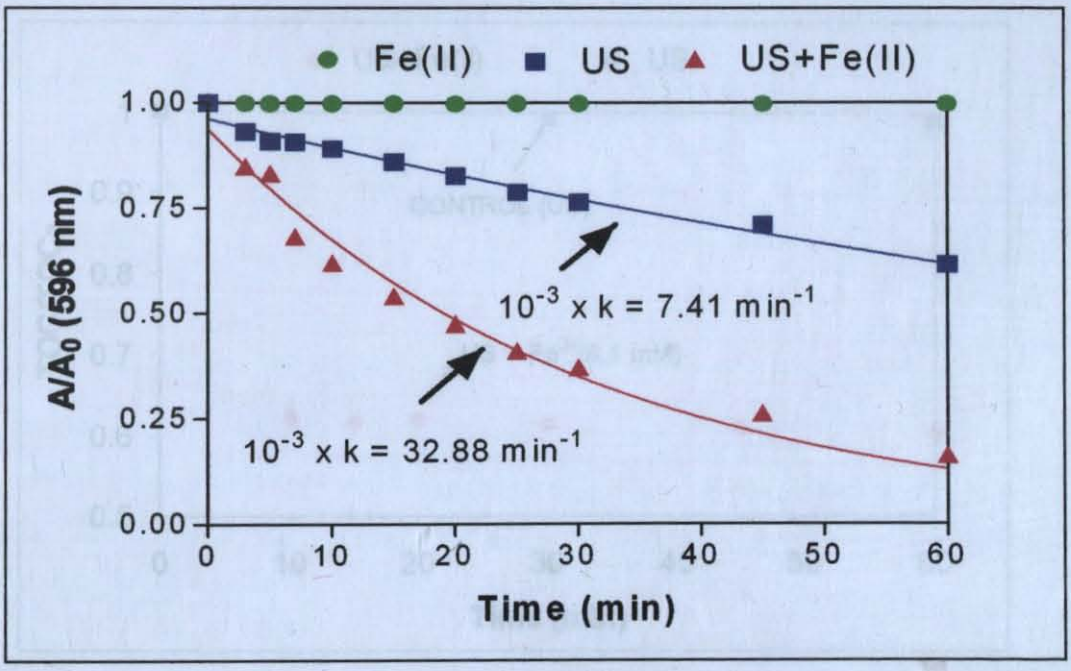

Figure 5.9. Profiles of color degradation of RB5 during US, Fe^{2+} (0.1 mM), and US+Fe^{2+}.

5.2.3.3. Contribution of Fe^{2+} to Dye Mineralization

The effect of Fe^{2+} addition (0.1 mM) on dye mineralization is presented in Figure 5.10. The remarkable enhancement in the overall degradation of the dye by Fe^{2+} addition shows that Fenton Reaction not only accelerated the destruction of the chromophore but that of all other compounds of the dye.

In the presence of 0.1 mM Fe^{2+}, the extent of mineralization was reached to its maximum (40 per cent depletion) and no further decrease was observed after 10 min. The steadiness of TOC removal after 10 min of reaction implies the depletion of Fe^{2+} (Equation (5.6)). Since the conversion of Fe^{3+} to Fe^{2+} was not possible without a source of UV light (see Chapter 2.1.1.1.4), additional •OH could not be generated in the absence of ferrous ion. As can be seen in Figure 5.9., the color of the dye continued to reduce probably due to the reaction with sonochemically produced •OH in bulk liquid, and this amount was not sufficient for mineralization (highly hydroxylated intermediates formed during irradiation are more hydrophilic than the parent molecule. Therefore, the degradation will slow down, because the only degradation pathway is the •OH oxidation in bulk liquid, they do not tend to accumulate at the interface of the bubble and •OH oxidation at the bubble-liquid interface can not be a degradation pathway anymore (Pétrier *et al.*, 2002)) .

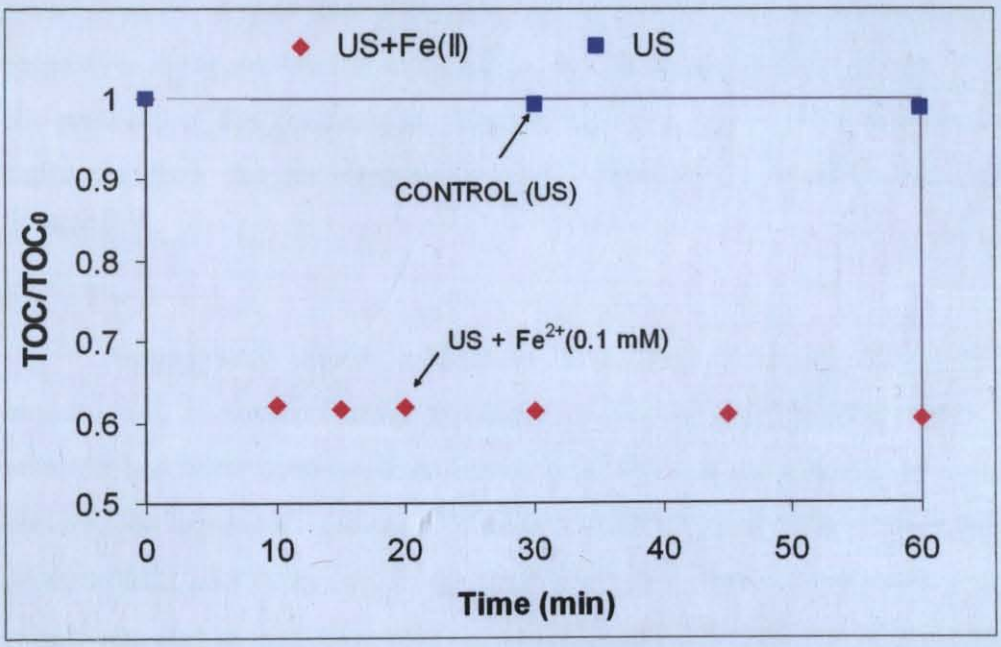

Figure 5.10. Total organic carbon degradation during ultrasonic irradiation of RB5 with (0.1 mM) or without Fe^{2+}.

The result of TOC depletion by Fe^{2+} catalyzed ultrasonic irradiation seems satisfactory but the disposal of sludge should be considered.

5.2.4. Conclusions

The addition of ferrous ion significantly increased ultrasonic decomposition of C.I. Reactive Black5 at 520 kHz. The Fenton process enhanced both the decolorization rate and mineralization to be attributed to the formation of additional •OH. The highest color degradation rate was observed in the presence of 0.1 mM Fe^{2+}, and further increases in Fe^{2+} concentration decreased the decolorization rate due to the scavenging of •OH by Fe^{2+}.

Although it is possible to obtain high decolorization and mineralization yields, final disposal of the ferrous ion requires additional treatment. Therefore, the system studied in Section 5.1. can be more reasonable for dye degradation. Higher degradation yields can be achieved in a shorter time by combining ultrasonic irradiation with the addition of strong oxidant O_3, which is also able to attack some intermediates such as organic acids.

CHAPTER 6. DEGRADATION AND TOXICITY REDUCTION OF TEXTILE DYESTUFF BY ULTRASOUND: APPLICATIONS IN SYSTEM II

This chapter is the paper entitled "Degradation and Toxicity Reduction of Textile Dyestuff by Ultrasound." which was published in *Ultrasonics Sonochemistry*, 10, 235-240, 2003.

6.1. Background

Effluents of textile dyeing processes are intensely colored and contaminated with high concentrations of chemical oxygen demand, suspended and dissolved salts and traces of recalcitrant material (Gurnham, 1965; Ince *et al.*, 1997). If improperly processed, these effluents not only deteriorate the aesthetics of receiving waters and may hinder the penetration of oxygen, but also pose significant threat to life forms upon hydrolysis of some dyes in the wastewater to form toxic products (Robinson *et al.*, 2001). The reason for the presence of dye residuals in wasted effluents is that some dyes have poor exhaustion capacities such that an important fraction of them is ultimately discharged with spent dyebaths.

Among such poorly exhausting dyes, those with azo bonds have the largest consumption in textile dyeing processes owing to their brilliant shades. Hence, much research has been conducted on methods of azo dye destruction, many of them being centered on advanced oxidation processes (AOP). Treatability of azo dye solutions by AOP, which generate hydroxyl radicals (•OH) via a variety of common methods, has been widely reported in the literature (Ince and Tezcanli, 1999; Arslan *et al.*, 2001; Gouldm and Groff, 1987). A less common way of onsite •OH generation is ultrasonic irradiation of the liquid. By such, the dissolved vapors and gases in the liquid are entrapped by cavitation

bubbles, which release very high temperatures during their adiabatic collapse (Suslick *et al.*, 1990; Dahlem *et al.*, 1998). In sonolysis of water containing hydrophilic compounds such as textile dyes, hydroxyl radicals are generated only by water fragmentation in the collapsing bubbles, and oxidative dye destruction is possible if the radicals are effectively ejected into the solution bulk. The efficiency of •OH diffusion into the aqueous phase is related to system parameters such as frequency, reactor geometry, presence of cavitation nuclei, and the ambient conditions (Mason and Cordemans, 1998; Mason *et al.*, 1990). The mechanism and kinetics of ultrasonic azo dye degradation has been recently investigated in pure dye solutions using simple compounds such as azo benzene and methyl orange (Joseph *et al.*, 2000; Destaillattes *et al.*, 2000).

The purpose of this study was to investigate the effectiveness of 520 kHz ultrasonic pressure waves on the destruction of textile dyestuff in aqueous solutions. The method involved exposure of three azo and one oxazine dye of various strengths to ultrasound for 4 h, during which effluent samples were analyzed for color, aromatic/olefinic content and Microtox toxicity. Test solutions were made in mass concentrations (rather than molar) to be consistent with actual dyeing recipes made of fixed mass concentrations of dyes and dyebath auxiliaries, dictated by the desired shade depth and not the structure of the dye (Pisa Corp., 2000). The test concentrations were selected by referring to typical dye concentrations found in dyeing mill effluents, and operation parameters were set in accordance with the maximum rate of color removal obtained during 1 h sonolysis of a model dye at various ultrasonic power and dye concentrations.

6.2. Materials and Methods

6.2.1. Dyes

Two "reactive" and two "basic" dyes were used as probe chemicals throughout the study. Color Index (C.I) codes, molecular properties, maximum visible absorption bands, characteristic chromophore, manufacturing source and the purity of commercially available products are presented in Table 6.1.

Table 6.1. Physicochemical and commercial properties of the test dyes

Chemical Structure C.I./Symbol	Vis-ABS/type Functional Gr	MW g mol^{-1}	Source/Purity
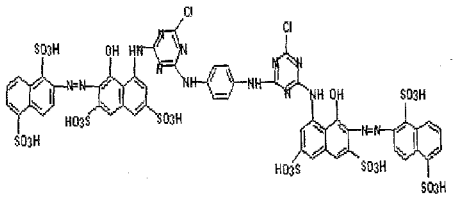 C.I.Reactive Red141 (RR141)	544 nm disazo 2x (–N=N-)	1791	BASF 75 %
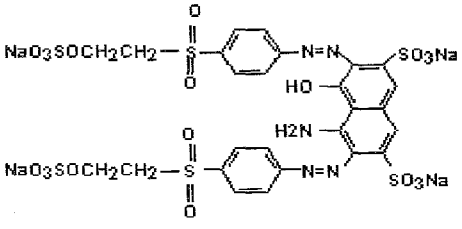 C.I. Reactive Black5 (RBk5)	596 nm disazo 2x(–N=N-)	991.8	DYESTAR- HOECHST 80-85 %
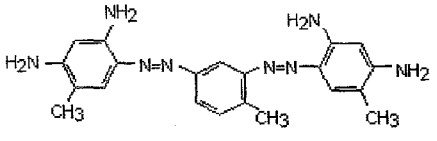 C.I. Basic Brown4 (BBr4)	464 nm disazo 2x(–N=N-)	461.4	Aldrich 40 %
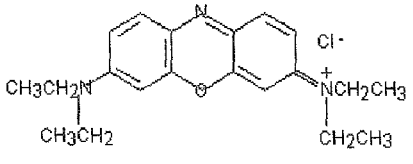 C.I. Basic Blue3 (BBl3)	654 nm oxazine 	359.9	Aldrich 50 %

No information was provided by the companies about the impurities except for the common knowledge that "basic" dyes contained heavy metals such as zinc and chromium (U.S. EPA, 1996). All of Microtox reagents and supplies were obtained from Azur Environment, UK.

6.2.2. Optimized System Parameters

Optimized system parameters used in this study (given in Chapter 4.2.2) are summarized in Table 6.2.

Table 6.2. Experimental parameters of System II

System	Transducer Frequency (kHz)	Reaction Volume (mL)	Power Density ($W\ mL^{-1}$)	Type of Gas / Flow Rate ($L min^{-1}$)
II	520	300	0.126	Ar / 1

6.2.3. Preparation of the Test Solutions

Stock dye solutions were prepared by dissolving 5 g of each dye in 1 L of boiling deionized water in accordance with dyeing recipes provided by a textile dyehouse for 5% shade depth (Pisa Corp., 2000). The reactive dyes were transformed to their hydrolyzed forms by adjusting the pH to 11 using 5 N sodium hydroxide, followed by heating to 90 °C. The reactive dye stock solutions were kept at that temperature for 6 hours for complete hydrolysis. Test solutions were made by diluting the stocks to typical effluent dye concentrations (20-60 mg L^{-1}) using deionized water followed by 1 h aeration. The pH of all test solutions was adjusted to a range of 5.5-6.5 prior to sonication.

It is well known that reactive dyes used for shading cellulosed fibers have poor exhaustion capacities, while the majority of basic dyes used in shading of synthetic fibers are fixed quite well on the fabric (U.S. EPA, 1996). Despite this fact, the degradability of basic dyes was investigated as well, because even at very low concentrations most of them are toxic in the aquatic environment, owing to traces of heavy metals in the dye matrix (U.S. EPA, 1996).

6.2.4. Analytical

Spectrophotometer

The optical absorption spectra (200-800 nm) of the test solutions during sonication were recorded by a Unicam. Helios Alpha/Beta double beam spectrophotometer through a 1 cm optical path length.

Toxicity

Toxicity of the dye solutions was determined using a Microtox Model 500 Analyzer, which utilizes freeze-dried luminescent bacteria (*V. fisheri*) as test organisms. The test system is based on the principle that bacterial luminescence is tied directly to cell respiration, so that any inhibition of cellular activity (due to toxicity) results in a reduction in the degree of luminescence. The Microtox analyzer is made of an array of sample wells for holding dilutions of bacterial suspensions, and a photometer to measure the light output of *V. fisheri* at 0, 5 and 15 min after contact with the toxicant. Light readings are compared to those of control bacteria (healthy) to determine the inhibition of light emission, and to estimate the EC_{50} of the sample. (EC_{50} is defined as the effective concentration of the toxicant- expressed as percentage relative to the original sample strength- that causes a 50 per cent reduction in the light output of the test organisms during the designated time interval.) Sample preparation, osmotic adjustment and serial dilution procedures were carried out by reference to the Basic Protocol of the Microtox assay (Microtox Manual, 1992). A photograph of Microtox Analyzer is given in Figure 6.1.

Figure 6.1. Photographic view of the Microtox toxicity analyzer.

6.2.5. Experimental

Determination of Dye Degradability

Three hundred milliliter of pre-aerated dye solutions of 20 mg L^{-1} (working dye concentration) were irradiated at 0.126 W mL^{-1} (optimum power density) for 4 h to monitor absorption abatements at the visible and UV_{254} bands. The degradability of the dyes was also assessed by monitoring the toxicity of the reactor effluents at various intervals during sonication. Argon was bubbled into the reactor at a flow rate of 1 mL min^{-1} to promote cavity formation and to overcome degassing.

Toxicity Measurements

The toxicity of all dye solutions was determined prior to sonication, and those that were found toxic were monitored throughout the contact time to follow the trends for detoxification. "Color correction" was found necessary in those samples collected during the first 30 minutes of irradiation, and was performed in accordance with the procedure

described in the Basic Protocol for colored samples (Microtox Manual, 1992). The referred protocol is aimed to overcome the potential hindrance of bacterial luminescence by the visible absorption of the dye solution.

During the first 30 min sonication, all dye solutions had color which could interfere with bacterial luminescence. So, those samples were re-analyzed according to the color correction test. Very special cuvettes were used for color correction. They are made up of two glass cuvettes, one within the other to prevent the contact of the sample and the bacteria. So the interference of color was easily determined by eliminating the probable toxicity of the sample o bacteria. First, the bacterial suspension was transferred into the inner chamber, and the non-toxic dilution water was transferred into the outer chamber and the luminescence of the bacteria was recorded by Microtox Analyzer. Then, dilution water was discarded from the outer chamber and the colored sample was transferred and the bacterial luminescence was recorded again. The results were added to the old data and re-analyzed by Microtox software.

6.3. Results and Discussion

6.3.1. Selection of Working Dye Concentration

The working dye concentration was selected by monitoring the rate of color decay in 20, 30 and 40 mg L^{-1} of RB5 during 1 h sonication at 0.126 W mL^{-1} (optimum system conditions was given in Chapter 4.2.2.). The degradation of color was found to follow pseudo-first order kinetics with respect to the absorption maximum of the dye in the visible band. Comparison of color degradation rate profiles in three concentrations of RB5 and estimated rate coefficients are presented in Figure 6.2.

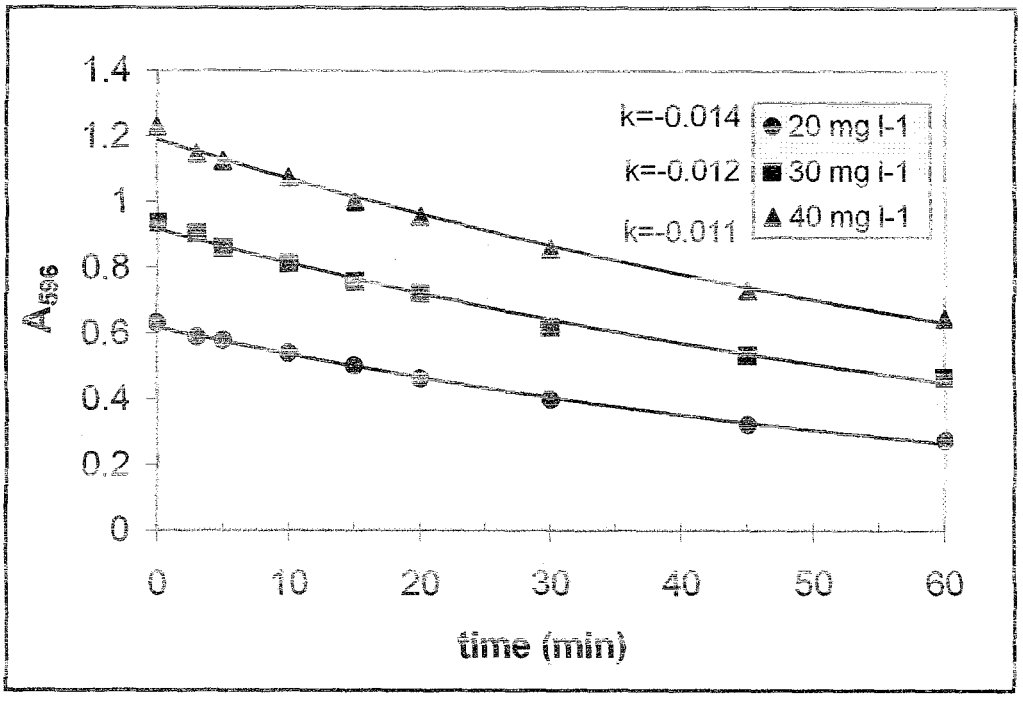

Figure 6.2. Selection of the working dye concentration based on color decay rates. The solid lines represent the fit of Equation (4.2) to each data set with $R^2 \geq 0.98$.

The rate coefficient was found to be only slightly sensitive to the mass concentration of the dye, being a maximum at 20 mg L^{-1}, which was therefore selected as the working initial dye concentration.

6.3.2. Dye Degradation by Color and Organic Carbon

The degradation of all dyes during the reaction period was assessed by absorption abatements at two bands: the visible, which is responsible for the chromophoric components and the UV-254, which represents the absorption of aromatic and/or olefinic carbons in the dye. The rate of absorption decay at 254 nm did not follow a common kinetic pattern as it did in the visible band as a consequence of aromatic intermediate formation by oxidative degradation of the dyes. Moreover, it was found that complete decolorization was achieved in all dye solutions within 150 min, while 4 h of sonication was required for appreciable degrees of aromatic/olefinic carbon destruction. Comparative fractions of color and organic component decay in 2 and 4 hours of sonication respectively are listed in Table 6.3.

Table 6.3. Fractions of color and organic carbon removal during 2 and 4 hours of sonolysis and estimated coefficients of color decay

Dye	$A_{visible}$		A_{254}
	reduction in 2 h	$kx10^{-3}$ (min^{-1})	reduction in 4 h
RR141	82.9 %	14.8	11.2 %
RB5	81.1 %	13.9	18.8 %
BB4	86.3 %	15.6	49.0 %
BB3	99.8 %	53.7	92.7 %

Note that the degree of UV-254 destruction in the first three azo dyes is significantly lower than that of color, signifying the priority of OH attack on N=N bonds and the increased mass of aromatic intermediates upon oxidation, which likely absorb UV light at 254 nm. The fact that the basic dye BB3 bleached much faster than the others and the abatement in its UV-254 band was close to that in the visible band may be attributed to its non-azo character, the oxazine chromophore and/or its lower molecular mass (Tezcanli-Guyer and Ince, 2003).

The effect of sonolysis on the absorption of the dyes in 200-800 nm band is presented in Figure 6.3. Note that the two reactive dyes had absorption peaks at 310 nm in addition to their absorption in the visible band, and both of them faded with increased contact. On the other hand, the spectra of the basic dyes were different; while BB3 had a peak at 253 nm, which also faded with time, BBr4 had no distinct peaks in the same region. Note also that despite the slight pH reduction (5-7 per cent) observed in all test solutions during the first 15 min of contact (indicating the formation of organic acids), no shift in the absorption peaks occurred during the same period.

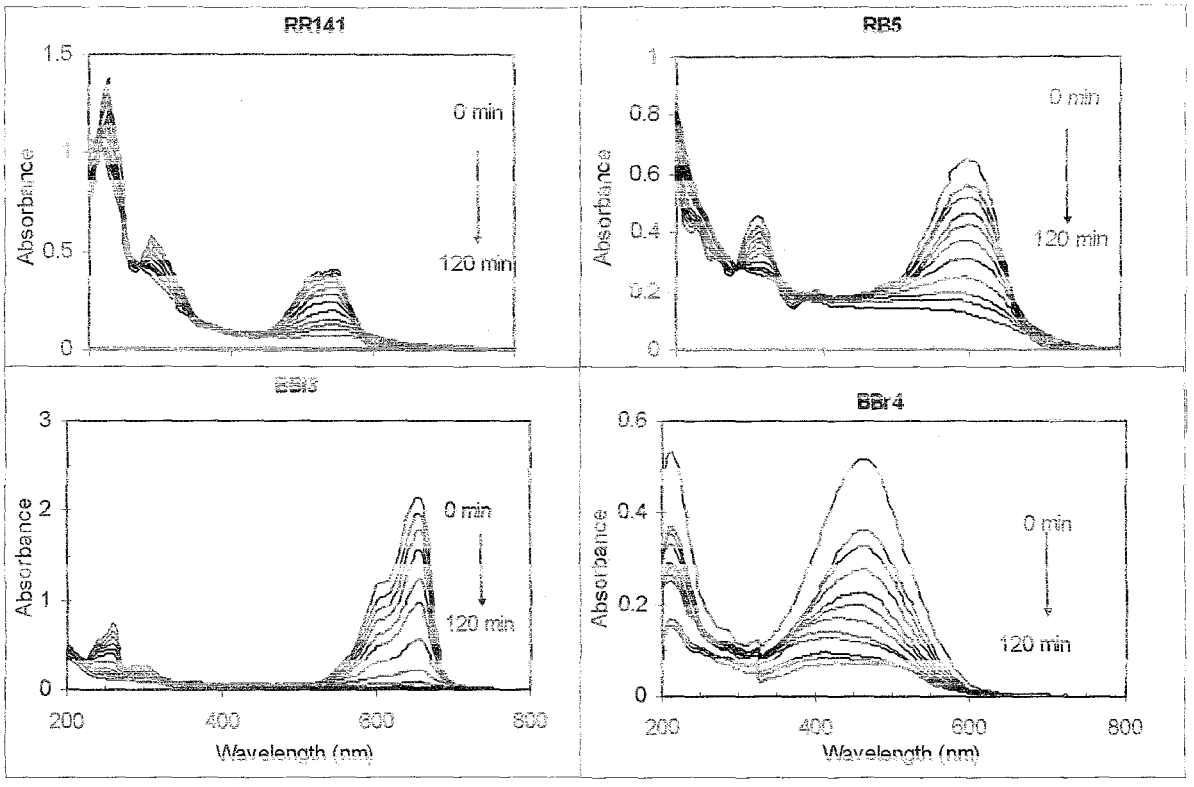

Figure 6.3. Spectral changes in 20 mg L^{-1} of the test dyes during 1 h exposure to US.

6.3.3. Dye Degradation by Toxicity

Five and fifteen min toxicity of the dye solutions prior to sonolysis showed that RR141 and RB5 were non toxic at 20 and 30 mg L^{-1}, while BB3 and BB4 were toxic at both concentrations. Hence, toxicity was monitored only in the latter two dyes during 240 min of sonolysis. Estimated values of EC_{50} were converted to a relative index TI as:

$$TI = \frac{\%\,EC\ 50\,(t=0)}{\%\,EC\ 50\,(t=t)} \qquad (6.1)$$

where TI is the relative toxicity index, and EC50 is the 5-min Microtox toxicity of the sample.

Besides these dyes the toxicity of representative dyes of acid group "C.I. Acid Black I" and "C.I Acid Orange 7" were also investigated and found as non-toxic. These result are consistent with the data given by Little and Lamb (1972). They investigated the

effect of 46 selected dyes on the Fathead Minnow and the toxicity results were expressed as LC_{50}, 96 Hour (mg l^{-1}) (the concentration that causes mortality to 50 per cent of the test population after 96-hour exposures). In this report, the toxicity of C.I. Acid Orange 7, C.I. Acid Black 1, C.I. Basic Brown 4, C.I. Basic Blue 3 were reported as 165, >180, 5.6, and 4 respectively (the higher the LC_{50}, the less toxic the sample is).

Comparable profiles of color, organic component and toxicity decay in the two originally toxic dyes are presented in Figure 6.4. It was found that despite the slower rate of color and organic carbon degradation in BB4 than that in BB3, the reduction in the toxicity of the former was faster, with complete detoxification before color decay was completed. This implies that toxicity causing components in BB4 were primarily due to the chromophoric characteristics of the dye, which may have been further enhanced by the addition of some impurities in the commercial product (Tezcanli-Guyer and Ince, 2003).

Since some of these impurities are made of heavy metals, it is likely that changes in the valence state of the metals upon their potential combination with organic sites resulted in detoxification of the effluents. The observed rise in toxicity after 120 min of irradiation may be attributed to the production of some toxic intermediates at this stage and the accumulation of hydrogen peroxide upon enhanced sonication. The detoxification of BB3 proceeded at a slower rate than that of BB4, implying that toxicity was due both to color and other aspects of the structure, but no further toxicity rise was observed once the effluents were totally detoxified.

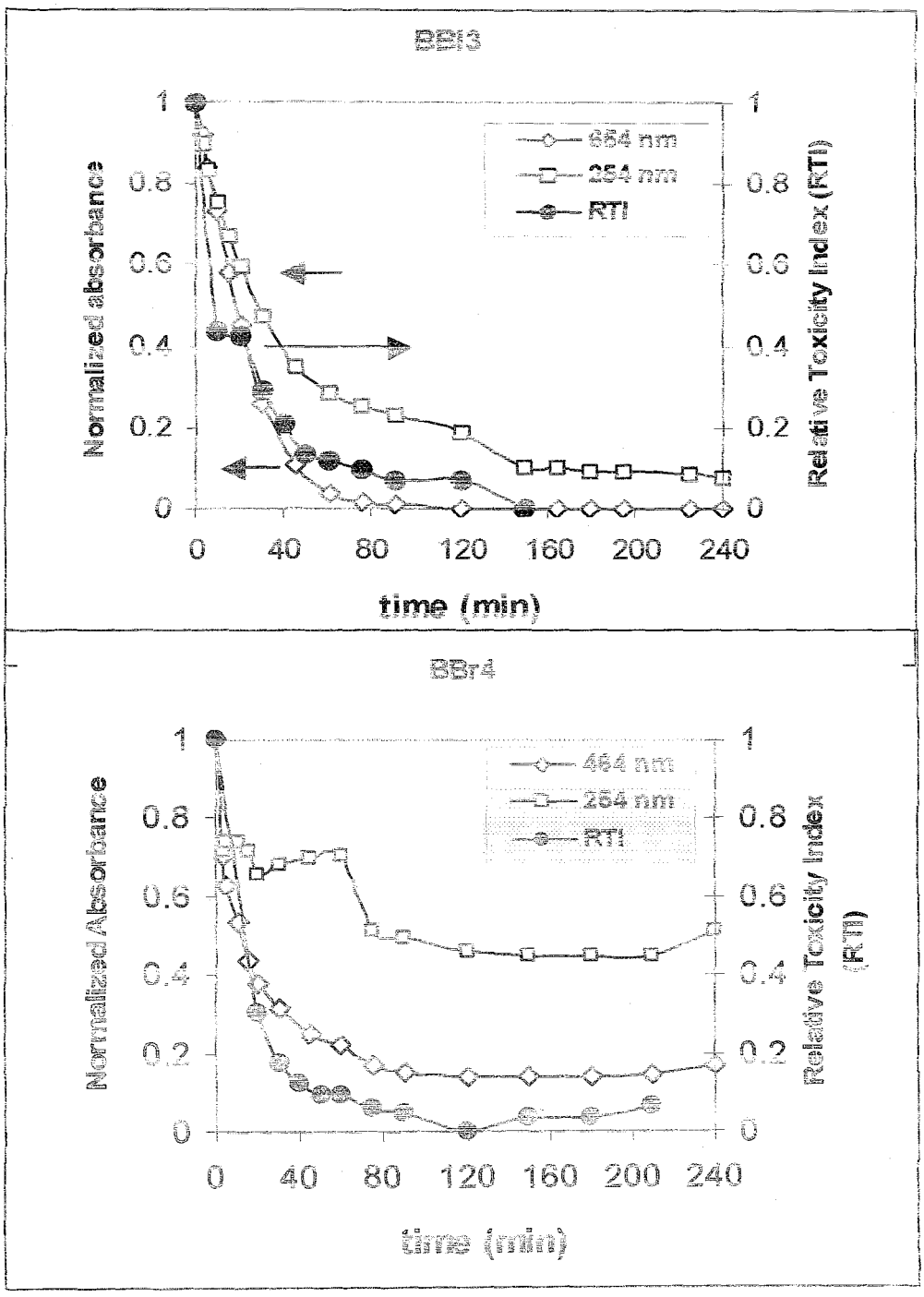

Figure 6.4. Relative profiles of color, organic carbon and toxicity degradation in 20 mg L^{-1} of C.I.Basic Blue3 and C.I. Basic Brown4 during 4 h exposure to ultrasound.

6.4. Conclusions

Textile dyehouse effluents are of significant environmental concern, due to the presence of dye residuals in wasted dyebaths. The study presented herein signifies features of dye degradability by ultrasonically generated hydroxyl radicals. It was shown that the degradation of azo and oxazine dyes is initiated by color decay followed by the destruction of organic and/or aromatic carbons in the molecule. The rate of color degradation was first order in the visible absorption of the dyes and slower in azo dyes than that in oxazine-origin dye structures. The degradation of aromatic/olefinic contents in azo dyes proceeded at a slower rate than that of color, as a consequence of increased mass of organic intermediates, which absorb at the UV-254 band. The slower destruction of aromatic/olefinic carbons in azo dyes than that of color was attributed to the priority of hydroxyl radical attack on the N=N bonds, and to the formation of numerous oxidation intermediates of organic character during the course of dye degradation. Toxicity analysis of the dye solutions prior to sonolysis revealed that "reactive" dyes were non-toxic, but "basic" ones were toxic at the test concentrations employed in this study. It was also shown that if the parent dye were toxic, the degradation products were less so, and total toxicity removal was accomplished within shorter contact than necessary for total dye degradation.

CHAPTER 7. DYE-STRUCTURE RELATED DEGRADABILITY OF TEXTILE DYESTUFF IN WASTED DYEBATHS: APPLICATIONS IN SYSTEM I

7.1. Sonochemical Destruction of Textile Dyestuff in Wasted Dyebaths

The study presented in this chapter is a copy of the article entitled "Sonochemical Destruction of Textile Dyestuff in Wasted Dyebaths" which was published in *Coloration Technology*, 5, October, 2003.

7.1.1. Background

Effluents of textile dyeing processes contain residuals of dyebath auxiliaries and unfixed dyestuff, which are wasted with exhausted dyebaths upon completion of a dyeing batch. Dyehouse wastewaters, therefore, are distinguished with high concentrations of chemical oxygen demand (COD), solids, color and traces of recalcitrant material (Gurnham, 1965; Boeniger, 1980). If improperly processed, they not only deteriorate the aesthetics of receiving waters, but also threaten aquatic life forms via hydrolysis and reduction reactions of some dyes to form toxic and carcinogenic end products (Brown *et al.*, 1993).

Dyebath effluent can be effectively treated with advanced oxidation processes (AOP), where it undergoes oxidative degradation via hydroxyl radicals (•OH) (Ince and Tezcanli, 2001; Arslan and Balcioglu, 2000). Radical species in AOP are produced onsite by common methods such as ultraviolet (UV) irradiation of the solution with hydrogen peroxide, titanium dioxide, Fenton's reagent, and ozone, or less commonly by ultrasonic irradiation. During sonication of a liquid, dissolved gases and water vapour are entrapped by cavitation bubbles, which expand at rarefaction cycles of the bubbles and release extreme temperatures upon adiabatic collapse (Suslick, 1990; Mason *et al.*, 1992). Under

these conditions, bubble contents are pyrolytically fragmented into radical species, some of which diffuse into the aqueous phase to initiate a series of oxidation reactions called "sonochemistry" (Ince *et al.*, 2000).

There are three possible mechanisms by which organic impurities in sonicated water are destroyed: i) pyrolytic fragmentation within the bubble if the substance is hydrophobic; ii) supercritical phase reactions at the gas-liquid interface; or iii) oxidation by hydroxyl radicals (•OH) and other reactive species in the bulk liquid (Ince *et al.*, 2000; Serpone *et al.*, 1994; Joseph *et al.*, 2000; Mason and Cordemans, 1996). Experience has shown that medium frequency ultrasound (300-600 kHz) is more favorable for sonochemical effects in the aqueous phase than short frequencies (20-100 kHz), and radical production yields are enhanced via bubbling of the liquid with a proper gas and/or by adding solid catalysts to overcome the effect of degassing and to promote cavity formation (Serpone *et al.*, 1994).

Advanced oxidation of textile dyes by ultrasonic techniques is an emerging field of research. The studies reported in the literature involve sonication of azo dye-deionized water solutions with medium frequency ultrasound during gas injection and/or catalysis with Fenton's agent, titanium dioxide or ozone (Joseph *et al.*, 2000; Destaillattes *et al.*, 2002; Vinodgopal *et al.*, 1998; Lorimer *et al.*, 2001). There is mutual agreement in all for the initiation of oxidation reactions by hydroxyl radical attack on the N=N double bond in the aqueous phase and that mineralization is a much longer process, starting only after bleaching is fairly complete. There are no reported studies so far on sonolytic degradation of dyestuff in spent dyebath effluents, which contain residuals of organic and inorganic auxiliaries added to enhance the efficiency of the process and the fixing capacity of the dye on the fiber.

The purpose of this study was to investigate the degradation of textile dyestuff in wasted dyebaths by ultrasonic irradiation at 300 kHz and to assess the impacts of dye structure, dyebath auxiliaries, pH and H_2O_2 addition on the rate of color decay and dye degradation. Three model dyes were selected from "basic" and "reactive" classes of commercial dyestuff, the reactive dye having a benzoquinone component, and the two basic dyes having a both common (azo bond) and uncommon chromophore (phenazine).

The dyebaths were prepared by reference to dyeing recipes provided by a commission-based dyehouse for 2 % shade depth (Pisa Corp. 2000). The degradation of dyebaths was monitored by the reduction in the visible absorption and chemical oxygen demand (COD) of the test solutions during irradiation with ultrasound.

7.1.2. Materials and Methods

7.1.2.1. Dyes and Dyebaths

The test dyes C.I. Reactive Blue19 (RB19), C.I. Basic Blue16 (BB16) and C.I. Basic Brown4 (BB4), were obtained from Aldrich in 45, 70 and 40 per cent purity, respectively. Note that the chromophoric components are different in all dyes: RB19 is made of an anthraquinone structure, BB16 contains a phenazine-monoazo component and BB4 is made of two azo linkages between aryl groups. Upon preparation of the dyebaths in accordance with the provided recipes, the bath containing RB19 was heated to 90°C following pH adjustment to 11, and kept at this temperature for 6 hours to allow complete hydrolysis of the dye and to simulate actual reactive dyebaths. H_2O_2 (35 per cent w/w) and all other reagents were analytical Merck grade. The quality of simulated dyebaths and the chemical structure of the probe dyes contained are presented in Table 7.1.

Stock test solutions were prepared by 67-fold (v/v) dilution of the dyebaths presented in Table 7.1. with tap water to reproduce batch dyeing effluents post the final washing operation (Ince and Tezcanli, 1999). The dilution water contained 65.6 mg L^{-1} alkalinity as $CaCO_3$, and 33.8 mg l^{-1} chloride. All stock solutions following 2 h aeration were transferred to glass bottles, capped and maintained in the dark at 4°C. The final composition of the stocks that simulate actual dyebath effluents is presented in Table 7.2.

Table 7.1. Composition of simulated dyebaths and chemical structure of the dyes contained

DYEBATH COMPOSITION[1]	DYE STRUCTURE
SYNONYM: **DB1** Max.Abs: 592 nm Dye: C.I. Reactive Blue19 (2 g/L) Acetic Acid: 0.3 g L^{-1} Sequestering agent[2]: 0.5 g L^{-1} Anti-creasing agent [3]: 1 g L^{-1} NaCl: 60 g L^{-1} Buffering agent [4]: 20 g L^{-1} Temp: 90 °C pH=11.1	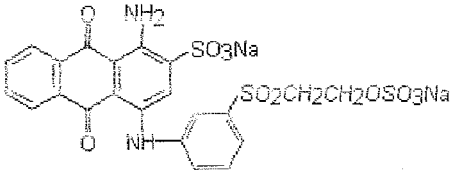 **C.I. Reactive Blue19** Type: anthraquinone
SYNONYM: **DB2** Max.Abs: 552 nm Dye: C.I. Basic Blue16 (2 g L^{-1}) Leveling agent[5]:1 g L^{-1} Acetic Acid:1.5 g L^{-1} Na_2SO_4: 6 g L^{-1} Temp: 120 °C pH=4.5	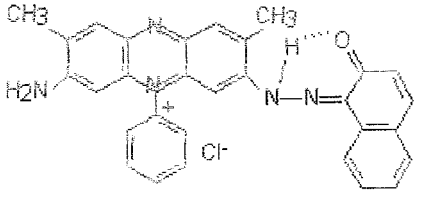 **C.I. Basic Blue16** Type: phenazine-monoazo
SYNONYM: **DB3** Max. Abs: 448 nm Dye: C.I. Basic Brown4 (2 g L^{-1}) Leveling agent:1 g L^{-1} Acetic Acid:1.5 g L^{-1} Na_2SO_4: 6 g L^{-1} Temp: 120 °C pH=4.5	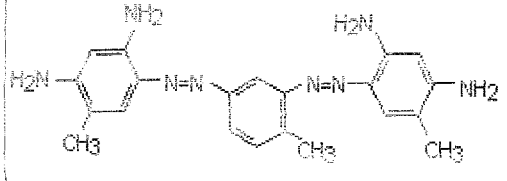 **C.I. Basic Brown4** Type: phenyl-disazo

[1]The concentration of auxiliaries is process and company specific.
[2]Verolan NBO
[3]Slipper
[4]Na_2CO_3
[5]Avolan IV

Table 7.2. Final compositions of the simulated dyebaths following 2-h aeration

DYEBATH COMPOSITION	Final Concentration
SYNONYM: **DB1**	
Max.Abs: 592 nm	
Dye: C.I. Reactive Blue19	0.048 mM
Acetic Acid	0.005 g L^{-1}
Sequestering agent	0.008 g L^{-1}
Anti-creasing agent	0.015 g L^{-1}
NaCl	0.900 g L^{-1}
Buffering agent	0.300 g L^{-1}
pH	9.4
SYNONYM: **DB2**	
Max.Abs: 552 nm	
Dye: C.I. Basic Blue16	0.059 mM
Leveling agent	0.015 g L^{-1}
Acetic Acid	0.022 g L^{-1}
Na_2SO_4	0.090 g L^{-1}
pH	6.7
SYNONYM: **DB3**	
Max. Abs: 448 nm	
Dye: C.I. Basic Brown4	0.065 mM
Leveling agent	0.015 g L^{-1}
Acetic Acid	0.022 g L^{-1}
Na_2SO_4	0.090 g L^{-1}
pH	6.7

7.1.2.2. Optimized System Parameters and Procedure

Optimized system parameters are given in Table 7.3. Optimization of system parameters were presented previously in Section 4.2.1.

Table 7.3. Experimental parameters of System I

System	Transducer Frequency (kHz)	Reaction Volume (mL)	Power Density (W mL^{-1})	Type of Gas / Flow Rate (L min^{-1})
I	300	100	0.184	Ar / 1

Sonication

Two test samples differing in pH (4.5 and 3.0) were prepared by adding adequate amounts of 0.1 N H_2SO_4 to 100 mL aliquots withdrawn from the stocks. The natural pH of the DB1, DB2, and DB3 (after 67-fold dilution from the stock dyebath) was 9.4, 6.7 and 6.7, respectively. The experiments involved 1 h sonication of these aliquots in the absence and presence of 7 mM H_2O_2 during argon bubbling at 1 l min^{-1}. Effluent samples were collected at 0, 3, 5, 10, 15, 20, 30, 45 and 60 min to run spectrophotometric analysis. In addition, the effluents collected at t=0 and t=60 min were analyzed for COD and H_2O_2.

Analytical

The absorption spectra of raw and sonicated samples were monitored at 200-800 nm using a Unicam, Helios Alpha/Beta double beam spectrophotometer through a 1 cm path length. Hydrogen peroxide was analyzed by the "triodide" method (Klassen *et al.*, 1994). COD was determined by reference to the Standard Methods of Water and Wastewater Analysis (APHA, 1992), and that of H_2O_2 containing samples was estimated by subtracting the COD of residual H_2O_2 from that of the sample (Kang *et al.*, 1999). The interference of chlorine in COD analysis was overcome by the addition of excess Hg_2SO_4 to the COD reagent.

7.1.3. Results and Discussion

7.1.3.1. Rate of Color Decay and the Effect of pH

It was found that the initial pH of the test solutions made no difference in their UV-visible spectra. However, a slight pH reduction was observed during the first 10 min of sonication (upon formation of organic acids) in samples originally at pH 4.5, while no variations were recorded in those buffered to pH 3. Changes in the UV-visible spectra of the test samples originally at pH=4.5 during 1 h irradiation are presented in Figure 7.1.

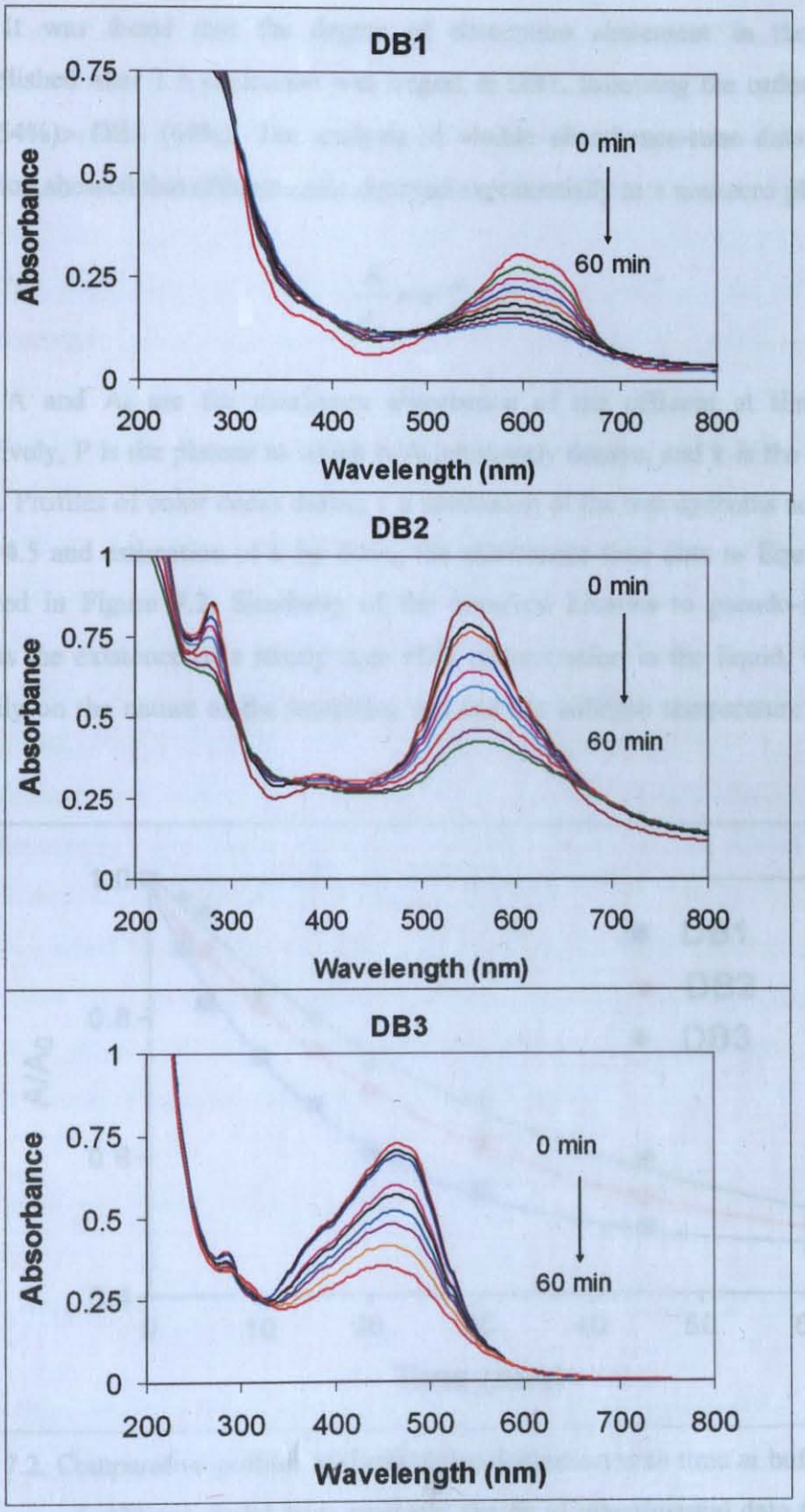

Figure 7.1. UV-Visible absorption spectra of the dyebaths (pH 4.5) at 0, 3, 5, 10, 15, 20, 30, 45 and 60 min of sampling.

It was found that the degree of absorption abatement in the visible band accomplished after 1 h sonication was largest in DB1, following the order: DB1 (68%)> DB2 (54%)> DB3 (49%). The analysis of visible absorbance-time data by non-linear regression showed that effluent color decayed exponentially to a non-zero plateau as:

$$\frac{A}{A_0} = e^{-kt} + P \qquad (7.1)$$

where A and A_0 are the maximum absorbance of the effluent at time t and zero, respectively, P is the plateau to which A/A_0 ultimately decays, and k is the decay constant (min^{-1}). Profiles of color decay during 1 h sonication of the test dyebaths adjusted initially to pH=4.5 and estimation of k by fitting the absorbance-time data to Equation (7.1). are presented in Figure 7.2. Similarity of the observed kinetics to pseudo-first order law suggests the existence of a steady-state •OH concentration in the liquid, which depends primarily on the nature of the saturating gas and the collapse temperature (Joseph *et al.*, 2000).

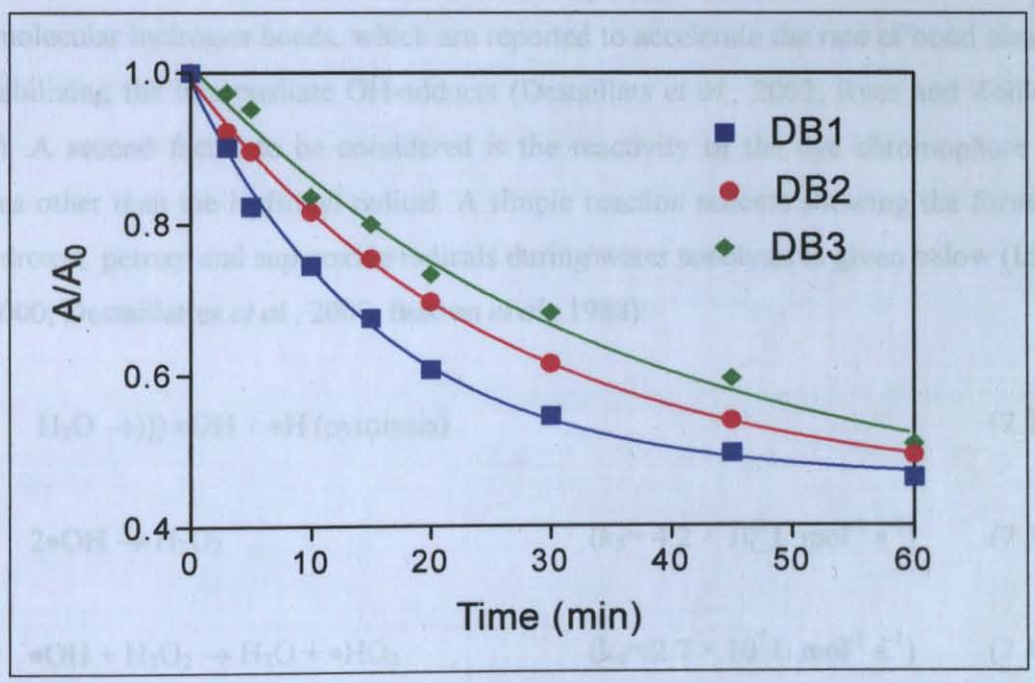

Figure 7.2. Comparative profiles of dyebath decolorization with time at buffered (pH=4.5) conditions. Solid lines represent the fit of experimental data to Equation 7.1 with k_{DB1}=0.062 min^{-1}, k_{DB2}=0.038 min^{-1}, k_{DB3}=0.028 min^{-1}.

The difference in the bleaching rates of DB2 and DB3, which are identical in their auxiliaries (Table 7.2.), must be due merely to differences in the structure and molar concentration of the dyes. The faster degradation of DB2 can be attributed to the combined effects of: i) the hydroxyl group in α-position to the azo bond that favors the hydrazine against the azo structure (hydrazine is more reactive with secondary radicals such as $\bullet HO_2/\bullet O_2^-$ (Nappolian *et al.*, 2002; Buxton *et al.*, 1988)); and ii) a relatively lower initial dye concentration (0.059 mM as opposed to 0.065 mM in DB3). On the other hand, DB1 (with a non-azo dye) bleached faster than both of DB2 and DB3 despite the apparent disadvantages of the dyebath, i.e. having a larger quantity of carbonates and chlorides (both of which are scavengers of OH radicals) and a lower reactivity coefficient of benzoquinones (i.e. the chromophore of the dye) with hydroxyl radicals than that of azobenzene or azo bonds ($k^{\bullet OH}_{benzoq}=1.2x10^9\ M^{-1}\ s^{-1}$, $k^{\bullet OH}_{azobenz}=2x10^{10}\ M^{-1}\ s^{-1}$ (Buxton *et al.*, 1988). Although an apparent advantage of DB1 is its relatively low initial dye concentration, it is most likely that there were more important factors affecting the overall enhancement of color degradation in the dyebath. One of these might be the potential of NH_2 substituents in α-position to the carbonyl group of the dye chromophore to form intramolecular hydrogen bonds, which are reported to accelerate the rate of bond cleavage by stabilizing the intermediate OH-adducts (Destaillats *et al.*, 2002; Rves and Zollinger, 1992). A second factor to be considered is the reactivity of the dye chromophore with species other than the hydroxyl radical. A simple reaction scheme showing the formation of hydroxyl, peroxy and superoxide radicals during water sonolysis is given below (Ince *et al.*, 2000; Destaillattes *et al.*, 2000, Buxton *et al.*, 1988):

$$H_2O \rightarrow))) \bullet OH + \bullet H \text{ (pyrolysis)} \qquad (7.2)$$

$$2\bullet OH \rightarrow H_2O_2 \qquad (k_3 = 4.2 \times 10^9\ L\ mol^{-1}\ s^{-1}) \qquad (7.3)$$

$$\bullet OH + H_2O_2 \rightarrow H_2O + \bullet HO_2 \qquad (k_4 = 2.7 \times 10^7\ L\ mol^{-1}\ s^{-1}) \qquad (7.4)$$

$$\bullet HO_2 + H_2O_2 \rightarrow H_2O + \bullet O_2^- + \bullet OH \qquad (k_5 = 5.0 \times 10^{-1}\ L\ mol^{-1}\ s^{-1}) \qquad (7.5)$$

$$\bullet O_2^- + H_2O_2 \rightarrow \bullet OH + O_2 + OH^- \qquad (k_6 = 1.3 \times 10^{-1}\ L\ mol^{-1}\ s^{-1}) \qquad (7.6)$$

Although $\bullet HO_2$ and $\bullet O_2^-$ are selective and less powerful than $\bullet OH$ as oxidizing agents, they are more stable and unlike $\bullet OH$ may accumulate in the aqueous phase. Moreover, a rate coefficient of $1x10^9$ M^{-1} s^{-1} is reported for the reaction of $\bullet HO_2/\bullet O_2^-$ pair with benzoquinone, while no reaction was observed with azobenzene or azo dyes (Buxton *et al.*, 1988). As a consequence, the more rapid rate of decolorization in DB1 despite the larger presence of $\bullet OH$ scavenging species (which are not completely destroyed at pH 4.5), and the lower reactivity of the dye chromophore with hydroxyl radicals must be due to combinative effects of α-NH_2 substituents, selectivity of superoxide radicals in favor of benzoquinone structures, and a lower initial dye concentration.

Reactive Dyebath matrix had an adverse effect on dye decolorization, while there was no significant change in decolorization at both non-buffered basic dyebath solutions. The scavenging effect of buffering agent (Na_2CO_3, 0.300 $g.L^{-1}$) was significant during sonication of non-buffered DB1 solutions. Alkalinity of tap water and the auxiliaries of basic dyebath solution had no adverse effect on dye bleaching. When the dyebaths were buffered to pH 3, the rate of bleaching in all slowed down, as apparent by estimated kinetic coefficients listed in Table 7.4. (Note, however, that the deceleration in DB3 is not statistically significant within 95% confidence.) Since reaction of OH radicals with aromatic compounds occurs at diffusion-controlled rates and $\bullet OH$ scavenging effects of carbonate/bicarbonate species are minimized at pH=3, retarded degradation rates in highly acidic solutions must be due to high concentrations of proton, as was reported in the literature for photocatalytic degradation of Reactive Blue4 (Nappolian *et al.*, 2002).

Table 7.4. Kinetic coefficients of color degradation at non-buffered and buffered conditions during sonication

DYEBATH	Condition[1]	$kx10^{-3}$ min^{-1}	R^2	*P*
DB1	N (pH=9.41)	0.30 ± 16.00	0.91	-
	B (pH=3.04)	29.64 ± 1.93	0.99	0.13
	B (pH=4.50)	62.99 ± 4.20	0.99	0.46
DB2	N (pH=6.60)	16.44 ± 5.70	0.98	0.64
	B (pH=3.06)	13.40 ± 4.42	0.99	0.05
	B (pH=4.62)	38.43 ± 1.52	0.99	0.44
DB3	N (pH=6.69)	16.16 ± 4.19	0.99	0.20
	B (pH=3.06)	17.82 ± 7.73	0.98	0.22
	B (pH=4.78)	28.93 ± 5.59	0.99	0.41

[1] The symbols "N" and "B" refer to non-buffered and buffered (pH=3 and pH=4.5) test solutions, respectively.

7.1.3.2. Effect of Hydrogen Peroxide

The rate of color removal in the dyebaths was accelerated at both pH test levels by H_2O_2 addition, which was shown to form O_2H and O_2^- radicals upon reaction with aqueous phase hydroxyl radicals (Equations (7.4)-(7.5)). Kinetic coefficients of color degradation at non-buffered and buffered conditions during sonication in the presence of 7 mM H_2O_2 is given in Table 7.5. Comparative rates of sonolytic color decay (and corresponding rate coefficients) with and without H_2O_2 are presented in Figure 7.3. Note that the same kinetic model governed H_2O_2-added reactions as those without H_2O_2.

Table 7.5. Kinetic coefficients of color degradation at non-buffered and buffered conditions during sonication after the addition of 7 mM H_2O_2

DYEBATH	Condition[1]	kx10^{-3} min^{-1}	R^2	*P*
DB1	N (pH=9.41)	-	-	-
	B (pH=3.04)	41.64 ± 3.38	0.99	0.17
	B (pH=4.50)	67.04 ± 8.10	0.98	0.11
DB2	N (pH=6.60)	-	-	-
	B (pH=3.06)	30.33± 3.72	0.99	0.04
	B (pH=4.62)	41.32 ± 2.28	0.99	0.32
DB3	N (pH=6.69)	-	-	-
	B (pH=3.06)	33.30 ± 3.73	0.99	0.21
	B (pH=4.78)	33.46 ± 6.98	0.98	0.20

[1] The symbols "N" and "B" refer to non-buffered and buffered (pH=3 and pH=4.5) test solutions, respectively.

Although color removal rates were faster during sonication at pH=4.5, the effect of H_2O_2 on color degradation was more pronounced at pH=3. Color removal rates during H_2O_2 coupled ultrasonic irradiation were higher at pH=4.5 but the increase in color degradation rates were higher at pH=3. This result may be attributed to the enhanced formation of H_2O_2 (and $^{\bullet}HO_2/^{\bullet}O_2^-$ radicals) at pH 3 (Jiang *et al.*, 2002).

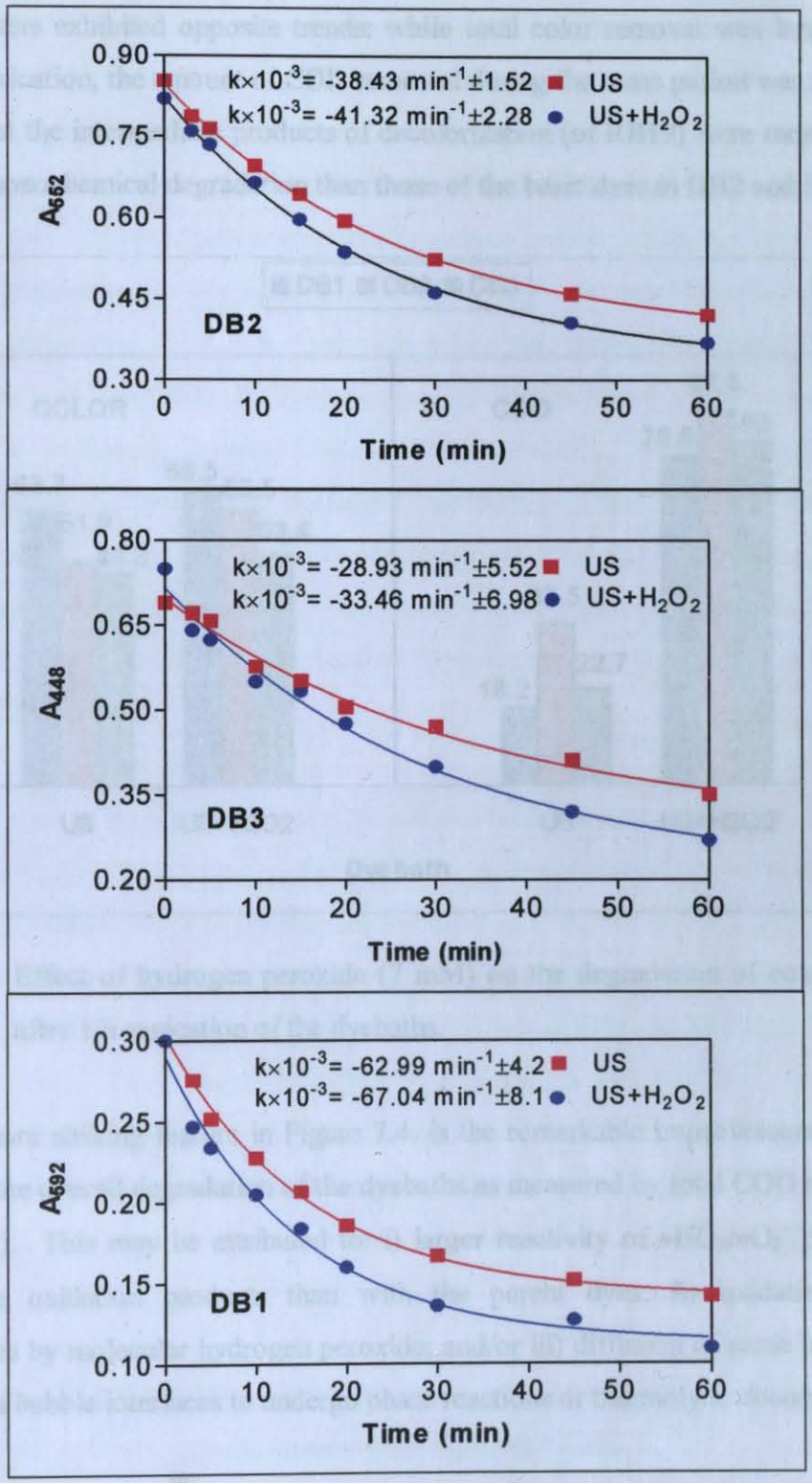

Figure 7.3. Relative rates of ultrasonic color decay at pH=4.5 with and without H_2O_2. The solid lines represent the fit of experimental data to $A=A_0e^{-kt} + P$.

The effect of H_2O_2 on total color and COD removal is presented in Figure 7.4. for those test samples initially at pH=4.5. Note that regardless of H_2O_2, the elimination of the

two parameters exhibited opposite trends: while total color removal was largest in DB1 upon 1 h sonication, the amount of COD removed during the same period was a minimum, implying that the intermediate products of decolorization (of RB19) were more stable and resistant to sonochemical degradation than those of the basic dyes in DB2 and DB3.

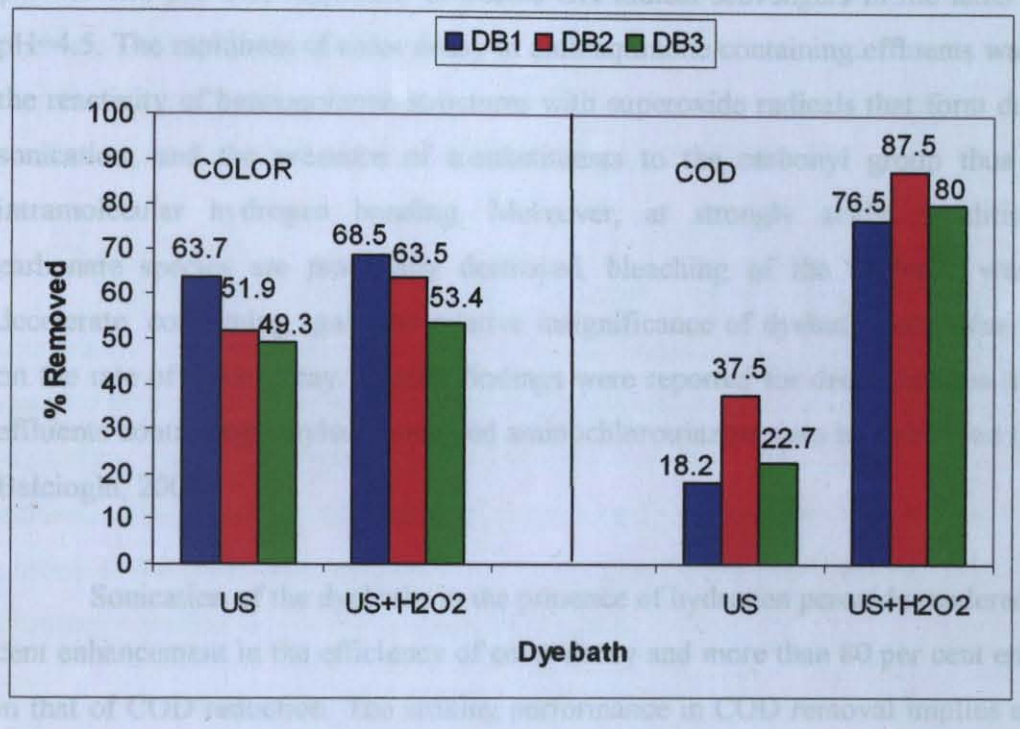

Figure 7.4. Effect of hydrogen peroxide (7 mM) on the degradation of color and COD after 1 h sonication of the dyebaths.

A more striking feature in Figure 7.4. is the remarkable improvement upon H_2O_2 addition in the overall degradation of the dyebaths as measured by total COD removal (80-85 per cent). This may be attributed to: i) larger reactivity of $\bullet HO_2/\bullet O_2^-$ pair with the intermediate oxidation products than with the parent dyes; ii) oxidation of some intermediates by molecular hydrogen peroxide; and/or iii) diffusion of some intermediates into gaseous bubble interfaces to undergo phase reactions or thermolytic decomposition.

7.1.4. Conclusions

Unfixed dye residuals wasted with exhausted dyebaths may find their way to natural waters unless dyehouse effluents are adequately processed. Radicals produced under ultrasonic pressure waves at 300 kHz can effectively destroy the residual color in

textile dyebath effluents at acidic and near-acidic pH, but the overall degradation of the effluents is relatively slow. The rate of color decay is more closely related to the structural and chromophoric properties of the dye than to the composition of the dyebath. This was justified by the observation that azo dyes bleached more slowly than anthraquinone dyes at pH=4.5 and pH=3.0, regardless of excess OH radical scavengers in the latter dyebath at pH=4.5. The rapidness of color decay in anthraquinone containing effluents was related to the reactivity of benzoquinone structures with superoxide radicals that form during water sonication, and the presence of α-substituents to the carbonyl group thus promoting intramolecular hydrogen bonding. Moreover, at strongly acidic conditions, where carbonate species are practically destroyed, bleaching of the dyebaths was found to decelerate, confirming again the relative insignificance of dyebath matrix (or auxiliaries) on the rate of color decay. Similar findings were reported for decolorization of dyehouse effluents containing vinylsulphone and aminochlorotriazine dyes by ozonation (Arslan and Balcioglu, 2000).

Sonication of the dyebaths in the presence of hydrogen peroxide rendered 10-12 per cent enhancement in the efficiency of color decay and more than 80 per cent enhancement in that of COD reduction. The striking performance in COD removal implies either or all of the following: i) the intermediate products of decolorization reactions formed in the presence of H_2O_2 are more reactive with peroxy and superoxide radicals than those formed without; ii) some of these intermediates undergo degradation by molecular H_2O_2; and iii) some have sufficiently large vapor pressures to migrate into the bubble-liquid interfacial region for phase reactions or thermolytic cleavage.

7.2. Sonochemical Destruction of Textile Dyestuff in Wasted Dyebaths: Impacts of Dye Structure and Dyebath matrix

The study presented here is the extension of the study presented here is the extension of the copy of the poster presented in ColorChem02. Czech Republic, 2002. which was printed in the *Proceedings*.

7.2.1. Background

Textile industry accounts for two thirds of the total dyestuff market, and effluents of dyeing processes are of considerable environmental concern due to their intense color, high chemical oxygen demand and traces of hazardous material. Hence, if improperly treated, dyehouse effluents not only deteriorate the aesthetics of receiving waters, but also pose significant threat to living systems via the formation of toxic and potentially carcinogenic products upon hydrolysis of some azo dyes (Boeniger, 1980).

Textile Dyes are classified as "reactive", "acid", "disperse", and "basic" in accordance with the type of fabric processed. Despite their poor exhaustion properties, reactive dyes with azo bonds have the largest consumption in dyeing processes due to the expanding market for cellulosed products and brilliant colors (Soares *et al.*, 2001). The environmental problem with azo and other poorly exhausting dyes is that a significant portion of the initial dye (in some cases as much as 50 per cent) remains in the bath, being ultimately discharged with the exhausted dyebath.

Advanced oxidation of textile dyes by ultrasonic techniques is a novel technology. In all reported studies so far, azo dyes dissolved in deionized water are sonicated with medium frequency ultrasound during gas injection and/or catalysis with Fenton's agent, TiO_2 or ozone (Joseph, *et al.*, 2000; Destaillats *et al.*, 2002; Vinodgopal, *et al.*, 1998; Lorimer *et al.*, 2001). It is reported that azo dye degradation is initiated by hydroxyl radical attack on the N=N double bond in the aqueous phase and mineralization is a much longer process, starting only after complete decolorization.

The purpose of this study was to investigate the degradability of textile azo dyes by ultrasonic irradiation at 300 kHz and to assess the effects of dye structure, dyebath auxiliaries and pH on the rate of color degradation. The dyes were dissolved either in deionized water to generate pure dye solutions (PDS), or in tap water spiked with dyebath auxiliaries to simulate synthetic dyebath effluents (DBE). Structural and matrix effects were assessed by comparing individual color degradation rates in PDS samples with one another, and with the rate observed in the corresponding DBE, respectively. The

degradation of textile dyestuff in wasted dyebaths by ultrasonic irradiation at 300 kHz in the presence of H_2O_2 was also investigated. In addition, the tests were repeated in a solution containing a mixture of 8 dyebaths (the dyes presented in Section 7.1 and 7.2), to reproduce a typical dyehouse process wastewater.

7.2.2. Materials and Methods

7.2.2.1. Dyes

All dyes except C.I Reactive Black-5 were obtained from Aldrich, and the latter from Dyestar Hoechst. The chemical structure of the test dyes and their Color Index (C.I) labels are presented in Figure 7.5. The characters in parenthesis are the abbreviations with which they are referred in the text. H_2O_2 (35% w/w) and all other reagents were analytical Merck grade.

A summary of commercial and molecular dye properties is presented in Table 7.6. The fixing capacity of the dye (last column) reveals the fraction of dye that is fixed on the fabric at the completion of a typical dyeing batch, the rest being wasted with the exhausted dyebath. Fixation values were calculated from the difference between the initial and final dye concentrations in dyebath. Each dyebaths were prepared separately in the Textile Dyehouse in Istanbul (Pisa Corp., 2002) with respect to dyeing recipes for 2 per cent shade depth (0.02 g dye/ g fabric). Initial ratio of fabric to water in tank was 1:10, which means for every 1 g of fabric, 10 ml of water is used. According to the 2 per cent shade depth procedure, 2 g dye with auxiliaries was used to color 100 g fabric in 1 l of tap water. Cotton and polyamide fabrics were colored with reactive and acid dyes, respectively. The absorbances of the dyebath effluents were determined by a spectrophotometer and final dye concentrations in the dyebaths were calculated by using Beers Law as represented by Equation (4.7):

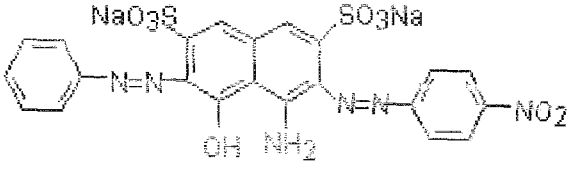

C.I. Acid Black1 (AB1)

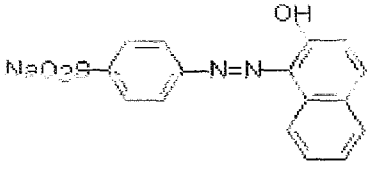

C.I. Acid Orange7 (AO7)

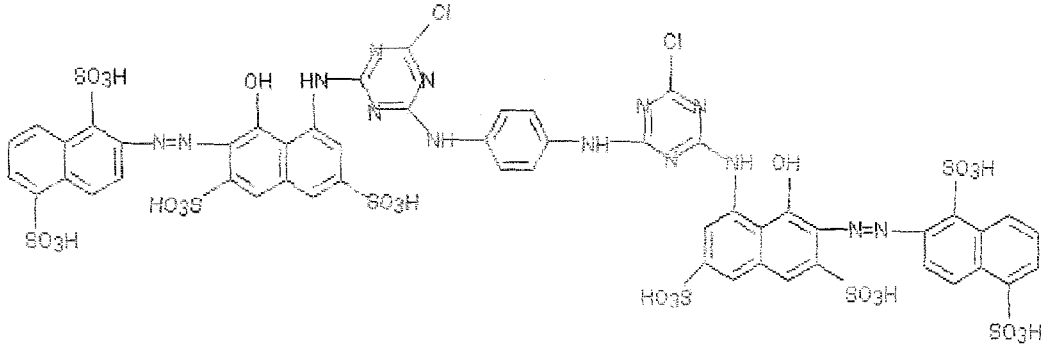

C.I. Reactive Red 141 (RR141)

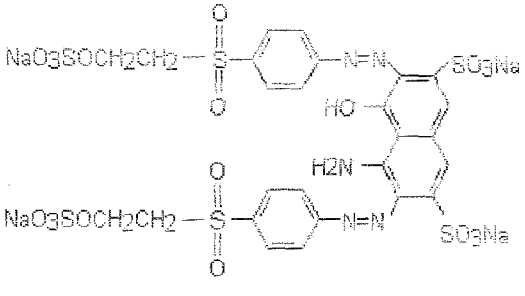

C.I. Reactive Black 5 (RB5)

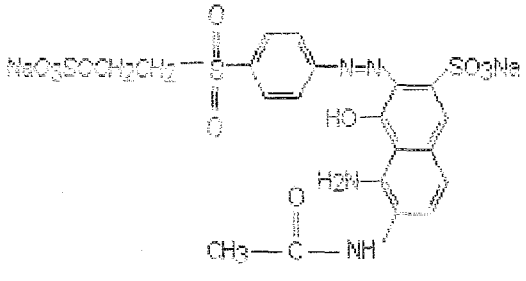

C.I. Reactive Orange 16(RO16)

Figure 7.5. Chemical structures and C.I. identification of the test dyes.

The following calculations are given only for calculating the fixation of RR141:

First the molar absorptivity coefficient (ε_{max}) was calculated by Equation (4.7) for λ = 544 nm:

A_o = 0.590 (average of 10 experiments, 30 mg/l dye at pH=3)

C_o = (30 mg L^{-1} x 10^{-3} g mg^{-1}) x (1 / 1781 g mol^{-1}) x (0.75 purity)

$$= 30 \frac{mg}{L} \times 10^{-3} \frac{g}{mg} / 1781 \frac{mol}{g} \times 0.75 = 1.26 \times 10^{-5} \text{ M}$$

$\varepsilon_{max} = (A_o / (C_o \times d)) = 4.67 \times 10^4 \text{ M}^{-1} \text{ cm}^{-1}$

The absorbance (at 544 nm) of the effluent was recorded as 1.012 in 1/10 dilution of the final effluent. The concentration of the RR141 in solution after dyeing ($C_{effluent}$) was then calculated by substituting the absorbance value into Equation (4.7) as follows:

$C_{effluent}$ = 1.012 / 4.67 x 10^4 M^{-1} cm^{-1} / 1 cm = 216 × 10^{-6} M

Fixation of RR141 was then calculated from the difference between the initial ($C_{influent}$ = 842× 10^{-6} M (2 g L^{-1})) and final dye concentration ($C_{effluent}$ = 216 × 10^{-6} M) and it was found that 25 per cent of the dye was wasted with the effluent and 75 per cent of the dye was fixed on the fabric as presented in Table 7.6.

Table 7.6. Identification and some selected properties of the test dyes

Dye Class	Dye C.I. Number	Typical Structure	Purity (%)	Molecular Weight (g mol^{-1})	UV Absorption	Fixation (%)
Reactive	R.Red141 (RR141)	disazo	75	1781.00	544 nm	75
	R.Black5 (RB5)	disazo	85	991.82	596 nm	80
	R.Orange16 (RO16)	monoazo	50	617.54	492 nm	60
Acid	A.Black1 (AB1)	disazo	80	616.50	620 nm	95
	A.Orange7 (AO7)	monoazo	85	350.33	484 nm	93

7.2.2.2. Preparation of Test Solutions

Two type of dye solutions were prepared: i) PDS: These were pure dye solutions made by dissolving 30 mg of each dye in 1 l of boiling deionized water during magnetic stirring. ii) DBE: These were dilutions of synthetic dyebaths prepared by reference to original dyeing recipes supplied by a commission based dyehouse for 2 per cent shade depth (Pisa Corp., 2002). Each dyebath was heated to 90-120°C in accordance with the corresponding recipe, and those with reactive dyes were adjusted to basic pH (with NaOH), and maintained at this temperature for 6-8 hours to allow hydrolysis. The dyebaths were brought to 30 mg L^{-1} as dye with tap water (67-fold dilution) to represent batch dyeing effluents post the final washing operation. The dilution water contained 65.55 mg L^{-1} alkalinity as $CaCO_3$, and 33.75 mg L^{-1} chlorine. The composition of simulated dyebath effluents used as test solutions is presented in Table 7.7. The degradation of textile dyestuff in DBE by ultrasonic irradiation coupled with 7 mM H_2O_2 was also investigated. In addition, the tests were repeated in a solution containing a mixture of 8 dyebaths to reproduce a typical dyehouse process wastewater.

Table 7.7.Composition of final dyebath effluents by auxiliary chemicals[1]

Type of dyebath	Auxiliaries Added	Concentration (mg L^{-1})
Reactive	Dye	30.0
(T = 90°C)	Sequestering agent[2]	7.5
	Anti-creasing agent[3]	15.0
	Acetic acid	4.5
	Sodium chloride	900.0
	Sodium carbonate	300.0
	Sodium hydroxide[4]	67.5
Acid	Dye	30.0
(T = 110°C)	Leveling agent[5]	15.0
	Acetic acid	22.5

[1] in addition to these auxiliaries, each dyebath effluent contained 65.6 and 33.8 mg L^{-1} of carbonate alkalinity and Cl^{-1}, respectively, [2] Verolan NBO, [3] Slipper, [4] added only to RB5 dyebath to produce covalent bonds with the fabric, [5] Uguar TP

7.2.2.3. Experimental Procedure

Experimental system and parameters were the same as previously presented in Section 7.1., in Table 7.3.

Hundred milliliters of PDS and DBE samples following 2 h aeration were exposed to ultrasonic irradiation at 300 kHz for 1 h at natural pH of the test dyes (5-6) and at pH=3 (buffered with 0.1 N H_2SO_4) in the presence of Argon gas. Samples were withdrawn at 0, 3, 5, 10, 15, 20, 30, 45 and 60 min for spectrophotometric analysis. The degradation of dyes in DBE by ultrasonic irradiation in the presence of 7 M H_2O_2 was also investigated. In addition, the tests were repeated in a solution containing a mixture of 8 dyebaths (CI Reactive Red141, CI Reactive Black 5, CI Reactive Orange 16, CI Acid Black1, CI Acid Orange7, Reactive Blue19, CI Basic Brown4, CI Basic Blue16), to reproduce a typical dyehouse process wastewater.

Analytical

Samples of PDS and DBE withdrawn from the reactor during sonication were analyzed spectrophotometrically at 200-800 nm and at the visible absorption of the solutions using a Unicam, Helios Alpha/Beta double beam spectrophotometer through a 1 cm path length. The concentration of hydrogen peroxide in the effluent was monitored by triiodide method (Klassen *et al.*, 1994). COD was determined in accordance with the Standard Methods of Water and Wastewater Analysis (APHA, 1992). Knowing that H_2O_2 also exerts a chemical oxygen demand, the COD of the residual H_2O_2 was subtracted from that of the sample (Kang *et al.*, 1999). The interference of chlorine in COD analysis was overcome by the addition of excess Hg_2SO_4. TDS was measured by WTW LF320 model conductivity meter.

7.2.3. Results and Discussion

7.2.3.1. Rate of Color Degradation

Profiles of color degradation during 1 h irradiation of PDS at non-buffered conditions and the fit of Equation 7.1. are presented in Figure 7.6. For each case, a correlation coefficient of at least 0.98 was obtained in the regression analysis.

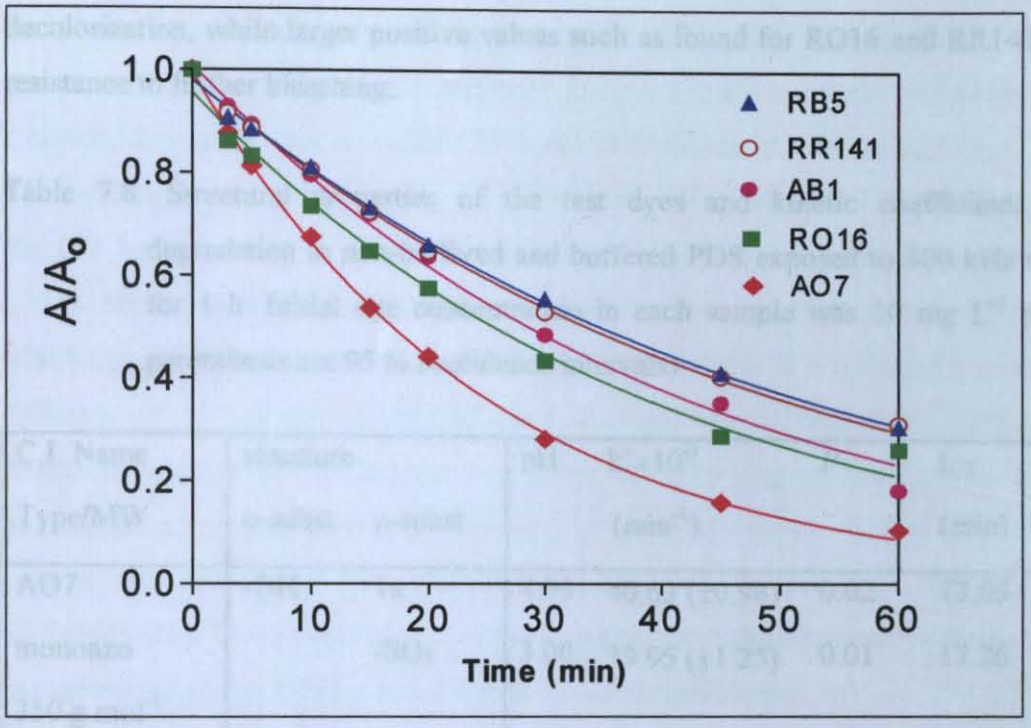

Figure 7.6. Relative profiles of absorbance decay with time in PDS containing 30 mg L^{-1} dye initially. The solid lines represent the fit of Equation 7.1 to the related data set.

The degradation of color in all test samples was pseudo-first order with respect to the absorbance of the dye in the visible band. The analysis of Absorbance versus time data by non-linear regression showed that absorbance decays exponentially as depicted by the integration of Equation 7.1.

7.2.3.2. Structural Effects

7.2.3.2.1. Study with Pure Dye Solutions

The effect of dye structure on color decay was investigated in pure dye solutions (PDS) at near-neutral and acidic conditions. The azo character of the dyes and the functional groups in ortho and para-position to the azo bonds are listed in Table 7.8. together with the estimated first order color decay coefficients and the "plateau". Note that a P value less than or slightly above zero indicates the tendency of the dye to complete

decolorization, while larger positive values such as found for RO16 and RR141 imply its resistance to further bleaching.

Table 7.8. Structural properties of the test dyes and kinetic coefficients of color degradation in non-buffered and buffered PDS exposed to 300 kHz ultrasound for 1 h. Initial dye concentration in each sample was 30 mg L^{-1} (figures in parenthesis are 95 % confidence intervals)

C.I. Name	structure		pH	$k' \times 10^{-3}$	P	$t_{1/2}$
Type/MW	o-subst	p-subst		(min^{-1})		(min)
AO7	-OH	1x	4.95	40.63 (±0.98)	0.02	17.05
monoazo		$-SO_3^-$	3.00	39.95 (±1.25)	0.01	17.26
350 g mol^{-1}						
RO16	$-SO_3^-$	1x	5.07	30.25 (±1.28)	0.14	20.17
monoazo	-OH	O=S=O	3.00	29.63 (±1.12)	0.11	20.43
618 g mol^{-1}						
AB1	SO_3^-	1x	5.32	24.50 (±0.98)	-0.29	28.30
disazo	OH	NO_2	3.00	26.66 (±0.86)	-0.17	30.04
617 g mol^{-1}	NH_2					
RR141	SO_3H	none	5.25	19.98 (±0.41)	0.11	34.70
disazo	OH		3.00	22.17(±1.00)	0.09	31.27
1791 g mol^{-1}						
RB5	$-SO_3^-$	2x	5.31	19.29 (±0.38)	0.03	35.94
disazo	-OH	O=S=O	3.00	21.72 (±0.47)	0.05	31.91
992 g mol^{-1}	NH_2					

The faster rate of bleaching of monoazo dyes confirms that color decay is •OH diffusion-controlled, and is therefore limited by the steady state •OH concentration in the aqueous phase. Hence, at limited $•OH_{aq}$, the rate of bleaching slows down as the number of chromophores in the dye molecule increases. On the other hand, other attributes of structure must have been responsible for the observed rate differences in structures

containing equivalent number of chromophores. These may include factors such as the character of o- and p-substitution about the azo bond(s) and the molecular mass of the dye. Recently, Destaillats and coworkers have shown that a carboxylic group vicinal to the azo bond enhances the rate of degradation by a strong intramolecular H-bond formation with the OH radical added to the N=N bond, thus stabilizing the adduct (Destaillats *et al.*, 2002). As shown in Table 7.8., the azo bonds in all test dyes had an o-OH substituent, which can also form strong intramolecular H-bonds with the OH adduct. Consequently, the difference in the bleaching rates of monoazo dyes is attributed to differences in their molecular weights and o-substituents. The slower bleaching of RO16 than AO7 implies that the presence of an additional substituent such as SO_3^- in the vicinity of the azo group reduces the stability of the intermediate adduct by the potential competition of o-substituents for intramolecular H bonding, and/or the enhancement of solvent effects via the anionic character of SO_3^- to form H-bonds with the solvent.

Comparison of disazo dye bleaching rates with one another reveals that each additional o-substituent, such as NH_2 (as in AB1 and RB5) inhibited the rate of bleaching, probably by the same principle discussed above (competition for intramolecular H-bonding) and the potential effects of steric hindrance. The exception was RR141, which bleached slower than AB1 despite the lack of o-NH_2 or o-SO_3^- substituents in the vicinity of its azo bonds. This must be due to its considerably larger molecular weight and the attachment of two naphthalene groups to each of its azo bonds. However, RR141 was found to bleach nearly at the same as RB5 (within statistical significance), which had a much smaller mass and no naphthalene attachments to its azo bonds. This was attributed to its neutral character, or the lack of anionic o-substituents to the azo bonds, which reduce the stability of its adduct. Moreover, the fact that RR141 had no p-substituents (to N=N bonds) while RB5 had two of them might be an additional factor in the unexpected bleaching rate of RR141. Similarly, the faster bleaching rate of AB1 than RB5, despite the similarity of their azo groups and o-substituents, must be assessed both in terms of their mass differences and difference of p-substituents to their azo bonds.

When PDS's were buffered to pH=3, the rate of color degradation was slightly accelerated (nearly by 10 per cent) in RR141, RB5 and AB1, while no effect was observed in AO7 and RO16 within statistical significance. The insensitivity of the latter to

acidification confirms the statement that the rate of color decay was merely controlled by the steady state •OH concentration in the aqueous phase, which has likely remained constant upon pH adjustment with sulfuric acid. The slight enhancement of degradation in three of the test dyes and the unchanging trend in the other two upon acidification with sulfuric acid implies that the effect of protonation (of SO_3^- or other sites) to lower H-bonding with the solvent was insignificant, and there were no additional •OH production routes that raised its steady state concentration in the liquid bulk.

7.2.3.3. Matrix Effects

7.2.3.3.1. Study with Dyebath Effluents

It was found that ranking of bleaching rates in dyebath effluent (DBE) followed the same order as that in the corresponding deionized water solutions: with however lower coefficients except for AO7, as shown in Table 7.9. The constant rate of bleaching of AO7 at all conditions (within statistical significance at 0.05 level) can be explained by its structural simplicity (low molecular weight, single o-substituent), the lack of large concentrations of •OH scavengers in its dyebath, and the sufficiency of aqueous •OH at both conditions to satisfy the minimum requirements for the destruction of its azo bond.

The slower degradation of the other dyebaths than their PDS is due to matrix effects, or the interaction of dyebath auxiliaries with •OH addition to azo bonds. The composition of DBE's in Table 7.7. shows that reactive dyebaths contained large concentrations of sodium salts (used for enhancing the fixation of the dye on the fabric), 900 and 300 mg L^{-1} of NaCl and Na_2CO_3, respectively. In addition, the dilution water had approximately 66 and 34 mg L^{-1} of $CaCO_3$ and Cl^-, respectively.

Table 7.9. Kinetic coefficients of color degradation in non-buffered and buffered dyebath effluent, containing the all dyebath auxiliaries (specified in Table 7.7.) and 30 mg L^{-1} dye

DYEBATH	pH	$k' \times 10^{-3}$ (min^{-1})	P	R^2	$t_{1/2}$ (min)
AO7	4.95	39.72 (±1.26)	0.06		
	3.00	41.72 (±1.30)	0.02	0.99	15.02
RO16	5.09	24.82 (±3.62)	0.24		
	3.00	26.78 (±1.82)	0.31	0.998	25.88
AB1	5.32	21.41 (±0.68)	-0.20		
	3.00	26.45 (±0.95)	-0.14	0.99	29.51
RR141	5.25	15.97 (±0.44)	0.01		
	3.00	18.78 (±0.14)	0.11	0.99	36.96
RB5	5.31	16.41 (±0.32)	0.04		
	3.00	19.57 (±1.75)	0.05	0.99	42.25

The delayed rate of color decay in reactive DBE is due, therefore, to the competition of target and non-target species for •OH as shown by the following reactions and bimolecular rate constants (Buxton *et al.*, 1988):

$$\text{Dye(azo)} + {}^{\circ}OH \rightarrow \text{Products} \qquad k=10^{8}\text{-}10^{10}\ M\ s^{-1} \qquad (7.7)$$

$$CO_3^{-2} + {}^{\circ}OH \rightarrow HO^{-} + {}^{\circ}CO_3^{-} \qquad k=3.8 \times 10^{8}\ M\ s^{-1} \qquad (7.8)$$

$$HCO_3^{2-} + {}^{\circ}OH \rightarrow H_2O + {}^{\circ}CO_3^{-} \qquad k= 8.5 \times 10^{6}\ M\ s^{-1} \qquad (7.9)$$

$$Cl^{-1} + {}^{\circ}OH \rightarrow HO^{-} + Cl^{\circ} \qquad k= 4.3 \times 10^{9}\ M\ s^{-1} \qquad (7.10)$$

Although, the generated carbonate radical anion has been shown to be an oxidant itself, its oxidation potential is much lower than that of the •OH. After it is formed, some of the formed $^{\circ}CO_3^{-}$ will further react with the dye molecules to form more oxygenated

products (Acero and Gunten, 2000) (Equation (7.11)), and some will react with •OH and again compete with the target molecule (Equation (7.8)).

$$\bullet CO_3^- + \text{Dye} \rightarrow CO_3^{-2} + \text{Products} \qquad k=1 \times 10^7\ M\ s^{-1} \qquad (7.11)$$

The fact that AB1 bleached slower in the dyebath than in PDS, but AO7 bleached at the same rate in both media, although neither of the dyebaths contained sodium salts must be due to the disazo structure of AB1, which requires larger •OH concentrations for the destruction of its chromophore than the monoazo AO7. It is likely that the concentration of •OH is slightly reduced in both dyebaths by the impurities in the matrix such as ions of acetate, carbonate and chloride (the latter two coming with the dilution water), the effect of which was insignificant for monoazo but significant for disazo dye bleaching rates.

The observed color decay coefficients in reactive dyebath effluents were found to increase by about 20 per cent upon acidification. The enhancement is due to the conversion of carbonates at pH=3 to carbonic acid, which is not an effective hydroxyl radical scavenger. The slight degree of rate inhibition still observed at acidic pH is due to the •OH scavenging of Cl^- alone, which unless at very high concentrations is not a strong rate inhibitor in advanced oxidation of azo dyes (Arslan and Balcioglu, 2000).

The effect of pH in reactive dyebaths was more closely investigated by monitoring the rate of color decay within a wider range of pH levels. Relative profiles of absorbance abatement in RR141 dyebath during ultrasonic irradiation at various pH levels are presented in Figure 7.7. It was found that rates of dyebath bleaching at highly acidic, slightly acidic (near neutral) and neutral pH were close, although at pH=5.25 bicarbonate species predominated. This is due to the fact that bimolecular reaction rate constant of bicarbonates with hydroxyl radicals is not competitive with that of azo dyes ($k=8.5 \times 10^6\ M\ s^{-1}$) (Buxton *et al.*, 1988).

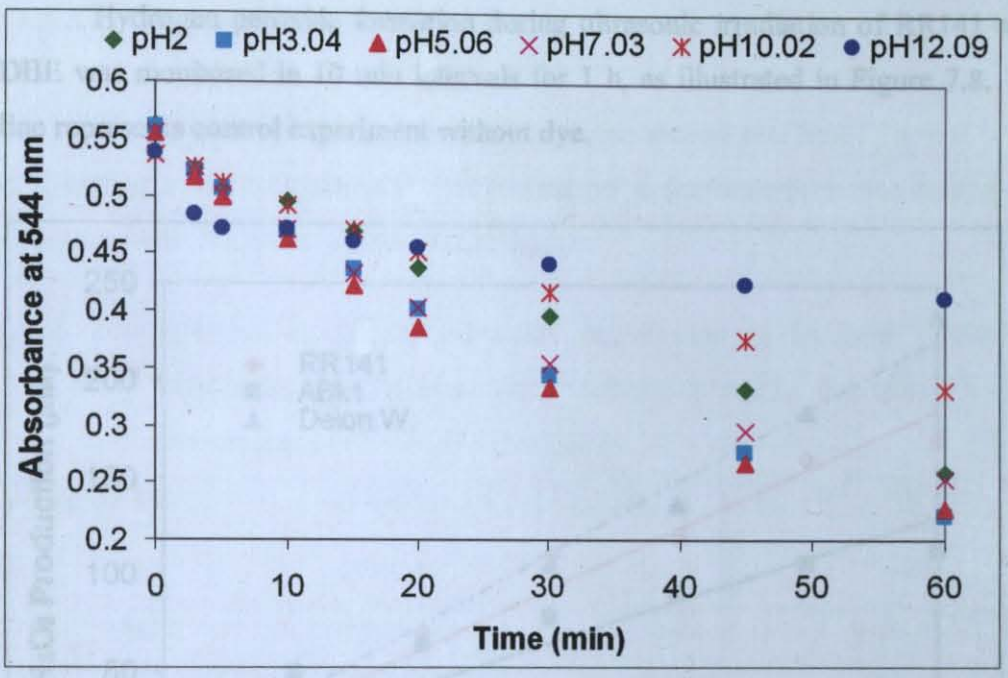

Figure 7.7. Comparative profiles of absorbance decay during 1 h sonolysis of a reactive DBE with 30 mg L^{-1} of RR141 at varying pH levels.

Sequential lowering of pH from 12 to 2 showed that the process becomes remarkably effective with increased acidity, but further decrease from pH 3 to 2 yielded a significant decrease in the rate of color degradation. This result can be attributed to the scavenging effect of H_2SO_4 (at high concentration) which was used for pH adjustments (Equation (7.12) and (7.13)) (Buxton *et al.*, 1988).

$$\bullet OH + H_2SO_4 \rightarrow H_2O + H^+ + SO_4^{-}\bullet \qquad (pK_a = -3) \qquad k = 1.4\times10^7\ M^{-1}\ s^{-1} \quad (7.12)$$

$$\bullet OH + HSO_4^{-} \rightarrow H_2O + SO_4^{-}\bullet \qquad (pK_a = 1.9) \qquad k = 4.7\times10^5\ M^{-1}s^{-1} \quad (7.13)$$

The lower rate of decolorization at pH 2 than at pH 3 can be attributed to the scavenging effect of HSO_4^{2-} (Equation. (7.13)), where sulphuric acid dissociates into H^+ and SO_4^{2-} at pH ≥ 1.9 (Droste, 1997). At pH 2, per cent H_2SO_4 is approximately equal to per cent SO_4^{2-}, and at pH 3 per cent H_2SO_4 is much less than per cent SO_4^{2}, and sulphate is a weaker scavenger of •OH.

Hydrogen peroxide formation during ultrasonic irradiation of RR141 and AB1 in DBE was monitored in 10 min intervals for 1 h, as illustrated in Figure 7.8. The dashed line represents control experiment without dye.

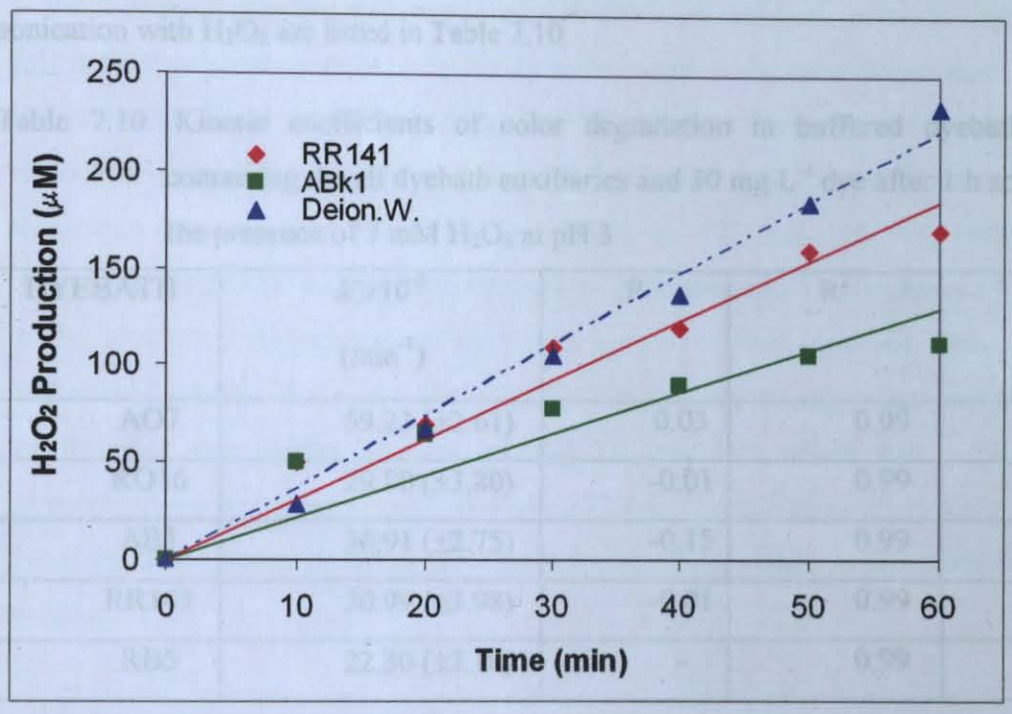

Figure 7.8. H_2O_2 production at 300 kHz in DBE containing AB1 and RR141 at pH 3. Initial dye concentrations were 30 mg L^{-1} (solid and dashed lines represent the fit of related data Set to $H_2O_2 = kt$).

As can be seen in Figure 7.8., the apparent kinetics are zero-order, with the observed rate coefficients as 2.17 μM min^{-1}, 3.09 μM min^{-1}, and 3.86 μM min^{-1}, for AB1, RR141, and deionized water solutions, respectively. H_2O_2 is accepted as an indirect measurement of net •OH concentration in solution. It is apparent that the •OH consumption is higher in AB1 dyebath, than that in RR141. This is consistent with the results of the previous study in this section, where a higher color removal was found for AB1. This can be explained due to i) higher reactivity of H_2O_2 (and also $•HO_2/•O_2^-$) with the intermediate oxidation products ; or ii) lower reactivity of RR141 with •OH to result in larger H_2O_2 production.

7.2.3.3.2. Effect of Hydrogen Peroxide

The addition of hydrogen peroxide into the reactor was found to accelerate the rate of bleaching in all dyebaths. The pseudo-first order decolorization rate constants after 1 h sonication with H_2O_2 are listed in Table 7.10.

Table 7.10. Kinetic coefficients of color degradation in buffered dyebath effluent, containing the all dyebath auxiliaries and 30 mg L^{-1} dye after 1 h sonication in the presence of 7 mM H_2O_2 at pH 3

DYEBATH	$k' \times 10^{-3}$ (min^{-1})	P	R^2	$t_{1/2}$ (min)
AO7	59.23 (±2.61)	0.03	0.99	11.70
RO16	29.80 (±3.80)	-0.01	0.99	23.26
AB1	30.91 (±2.75)	-0.15	0.99	22.38
RR141	20.99 (±3.98)	-0.01	0.99	33.03
RB5	22.30 (±2.18)	-	0.99	31.08

The rate of color removal by H_2O_2 addition was accelerated by 10 - 40 per cent, as a result of higher $^{\bullet}OH$ yields and the production of additional radicals (peroxy and superoxide), which may also migrate to the solution bulk to act as oxidizing agents (Hart and Henglein, 1987; Drijivers *et al.*, 1999).

When the dyebath solutions were spiked with H_2O_2, the highest increase in color removal rate was observed for AO7 solution (40 per cent), while the other dye decolorization rates were close to each other. The enhancement can be due to its simpler molecular structure and may be related to the higher reactivity toward superoxide radicals (Equation (7.4) and (7.5)). The dyes that contain a hydroxyl group in *ortho* position to the azo bond exist in equilibrium with two tautomeric forms, azo and hydrazone (Oakes and Gratton, 1998) and this hydrazone form may be more reactive with superoxide radicals than azo forms. Although all of the dyes in this Chapter probably mostly exist in their hydrazone forms, they seem to be more resistant to the attack of superoxides due to their more complex structures.

7.2.3.3.3. Dyebath Mixture

7.2.3.3.3.1. Color Decay

To simulate actual wastewater compositions, all test dyes (given in Section 7.1 and 7.2) in their original dyebath composition were mixed in the ratio 50 per cent reactive: 25 per cent acid: 25 per cent basic dyes. The mixture was then exposed to ultrasound and ultrasound coupled hydrogen peroxide at pH 3. The test solution was found to exhibit two absorption bands in the visible range, namely at 492 and 596 nm, which must be responsible for the red and greenish blue color of the solution. The tendency of degradation in the absence and presence of H_2O_2 was similar to that observed with unmixed or individual dyebaths. The concentration of H_2O_2 added was an important control parameter, for the fact that excess amounts induced an inhibitory effect due to the increased competition for hydroxyl radicals (Equation (7.4)). The selection of optimum H_2O_2 was, therefore, based on the observed color degradation rate constant, as presented in Figure 7.9 as bars.

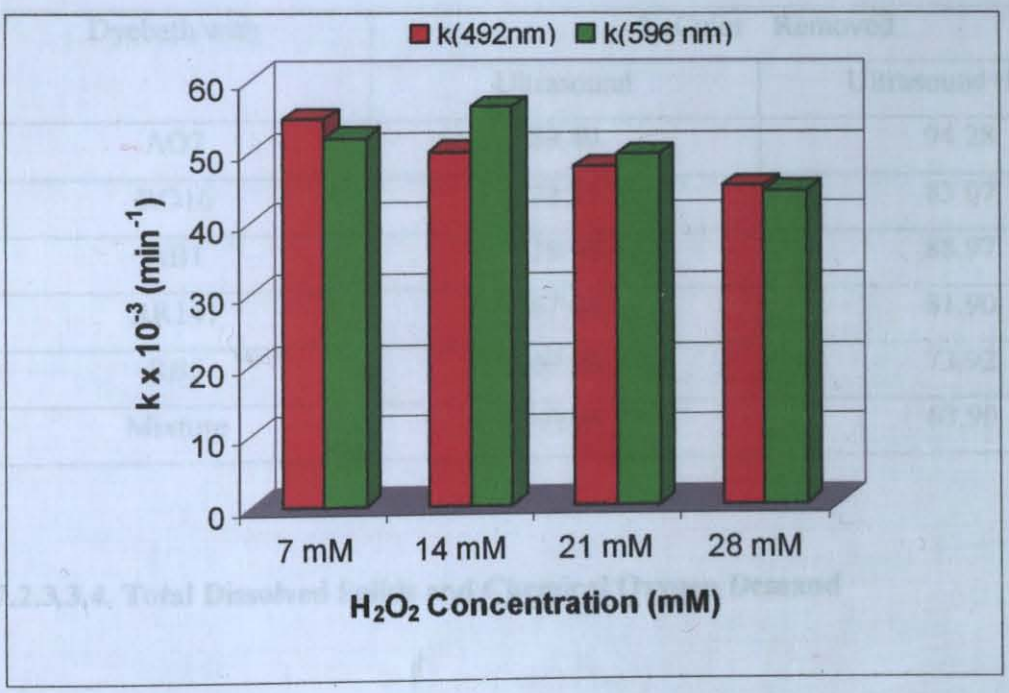

Figure 7.9. Effect of H_2O_2 concentration on decolorization kinetics. Dyebath mixture was exposed to 300 kHz Irradiation in the presence of differing H_2O_2 concentrations for 1 h.

Note that the rate increases with doubling the concentration of H_2O_2, whereas further increases retard the reaction as a result of increased competition between H_2O_2 and the dye for hydroxyl radicals. First order color degradation rate constants after 1 hr ultrasonic irradiation in the absence and presence of 14 mM H_2O_2 were 30.15 min^{-1} and 56.21 min^{-1}, respectively.

Per cent color removal in the test solutions together with dyebath mixture upon 1 h sonication with and without hydrogen peroxide is presented in Table 7.11.

The rate of color removal by H_2O_2 addition was accelerated by 5-15 per cent, as a result of higher •OH yields and the production of additional radicals (peroxy and superoxide), which may also migrate to the solution bulk to act as oxidizing agents.

Table 7.11. Degradation of color in the dyebaths and the dyebath mixture upon 1 h sonication with or without hydrogen peroxide (H_2O_2 Concentration was 7 mM and 14 mM for DBE and DBE mixture, respectively)

Dyebath with	% Color Removed	
	Ultrasound	Ultrasound+H_2O_2
AO7	89.49	94.28
RO16	74.91	83.07
AB1	78.98	88.97
RR141	67.04	81.90
RB5	69.58	73.92
Mixture	49.90	63.90

7.2.3.3.4. Total Dissolved Solids and Chemical Oxygen Demand

The dissolved solids (TDS) content of the dyebath effluents increased during sonication, as a result of the formation of intermediate oxidation products. The initial TDS concentration is recipe-dependent. Reactive dyebath effluents have the highest TDS

concentration due to the addition of excess salts to the dyebaths to enhance dye fixation to the fiber. The initial and final TDS content of different samples are presented in Table 7.12.

Table 7.12. Total dissolved solids concentrations of some selected dyes upon exposure to 1 h ultrasonic irradiation with or without H_2O_2

Dyebath with	Initial TDS (mgL^{-1})	Final TDS (mgL^{-1})	
		Ultrasound alone	Ultrasound+H_2O_2
Reactive Orange16	1296	1436	1530
Acid Black1	398	439	481
Basic Brown4	504	528	534
Dyebath Mixture	1060	1112	1286

Monitoring of Chemical Oxygen Demand (COD) of the test samples during sonication with and without hydrogen peroxide showed that ultrasound alone provided no more than 6 per cent reduction in COD, while at least 70 per cent COD reduction was possible when hydrogen peroxide was present. Comparison COD removal in the test solution upon 1 h sonication with and without hydrogen peroxide is presented in Table 7.13. for those dyebath effluent (DBE) and DBE mixture.

Table 7.13. Degradation of COD in dyebath and dyebath mixture upon 1 h sonication with or without hydrogen peroxide (H_2O_2 concentration was 7 mM and 14 mM for DBE and DBE mixture, respectively)

Dyebath with	% COD Removed	
	Ultrasound	Ultrasound+H_2O_2
AO7	4.93	86.29
RO16	3.34	82.32
AB1	4.05	89.54
RR141	4.88	75.29
RB5	4.69	74.61
Mixture	5.92	70.77

The effectiveness of combined system to COD removal, which is a measure of the overall degradation of the dye involved can be attributed to larger reactivity of $\bullet HO_2/\bullet O_2^-$ pair with the intermediate oxidation products than with the parent dyes, and the oxidation of some intermediates by molecular hydrogen peroxide. The COD removal in DBE mixture can be due to the reactivity of intermediates with peroxy radicals/hydrogen peroxide, and additionally with carbonate radicals. Carbonate radicals (where higher amounts were present in the mixture) may further react with the dye molecules to form more oxygenated products (Equation (7.11)). The efficiency of ultrasonic system can be increased by enhanced detention time, which however would lower the cost-effectiveness of a potential ultrasonic system to be designed for the pre-treatment of textile dyebath effluents.

7.2.4. Conclusions

Sonochemical bleaching of textile azo dyes was investigated in deionized water-dye solutions and synthetic dyebath effluents during irradiation at 300 kHz. It was found that the rate of bleaching was closely related to the chemical structure of the dye such as the number of azo groups, the relative position and character of the substituents about the azo bonds, and the molecular mass. Color removal as based on hydroxyl radical addition to the azo bonds exhibited an exponential decay rate profile in both of the test media. The •OH–limited rate of color decay in deionized water solutions of test dyes depends on their molecular mass and structural properties, particularly the number of azo bonds and substituents in their vicinity. The rate of bleaching follows the order: monoazo>disazo; small molecules>large molecules; single o-OH substituent>multiple substituents.

In dyebath effluents simulated by adding exact quantities of auxiliary chemicals (specified in dyeing recipes) into azo dye solutions made in ordinary tap water, bleaching is inhibited only if the concentrations of carbonate and chloride ions in the matrix are sufficiently large to allow competition of these species with the dye for hydroxyl radicals. Otherwise, the rate is controlled by the structure of the dye as in deionized water-dye solutions. Buffering of the dyebaths to acidic pH accelerated the rate of bleaching in those dyebaths containing significant quantities of carbonate species, which at non-buffered conditions competed with the dye for hydroxyl radicals. In deionized water-dye solutions,

where no competition was present, acidification rendered a slight enhancement in the bleaching of disazo dyes, but no change in those with monoazo character.

The addition of H_2O_2 was found to enhance the rate of decolorization. Furthermore, the overall degradation of the dye as monitored by the reduction in COD of the effluent samples was remarkably faster in the presence of H_2O_2 and insignificant in its absence. The total dissolved solids were found to increase upon ultrasonic bleaching and degradation, implying the formation of soluble intermediate byproducts within the oxidation process. Ultrasonic destruction of dyestuff in a dyebath mixture, which resembled real dyehouse process effluents, was observed to follow the same trend as that of individual dyebaths.

CHAPTER 8. IMPACTS OF pH AND MOLECULAR STRUCTURE IN ULTRASONIC DEGRADATION OF AZO DYES: APPLICATIONS IN SYSTEM I

8.1. C.I. Acid Orange7 and C.I. Reactive Orange16

The study presented in this section is an extension of the paper presented in "Ultrasonics 2003, held on 30 June-4 July 2003, in Granada, Spain". The complete work is submitted to *Ultrasonics*, and is currently under review.

8.1.1. Background

Azo dyes are chemically described with structures made up of single or multiple units of N=N bonds connected to aryl and/or naphthalene groups, the whole unit making the characteristic chromophore in the dye. The large consumption of such dyes in the industry, and the practice of discharging exhausted dyebaths with residuals of unfixed dyestuff and spent chemicals have challenged environmental engineers and water quality managers over the years. A promising solution alternative to the protection of water environment from these effluents is to pre-treat them with well-selected advanced oxidation processes (AO), which in situ generate extremely powerful oxidants such as the hydroxyl radical (•OH).

Ultrasonic cavitation is an emerging AO technology for use in decontaminating natural waters or industrial process effluents from refractory organic materials. The rate of target chemical destruction during sonication of contaminated waters is limited by the rate of •OH diffusion into the bulk liquid and the partial pressure of the compound, which dictates its ability to migrate into the gaseous or the gas-liquid interfacial layers for pyrolytic and supercritical phase reactions, respectively (Suslick, 1990; Mason *et al.*, 1992;

Ince *et al.*, 2000; Joseph *et al.*, 2000). Because azo dyes are highly water soluble and thus largely hydrophilic, their partitioning into the gas phase is not likely. Hence, the major route for destruction of such dyes must be chemical oxidation by OH radicals in the bulk liquid.

Sonochemical oxidation of azo dyes has been investigated by some researchers during the last few years. In the reported studies, deionized water solutions of azo dyes are sonicated with medium frequency ultrasound during gas injection and/or catalysis with Fenton's agent, TiO_2 or ozone (Joseph *et al.*, 2000; Destaillats *et al.*, 2002; Vinodgopal *et al.*, 1998; Lorimer *et al.*, 2001). It is predicted by proposed reaction mechanisms that color decay is mainly governed by hydroxyl radical addition to the azo bond in the aqueous phase and the overall degradation of the dye is a longer process, involving a number of intermediate oxidation states (Destaillats *et al.*, 2002; Joseph *et al.*, 2000; Stock *et al.*, 2000).

The purpose of this study was to investigate and compare degradability of azo dyes by ultrasonic irradiation at 300 kHz and to assess the effects of dye structure and pH on the rate of color decay. Two sulphonated monoazo dyes of 1-aryl-azo-2-naphtol structure were selected from commercial dyestuff and used as surrogate compounds throughout.

8.1.2. Materials and Methods

8.1.2.1. Dyes

The dyes C.I. Acid Orange7 (AO7) and C.I. Reactive Orange16 (RO16) were both obtained from Aldrich in 85 and 50 per cent purity, respectively. (No information was provided about impurities.) All other reagents were analytical Merck grade.
General structure of the "aryl-azo-naphtol" type model dye is given below:

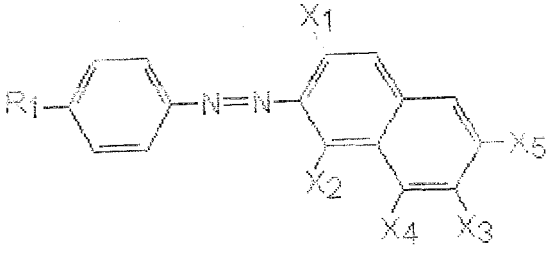

The commercial and chemical properties of the model dyes are given in Table 8.1.

Table 8.1. The commercial and chemical properties of the model dyes

Dye C.I. Manufacturing Company-Purity (Molecular Weight)	X_1, X_2, R_1 substituents	X_3, X_4, X_5 substituents	Visible Absorbance
AcidOrange7 ALDRICH-85% (350 $gmol^{-1}$) 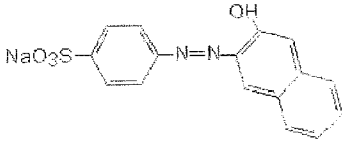	$X_1 = -OH$ $X_2 = -H$ $R_1 = -SO_3Na$	$X_3 = -H$ $X_4 = -H$ $X_5 = -H$	484 nm
ReactiveOrange16 ALDRICH-50 % (618 $gmol^{-1}$) 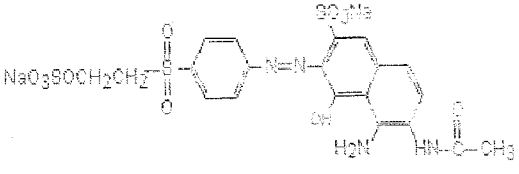	$X_1 = -SO_2Na$ $X_2 = -OH$ $R_1 = -SO_2C_2H_4S$	$X_3 = -NH_2$ $X_4 = -NHMe$ $X_5 = -H$	492 nm

8.1.2.2. Preparation of the Test Solutions and Experimental Procedure

The optimized system parameters were the same as previously given in Table 7.3. Stock dye solutions were prepared by dissolving 1 g of dye (as received) in 1 L of boiling deionized water during magnetic stirring. The solution with C.I. Reactive Orange16 was heated to 90 °C following pH adjustment to 1L. and maintained for 6 hours there to allow complete hydrolysis of the dye. The stocks were then transferred into opaque bottles and stored at 4°C in the dark.

Test solutions were made by proper dilution of the stocks to 30 μM as dye using ultra pure deionized water. 100 mL aliquots of the test samples following 2 h aeration were irradiated for 1 h under the following conditions: i) without any pH adjustment; ii) after the addition of H_2SO_4 (1 N) to adjust pH to 3.0; iii) after the addition of Na_2CO_3 to obtain basic solution and they are summarized in Table 8.2. The solution containing RO16 was adjusted to basic pH with varying concentrations of Na_2CO_3 as well as NaOH in order to investigate the effect of carbonate scavenging. The other test solution was adjusted to basic pH with Na_2CO_3 only. Samples were withdrawn at 0, 3, 5, 10, 15, 20, 30, 45 and 60 min of contact for spectrophotometric analysis.

Table 8.2. Properties of the test solutions in terms of pH and chemical buffer

Dyestuff	pH	Buffer
AO7	3.05	1 N H_2SO_4
	6.21	none (natural)
	8.50	0.2 mM CO_3^{2-}
	9.35	1 mM CO_3^{2-}
	10.28	5 mM CO_3^{2-}
	10.72	10 mM CO_3^{2-}
RO16	3.04	1 N H_2SO_4
	6.97	none (natural)
	8.58	1 N NaOH
	8.40	0.2 mM CO_3^{2-}
	9.44	1 mM CO_3^{2-}
	10.36	5 mM CO_3^{2-}

Analytical

Spectrophotometric analyses were carried out using a Unicam-Helios Alpha/Beta double beam spectrophotometer through a 1 cm path length and the degree of decolorization was assessed by relating the amount of visible absorption abatement in time to the original absorption at time zero. Total organic carbon (TOC) degradation was monitored with Shimadzu TOC-V CSH analyzer. H_2O_2 was analyzed spectrophotometrically at 351 nm based on KI (potassium iodide) method (Klassen *et al.*,

1994). Total alkalinity was determined titrimetrically by titrating the solutions with 0.023 N H_2SO_4 to pH 4.5 (APHA, 1992). Alkalinity of the solutions were then calculated by Equation (8.1.).

$$\text{Alkalinity (mg } CaCO_3\ L^{-1}) = \frac{0.023 \times acidconsumptionuntilpH4.5(ml) \times 50000}{samplevolume(ml)} \qquad (8.1)$$

8.1.3. Results and Discussion

8.1.3.1. Dye Degradation at Neutral State

Upon dissolution, both dyes were found to be slightly acidic with pH=5.08 in AO7 and 5.22 in RO16, to be attributed to deprotonation of naphtol OH. The higher value in RO16 must be due to excess sulphonation of the molecule. When the stocks were diluted with deionized water at pH=6.1, the final pH levels were recorded as 6.1 (AO7) and 6.9 (RO16), which were labeled as "non-buffered" solutions. Comparable profiles of the dye spectra (C_0=30 μM) at these conditions before and during sonication are presented in Figure 8.1. and Figure 8.2.

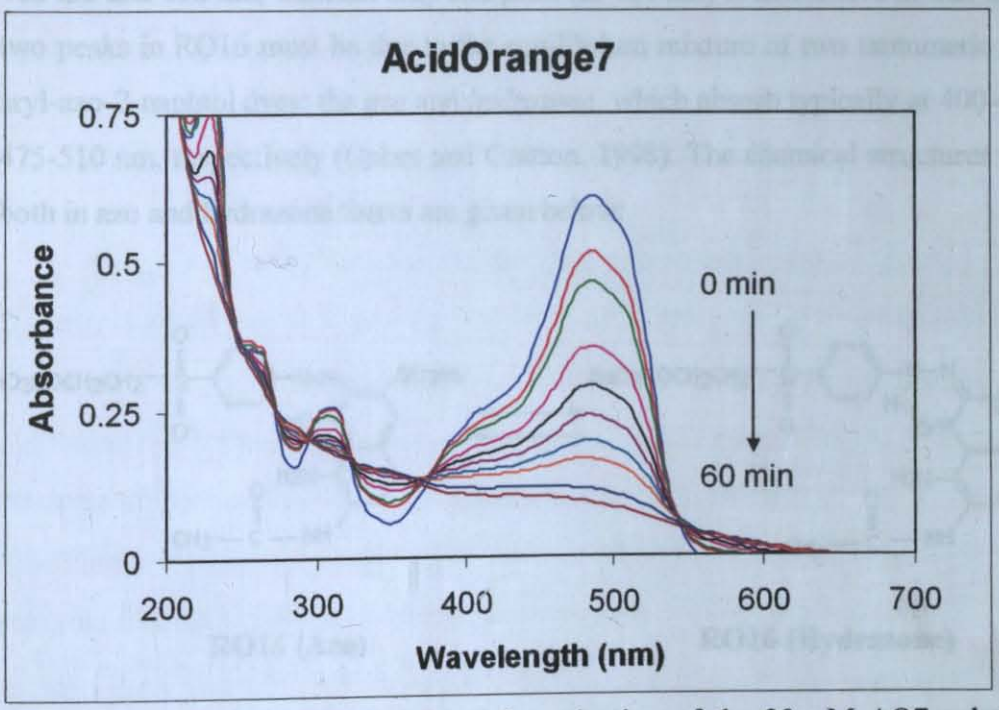

Figure 8.1. Spectral changes during 1 h sonication of the 30 μM AO7 solution at near neutral pH (non-buffered conditions).

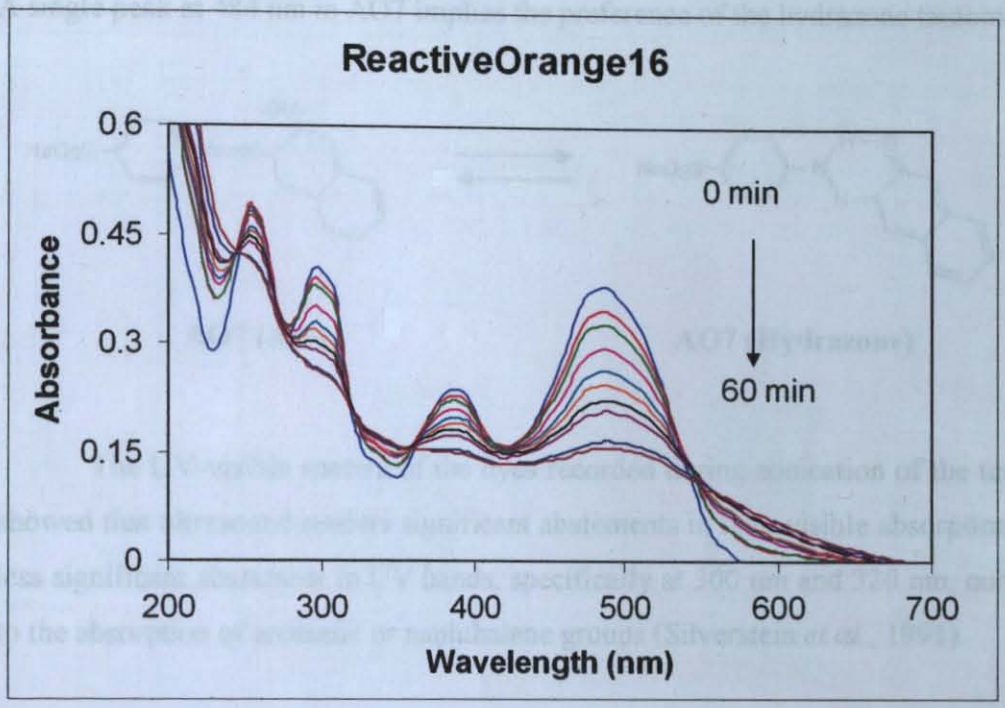

Figure 8.2. Spectral changes during 1 h sonication of the 30 μM RO16 solution at near neutral pH (non-buffered conditions).

Note that there are two distinct visible absorption peaks in the spectrum of RO16; at 400 nm and 492 nm, whereas only one peak (at 484 nm) is distinctive in that of AO7. The two peaks in RO16 must be due to the equilibrium mixture of two tautomeric forms in 1-aryl-azo-2-naphtol dyes: the *azo* and *hydrazone*, which absorb typically at 400-440 nm and 475-510 nm, respectively (Oakes and Gratton, 1998). The chemical structures of test dyes both in azo and hydrazone forms are given below:

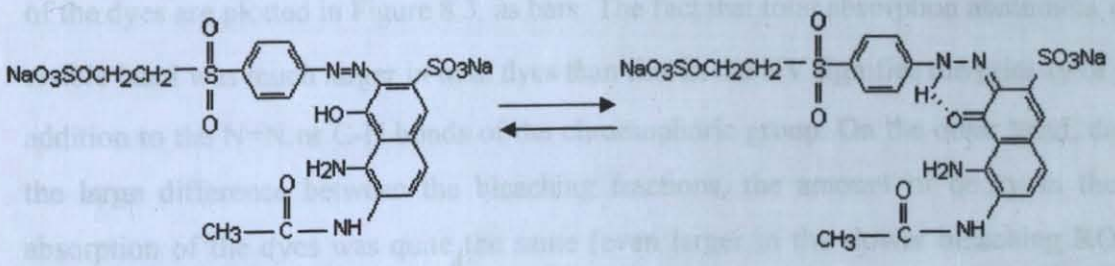

RO16 (Azo) **RO16 (Hydrazone)**

A single peak at 484 nm in AO7 implies the preference of the hydrazone tautomer:

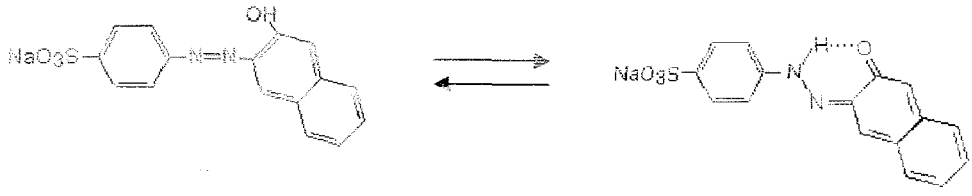

AO7 (Azo) **AO7 (Hydrazone)**

The UV-visible spectra of the dyes recorded during sonication of the test solutions showed that ultrasound renders significant abatements in their visible absorption, and some less significant abatement in UV bands, specifically at 300 nm and 320 nm, corresponding to the absorption of aromatic or naphthalene groups (Silverstein *et al.*, 1991).

The main reaction pathway for sonicated azo dye solutions is oxidation by •OH attack in the bulk liquid (Equation (8.2)), while thermal reactions may occur at the bubble-liquid interface provided that the conditions are suitable for some of the dye molecules to approach gaseous bubble surfaces (Equation (8.3)):

$$\bullet OH + Dye \rightarrow [Dye\text{-}OH\ adduct]^{\bullet} \rightarrow\rightarrow Oxidized\ dye + CO_2 + H_2O \quad (8.2)$$

$$Dye \rightarrow))) Organic\ radicals + Dissociated\ dye\ fragments + C_2H_4 \quad (8.3)$$

Relative fractions of color and aromatic component removal during 1 h sonication of the dyes are plotted in Figure 8.3. as bars. The fact that total absorption abatement in the visible band was much larger in both dyes than that in the UV signifies the priority of •OH addition to the N=N or C-N bonds of the chromophoric group. On the other hand, despite the large difference between the bleaching fractions, the amount of decay in the UV absorption of the dyes was quite the same (even larger in the slower bleaching ROr16), implying that the oxidation of aromatic components was not •OH limited, involving other oxidants such as H_2O_2, $^{\bullet}HO_2$ and $^{\bullet}O_2^-$ (which are products of water sonolysis), and/or other destruction pathways, such as proposed in Equation (8.3).

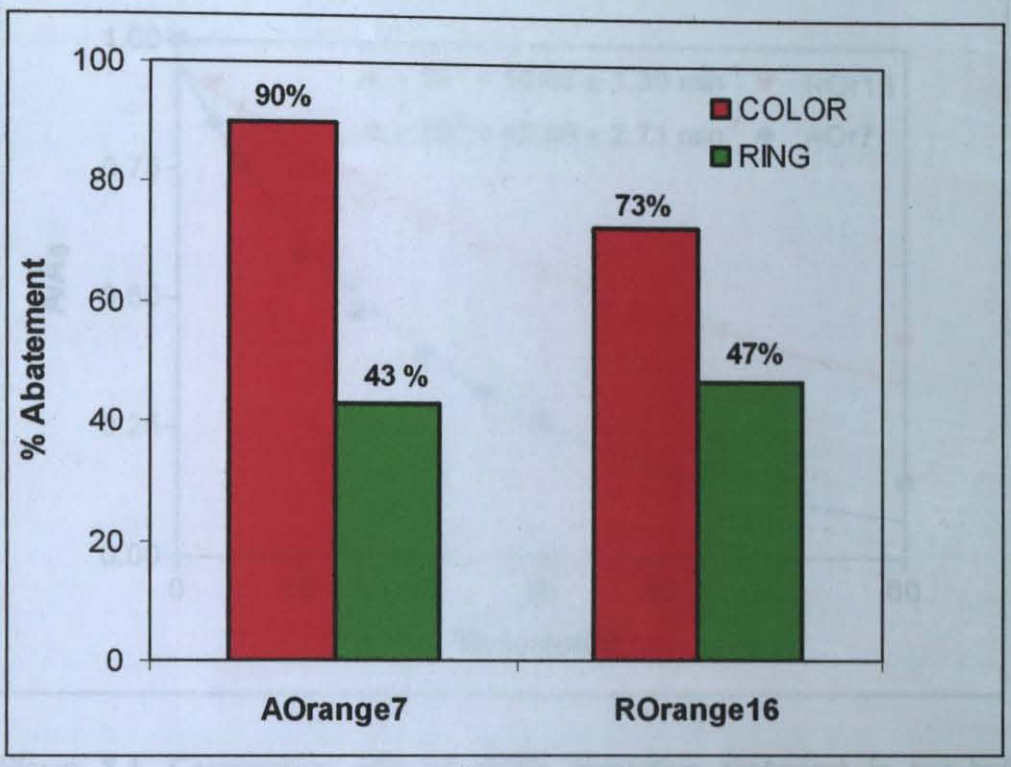

Figure 8.3. Relative fractions of UV and Visible absorption abatement in non-buffered test solutions with initial dye concentration = 30μM.

The rate of color decay followed pseudo-first order kinetics with respect to the visible absorption of the dyes. Profiles of color degradation during 1 h sonication of the test solutions at neutral conditions and the fit of data to the integrated or exponential form of Equation (4.2) are presented in Figure 8.4.

The fact that AO7 bleached remarkably faster than RO16 can be attributed to its: i) relatively simpler chemical structure and lower molecular weight; ii) lower initial pH and lower SO_3^- content (which increases anionicity of a molecule); and iii) hydrazone preference, which is reported to be more reactive with $H_2O_2/\bullet HO_2^-$ pair (that form by water sonolysis) than the azo form (Oakes and Gratton, 1998). The first two properties are also believed to enhance the probability of AO7 to approach the negatively charged cavity bubbles, where OH radicals are most abundant, and undergo additional degradation (oxidation/pyrolysis) at the gas-liquid interface.

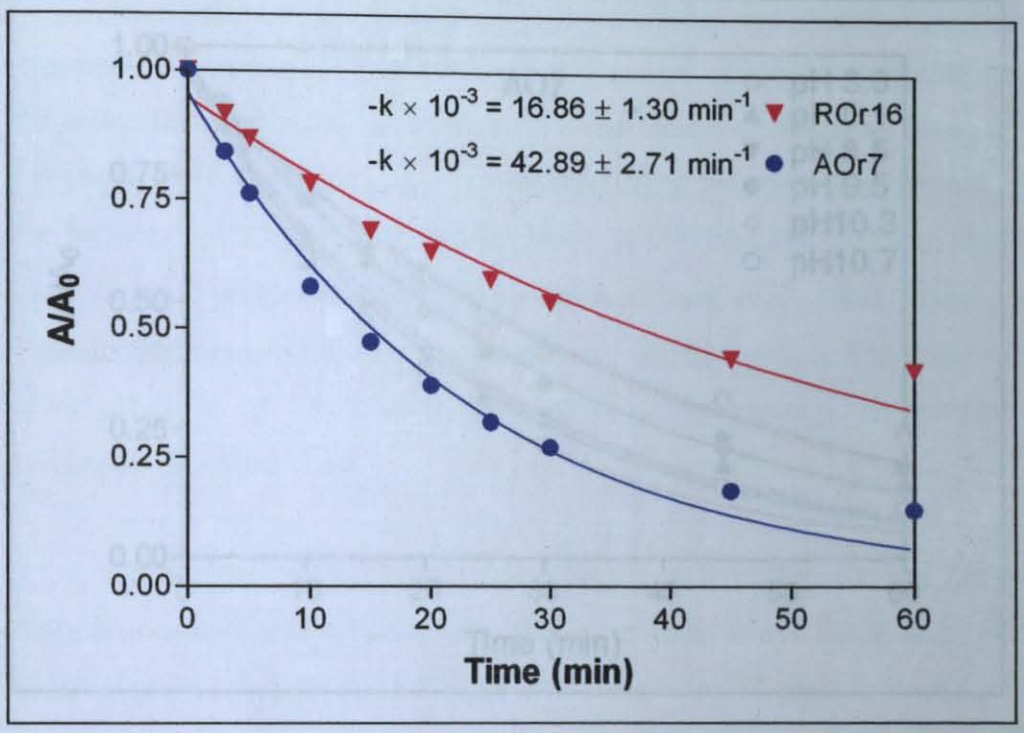

Figure 8.4. Comparative rates of visible absorption abatement in non-buffered dye solutions with initial dye concentration of 30 μM. The solid lines represent the fit of experimental data to $A/A_0 = e^{-kt}$ with regression coefficients $R^2>0.98$ in both fits.

8.1.3.2. Effect of pH and Molecular Structure

Kinetics of color degradation at all conditions followed first order law regardless of pH adjustments, and the fit of all data to first order rate equation revealed excellent statistics. The effect of pH on the rate of color degradation is presented in Figure 8.5. and Figure 8.6., and estimated rate coefficients are listed in Table 8.3. together with the azo forms of the dye structures.

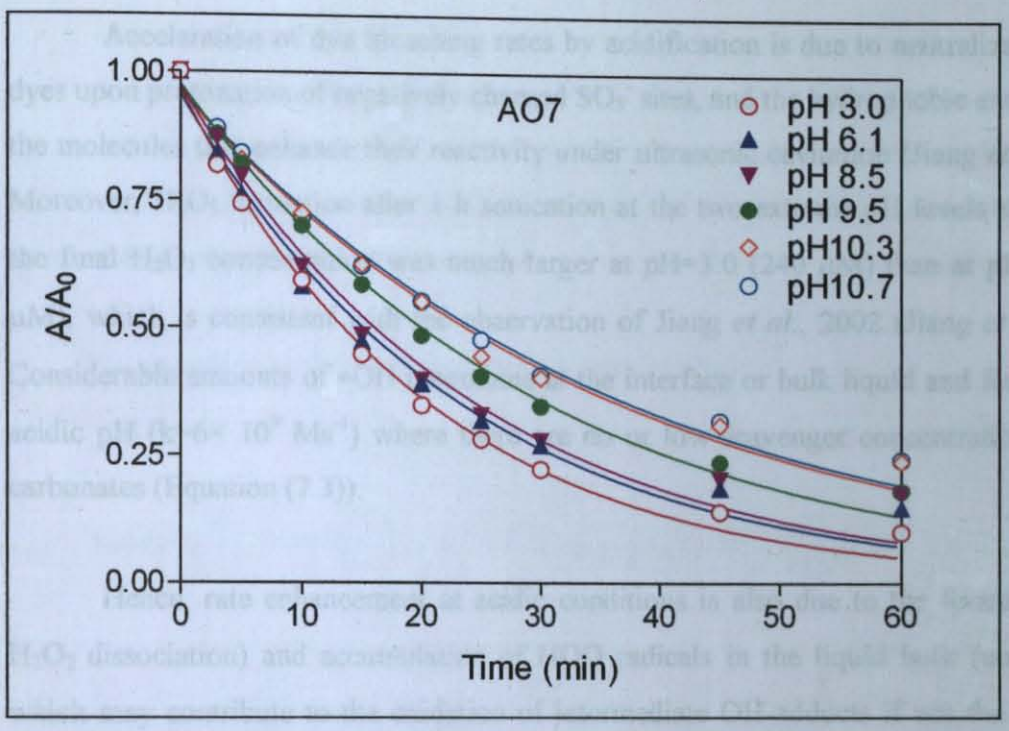

Figure 8.5. Impact of pH and carbonate alkalinity on pseudo-first order 30 μM AO7 bleaching rates. The solid lines are the fit of experimental data to $A/A_0 = e^{-kt}$.

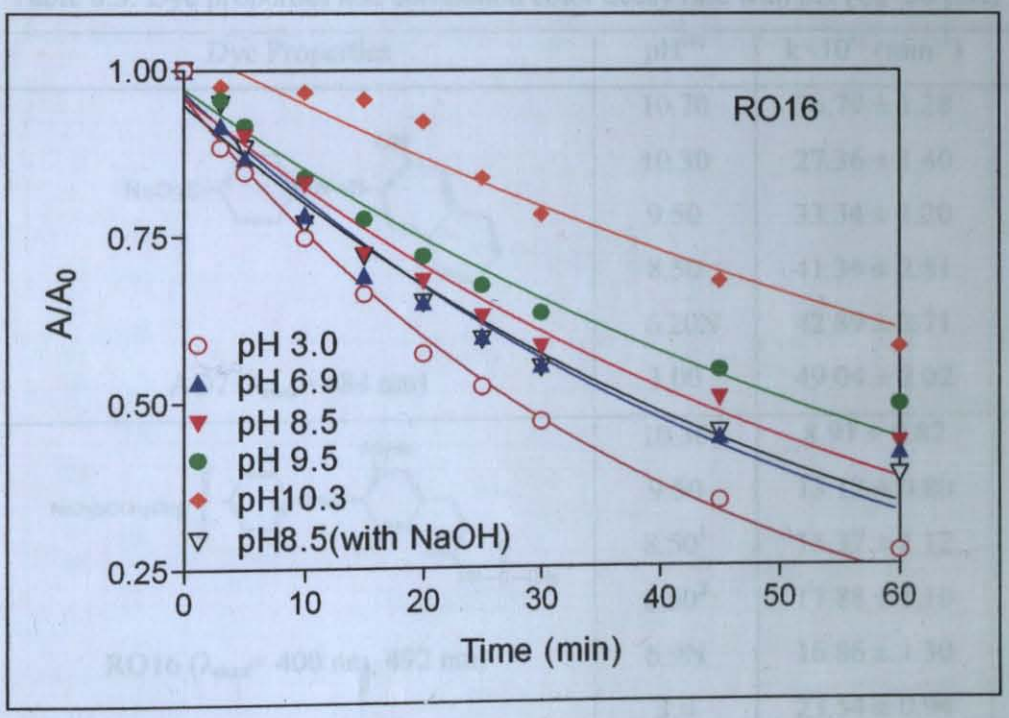

Figure 8.6. Impact of pH and carbonate alkalinity on pseudo-first order 30 μM RO16 bleaching rates. The solid lines represent the fit of experimental data to $A/A_0 = e^{-kt}$.

Acceleration of dye bleaching rates by acidification is due to neutralization of the dyes upon protonation of negatively charged SO_3^- sites, and the hydrophobic enrichment of the molecules that enhance their reactivity under ultrasonic cavitation (Jiang *et al.*, 2002). Moreover, H_2O_2 formation after 1 h sonication at the two extreme pH levels showed that the final H_2O_2 concentration was much larger at pH=3.0 (240 μM) than at pH=9.5 (130 μM), which is consistent with the observation of Jiang *et al.*, 2002 (Jiang *et al.*, 2002). Considerable amounts of •OH recombine at the interface or bulk liquid and form H_2O_2 at acidic pH ($k=6\times 10^9$ Ms^{-1}) where there are no or low scavenger concentrations such as carbonates (Equation (7.3)).

Hence, rate enhancement at acidic conditions is also due to the formation (upon H_2O_2 dissociation) and accumulation of HOO radicals in the liquid bulk (unlike •OH), which may contribute to the oxidation of intermediate OH-adducts if not the parent dye (Equation (7.4)).

($\bullet OH + H_2O_2 \rightarrow H_2O + HOO^{-}\bullet$ $k = 2.7 \times 10^7\ M^{-1}\ s^{-1}$).

Table 8.3. Dye properties and correlation color decay rate with pH (C_0=30 μM)

Dye Properties	pH[a]	$k\times10^{-3}$ (min^{-1})	R^2
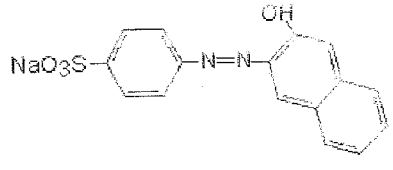 AO7 (λ_{max}= 484 nm)	10.70	26.79 ± 1.28	0.98
	10.30	27.36 ± 1.40	0.98
	9.50	33.34 ± 1.20	0.99
	8.50	41.35 ± 2.81	0.97
	6.20N	42.89 ± 2.71	0.98
	3.00	49.04 ± 2.02	0.99
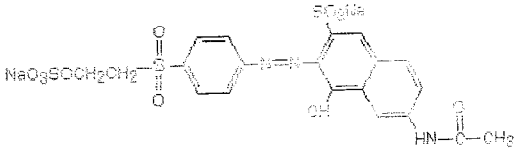 RO16 (λ_{max}= 400 nm, 492 nm)	10.30	8.91 ± 0.87	0.95
	9.50	13.12 ± 0.80	0.97
	8.50[1]	15.37 ± 1.12	0.97
	8.50[2]	17.88 ± 1.10	0.97
	6.9N	16.86 ± 1.30	0.96
	3.0	23.54 ± 0.94	0.99

(a)"N" refers to neutral, i.e. non-buffered conditions

[1] buffered with 1 N CO_3^{2-}, [2] buffered with 0.2 mM NaOH

Inhibition of color decay at alkaline conditions is a consequence of ionization of the dyes by hydrogen loss from protonated sites and naphthol –OH, resulting in enriched hydrophilic character. In fact, at pH above 9, the common ion (naphtalate) predominates over the azo and hydrazone forms owing to the fact that pK_a of aryl-azo-naphtol dyes is larger than 9.0 (Oakes and Gratton, 1998).

The common ion forms of test dyes are shown below:

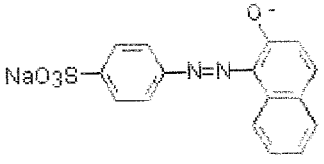

AO7 (common ion)

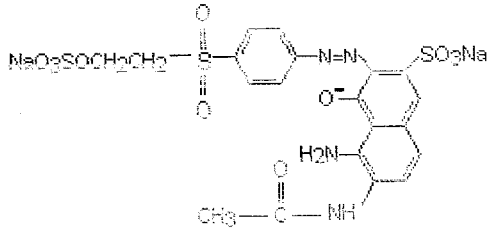

RO16 (common ion)

Relative effect of pH on first order bleaching rate is given in Figure 8.7., and the results show that at pH greater than 9, both of the dyes were in their common ion forms.

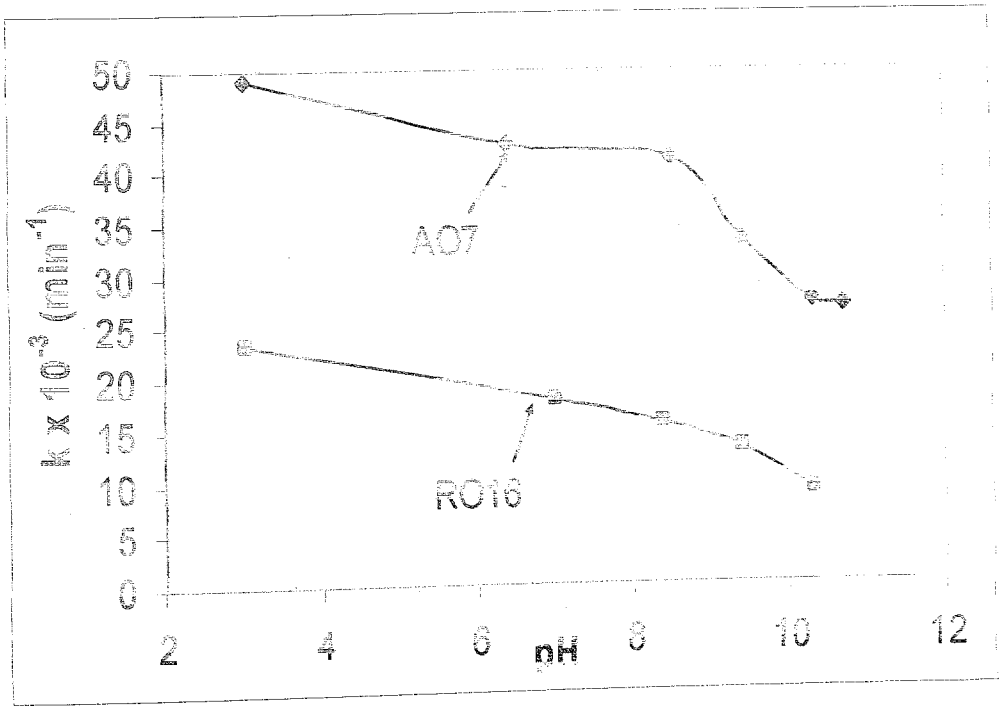

Figure 8.7. Relative effect of pH on first order bleaching Rate (C_o = 30 μM).

There was a significant reduction in decolorization rates above pH 9 for AO7 and RO16. Probably the pKa of test dyes were close to 9. and at pH above 9 the dyes began to dissociate and lose hydrogen, resulting in enriched anionic character. Because of their increased hydrophilic character, they tended to stay in bulk liquid and degraded with radicals only where as the dyes at acidic pH probably degraded both via oxidation in bulk liquid and at bubble-liquid interface.

Moreover, at such and higher levels of pH, •OH scavenging effects become significant, particularly when the scavengers are anions such as HCO_3^- and CO_3^{2-} that were introduced to the reactor by the addition of a sodium carbonate buffer. As can be seen in Table 8.3.and Figure 8.8., pseudo-first order decolorization rate constants for both dye solutions were decreased along with the addition of Na_2CO_3. When the pH of the RO16 solution was adjusted to 8.5 with 1 N NaOH and 2 mM Na_2CO_3, no significant carbonate scavenging was observed. Formed carbonate radicals (Equation (7.9) and (7.10)) are in principle also capable of oxidizing pollutants but in general they have lower rates than •OH (Equation (7.12)). Thus, on one hand, carbonate ions can even promote the efficiency of the treatment process, but on the other hand, these ions are effective radical scavengers reducing the amount of •OH available for pollutant oxidation (Equation. (7.9)). By the addition of 5 mM soda ash (Na_2CO_3) which is a typical dose for reactive dyebaths (≈ 4 mM CO_3^{2-} in 30 µM reactive dyebath solution), two fold and three fold decrease in color and UV_{312} removals were evident, respectively. This implied the •OH scavenging effect of soda that became particularly pronounced for the color and aromatic removal of the dye after pH 10.3.

The observed difference in the reactivity and/or rate of degradation of the test dyes at equivalent conditions is a consequence of differences in their structural features. Although the mechanism of •OH reactions with azo dyes is still not clear, theoretical methods using quantum mechanical calculations and proposed reaction mechanisms based on product analysis have revealed that the addition of •OH to the azo bond is more favorable than addition to the C-N bond (Joseph *et al.*, 2000; Ozen *et al.*, 2003). It has also been proposed that reactions of OH radicals with azo dyes involve both hydroxyl adduct formation and electron transfer processes (Das *et al.*, 1999).

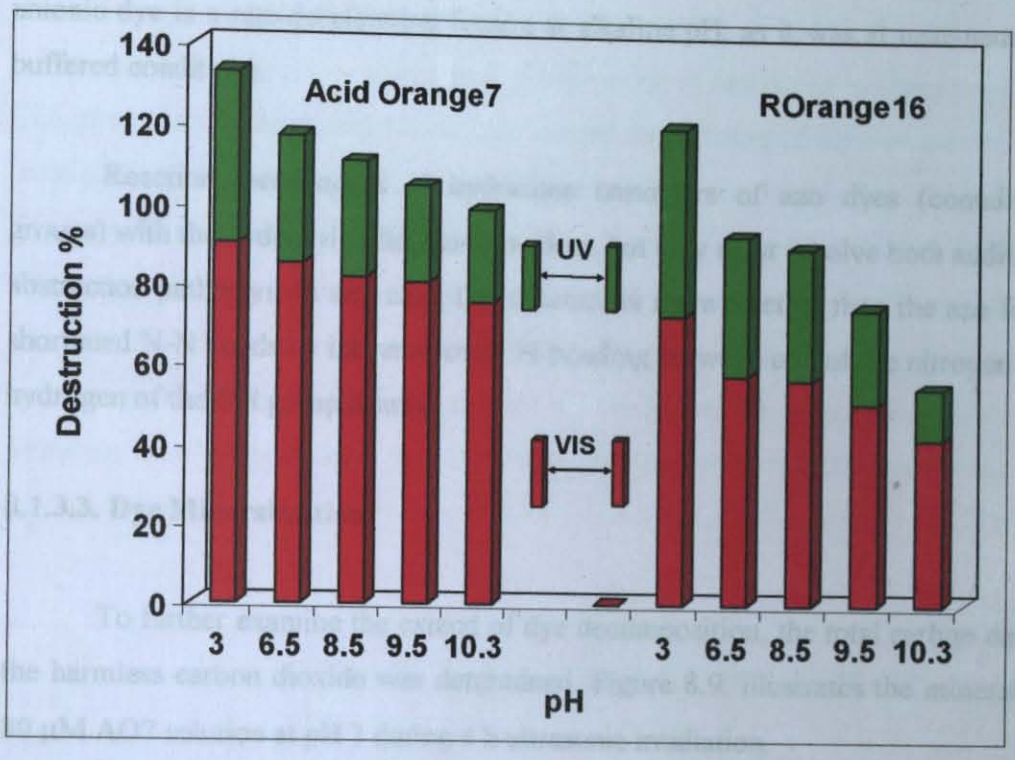

Figure 8.8. Effect of pH and carbonate alkalinity on dye decolorization and ring destruction.

When the test dyes are in azo form, addition of •OH to the naphtol nitrogen results in strong intermolecular hydrogen bonding between hydrogen of the OH-adduct and oxygen of the naphtol OH, positioned *ortho* to the N-N bond. A similar reasoning reported for *ortho*-carboxyl substituents in aryl-azo dyes was confirmed by DFT calculations, showing that the enhancement in the rate of reaction with •OH was due to internal H-bonding, by which the N-N bond distance shortened and the activation energy was lowered (Destaillats *et al.*, 2002). In RO16, which had a second *o*-substituent at the naphtol ring (SO_3^-), internal H-bonds are weakened (due to steric effects and the competition between two *o*-substituents for H-abstraction from the OH-adduct), and hence the reactivity of the dye is reduced. Moreover, delocalization of the C-O bond electrons of the carboxyl amine group attached to the naphtol ring stabilizes RO16 molecule, thus lowering its reactivity. It is also possible that solvent effects in RO16 are stronger than in AO7 due to more complex substituent structures in the former (such as p-positioned SO_2RSO_3Na at the benzene ring, as opposed to SO_3Na in AO7). Finally, the relative ease of ionization in RO16 to form the

anionic dye is a rate-decelerating feature at alkaline pH, as it was at near-neutral or non-buffered conditions.

Reaction mechanisms of hydrazone tautomers of azo dyes (containing α-OH groups) with the hydroxyl radical are not clear, but they must involve both addition and H-abstraction pathways. In any case, the structure is more reactive than the azo form due to shortened N-N bonds by intramolecular H-bonding between one of the nitrogen atoms and hydrogen of the OH group nearby.

8.1.3.3. Dye Mineralization

To further examine the extend of dye decomposition, the total carbon converted to the harmless carbon dioxide was determined. Figure 8.9. illustrates the mineralization of 30 μM AO7 solution at pH 3 during 4 h ultrasonic irradiation.

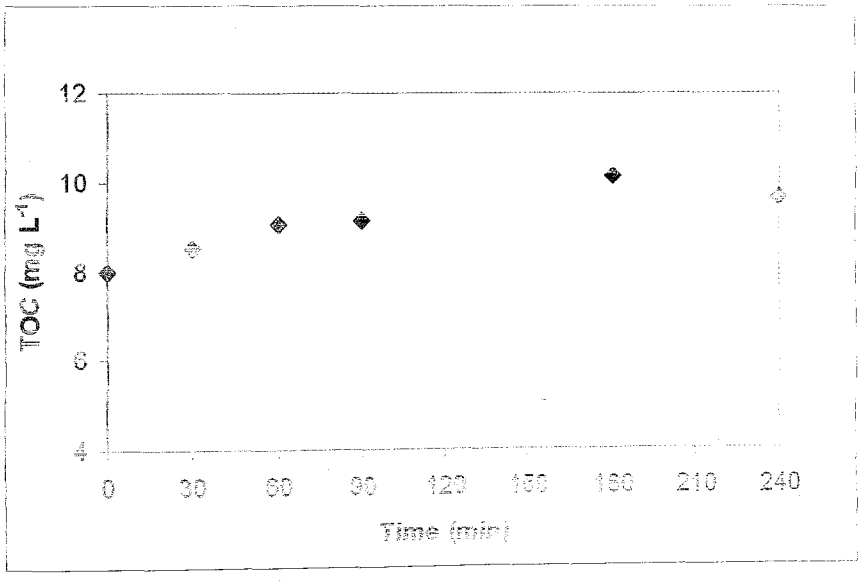

Figure 8.9. Mineralization of AO7 during ultrasonic irradiation (Initial dye concentration 30 μM, pH 3).

Although appreciable color and aromatic degradation was achieved, no TOC degradation (even a slight increase in total organic content) was observed during 4 h ultrasonic irradiation of the test dye. This increase may be due to the diffusion of atmospheric carbon dioxide into the reactor solution (the system was open to the

atmosphere) (Harada, 1998). Hence, longer contact is needed for more appreciable mineralization of the dye. However, we believe that in ultrasonic systems reliable TOC or CO_2 production is not a measure of the overall degradation of organic matter, because in most cases, pyrolysis results in the production of acetylene, which may not be converted to CO_2. As Beckett and Hua (2003) have shown, lower frequencies (300-400 kHz) tend to draw nonvolatile species such as dyestuffs into the extreme conditions of gas phase through microstreaming effects. Therefore, AO7 could additionally be degraded within the bubble by additional thermolytic mechanism and harmless pyrolysis products, such as acetylene could be generated, which can not be monitored during TOC analysis.

8.2. C.I. Acid Black1 and C.I. Reactive Black5

In this part of the study, the same dye model was investigated, using two different test dyes: C.I. Acid Black1 (AB1) and Reactive Black5 (RB5).

8.2.1. Materials and Methods

8.2.1.1. Dyes

C.I. Reactive Black5 was obtained from Dyestar Hoechst and the latter was obtained from Aldrich. A summary of commercial and molecular dye properties is presented in Table 8.4. All reagents consumed in this study were analytical Merck grade.

Table 8.4. Commercial and chemical properties of C.I. Acid Black1 and C.I. Reactive Black5

Dye C.I./ Company-purity (Molecular Weight)	X_1, X_2, R_1 substituents	X_3, X_4, X_5 substituents	Maximum Absorption
AcidBlack1/ ALDRICH-80% 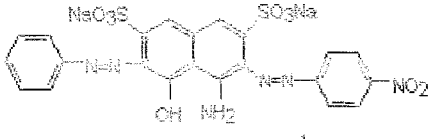 (517 $gmoL^{-1}$)	X_1= $-SO_3Na$ X_2= $-OH$ R_1= $-H$	X_3= $-NH_2$ X_4= $-Aryl-azo$ X_5= $-SO_3Na$	620 nm
ReactiveBlack5/ DYESTAR/HOECHST-85% 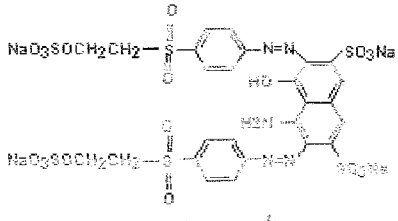 (992 $gmoL^{-1}$)	X_1= $-SO_3Na$ X_2= $-OH$ R_1= $SO_2C_2H_4S$	X_3= $-NH_2$ X_4= $-Aryl-azo$ X_5= $-SO_3Na$	596 nm

8.2.1.2. Experimental Procedure

Operating parameters and test dye solution preparation procedure were the same as previously indicated in Section 8.1. Test solutions were diluted to 30 μM as dye with deionized water or alkaline tap water, respectively. The solutions were sonicated for one hour under the following conditions: i) without the addition of a buffer, i.e. at their natural pH; ii) after the addition of 1 N H_2SO_4 to buffer to pH=3.0; iii) after the addition of Na_2CO_3 to buffer to pH=8.5 and 9.5, as summarized in Table 8.5. Hundred milliliters of samples were aerated for 2 h and then irradiated for 1 h for UV-Vis spectrometry analysis. Experiments were extended to 4 h to monitor the ultrasonic mineralization of the dyes.

Table 8.5. Properties of the test solutions in terms of pH and chemical buffer

Dyestuff	pH	Buffer
AB1	3.02	1 N H_2SO_4
	6.98	none (natural)
	8.50	0.2 mM CO_3^{2-}
RB5	3.00	1 N H_2SO_4
	7.50	none (natural)
	8.50	0.2 mM CO_3^{2-}

Analytical

UV-VIS spectrophotometry analyses were carried out using a Unicam, Helios Alpha/Beta double beam spectrophotometer through a 1 cm path length. Dye mineralization was followed by a Shimatzu TOC V analyzer during 4 h irradiation.

8.2.2. Results and Discussion

8.2.2.1. Dye Degradation at Neutral State

The effect of dye structure on color decay was investigated in deionized water solutions at their neutral (non-buffered) conditions. The azo and hydrazone forms of the test dyes are illustrated in Figure 8.10.

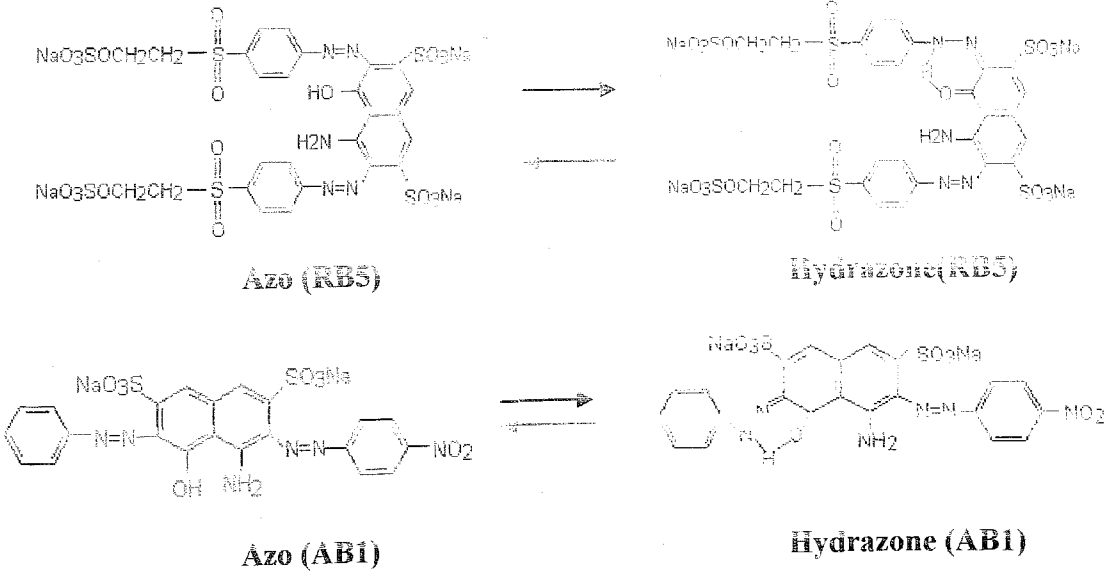

Figure 8.10. Azo and hydrazone forms of the test dyes.

Both test dyes contain a hydroxyl group in *ortho* position to the azo bond and exist in equilibrium with two tautomeric forms, azo and hydrazone which absorb at different visible wavelengths. The spectra of 30 μM AB1 and RB5 solutions at their non-buffered conditions before and during sonication are presented in Figure 8.11. and Figure 8.12., respectively.

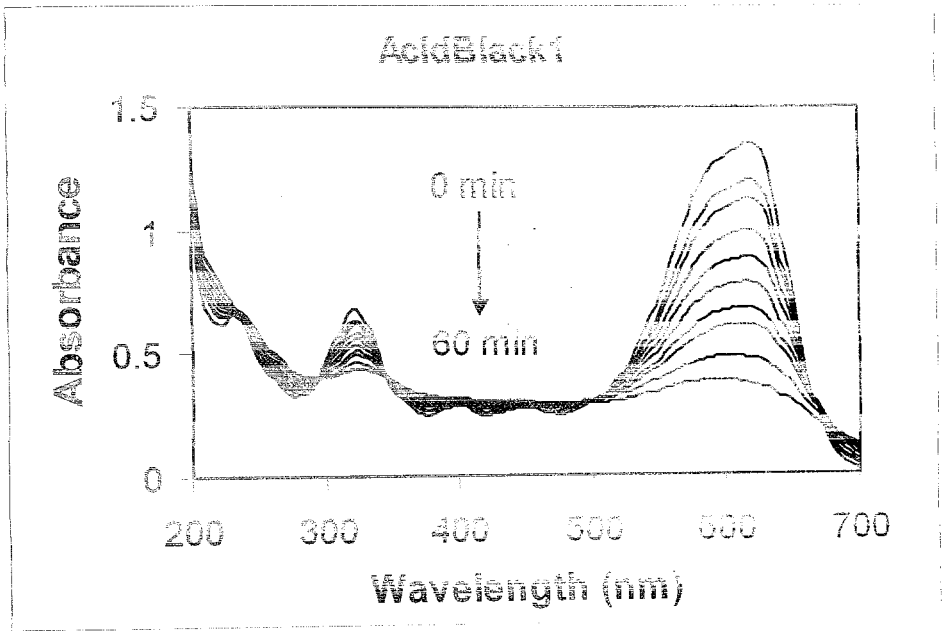

Figure 8.11. Spectral changes during 1 h sonication of the 30 μM AB1 solution at near neutral pH (non-buffered conditions)

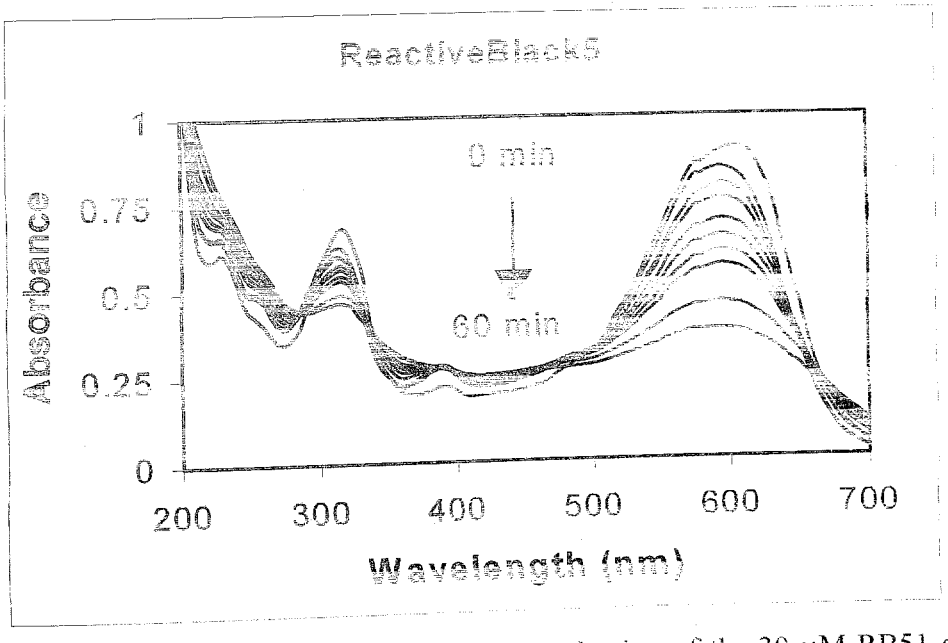

Figure 8.12. Spectral changes during 1 h sonication of the 30 μM RB51 solution at near neutral pH (non-buffered conditions).

From the above spectra of the test dyes, AB1 is expected to favor the hydrazone form, because it has a high absorption at 484 nm. RB5 is expected to exist in both hydrazone and azo form, because there is also another peak between 390-440 nm (not as high as the peak at 596 nm).

Color and aromatic fragment degradation after 1 h ultrasonic irradiation are given in Figure 8.13. Color degradation of AB1 and RB5 was greater than the aromatic fragment removal which is consistent with the results of previous dyes. This again confirms the priority of •OH attack to the N=N or C=N bonds. Aromatic fragment abatement was not as large as color abatement, again implying that the aromatic degradation was not •OH limited. Other sonochemically generated radicals, such as $•HO_2$ and $•O_2$ can play role in aromatic fragment degradation.

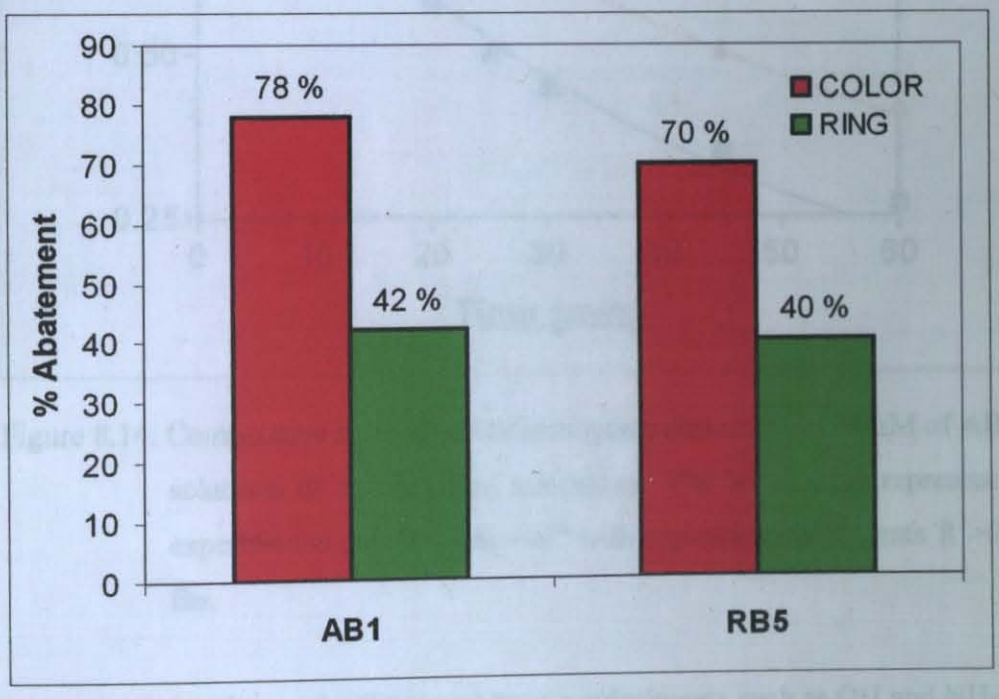

Figure 8.13. Relative fractions of UV and visible absorption abatement in non-buffered AB1 and RB5 solutions with initial dye concentration = 30μM.

Faster color removal of monoazo dyes RO16 and AO7 (Section 8.1) than disazo dyes AB1 and RB5 confirms that color decay is •OH diffusion controlled, and is limited by the steady state •OH concentration in bulk liquid. Hence, at limited •OH, the rate of bleaching slows down as the number of chromophores (in our case azo bonds) in dye

increases. Also, the character of o- and p- substituents about the azo bonds and the molecular weight of the dye are responsible for the deceleration in color removal.

The rate of color removal was pseudo-first order, and profiles of color removal during 1 h sonication of the test dye solutions at non-buffered conditions are illustrated in Figure 8.14.

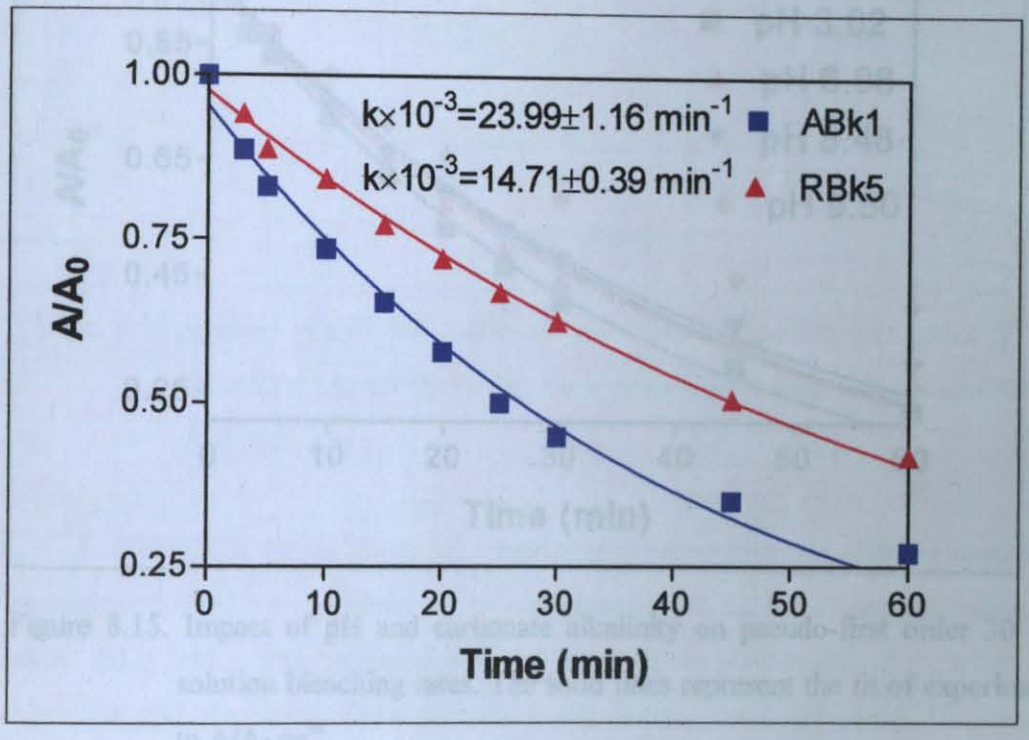

Figure 8.14. Comparative rates of visible absorption abatement in 30 μM of AB1 and RB5 solutions at non-buffered conditions. The solid lines represent the fit of experimental data to $A/A_0 = e^{-kt}$ with regression coefficients $R^2>0.98$ in both fits.

Both test dyes were disazo and have o-substituents such as OH and NH_2. Similarity of their azo groups and o- substituents, the higher color removal rate in AB1 solution can be attributed to i) lower molecular mass and simpler structure, ii) difference of p-substituents, iii) lower SO_3^- content (will be less anionic and will tend to approach to bubble to degrade additionally at the bubble/liquid interface), and iv) and the preference of the reactivity $H_2O_2/{\bullet}HO_2^-$ pair with hydrazone form.

8.2.2.2. Effect of pH and Molecular Structure

The impact of pH on color degradation is illustrated in Figure 8.15. and Figure 8.16., and estimated rate coefficients are given in Table 8.6.

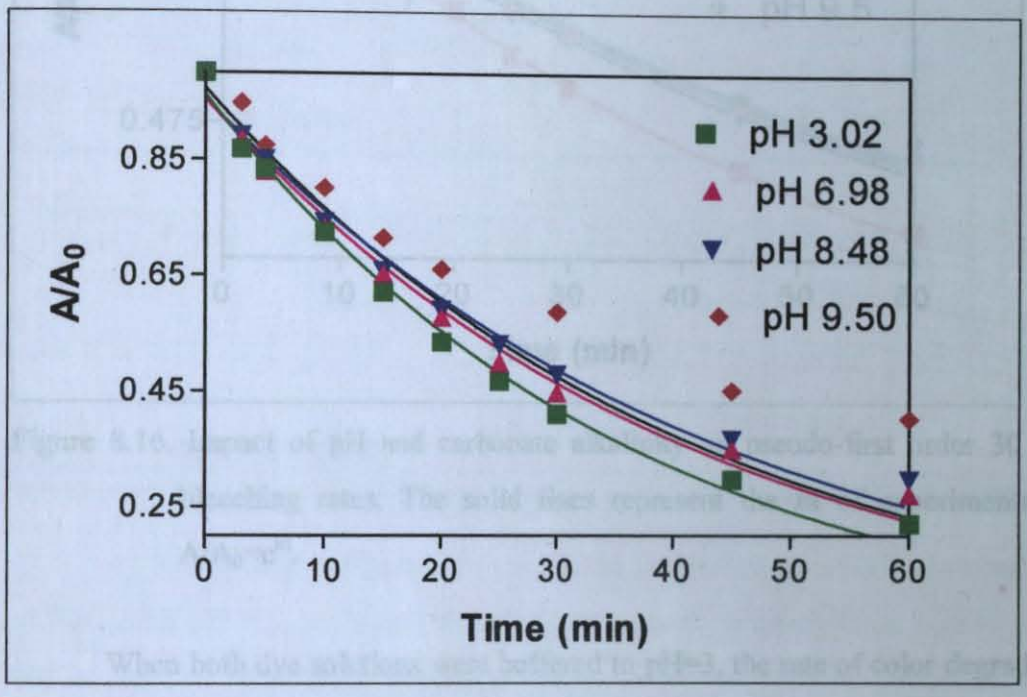

Figure 8.15. Impact of pH and carbonate alkalinity on pseudo-first order 30 μM AB1 solution bleaching rates. The solid lines represent the fit of experimental data to $A/A_0 = e^{kt}$.

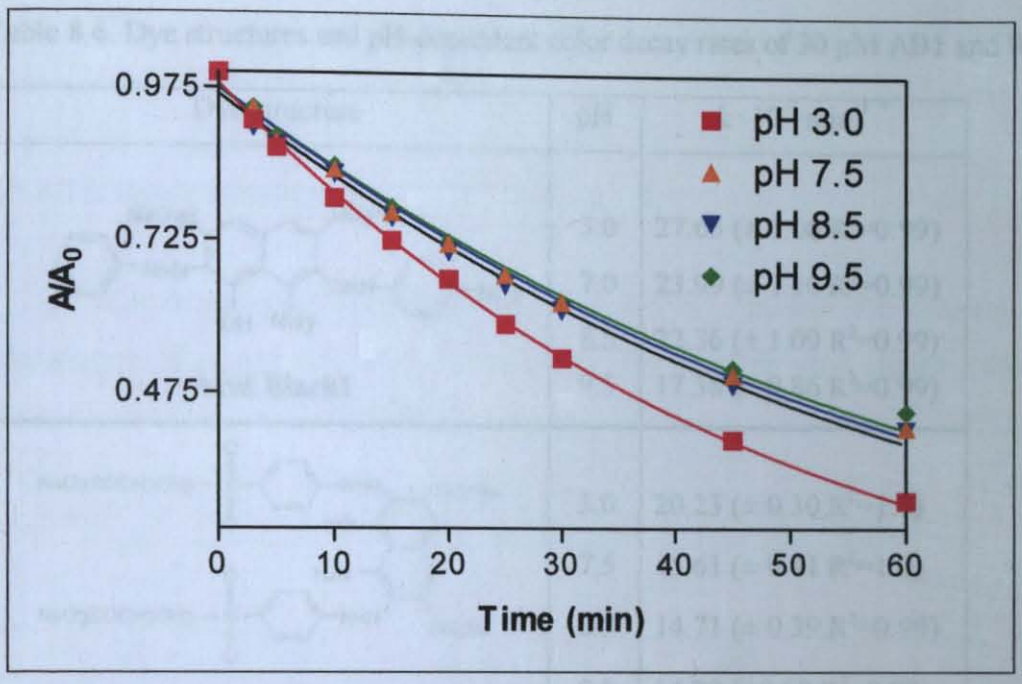

Figure 8.16. Impact of pH and carbonate alkalinity on pseudo-first order 30 μM RB5 bleaching rates. The solid lines represent the fit of experimental data to $A/A_0=e^{kt}$.

When both dye solutions were buffered to pH=3, the rate of color degradation was accelerated which can be attributed to neutralization of the dyes upon protonation of SO_3^- sites. As a result, dye molecule becomes more hydrophobic and approaches to bubble interface and also reacts with radicals at the bubble-liquid interface. The rate of color degradation in AB1 accelerated by 17 per cent, while decolorization in RB5 solution accelerated by 33 per cent. This implies the importance of hydrophobicity of the molecule.

At higher levels of pH, decrease in color removal rates was observed. This can be due to i) the ionization of the dyes by hydrogen loss, resulting in increased hydrophilic character. Such hydrophobic compounds tend to stay in the bulk liquid and degrade with radicals only in solution, where more hydrophilic dyes react with radicals both in solution and bubble-liquid interface; ii)•OH scavenging effect of HCO_3^- and CO_3^{2-}, which were added with sodium carbonate buffer during pH adjustment.

Table 8.6. Dye structures and pH-dependent color decay rates of 30 μM AB1 and RB5

Dye structure	pH	k 10^{-3} min^{-1} *
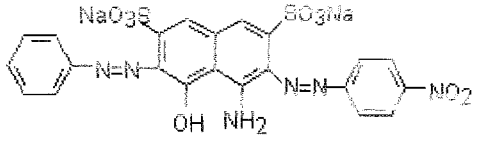 **Acid Black1**	3.0	27.65 (± 1.06 R^2=0.99)
	7.0	23.99 (± 1.16 R^2=0.99)
	8.5	22.36 (± 1.09 R^2=0.99)
	9.5	17.38 (± 0.86 R^2=0.99)
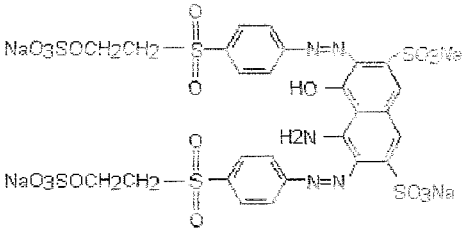 **Reactive Black5**	3.0	20.23 (± 0.30 R^2=1.0)
	7.5	15.61 (± 0.41 R^2=1.0)
	8.5	14.71 (± 0.39 R^2=0.99)
	9.5	14.20 (±0.50 R^2=0.99)

*figures in parenthesis are 95 % confidence intervals and the coefficients of regression.

As can be seen in Figure 8.17., there was a significant reduction in bleaching rates of AB1 after pH 8.5, implying that the dye was mostly existing in its common ion form. and because of its anionic structure probably it degraded only with radicals in solution bulk.

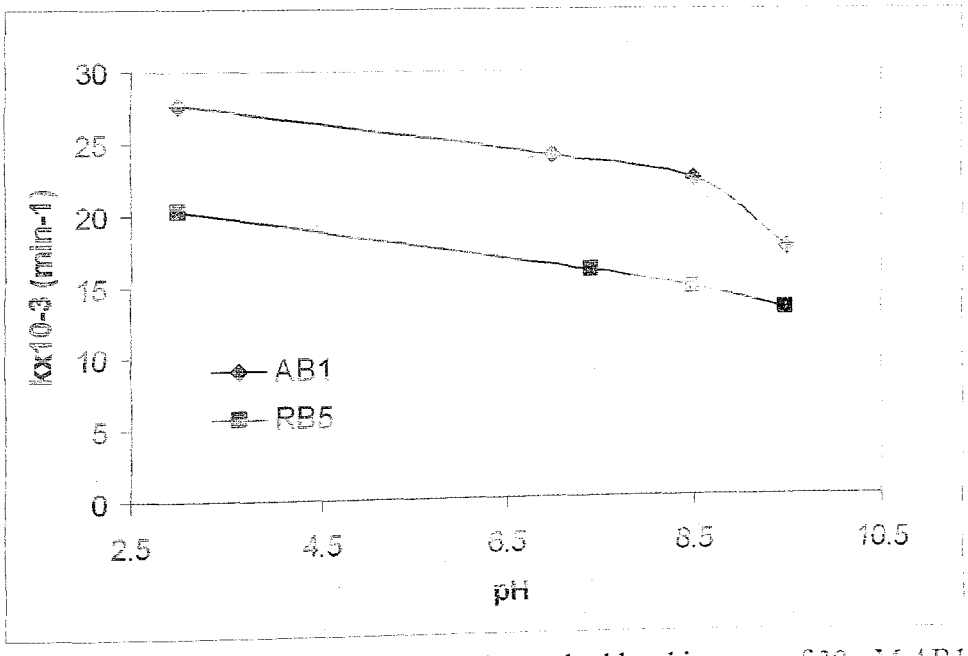

Figure 8.17. Relative effect of pH on first order bleaching rate of 30 μM AB1 and RB5.

The reduction in bleaching rates of RB5 was not considerable, and pKa of RB5 is thought to be much greater than pH 9.

8.2.2.3. Dye Mineralization

The extent of mineralization was monitored for a period of 4 h during ultrasonic irradiation of 30 μM AB1 and RB5 solutions. The obtained total organic carbon (TOC) data are displayed in Figure 8.18.

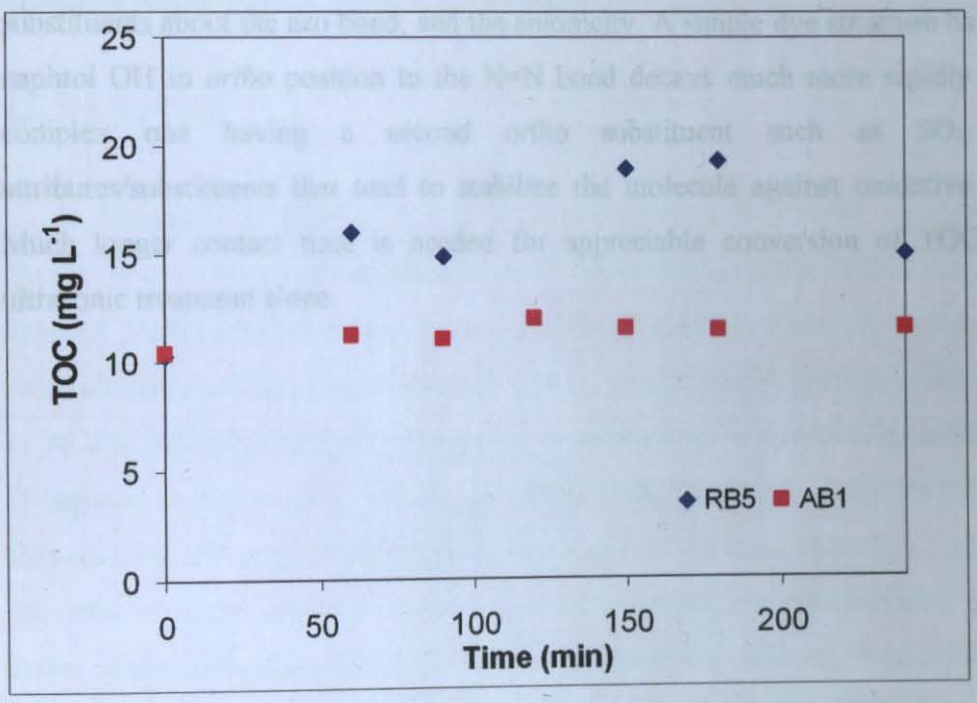

Figure 8.18. Total organic carbon variation in 30 μM AB1 and RB5 during 4 h ultrasonic irradiation at pH= 3.

During the course of treatment with ultrasonic irradiation, TOC of both solutions were slightly increased. The obtained results can be attributed to the diffusion of atmospheric carbon dioxide into the test solution.

8.2.3. Conclusions

Sonochemically generated hydroxyl radicals are shown to oxidize aryl-azo naphtol dyes by pseudo-first order reaction rates. Dye degradation is initiated by hydroxyl radical

attack onto the chromophore made up of an azo linkage between a benzene ring and a naphtol group. Conditions that favor neutral molecules such as acidic pH accelerate the rate of bleaching by hydrophobic enrichment of the molecules and the formation of excess H_2O_2, $\cdot HO_2$- and $\cdot O_2$-. Similarly, rate of bleaching is inhibited at alkaline pH upon the formation of negatively charged dye molecules and radicals, and OH radical scavenging effect of carbonate/bicarbonate species.

The rate of azo dye bleaching by ultrasound is also dependent on structural features, such as the largeness and complexity of the molecule, the type and position of the substituents about the azo bond, and the anionicity. A simple dye structure having only the naphtol OH in *ortho* position to the N=N bond decays much more rapidly than a more complex one having a second ortho substituent such as SO_3 and other attributes/substituents that tend to stabilize the molecule against oxidative degradation. Much longer contact time is needed for appreciable conversion of TOC to CO_2 by ultrasonic treatment alone.

CHAPTER 9. ULTRASOUND IN ADVANCED OXIDATION PROCESSES-A CASE STUDY WITH ACID ORANGE 7: APPLICATIONS IN SYSTEM III

Part of this chapter is the study presented in "Ultrasonics 2003, 30 June-4 July 2003, Granada, Spain" (published in conference proceedings), and the whole work is submitted to *Ultrasonics*, and is under review.

9.1. Background

Ultrasonic irradiation is a potential catalyzer of Advanced Oxidation Processes (AOPs) in environmental remediation, due to •OH and H_2O_2 production during cavitation-induced water decomposition. It is possible to achieve complete color removal and mineralization in refractory pollutants such as those found in textile dyeing mill effluents by AOPs. Advanced oxidation is a term commonly used to describe oxidative degradation of organic matter by free radicals, particularly the hydroxyl radical (•OH), which is a nonselective and very powerful oxidizing agent. Ultraviolet light (UV) coupled with a powerful oxidizing agent or a semi-conductor, Fenton and photo-Fenton processes are some of the common Advanced Oxidation Processes (Glaze *et al.*, 1987; Ince and Tezcanli, 1999; Vinodgopal and Kamat, 1998; Naffrechoux *et al.*, 2000).

Cavitation in liquids results in extreme temperatures and pressures upon collapsing of acoustic micro bubbles. This phenomena initiates and promotes chemical reactivity through thermolysis within the center of the bubble, free radical oxidation at the interface of the bubble and/or in the bulk liquid (Ince *et al.*, 2000; Joseph *et al.*, 2000). The efficiency of •OH diffusion into the aqueous phase is related to system parameters such as frequency, reactor geometry, sparge gases, and ultrasonic power (Mason and Cordemans, 1998). When the sparge gas is Argon and the medium is water, the reaction sequence is as follows (Ince *et al.*, 2000):

$$H_2O +))) \rightarrow \bullet OH + \bullet H \quad \text{(thermolysis)} \quad (9.1)$$

$$\bullet OH + \bullet H \rightarrow H_2O \quad (9.2)$$

$$\bullet OH + \bullet OH \rightarrow H_2O_2 \quad (9.3)$$

$$2\,\bullet OH \rightarrow H_2O + O \quad (9.4)$$

If the solution is saturated with oxygen, peroxyl and additional hydroxyl radicals are formed in the gas phase (Beckett and Hua, 2000) as:

$$O_2 +))) \rightarrow 2\bullet O \quad (9.5)$$

$$O_2 + O \rightarrow O_3 \quad (9.6)$$

$$O_2 + \bullet H \rightarrow \bullet O_2H \text{ (or } \bullet OH + O) \quad (9.7)$$

$$O + \bullet O_2H \rightarrow \bullet OH + O_2 \quad (9.8)$$

$$\bullet O_2H + \bullet O_2H \rightarrow H_2O_2 + O_2 \quad (9.9)$$

$$\bullet O + H_2O \rightarrow 2\bullet OH \quad (9.10)$$

Physical and chemical properties of the medium such as pH, vapor pressure and partition coefficient of the solutes are also significant parameters that affect sonochemical yields. In sonolysis of water containing hydrophilic compounds such as textile dyes, oxidative dye destruction is possible if the radicals are effectively ejected into the solution bulk. The optimum frequency range for degradation of these compounds is 200-600 kHz. (Pétrier and Francony, 1997).

Ozonation (coupled with or without a source of ultraviolet light) is one of the most common practice of free radical production in AOPs. Ozone reacts with organic compounds via two different pathways namely direct molecular and indirect radical chain type reaction depending upon pH of the water. Molecular O_3 is the major oxidant at acidic pH and reacts directly by electrophilic attack, whereas less selective and faster radical

reaction oxidations (mainly •OH) become predominant at pH > 7, as a consequence of acceleration of O_3 decomposition by OH^- (Glaze *et al.*, 1987). When ozonation is coupled with UV irradiation, additional •OH radicals are produced (Equation (9.11)) as:

$$O_3 + h\nu \rightarrow 2\,{\bullet}OH \qquad \lambda = 254\ nm \qquad (9.11)$$

When ozonation is combined with ultrasonic irradiation, thermal decomposition of ozone in cavitation bubbles results in increased •OH and H_2O_2 as shown (Destailattes *et al.*, 2000; Ince and Tezcanli, 2001, Weavers *et al.*, 1998):

$$O_3 +))) \rightarrow O_2(g) + O(^3P)\,(g) \qquad (9.12)$$

$$O(^3P)(g) + H_2O(g) \rightarrow 2{\bullet}OH \qquad (9.13)$$

$$O_3 + {\bullet}OH \rightarrow {\bullet}HO_2 + O_2 \qquad (9.14)$$

$$O_3 + H_2O \rightarrow 2HOO{\bullet} \qquad (9.15)$$

$$O_3 + HOO{\bullet} \rightarrow {\bullet}OH + 2O_2 \qquad (9.16)$$

$$O_3 + H_2O_2 \rightarrow {\bullet}OH + O_2 + HO_2 \qquad (9.17)$$

Recent studies have shown that the efficiency of ultrasound in wastewater treatment (degradation of aromatics) is low (Ince and Tezcanli, 2001, Vinodgopal *et al.*, 1998), however combination of US with other techniques (sonoelectrolysis, ultrasound/H_2O_2 and/or O_3, ultrasound/UV, ultrasound/Fenton's reagent) are very effective upon excess •OH formation and enhanced O_3 diffusion (Naffrechoux *et al.*, 2000; Beckett and Hua, 2003; Lorimer *et al.*, 2000).

The purpose of this study was to investigate the performance of 520 kHz ultrasound and its combinations with ozone, ultraviolet light and both. The test chemical was a textile azo dye C.I. Acid Orange 7. The degradation of the dye was monitored by the abatement in

its absorbance at the visible, UV_{254}, and UV_{312} bands; the reduction in total organic carbon; and the increase in biodegradability.

9.2. Material and Methods

9.2.1. Test Dye and Preparation of Dye Solutions

The test dye C.I. Acid Orange 7 (MW= 350 g mol^{-1}), was obtained from Aldrich in 85 per cent purity. The chemical structure of which was given in Chapter 8, a stock dye solution was prepared by dissolving 1 g of the dye in 1 L of boiling deionized water and test solutions for all runs were made by diluting the stock to typical effluent dye concentrations (57 μM) using deionized water. The pH of test solutions was 5.5 prior to sonication and no pH adjustment was made during the experiments. All samples were aerated for 1 h before sonication.

9.2.2. Experimental Methods

Optimum system parameters of System III which were previously defined in Chapter 4.2.3 are listed in Table 9.1.

Table 9.1. Optimum parameters of System III

System	Transducer Frequency (kHz)	Reaction Volume (mL)	Power Density (W mL^{-1})	Type of Gas and Flow Rate ($L min^{-1}$)
III	3 x 520	1200	0.075	Ar: O_2 (1 $L min^{-1}$:0.5 $L min^{-1}$)

Ozone was generated onsite from dry pure O_2 and supplied into the system through an OzoneLab 100 model generator (Ozone Services) at 0.25 L min^{-1} of O_2 flow rate, and 40 gm^{-3} O_3 output. During the experiments involving O_3, the solution was not sparged with any gas.

Experimental Scheme:

The experiments were grouped as:

i) Ozone + Ultrasound; (O_3+US),

ii) Ozone + UV irradiation; (O_3+UV),

iii) Ozone + Ultrasound + UV irradiation; (O_3+US+UV), and

iv) UV irradiation + Ultrasound (UV+US).

Control experiments were conducted with each run to assess the impact of single systems. The controls were: i) O_3, ii) UV, and iii) US. The conditions of each group are specified in results and discussion section.

Determination of Dye Degradability:

Air-saturated test solutions were irradiated in the presence or absence of ozone, UV light or both for 1 h for

i) spectrophotometric analysis in the UV-Visible band,

ii) total organic carbon analysis.

iii) five-day Biochemical Oxygen Demand (BOD_5) analysis. This determination involves the measurement of the dissolved oxygen consumed by microorganisms to biologically degrade the organic waste during the first 5 days of biodegradation. It has traditionally been one of the most important measurement of the strength of organic pollution.

iv) H_2O_2 analysis.

9.2.3. Analytical Methods

i) Spectrophotometric Measurements (for color and aromatic fragment degradation): The optical absorption spectra (200-700 nm) and the reduction in UV/visible absorption of the dye solutions were recorded by a Unicam, Helios Alpha/Beta double

beam spectrophotometer through a 1 cm path length. Color degradation was monitored by the abatement in UV_{484} nm, and aromatic fragment degradation was monitored by the abatement in UV_{254}, and UV_{312} nm bands.

ii) Hydrogen Peroxide and UV Intensity Measurements: The concentration of hydrogen peroxide was measured in sonicated deionized water in the absence and presence of UV light, using the KI method (Klassen *et al.*, 1994). UV light intensity was measured by peroxodisulphate/tert butanol chemical actinometer (Mark *et al.*, 1990). Upon photolysis of this solution, sulphuric acid is formed, whose liberation can be directly followed with a pH meter. Details of UV intensity measurement are given in Appendix C.

iii) Total Organic Carbon Measurements: Total organic carbon (TOC) monitored with a Shimadzu TOC-V CSH analyzer. The instrument was calibrated by standard solutions of KHP (5-30 ppm).

iv) BOD_5 Measurements: BOD_5 tests were run in accordance with the dilution method described in Standard Methods of Water and Wastewater Analysis (APHA, 1989). BOD_5 test involve putting a sample of waste into stoppered bottles (300 mL), measuring the concentration of dissolved oxygen in the sample at the beginning of the test and again 5 days later after incubating at 20 °C. All samples were seeded with a bacterial culture that has been acclimated to the organic matter that may be present in the effluent. Supernatants (1.5 mL) of acclimatized mixed culture obtained from aeration tank of a local wastewater treatment plant were mixed with 300 mL of raw and sonicated test solutions. Acclimization of biomass was conducted during several weeks by synthetic domestic wastewater. The feed base was diluted to obtain a COD rate of 250 mg L^{-1} O_2/day. Dissolved oxygen is measured initially and after incubation, and the difference between initial and final (5 days later) dissolved oxygen concentrations were determined by WTW Oxymeter 3000 dissolved oxygen apparatus with membrane electrode. The BOD of the samples was determined by calculating the difference between the sample BOD and the blank BOD (seeded dilution water).

v) Ozone Measurements: The concentration of ozone in solution was determined using the Indigo colorimetric method described in Standard Methods of Water and WasteWater Analysis (APHA,1989).

9.3. Results and Discussion

9.3.1. Comparison of US/O_3 with UV/O_3

9.3.1.1. Selection of the Ozone Concentration

Ozone was injected into the reactor at a generator O_3 output of 10, 20, 40 and 60 g m^{-3} during ultrasonic irradiation of the dye solution (pH= 5.5) for 1 h, and samples were collected within short intervals for spectrophotometric analyses at the UV-visible region. The absorbance decay curves were obtained by fitting the absorption data (at 484 nm) to Equation (4.2.) as presented in Figure 9.1. Maximum color degradation was observed at 60 gm^{-3}, but 40 gm^{-3} (corresponding to a rate oxygen flow rate of 0.25 L min^{-1}) was selected as the optimum value (working concentration) for economic reasons. All control experiments with ozone (40 gm^{-3}) and ultrasound alone were conducted on air-saturated dye solutions.

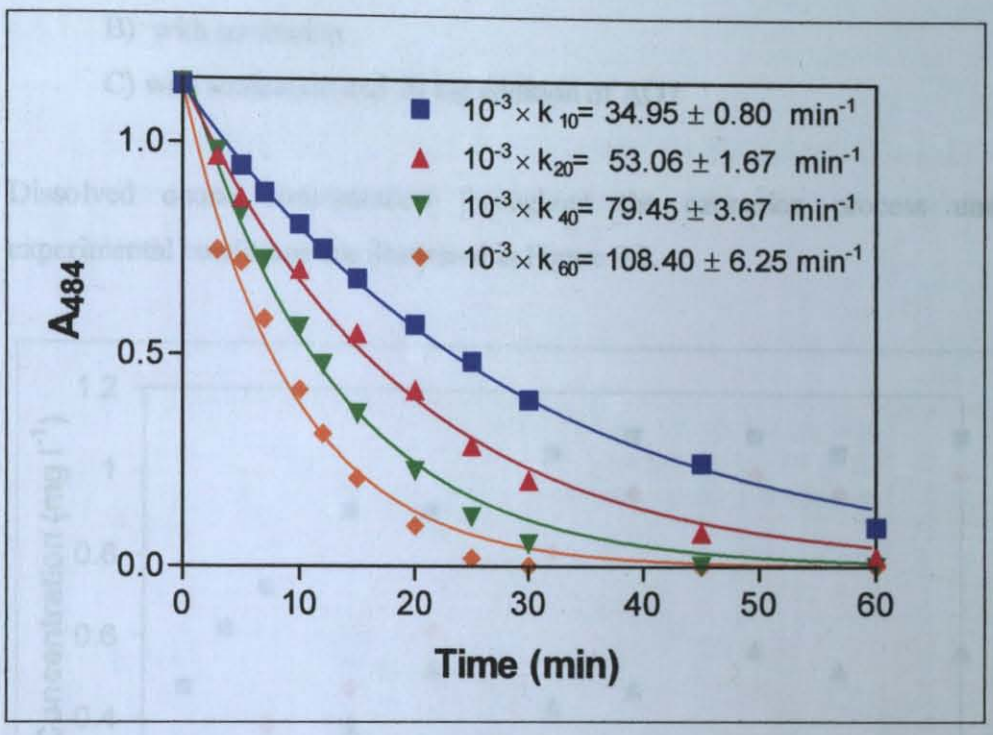

Figure 9.1. Color degradation of AO7 in the presence of US and O_3. Subscripts 10, 20, 40 and 60 refer to the O_3 outputs of the generator (g m^{-3}).

The ozone concentration in the dye solution increased for 12 min and then remained almost constant. The corresponding O_3 concentration in solution at 40 g m^{-3} input was analytically determined (Indigo method) as 0.95 mg L^{-1}. The details of the procedure are outlined in Appendix B.

The Concentration of Ozone in Solution

The enhancement of color and aromatic removal rates during US/O_3 combination was attributed to increased mass transfer of O_3 by sonolysis. This hypothesis was also supported by monitoring the O_3 concentration in sonicated and non-sonicated deionized water in accordance with the Indigo colorimetric method (APHA, 1989). The procedure and the experimental data of this section are given in Appendix B. Ozone concentration was monitored at varying experimental conditions as follows:

- 40 g m^{-3} ozone supply into deionized water at pH 2,

A) without sonication

B) with sonication

C) with sonication and 20 mg addition of AO7

Dissolved ozone concentration throughout the ozonation process under varying experimental conditions are illustrated in Figure 9.2.

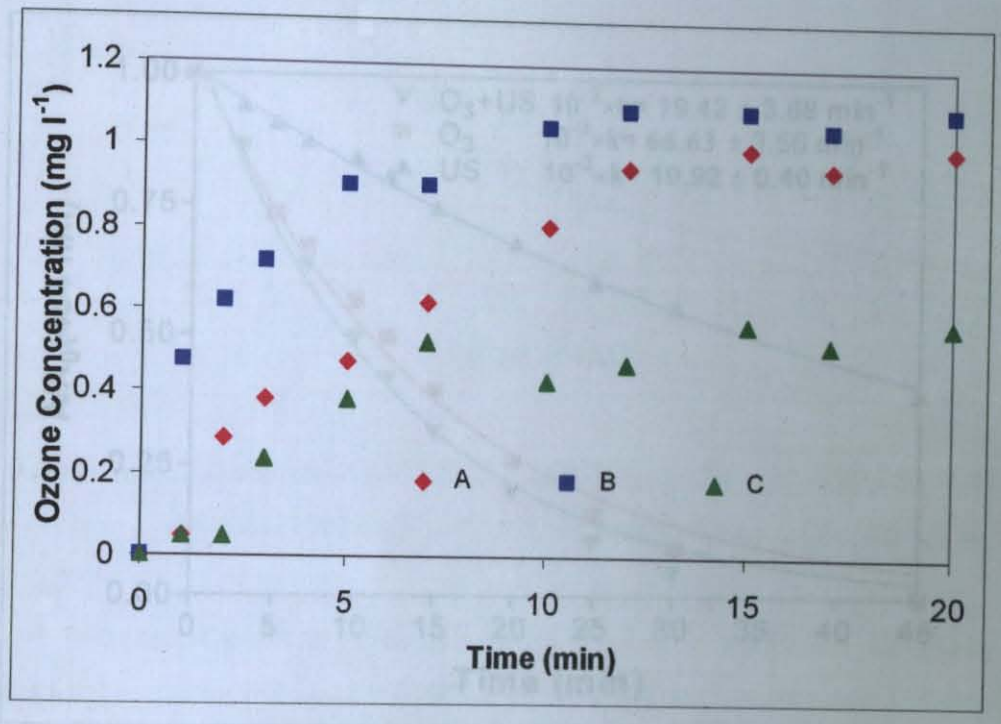

Figure 9.2. Dissolved O_3 concentrations in deionized water throughout the ozonation processes under varying experimental conditions (A: without sonication, B: with sonication, C: with sonication and 20 mg dye addition).

A and B in Figure 9.2. reveals that the mass transfer of O_3, and thus the O_3 concentration in solution is enhanced by sonolysis. The concentration of O_3 was increased with time, and it remained almost constant after 12 min during all runs. Dissolved O_3 concentration in sonicated deionized water (B) was approximately 15 per cent higher than the concentration in non-sonicated deionized water (A). Per cent color and aromatic removal of dye also support this observation (the above sections). Ozone concentration in dye solution (C) was lower than the concentration in deionized water (B) which was due to the scavenging effect of AO7. This might be due to the decomposition of O_3 by the direct reaction with the dye molecule.

9.3.1.2. Color Degradation

Comparative results of color degradation by the control sets (O_3 and US alone) and by combinations of US/O_3 and US/O_3/UV are presented in Figure 9.3. and Figure 9.4. for 57 μM AO7.

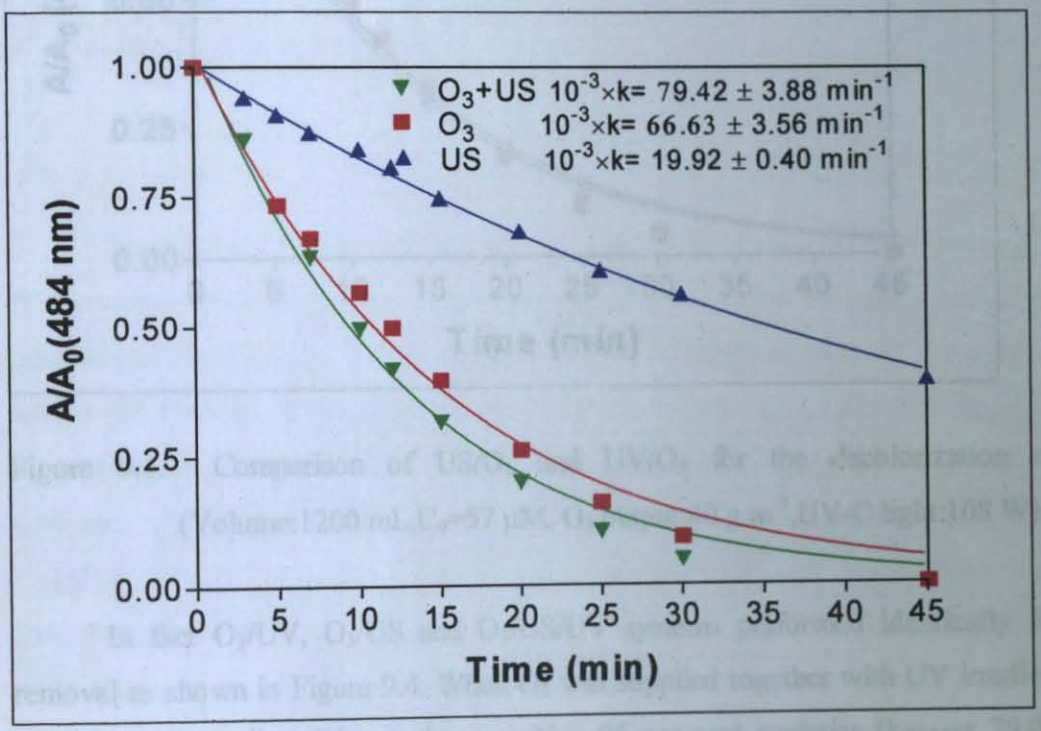

Figure 9.3. Effect of ultrasound on ozonation of 57 μM AO7 (Irradiated Volume: 1200 mL, Ozone: 40 g m^{-3}, $R^2 > 0.98$).

Decolorization by US alone was 3 times slower than by O_3 alone, and combined application of the two yielded more than 4 times enhancement with respect to US. Increased decolorization during US/O_3 combination is due to: increased mass transfer of O_3, which; i) reacts directly with the parent dye and its intermediates, ii) decomposes to produce excess •OH radicals (Equation (9.12)-(9.17)) and •OH generation by US (Equation (9.1)- (9.10)).

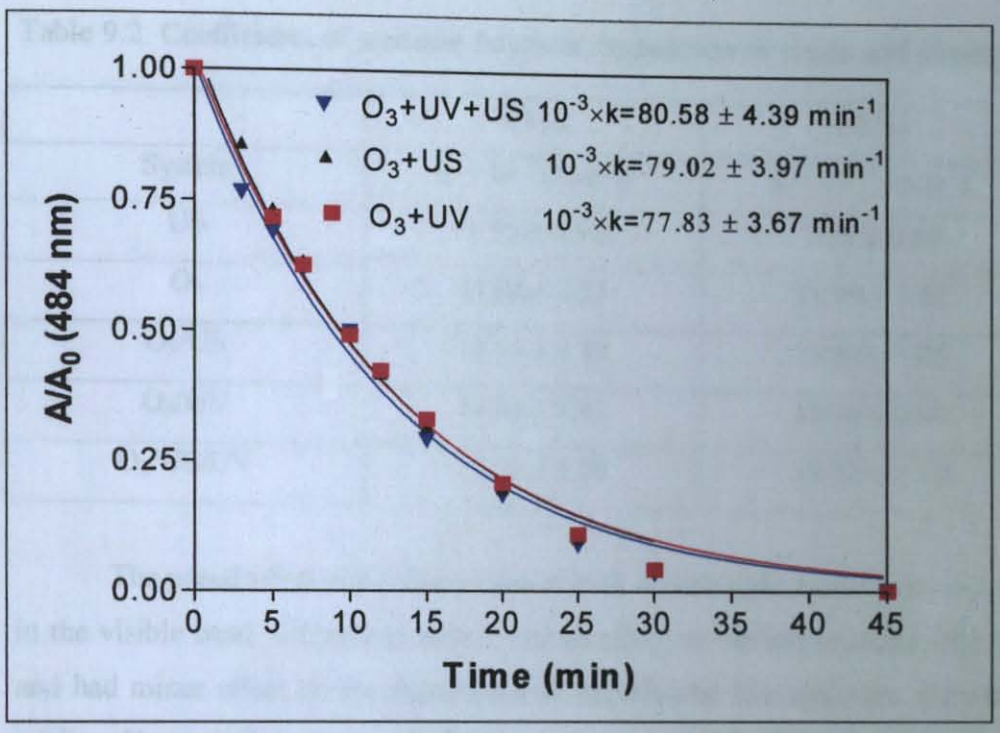

Figure 9.4. Comparison of US/O_3 and UV/O_3 for the decolorization of AO7 (Volume:1200 mL,C_0=57 μM, O_3 output:40 g m^{-3},UV-C light:108 W).

In fact O_3/UV, O_3/US and O_3/US/UV systems performed identically for color removal as shown in Figure 9.4. When O_3 was supplied together with UV irradiation, the rate of decolorization did not change within 95 per cent statistics ($k_{O3/US}$= 79.02 min^{-1}, $k_{O3/US/UV}$=80.58 min^{-1}).

9.3.1.3. Aromatic Fragment Degradation

To assess the overall degradation process, profiles of absorbance decay at 254 nm and 312 nm, which correspond to the absorption of olefinic/aromatic carbons and naphthalene-like structures, respectively, were monitored (Silverstein *et al.*, 1991). The pseudo-first order decay rate coefficients of UV_{254} and UV_{312} band decay are presented in Table 9.2.

Table 9.2. Coefficients of aromatic fragment degradation in single and combined systems

	UV_{254}	UV_{312}
System	$k \times 10^{-3}$ (min^{-1})	$k \times 10^{-3}$ (min^{-1})
US	1.75 ± 0.54	7.75 ± 0.55
O_3	11.08 ± 1.23	35.99 ± 1.12
O_3/US	16.74 ± 1.49	38.84 ± 1.05
O_3/UV	19.64 ± 1.91	38.91 ± 0.90
O_3/US/UV	21.71 ± 1.58	39.72 ± 1.12

The pseudo-first order decay rates at both wavelengths were much slower than that in the visible band. Ultrasound almost had no effect on olefinic/aromatic dye degradation, and had minor effect on the degradation of naphthalene like structure. Ozonation at near acidic pH resulted in more than 4 times faster aromatic fragment and naphtaline-like structure degradation rate coefficients with respect to US. This was not surprising since aromatic compounds are in general readily attacked by molecular ozone (Reife and Freeman, 1996). Comparative evaluation of rate coefficients of UV_{254} and UV_{312} shows that, the removal rates at 312 nm were faster than those at 254 nm. The increase in removal rates of aromatic compounds can be attributed to the fast O_3 addition reactions with olefins.

9.3.2. Comparison of US/UV with US

Control experiments with UV alone (at $I_0=2.1\times10^{-4}$ E m^2 s^{-1}) showed that AO7 did not undergo any degradation by photolysis. The light intensity was estimated by peroxodisulphate/tert butanol chemical actinometry (Mark *et al.*, 1990), and the data are given in Appendix C.

9.3.2.1. Color Degradation

In the literature, there are reported studies showing the enhancement of organic matter degradation by UV/US combinations (Naffrechoux *et al.*, 2000; Pétrier *et al.* 2002). In the present study, the combination of US/UV was investigated at increasing UV powers.

Rate of decolorizations were investigated at 3 different UV powers, 36, 72 and 108 W, and rate coefficients were compared in Figure 9.5. as bars.

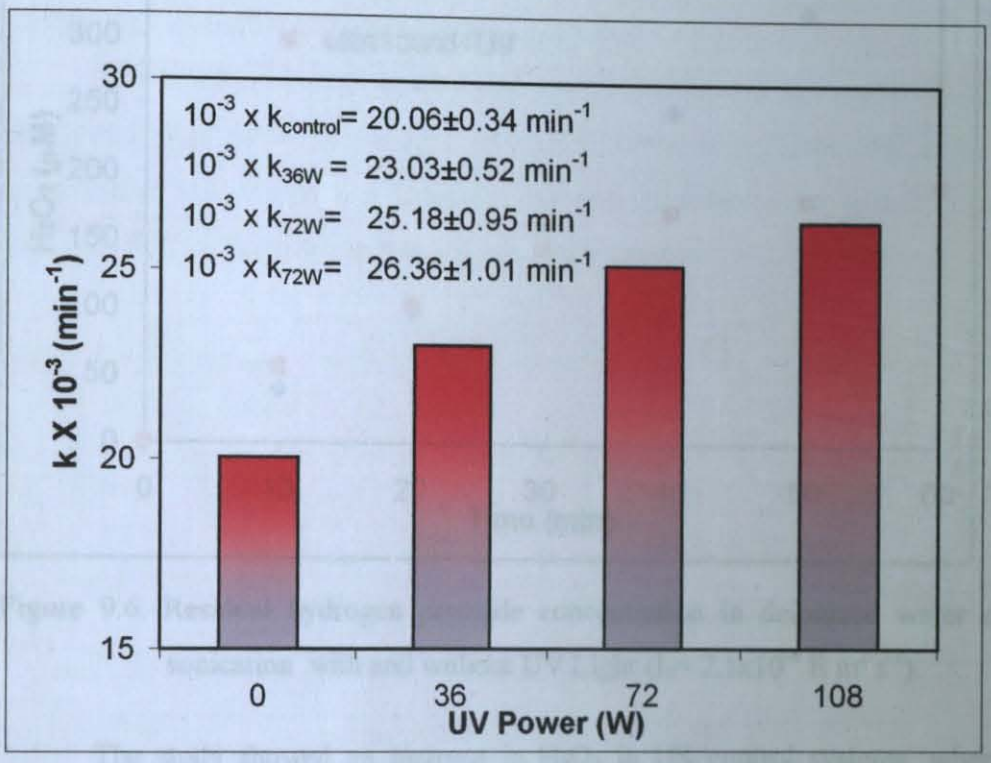

Figure 9.5. Pseudo-first order color degradation rate coefficients in AO7 during exposure to US and US/UV combinations at increasing UV powers.

Maximum degradation occurred at UV power of 108W at which the light intensity was $2.1x10^{-4}$ E m^2 s^{-1}. The increase in color degradation by US/UV combination can be attributed to the formation of excess •OH by UV photolysis of US generated H_2O_2 (H_2O_2 +hν→2 •OH).

This was justified by monitoring the residual H_2O_2 in US and US/UV combination (I_0= $2.1x10^{-4}$ E m^2 s^{-1}), and the results are presented in Figure 9.6.

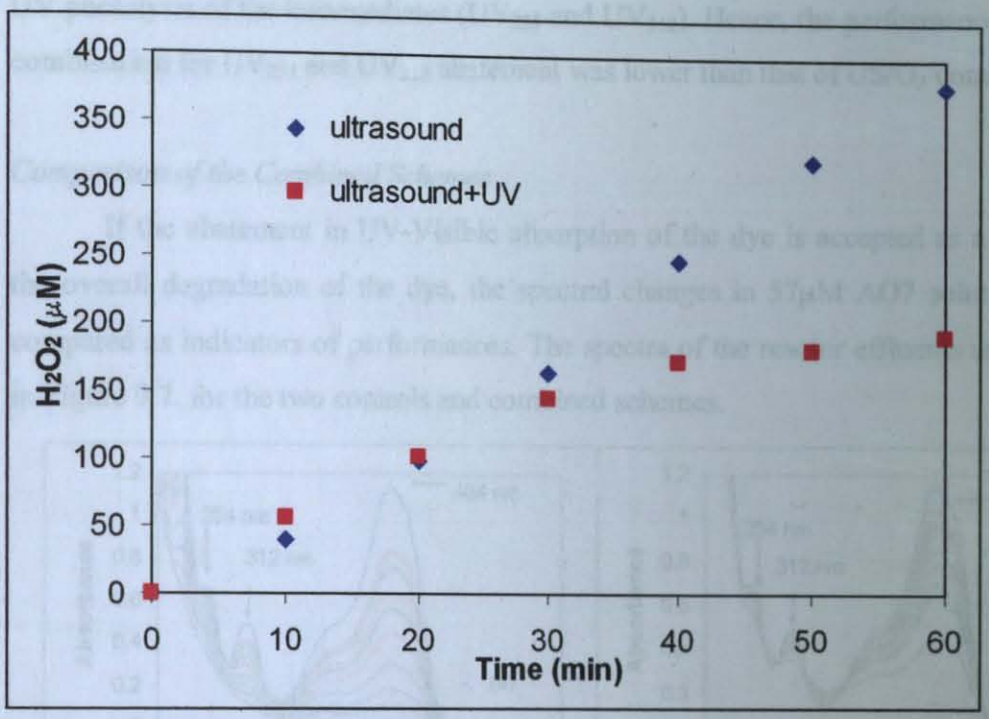

Figure 9.6. Residual hydrogen peroxide concentration in deionized water during 1 h sonication with and without UV Light (I_0= 2.1x10^{-4} E m^2 s^{-1}).

The study showed an increase in H_2O_2 in US control systems, whereas it was depleted and reached a steady state concentration in US/UV combination.

9.3.2.2. Aromatic Fragment Degradation

Rate of aromatic/olefinic carbon destruction was slower than that of color as presented in Table 9.3. The profile of aromatic band decay was similar to that of the visible.

Table 9.3. Estimated UV_{254} and UV_{312} degradation rate constants for US and US/UV combination

	254 nm	312 nm
System	k × 10^{-3} (min^{-1})	k × 10^{-3} (min^{-1})
US	1.75 ± 0.54	6.95 ± 0.55
US/UV	3.68 ± 0.26	9.18 ± 0.35

The increase in aromatic degradation by combined US/UV can be attributed to the formation of additional •OH by UV photolysis of H_2O_2 and the increased probability of

UV photolysis of the intermediates (UV_{254} and UV_{312}). Hence, the performance of US/UV combination for UV_{254} and UV_{312} abatement was lower than that of US/O_3 combination.

Comparison of the Combined Schemes

If the abatement in UV-Visible absorption of the dye is accepted as a measure of the overall degradation of the dye, the spectral changes in 57μM AO7 solutions can be compared as indicators of performances. The spectra of the reactor effluents are presented in Figure 9.7. for the two controls and combined schemes.

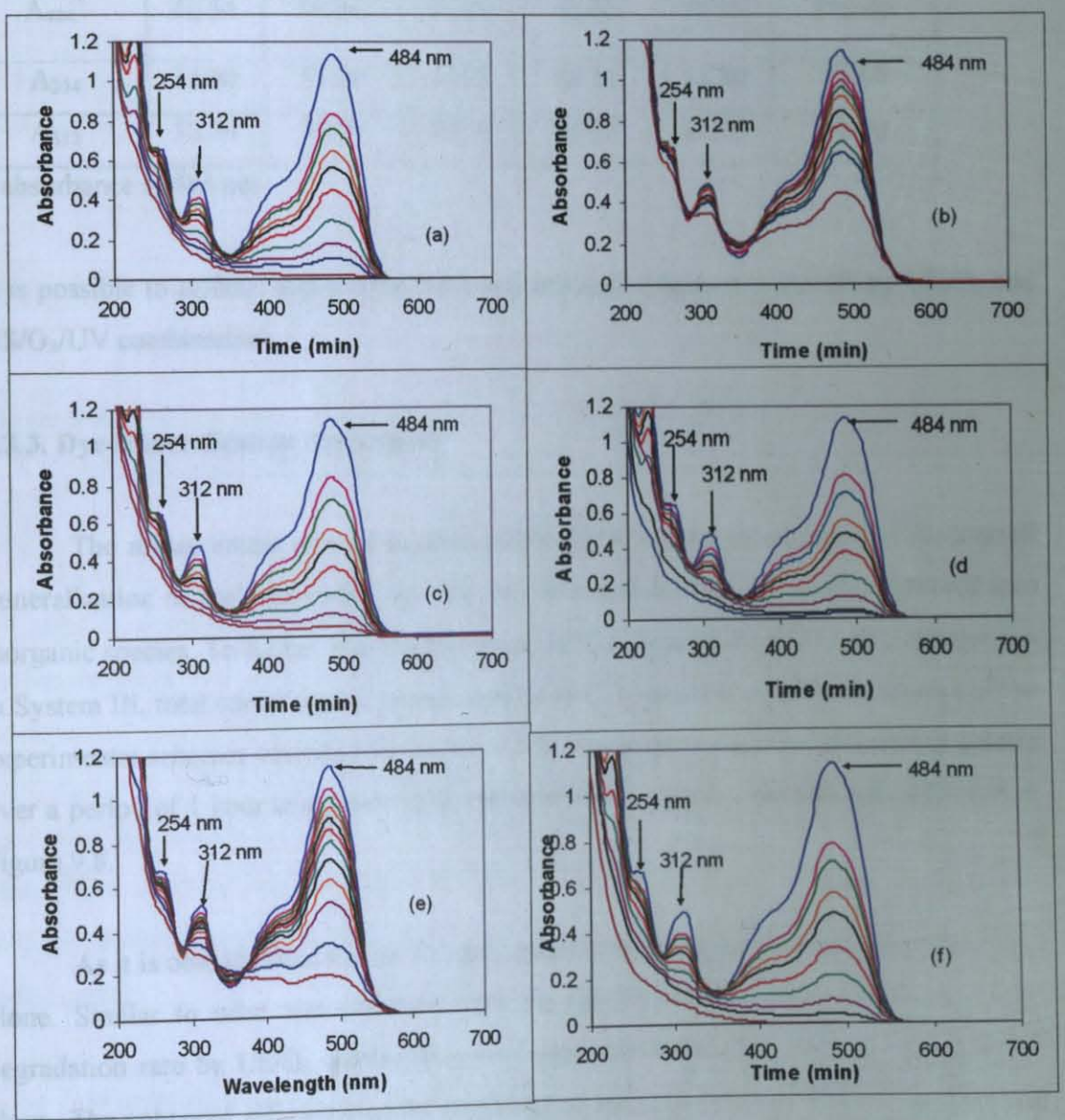

Figure 9.7. Spectral changes in 57μM AO7 during 1 h exposure to (a) O_3; (b) US; (c) O_3/US; (d) O_3/UV (e) US/UV (f) O_3/US/UV (Sampling times: 0,5,7,10,12,15 20,25,30, and 45 min).

Per cent removal at A_{484}, A_{312}, and A_{254} (45 min) are calculated from Figure 9.7., and the results are presented in Table 9.4.

Table 9.4. Comparison of dye degradability by different schemes

	Experimental Schemes					
Per cent Removal	US	O_3	US/O_3	UV/O_3	US/UV	$US/O_3/UV$
A_{484}^*	60.54	90.84	95.26	96.83	70.97	100.00
A_{254}	14.30	51.66	43.02	64.13	15.89	70.69
A_{312}	32.39	77.00	70.18	82.19	35.00	83.46

* absorbance at 484 nm

It is possible to achieve appreciable color and aromatic fragment removals by US/O_3 and $US/O_3/UV$ combinations.

9.3.3. Dye Mineralization Assessment

The measurement of total organic carbon (TOC) gives an estimate of the overall mineralization as both the parent dye and the intermediates that are totally degraded into inorganic species. To further examine the extent of C.I. Acid Orange7 (57 μM) destruction in System III, total conversion of organic carbon to CO_2 was determined in effluents of the experimental schemes described in Section 9.2.2. The extent of mineralization was probed over a period of 1 hour using individual and combined systems. The data are displayed in Figure 9.8.

As it is obvious from Figure 9.8. that, mineralization is not possible with ultrasound alone. Similar to what was observed with the decolorization of the parent dye, TOC degradation rate by US/O_3 combination was generally faster than those with US or O_3 alone. The enhanced efficiency of the combined system resulted from the increased mass transfer of ozone by ultrasound, which reacts directly with the intermediates and also decomposes to generate additional •OH. It appears that ultrasound coupled systems (except

US/UV combination) is certainly a positive step toward achieving quick mineralization with respect to ultrasound alone.

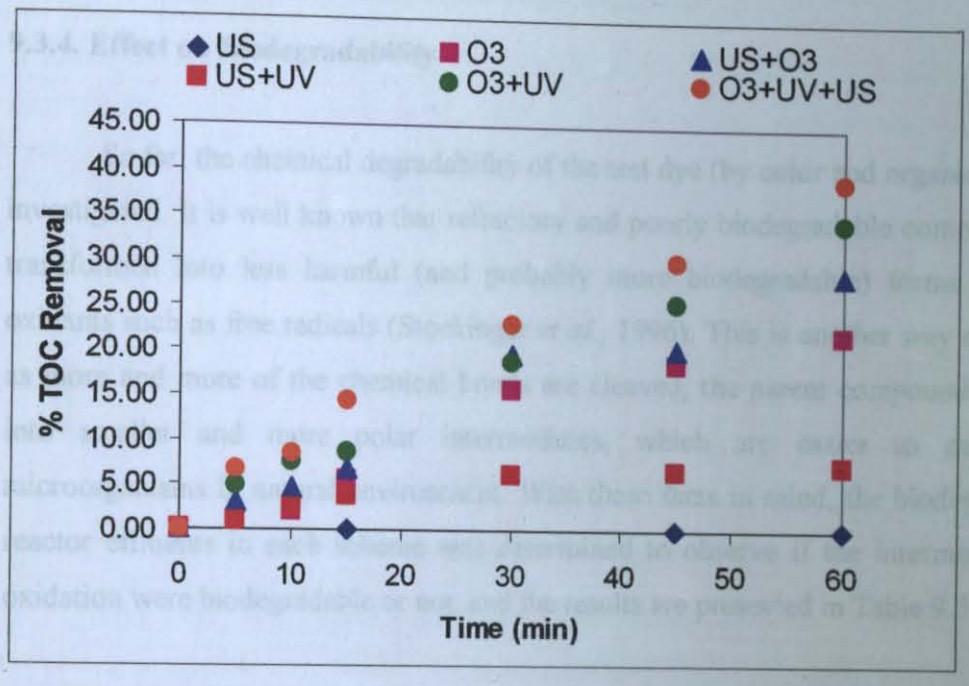

Figure 9.8. Total organic carbon removal of AO7 (C_0=57μM) during 1 h contact with individual and combined schemes.

During the first 15 min treatment with O_3, US/O_3, and UV/O_3, parallel TOC degradation efficiencies were observed. Probably the reaction mainly proceeded by direct molecular ozone reactions with the dye molecule. After 30 min treatment, oxidation of the intermediates with •OH began to be pronounced. Although ozonation showed rapid initial TOC destruction of over the first 15 min, the rates decreased as intermediates resistant to oxidation by O_3 were formed. As the reaction proceeded (after 45 min), UV/O_3 got faster than US/O_3 and O_3. The increased UV absorption of the intermediates and the additional •OH by the photolysis of sonochemically generated H_2O_2 can be the reason for the overall enhancement.

As a consequence, a quick mineralization of the pollutant should be the goal to minimize the survival time of possible harmful intermediates. Hence, US/O_3/UV triple combination would be more beneficial for dye mineralization. Although the color removal

rate of this triple combination was very close to the rates of US/O_3 and UV/O_3 combinations. $US/O_3/UV$ provided the highest dye mineralization rates.

9.3.4. Effect on Biodegradability

So far, the chemical degradability of the test dye (by color and organic carbon) was investigated. It is well known that refractory and poorly biodegradable compounds can be transformed into less harmful (and probably more biodegradable) forms by powerful oxidants such as free radicals (Stockinger *et al.*, 1996). This is another way of saying that as more and more of the chemical bonds are cleaved, the parent compound is converted into smaller and more polar intermediates, which are easier to metabolize by microorganisms in natural environment. With these facts in mind, the biodegradability of reactor effluents in each scheme was determined to observe if the intermediates of the oxidation were biodegradable or not, and the results are presented in Table 9.5.

Table 9.5. Five day Biochemical Oxygen Demand (BOD_5) of AO7 (C_0=57 μM) at 30 min and 60 min contact with single and combined schemes

Type of AOP	BOD_5 (mg L^{-1}) 30 min	BOD_5 (mg L^{-1}) 60 min
US	0	0
O_3	0.36	1.72
O_3/US	1.96	2.40
O_3/UV	-	3.00
US/UV	0	0.69
O_3/US/UV	2.32	3.18

As in the case of color and TOC degradation, the treatment performances of US/O_3, UV/O_3, and $US/O_3/UV$ combinations for biodegradability improvement far exceeded that of the ultrasonic irradiation or US/UV combination.

The ratio of BOD_5 to TOC is also an important parameter to assess the hazardous nature of a pollutant (Tchobanoglous and Burton, 1991). The computed values for each scheme are plotted as bars in biodegradability Figure 9.9.

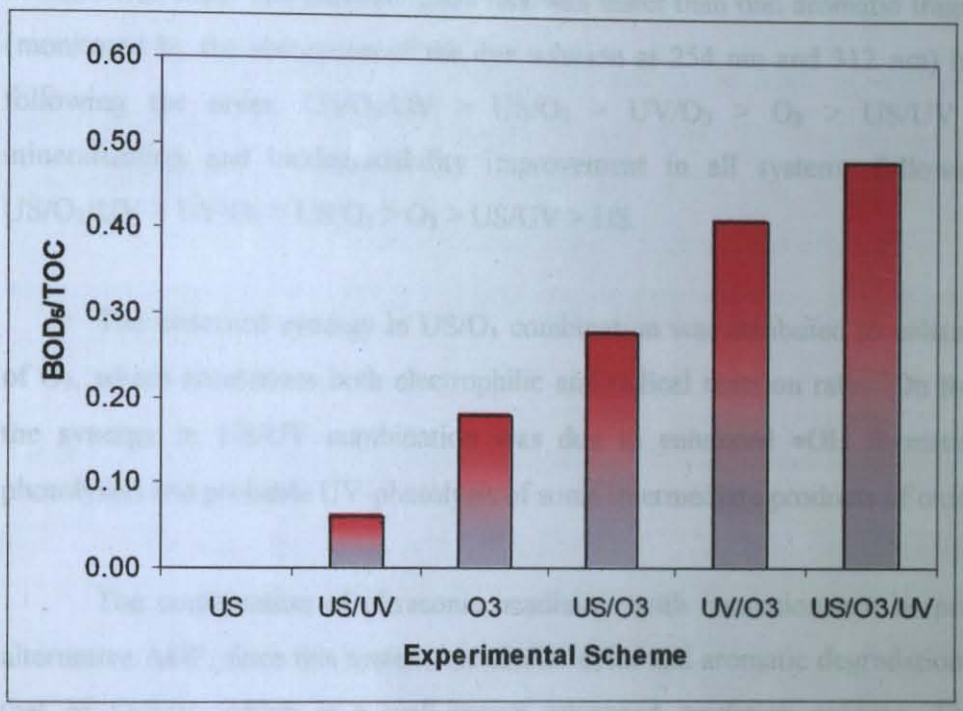

Figure 9.9. BOD_5:TOC ratios after 1 h exposure of 57 μM AO7 to single and combined test schemes.

The figure shows that the ratios of BOD_5 to TOC increases in the order: US < US/UV < O_3 < US/O_3 < UV/O_3 < US/O_3/UV. Hence the highest value (0.45) corresponds to the triple scheme with US, O_3, and UV irradiation, in which 45 per cent of total organic carbon is made of biodegradable or biochemically oxidizable carbon.

9.4. Conclusions

This and previous studies with textile dyes have shown that while ultrasound is effective in decolorizing textile wastewaters, no improvement in BOD_5/TOC ratio and/or mineralization is possible unless it is used in combination with O_3 and/or UV irradiation. In the present study, combination of ultrasound with ozone and/or UV irradiation was found effective in accelerating the rate of dye degradation.

The rate of color decay was pseudo-first order with respect to the visible absorption of the model dye, C.I. Acid Orange 7 in single and combinative operations, and all investigated systems performed best when a sparge gas ratio of 1:0.5 L min^{-1} Ar/O_2 mixture was used. The decolorization rate was faster than that aromatic fragment removal (monitored by the absorption of the dye solution at 254 nm and 312 nm) in all systems, following the order: $US/O_3/UV > US/O_3 > UV/O_3 > O_3 > US/UV > US$. Dye mineralization and biodegradability improvement in all systems followed the order: $US/O_3/UV > UV/O_3 > US/O_3 > O_3 > US/UV > US$.

The observed synergy in US/O_3 combination was attributed to enhanced diffusion of O_3, which accelerates both electrophilic and radical reaction rates. On the other hand, the synergy in US/UV combination was due to enhanced •OH formation (by H_2O_2 photolysis) and probable UV-photolysis of some intermediate products of oxidation.

The combination of ultrasonic irradiation with ozonation can be proposed as an alternative AOP, since this system has similar color and aromatic degradation efficiency as that of O_3/UV, which is a well-known advanced oxidation scheme. This system is especially beneficial for compounds, which have low reaction rates with O_3, because any •OH that is formed at the expense of increased O_3 concentration (by sonolysis) will increase the destruction of the substrate. The key for such a coupled system should lie in choosing processes that complement each other and lead to synergistic effects. In terms of applicability of the system, it must be economically competitive and the problems related to scale-up application should be addressed in the near future.

CHAPTER 10. KINETIC MODELING

This chapter presents a modeling approach to the study of •OH production and depletion kinetics in sonicated solutions of azo dyes. The model was based on the assumption that dye molecules are oxidized only in the bulk liquid upon reaction with hydroxyl radicals, which are generated by water sonolysis and depleted by recombination and scavenging reactions. The list of such reactions and the rate coefficients associated are given in Table 10.1

Table 10.1. List of chemical reactions and rate coefficients used in model development

Chemical Reactions in Bulk Liquid	Rate Constant
1. $H_2O +))) \rightarrow {}^{\bullet}OH + {}^{\bullet}H$	K_{FOH}
2. Dye + •OH → [Dye-OH adduct]* →→ products	k_{Dye}
3. $^{\bullet}OH + {}^{\bullet}OH \rightarrow H_2O_2$ [1]	$k_{R1,H2O2} = 6 \times 10^9\ M^{-1}s^{-1}$
4. $^{\bullet}OH + H_2O_2 \rightarrow {}^{\bullet}HO_2 + H_2O$ [1]	$k_{S,H2O2} = 2.7 \times 10^7\ M^{-1}s^{-1}$
5. $^{\bullet}HO_2 \Leftrightarrow {}^{\bullet}O_2^-$ [1] pKa=4.8	
6. $^{\bullet}OH + {}^{\bullet}O_2^- \rightarrow HO^- + O_2$ [1]	$k_{S,O2} = 1.01 \times 10^{10}\ M^{-1}s^{-1}$
7. $^{\bullet}HO_2 + {}^{\bullet}O_2^- + H^+ \rightarrow H_2O_2 + O_2$ [1]	$k_{R2,H2O2} = 9.7 \times 10^7\ M^{-1}s^{-1}$
8. $^{\bullet}HO_2 + {}^{\bullet}HO_2 \rightarrow H_2O_2 + O_2$ [1]	$k_{R3,H2O2} = 8 \times 10^5\ M^{-1}s^{-1}$

[1] Destaillats *et al.*, 2000

The first and second reactions describe the formation of •OH and the degradation of the dye by hydroxylation, respectively. Reactions 3, 7 and 8 represent the formation of H_2O_2, but the reported rate constants reveal that the contribution of the last one is insignificant. Reactions 4 and 6 describe the depletion of •OH by scavengers, specifically H_2O_2 and O_2^-; and reaction 5 describes the equilibrium between peroxy and superoxide radicals.

Using the information in Table 10.1, a kinetic model to represent the time rate of hydroxyl radical variation in the dye solution was developed as:

$$\frac{d[\bullet OH]}{dt} = K_{fOH} - k_{dye}[\bullet OH][dye] - k_{fH2O2}[\bullet OH]^2 - k_{sH2O2}[\bullet OH][H_2O_2] \qquad (10.1)$$

where K_{fOH} and k_{dye} are unknown rate coefficients or the parameters of the model, k_{fH2O2} and k_{sH2O2} are model constants, and the expressions in brackets are molar concentrations, or variables of the model. For the solution of Equation (10.1), the zero-order rate coefficient of hydroxyl radical formation K_{fOH} was used as the adjustable parameter, and the "dye" was represented by C.I. Acid Black1. Hence, the data for [dye] and $[H_2O_2]$ were generated experimentally by sonicating 30 μM of Acid Black1 in System I at pH=3.0 while monitoring color and H_2O_2 in the solution.

Note that the model is made simple by ignoring some of the reactions given in Table 10.1. These were i) reaction 8 (H_2O_2 formation) due to its much lower rate constant than that of Reaction 3, and ii) reactions 6 and 7 due to the equilibrium condition in reaction 5, which implies that molar concentration of $\bullet O_2^-$ is insignificant at pH=3.0.

At steady state, $d[\circ OH]/dt=0$, and the rate expression becomes:

$$k_{fH2O2}[\circ OH]_{ss}^2 + k_{sH2O2}[\circ OH]_{ss}[H_2O_2]_t + k_{dye}[\circ OH]_{ss}[dye]_t - K_{fOH} = 0 \qquad (10.2)$$

where $[\circ OH]_{ss}$ is the steady-state hydroxyl radical concentration (M), $[H_2O_2]_t$ and $[dye]_t$ are concentrations of hydrogen peroxide and dye at time t, respectively (M); k_{fH2O2}, k_{sH2O2}, are bimolecular reaction rate coefficients of H_2O_2 formation and H_2O_2 reaction with •OH, respectively ($M^{-1}s^{-1}$); k_{dye} is the second order reaction rate coefficient of the dye with •OH ($M^{-1}s^{-1}$); and K_{fOH} is the zero-order rate coefficient of •OH formation in SYSTEM I ($M\,s^{-1}$).

Since the rate of dye degradation was first order in the visible absorption of the dye, the bimolecular rate coefficient, k_{dye} in Equation (10.2) can be replaced by $k'/[\bullet OH]$ because of the following relation:

$$-\frac{d[dye]}{dt} = k_{dye}\,[\bullet OH]\,[dye] = k'\,[dye] \qquad (10.3)$$

where d[dye]/dt is the rate of dye degradation and k' is the pseudo-first order decay coefficient (s^{-1}). The final equation expressing the rate of •OH formation/depletion at steady-state is:

$$k_{fH2O2}\,[\bullet OH]_{ss}^{2} + k_{sH2O2}\,[\bullet OH]_{ss}\,[H_2O_2]_t + k'[dye]_t - K_{fOH} = 0 \qquad (10.4)$$

The solution of Equation (10.4) is possible using graphical or numerical methods initiated by assigning a hypothetical value to K_{fOH} and inserting experimental data of $[H_2O_2]_t$ and $[dye]_t$, the latter to be estimated by Lambert-Beer Law:

$$[dye]_t = \frac{A_t}{\varepsilon \times b} \qquad (10.5)$$

where A_t is the maximum absorbance of the solution ($A_{620\ nm}$) at time t, ε is the molar extinction coefficient of the dye at 620 nm ($4.41 \times 10^4\ M^{-1}cm^{-1}$), and b is the optical path length (1 cm).

The numerical method involved calculation of $[\bullet OH]_t$ for an initial assumption of K_{fOH} and insertion of the lowest $[\bullet OH]_t$ into Equation (10.4) to solve for K_{fOH}. This computed value of K_{fOH} was then used in the next solution to recompute a new set of $[\bullet OH]_t$. The procedure was repeated until the last substituted value converged with the last calculated K_{fOH}. The experimental data for 360 min sonication (at 300 kHz) of 30 μM dye at pH=3.0 and numerical estimations of $[\bullet OH]_t$ for $K_{fOH} = 4.0 \times 10^{-7}$ are listed in Table 10.2. Profiles of $[\bullet OH]_t$ variations with time for some selected solutions of Equation (10.4) are illustrated in Figure 10.1.

The figure shows that at all values of K_{fOH} the concentration of •OH increases linearly during the first 40 min, but with varying slopes that are proportional to the magnitude of K_{fOH}. This increase may be due to the presence of excess gas bubbles during initial contact (due to air-saturated dye solution) and lack of hydrogen peroxide. The

steady-state condition is reached approximately at t=40 min and sustained for about 35 min. As the rate of depletion/scavenging reactions exceeds that of formation (upon degassing and H_2O_2 accumulation), the steady-state is disturbed (t=80 min), and [•OH] begins to decline to fairly low concentrations until it is stable again (t=240 min).

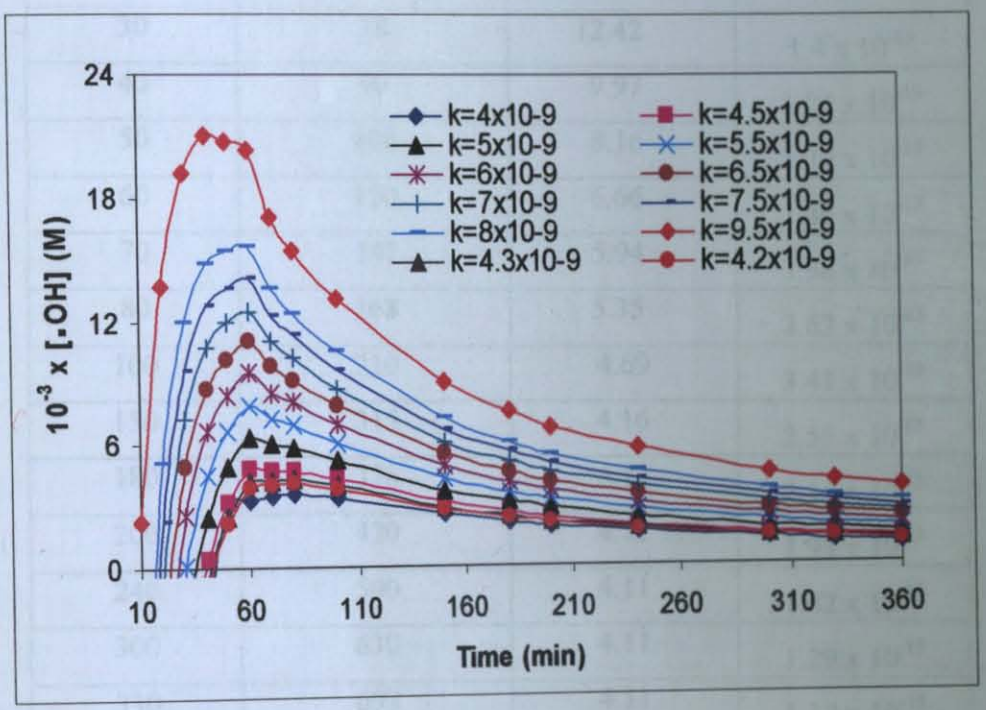

Figure 10.1 Model predictions of [•OH] variations during 360 min sonication.

Values of K_{fOH} and $[\bullet OH]_{ss}$ computed by the technique described above are 4.01×10^{-9} M s^{-1} and 3.62×10^{-13} M, respectively. Estimation of k_{dye}, the bimolecular reaction rate coefficient is possible by substituting model prediction of $[\bullet OH]_{ss}$ and the pseudo-first order color decay coefficient k' into Eq (10.3):

$$k_{dye} = \frac{4.41\times10^{-4}\ s^{-1}}{3.62\times10^{-13}\ M} = 1.22\times10^{9}\ M^{-1}s^{-1}$$

The calculated value is in good agreement with the reported bimolecular rate coefficients of azo dyes with hydroxyl radicals (10^9-10^{10} $M^{-1}s^{-1}$) (Destaillats *et al.*, 2000; Joseph *et al.*, 2000).

Table 10.2. Model variables

Time (min)	10^{-6} x H_2O_2 (M)	10^{-6} x dve (M)	•OH (M)
0	0	29.89	-
10	50	21.80	-
20	65	16.11	-
30	78	12.42	1.4×10^{-13}
40	90	9.97	3.04×10^{-13}
50	106	8.16	3.29×10^{-13}
60	120	6.66	3.48×10^{-13}
70	147	5.94	3.58×10^{-13}
80	168	5.35	3.62×10^{-13}
100	210	4.69	3.41×10^{-13}
150	315	4.16	2.55×10^{-13}
180	378	4.12	2.14×10^{-13}
200	420	4.11	1.93×10^{-13}
240	500	4.11	1.62×10^{-13}
300	630	4.11	1.29×10^{-13}
330	693	4.11	1.17×10^{-13}
360	756	4.11	1.07×10^{-13}

CHAPTER 11. ECONOMIC EVALUATION, CONCLUDING REMARKS AND RECOMMENDATIONS

11.1. Economic Evaluation

Cost-effectiveness (operational) of System I, II and III were investigated on the basis of 45 per cent color removal in 1 m^3 of wastewater containing 20 mg L^{-1} of an azo dye, represented by C.I. Acid Orange 7. Unit costs of materials and electrical power (local) that were used in the calculations are listed in Table 11.1. Despite the fact that argon was the most efficient bubbling gas in all systems, operational costs were estimated based on air as the injected gas (to be provided with the use of a simple air compressor) because of the fact that the cost of Ar is too large to use in large-scale operations.

Table 11.1. List of operating parameters and their costs

Parameter	Unit Cost (UC)
Electrical Power	0.055 USD kWh^{-1} (1)
H_2O_2	0.295 USD L^{-1} (1)
O_2	1.5 USD m^{-3} (2)

(1) Ince and Apikyan, 2000
(2) HABAŞ, Istanbul (2003)

Cost comparisons were made for singly operated ultrasound in all systems and for the combination of ultrasound and ozone in SYSTEM III. The reason why this combination was the only one considered was for consistency (only this one made use of C.I. Acid Orange 7).

The total operation cost (TC) in single operations was equal to the cost of electrical power used by the ultrasound generator and the aeration pump:

TC = (Generator Power Consumption+ Pump Power Consumption) $t_o \times UC_E$, i.e.

$$TC = (GP+PP)\ t_o \times UC_E \qquad (11.1)$$

where GP and PP are experimentally observed electrical power consumptions of the generator and pump, respectively (W); t_o is the estimated contact time for 1 m^3 wastewater treatment (h), and UC_E is the unit cost of electricity (USD kWh^{-1}). The operation time t_o for each system was estimated by multiplying the experimental contact time t_i by $1000/V_i$, where V_i is the test volume in liters.

11.1.1 Cost of Single Ultrasound Systems

SYSTEM I

t_i =14 min

V_i = 0.1 mL

t_o = 14/60 h × 1000/0.1

= 2334 h

TC_{s1}= [(25 W+ 2.5 W)/1000 W kW^{-1}] × 0.055 USD kWh^{-1} × 2344 h

= 3.52 USD

SYSTEM II

t_i = 23 min

V_i = 300 mL

t_o = 1277 h

TC_{s2} = [(40 W +2.5 W)/1000 W kW^{-1}] × 0.055 USD kWh^{-1} × 1277 h

= 3.37 USD

SYSTEM III

t_i = 33 min

V_i = 1200 mL

t_o = 458 h

TC_{s3} = [(390 W +2.5 W)/1000 W kW^{-1}] × 0.055 USD kWh^{-1} × 458 h

= 9.88 USD

Hence, cost effectiveness of the systems when operated alone is in the order: SYSTEM II > SYSTEM I > SYSTEM III.

11.1.2. Cost of System III Operated with US/O_3

In this combination, the total cost is equal to the sum of single US cost and the cost of operating the ozone generator, which consumes pure O_2 (0.25 L min^{-1} O_2) and electrical power:

$$TC_{s3}(US/O_3) = [V_{O2} \times UC_{O2} + (OP + GP)UC_E] \times t_o \qquad (11.2)$$

where V_{O2} is the volume rate of O_2 consumption in the system (l/min), UC_{O2} is the unit cost of O_2 (USD m^{-3}) and OP is the electrical power consumption of the ozone generator (W). (Note that no additional gas injection (no aeration cost) is applied in ozonated solutions.) System parameters were:

t_i = 8 min

V_i = 1200 mL

t_o = 111 h

$TC_{s3}(US/O_3)$= [(0.25 l min^{-1} × m^3/1000L × 60min h^{-1})× 1.5 USD m^{-3}+ (18W+390W)/1000 W kW^{-1} × 0.055 USD kWh^{-1}] 111 h

= 2.57 USD.

Note: If the system was operated without ultrasound, i.e. the wastewater was O_3-treated for 45 per cent decolorization; the operation cost would be 3.60 USD.

11.2. Concluding Remarks

Three ultrasonic systems and 9 textile dyes were investigated in this study to assess the impacts of system conditions, physical/chemical agents, dye properties and dyebath matrix on sonolytic destruction of textile dyes.

1. The systems were specified as:
   - SYSTEM I: Generator capacity=25W, frequency=300kHz, volume=150 mL.
   - SYSTEM II: Generator capacity=100W, frequency=520kHz, volume=1200 mL.
   - SYSTEM III: Generator capacity=600W, frequency=3x520 kHz, volume=2000 mL; equipped with 3 UV-C lamps emitting ultraviolet light at 254 nm.
2. The test media were:
   - deionized water solutions of textile dyestuff
   - simulated dyebath wastewater
3. The test dyes were:
   - C.I. Acid Black 1
   - C.I. Acid Orange 7
   - C.I. Basic Blue 3
   - C.I. Basic Blue 16
   - C.I. Basic Brown 4
   - C.I. Reactive Black5
   - C.I. Reactive Blue 19
   - C.I. Reactive Orange 16,
   - C.I. Reactive Red 141,
4. Gas injection was made with constant flow of Ar, O_2 or air, or with Ar/O_2 mixtures.
5. Analytical parameters were:
   - Color (visible absorption of the test dye)
   - Organic matter

     UV_{254} and UV_{312}

     Chemical Oxygen Demand (COD)

     Total Organic Carbon (TOC)

Five-day Biochemical Oxygen Demand (BOD_5)

- Toxicity
- Total Solids

6. Kinetics of dye degradation with hydroxyl radicals was modeled.

The conclusions drawn were:

1. Systems and Gases

- The efficiency of the studied systems in terms of decolorization of the test solutions was such that: System I > System II > System III. The technical efficiency of System III was enhanced when it was operated with O_3, and/or UV irradiation.

- Injection of different gasses showed that rate of decolorization increased in the sequence: Ar > O_2 > Air. Combination of an Ar:O_2 gas mixture further enhanced the rate, and maximum color degradation was obtained at a sparge gas ratio of 66 per cent Ar to 34 per cent O_2 in SYSTEM III.

- The efficiency of System I was most sensitive to the applied power, while efficiencies of System II and III were affected more by the geometry and volume of the reactor.

2. Dyes and Dyebaths

- The rate of color decay in all dye classes was more closely related to the structural and chromophoric properties of the dye than to the composition of the dyebath.

- The presence of α-substituents around the reactive component of dyes accelerated the rate of dye bleaching by promoting intramolecular hydrogen bonding.

- Dye structures having a single OH substituent in *ortho* position to the N=N bond decayed more rapidly than those with a second o-substiuent such as SO_3.

- Anthraquinone dyes bleached faster than azo dyes as a consequence of the reactivity of benzoquinone structures with superoxide radicals that form during water sonication.

- The rate of bleaching was decelerated by the formation of anionic sites, as a consequence of increased hydrophilicity.

- Decolorization in dyebath solutions was inhibited only if the concentrations of carbonate and chloride ions were sufficiently large to allow competition of these species with the dye for hydroxyl radicals.

3. **Analysis Parameters**

- The fraction of visible absorption abatement in sonicated dye solutions and dyebaths was always larger than the abatement in their UV absorption, indicating that chromophores were more reactive with hydroxyl radicals than non-chromophoric organic components.

- Ultrasound was not effective in the overall degradation of the dyes as measured by Chemical Oxygen Demand (COD) and Total Organic Carbon (TOC) of the test solutions, unless operated in combination with physical/chemical agents.

- Toxic dyes were detoxified by ultrasound within short contact, but in non-toxic dyes the ratio of 5-day BOD to TOC (which is an indicator of the degree of harmfulness of organic compounds) did not change significantly by ultrasonic irradiation alone.

4. **Combinations of Ultrasound**

- Sonication of dye solutions in the presence of chemical agents such as O_3 and Fe^{2+} increased degradation yields considerably with respect to those observed with sonication alone. Moreover, the effect of these combinations was larger than that of chemical oxidation with O_3 and Fe^{2+} applied individually. Hence, ultrasound is an effective tool in advanced oxidation processes for lowering chemical consumptions.

- Sonication of dyebaths with the addition of hydrogen peroxide rendered 10-12 per cent enhancement in the efficiency of color decay and more than 80 per cent enhancement in that of COD reduction.

- Combinations of ultrasound with O_3 resulted in dye mineralization, which was four times larger than mineralization with O_3 alone.

- The most effective combined scheme was ultrasound/ozone/UV irradiation, under which all analytic parameters related to organic quality were significantly degraded.

5. Kinetic Modeling

- A kinetic model was proposed to express the rate of •OH reactions in dye solutions sonicated with 300kHz, and it was shown that steady-state conditions were reached at t=40 min and t=150 min. Through model-predicted •OH concentrations at steady state, it was possible to compute the second-order reaction (decolorization) rate coefficient of azo dyes with hydroxyl radicals. The computed coefficient (1.22×10^9 $M^{-1}s^{-1}$) was in good agreement with values reported in the literature.

6. Economic Evaluation

- Estimated operational costs of System I, System II, and System III for 45 percent decolorization of azo dyes were 3.52 USD m^{-3}, 3.37 USD m^{-3}, and 9.88 USD m^{-3}, respectively. The cost of ozone-ultrasound combination in System III was 2.57 USD m^{-3}, which was much less than operation without ozone (9.88 USD m^{-3}).

11.3. Recommendations

In accordance with the results obtained within the experimental conditions employed in this study, it is recommended that System III be modified for geometry,

volume and electrical components of the generator. The inefficiency is due to its power/volume ratio and equipment with a single generator for three transducers. Similarly, reducing the cell volume can also modify SYSTEM III by increasing its power-volume ratio. An alternative method to improve SYSTEM I is to operate it with a more powerful generator.

A better understanding of chemical structure and sonochemical yield relations is recommended by studying simpler compounds as surrogate chemicals, and by running chromatographic analyses to depict intermediate products. This will also assist the examination of reaction pathways and mechanisms.

REFERENCES

Acero, J. L., Gunten, U., "Influence of Carbonate on the Ozone/Hydrogen Peroxide based Advanced Oxidation Process for Drinking Water Treatment," *Ozone Science and Engineering*, 22, 305-328, 2000.

Adewuyi, Y. G., "Sonochemistry: Environmental Science and Engineering Applications," *Industrial and Engineering Chemistry Research*, 40, 4681-4715, 2001.

Alegria, A. E., Lion. Y., Kondo, T., Riesz, P., "Sonolysis of Aqueous Surfactant Solutions-Probing the Interfacial Region of Cavitation Bubbles by Spin Trapping," *Journal of Physical Chemistry*, 93, 4908-4913, 1989.

APHA, AWWA, WPCP, *Standard Methods for the Examination of Water and Wastewater*, 17th Edition, American Public Health Association, Washington, D.C., 1992.

Arslan, I., Balcıoglu, I. A., "Degradation of Commercial Reactive Dyestuffs by Heterogeneous and Homogeneous Advanced Oxidation Process: A Comparative Study," *Dyes and Pigments*, 43, 95-108, 1999.

Arslan, I., Balcioglu, I. A., Tuhkanen, T., "Advanced Oxidation of Synthetic Dyehouse Effluents by O_3, H_2O_2/O_3 and H_2O_2/UV Processes," *Enviromental Technology*, 20, 921-926, 1999.

Arslan, I., Balcioglu, I. A., "Effect of Common Reactive Dye Auxiliaries on the Ozonation of Dyehouse effluents Containing Vinylsulphone and Aminochlorotriazine Dyes," *Desalination*, 130, 61-71, 2000.

Arslan, I., Balcıoğlu, I. A., Tuhkanen, T., "Advanced Treatment of Dyehouse Effluents by Fe(II) and Mn(II) Catalyzed Ozonation and the H_2O_2/O_3 Processes," *Water Science and Technology*, 42, 13-18, 2000.

Bahorsky, M. S., "Textiles," *Water Environment Research*, 69, 658-664, 1997.

Barbier, P., Pétrier, C., "Study at 20 kHz and 500 kHz of the Ultrasound-Ozone Advanced Oxidation System: 4-Nitrophenol Degradation," *Journal of Advanced Oxidation Technology,* 1, 154-161, 1996.

Bauman, L. C., Stensrom, M. K., "Removal of Organohalogens and Organohalogen Precorsurs in Re-Claimed Wastewater," *Water Research,* 24, 949-955, 1990.

Beckett, M. A., Hua, I., "Elucidation of the 1,4-Dioxine Decomposition Pathway at Discrete Ultrasonic Frequencies," *Environmental Science and Technology,* 3, 3944-3953, 2000.

Beckett, M. A., Hua, I., "Impact of Ultrasonic Frequency on Aqueous Sonoluminescence and Sonochemistry," *Journal of Physical Chemistry* A, 105, 3796-3802, 2001.

Bhatnagar, A., Cheung, H. M., "Sonochemical Destruction of Chlorinated C-1 and Chlorinated C-2 Volatile Organic Compounds in Dilute Aqueous Solution," *Environmental Science and Technology,* 28, 1481-1486, 1994.

Bird, C. L., Boston, W. S. (Eds), *The Theory of Coloration of Textiles,* The Dyers Company Publications Trust, White Rose Press Ltd., Mexborough and London, 1975.

Boeniger, M. F., *Carcinogenity of Azo Dyes Derived from Benzidine,* Pub No. 80-119., Department of Health and Human Services (NIOSH), Cincinnati, O.H., 1980.

Brown, M. A., De Vito, S. C., "Predicting Azo Dye Toxicity," *Critical Reviews in Environmental Science and Technology,* 23, 249-324, 1993.

Buxton, G. V., Greenstock, C. L., Helman, W. P., Ross, A. B., *Journal of Physical Chemistry Reference Data,* 17, 513, 1988.

Calgon Carbon Oxidation Technologies, *The AOT Handbook,* Volume1, No 1, 1996.

Carriere, J., Jones, J. P., Broadbent, A. D., *Decolourization of Textile Wastewaters by Ozonation,* AATCC Book., 1991.

Cheung, H. M., Kurup, S., "Sonochemical Destruction of CFC-11 and CFC-113 in Dilute Aqueous Solution," *Environmental Science and Technology*, 28, 1619-1622, 1994.

Colarusso, P., Serpone, N., "Sonochemistry Effects of Ultrasound on Homogeneous Chemical Reactions and in Environmental Detoxification," *Research on Chemical Intermediates*, 22, 61-89, 1996.

Colonna, G. M., Caronna, T., Marcandalli, B., "Oxidative Degradation of Dyes by Ultraviolet Radiation in the Presence of Hydrogen Peroxide," *Dyes and Pigments*, 41, 211-220, 1999.

Cooper, W. J., Curry, R. D., O'Shea, K. E. (Eds), *Environmental Applications of Ionizing Radiation*, John Wiley&Sons, Inc., New York, 1998.

Correia, V. M., Stephenson, T., Judd, S. J., "Characterization of Textile Wastewaters: A Review," *Environmental Technology*, 15, 917-929, 1994.

Cost, M., Mills, G., Glisson, P., Lakin, J. "Sonochemical Degradation of p-Nitrophenol in the Presence of Chemical Components of Natural Waters." *Chemosphere*, 27, 1737-1742, 1993.

Crum, L. A., "Sonoluminescence, Sonochemistry, and Sonophysics," *Journal of the Acoustical Society of America*, 95, 559-562, 1994.

Dahlem, O., Demaiffe, V., Halloin, V., Reisse, J., "Direct Sonication System Suitable for Medium-Scale Sonochemical Reactors." *AICHE Journal*, 44, 2724-2730, 1998.

Das, S., Kamat, P. V., Padmaja, S., Au, V., Madison, S. A., "Free Radical Induced Oxidation of the Azo Dve Acid Yellow 9. " *Journal of the Chemical Society - Perkin Transactions* 2, 1219-1223, 1999.

David, B., Lhote, M., Faure, V., Boule, P., "Ultrasonic and Photochemical Degradation of Chlorpropham and 3-Chloroaniline in Aqueous Solution." *Water Research*, 32, 2451-2461, 1998.

De-Aousa-Barboza, C., Luche, J. L., Pétrier, C., "Ultrasound in Organic Synthesis-Some Fundemental Aspects of the Sonochemical Barbier Reaction." *Journal of Organic Chemistry*, 53, 1212-1218, 1988.

Destaillats, H., Colussi, A. J., Joseph, J. M., Hoffmann, M. R., "Synergistic Effects of Sonolysis Combined with Ozonolysis for the Oxidation of Azobenzene and Methyl Orange," *Journal of Physical Chemistry*, 104, 8930-8935, 2000.

Destaillats, H., Turjanski, A. G., Estrin, D. A., Hoffmann, M. R., "Molecular Structure Effects on the Kinetics of Hydroxyl Radical Addition to Azo Dyes," *Journal of Physical Organic Chemistry*,. 15, 287-292, 2002.

Drijvers, D., van Langenhove, H., Beckers, M., "Decomposition of Phenol and Trichloroethylene by the Ultrasound/H_2O_2/CuO Process," *Water Research*, 33, 1187-1194, 1999.

EPA, *Best Management Practices for Pollution Prevention in the Textile Industry*, Cincinnati Ohio, USA, 1996.

Fischer, C. H., Hart, E. J., Henglein, A., "Ultrasonic Irradiation of Water in the Presence of O_{18}, O_{18}^2. Isotope Exchange and Isotopic Distribution of H_2O_2," *Journal of Physical Chemistry*, 90, 1954-1956, 1986.

Ganesh, R., Boardman, G. D., Michelsen, D., "Fate of Azo Dyes in Sludges," *Water Research*, 28, 1367-1376, 1994.

Glaze, W. H., Kang, J. W., Chapin, D. H., "The Chemistry of Water Treatment Processes Involving Ozone, Hydrogen Peroxide and Ultraviolet Radiation." *Ozone Science and Engineering*, 9, 335-352, 1987.

Gonze, E., Fourel, L., Gonthier, Y., Boldo, P., Bernis, A., "Wastewater Pretreatment with Ultrasonic Irradiation to Reduce Toxicity," *Chemical Engineering Journal*, 73, 93-100, 1999.

Gould, J. P., Groff, K. A., "The Kinetics of Ozonolysis of Synthetic Dyes," *Ozone Science and Engineering*, 9, 153-164, 1987.

Gregor, K. H., "Oxidative Decolorization of Textile Wastewater with AOP's". *Proceedings of the 2nd International Syposium on Chemical Oxidation Technology for the Nineties*, Nashville Tennessee, 19-21 February, 1992.

Gurnham, C. (Ed), *Industrial Waste Control*, Academic Press, New York, 1965.

Harada, H., "Sonochemical Reduction of Carbon Dioxide," *Ultrasonics Sonochemistry*, 5, 73-77, 1998.

Hart, E. J., Henglein, A., "Free Radical and Free Atom Reactions in the Sonolysis of Aqueous Iodide and Formate Solutions." *Journal of Physical Chemistry*, 89, 4342-4347, 1985.

Hart, E. J., Henglein, A., "Sonolysis of Ozone in Aqueous Solution," *Journal of Physical Chemistry*, 90, 3061-3062, 1986.

Hart E. J., Henglein A., "Sonochemistry of Aqueous Solutions-H_2O_2 Combustion in Cavitation Bubbles," *Journal of Physical Chemistry*, 91, 3654-3656, 1987.

Herrera, F., Kiwi, J., Lopez, A., Nadtochenko, V., "Photochemical Decolorization of Remazol Brilliant Blue and Uniblue A in the presence of Fe^{3+} and H_2O_2." *Environmental Science and Technology*, 33, 3145-3151, 1999.

Hua I, Höchemer R. H., Hoffmann, M. R., "Sonolytic Hydrolysis of p-Nitrophenyl Acetate: The Role of Supercritical Water," *Journal of Physical Chemistry*, 99, 2335-2342, 1995.

Hua, I., Hoffmann, M. R., "Kinetics and Mechanisms of the Sonolytic Degradation of CCl_4: Intermediates and Byproducts," *Environmenal Science and Technology*, 30, 864-861, 1996.

Hua, I., Hoffmann, M. R., "Optimization of Ultrasonic Irradiation as an Advanced Oxidation Technology," *Environmental Science and Technology*, 31, 2237-2243, 1997.

Huang, C. R., Shu, H. Y., "Wastewater Decolorization and TOC Reduction by Sequential Treatment," *American Dyestuff Report,* 83, 15-18, 1994.

Hung, H. M., Hoffmann, M. R., "Kinetics and Mechanisms of the Enhanced Reductive Degradation of CCl4 by Elemental Iron in the Presence of Ultrasound," *Environmental Science and Technology,* 32, 3011-3016, 1998.

Ince, N. H., Stefan, M. I., Bolton J. R., "UV/H_2O_2 Degradation and Toxicity Reduction of Textile Azo Dyes: Remazol Black-B, a Case Study", *Journal of Advanced Oxidation Technoogy,* 2, 442-448, 1997.

Ince, N. H., Gonenc, D. T., "Treatability of Textile Azo Dye by UV/H_2O_2", *Environmental Technology,* 18, 179-185, 1997.

Ince, N. H., "Light-enhanced Chemical Oxidation for Tertiary Treatment of Municipal Landfill Leachate," *Water Environment Research,* 70, 1161-1169, 1998.

Ince, N. H., and Tezcanli, G., "Treatability of Textile Dyebath Effluents by Advanced Oxidation: Preparation for Reuse." *Water Science and Technology,* 40, 183-190, 1999.

Ince, N. H., and Tezcanli, G., "Reactive Dyestuff Degradation by Combined Sonolysis and Ozonation," *Dyes and Pigments,* 49, 145-153, 2001.

Ince, N. H., Tezcanli, G., Belen, R. K., Apikyan, I. G., "Ultrasound as a Catalyzer of Aqueous Reaction Systems: the State of the Art and Environmental Applications," *Applied Catalysis B: Environmental,* 29, 167-176, 2001.

Ince, N. H., Belen, R., "Aqueous Phase Disinfection with Power Ultrasound: Process Kinetics and Effect of Solid Catalysts," *Environmental Science and Technology,* 35, 1885-1888, 2001.

Ince, N. H., Hasan, D. A., Üstün, B., Tezcanli, G., "Combinative Dyebath Treatment with Activated Carbon and UV/H_2O_2: A Case Study on Everzol Black-GSP," *Water Science and Technology,* 46, 51-58, 2002.

Ince, N. H., Tezcanli-Guyer, G., "Impacts of pH and Molecular Structure on Ultrasonic Degradation of Azo Dyes," *Ultrasonics International 03, UI03 Meeting*, Granada. Spain, 30 June-4 July, 2003.

IOA Standardisation Committee-Europe, 001/87 (F)., *Iodemetric Method for the Determination of Ozone in a Process Gas*, Brussels. 1987.

Jiang, Y., Pétrier, C., Waite, T. D., "Effect of pH on Ultrasonic Degradation of Ionic Aromatic Compounds in Aqueous Solution," *Ultrasonics Sonochemistry*, 9,163-168, 2002.

Joseph, J. M., Destaillats, H., Hung, H. M., and Hoffmann. M. R., "The Sonochemical Degradation of Azobenzene and Related Azo Dyes: Rate Enhancements via Fenton's Reactions," *Journal of Physical Chemistry A* 104, 301-307, 2000.

Kang, J. W., Hoffmann, M. R., "Kinetics and the Mechanisms of the Sonolytic Destruction of Methy-tert-buthyl Ether by Ultrasonic Irradiation in the Presence of Ozone," *Environmental Science and Technology*, 32, 3194-3199 , 1998.

Kang, J. W., Hung, H. M., Lin, A., Hoffmann, M. R., "Sonolytic Destruction of Methyl tert-Butyl Ether by Ultrasonic Irradiation: The Role of O_3, H_2O_2, Frequency, and Power Density," *Environmental Science and Technoogy*, 33, 3199-3205, 1999.

Kang Y. W., Cho M. J., Hwang K. Y. "Correction of Hydrogen Peroxide Interference on Standard Chemical Oxygen Demand Test," *Water Research*, 33, 1247-1251, 1999.

Klassen, N. V., Marchington, D., McGowan, H. C. E., "H_2O_2 Determination by the I_3^- method and by $KMnO_4$ Titration," *Analytical Chemistry*, 66, 2921-2925, 1994.

Kontronarou, A., Mills, G., Hoffmann, M. R., "Ultrasonic Irradiation of p-Nitrophenol in Aqueous Solution," *Journal of Physical Chemistry*, 95, 3630-3638, 1991.

Kuo, W. G., "Decolorizing Dye Wastewater with Fenton's Reagent," *Water Research*, 26, 881-886, 1992.

Kusakabe, K., Aso, S., Wada, T., Hayashi, J. I., Morooka, S., "Destruction of Volatile Organochlorine Compounds in Water by Ozonation with Ultraviolet Radiation," *Water Research*, 25, 1199-1203, 1991.

Law, S. E., Wu, J., Hitchcock, D. R., Eitemann, M. A., "Ozone Decolorization of Cotton Dyehouse Wastewater." *International ASAE Meeting*, Phoenix, Arizona, 1996.

Legrini, O., Oliveros, E., Braun, A. M., "Photochemical Processes for Water Treatment," *Chemical Reviews*, 93, 671-698, 1993.

Leighton T. G., *The Acoustic Bubble*, Academic Press, Harcourt Brace&Company, London, 1994.

Lepoint, T., Mullie, F., "What Exactly is a Cavitation Chemistry," *Ultrasonics Sonochemistry*, 1, 13-22, 1994.

Lepoint-Mullie, F., De Pauw, D., Lepoint, T., "Analysis of the New Electrical Model of Sonoluminescence," *Ultrasonics Sonochemistry*, 3, 73-76, 1996.

Lin, S. H., Lin, C. M., "Treatment of Textile Waste Effluents by Ozonation and Chemical Coagulation," *Water Research*, 27, 1743-1748, 1993.

Lin, S. H., Peng, C. F., "A Continuous Fenton's Process for Treatment of Textile Wastewater," *Environmental Technology*, 15, 693-699, 1995.

Lin, S. H., and Peng, C. F., "Continuous Treatment of Textile Wastewater by Combined Coagulation, Electrochemical Oxidation and Activated Sludge", *Water Research*, 30, 587-592, 1996.

Little, L. W., Lamb, J. C., "*Acute Toxicity of 46 Selected Dyes to the Fathead Minnow Pimephales promelas*," American Dye Manufacturers Institute, September 1972.

Lorimer, J., Mason, T., "Sonochemistry Part 1-The Physical Aspects," *Chemical Society Reviews*, 16, 239-274, 1987.

Lorimer, J. P., Mason, T. J., Plattes, M., Phull, S. S., "Dye Effluent Decolorization using Ultrasonically Assisted Electro-Oxidation," *Ultrasonics Sonochemistry*, 7, 237-242, 2000.

Lorimer, J. P., Mason, T. J., Plattes, M., Phull, S. S., Walton, D. J., "Degradation of Dye Effluent," *Pure and Applied Chemistry*, 73, 1957-1968, 2001.

Luche, J. L. *Synthetic Organic Sonochemistry*, Plenum Press, New York, 1998.

Majcen-Le Marachel, A., Slokar, Y. M., and Taufer T., "Decolorization of Chlorotriazine Reactive Azo Dyes with H_2O_2/UV" *Dyes and Pigments*, 33, 4, 281-298, 1997.

Makkino, K., Mossoba, M. M., Riesz, P., "Chemical Effects of Ultrasound on Aqueous Solutions" *Journal of American Chemical Society*, 104, 3537-3539, 1982.

Margulis, M. A., "Fundamental Aspects of Sonochemistry," *Ultrasonics*, 30,152-155, 1992.

Margulis, M., *Sonochemistry and Cavitation;* OPA (Amsterdam) B.V. Gordon and Breach Science Publication, New York, 1995.

Mark, G., Schuchmann, M. N., Schuchmann, H. P., von Sonntag, C., "A Chemical Actinometer for Use in Connection with UV Treatment in Drinking-Water Processing," *Journal of Water SRT-Aqua*, 39, 309-313, 1990.

Mark, G., Tauber, A., Laupert, R., Schuchmann, H. P., Schulz, D., Mues, A., von Sonntag, C., "OH-Radical Formation by Ultrasound in Aqueous Solution-Part II: Terephthalate and Fricke Dosimetry and the Influence of Various Conditions on the Sonolytic Yield," *Ultrasonics Sonochemistry*, 5, 41-52, 1998.

Mason, T. J., *Chemistry with Ultrasound Critical Reports on Applied Chemistry, No28* Society for Chemical Industry, Elsevier Applied Science, London, 1990.

Mason, T. J., Lorimer, J. P Walton, D. J., "Sonoelectrochemistry," *Ultrasonics* 28, 333-337, 1990.

Mason T. J., Lorimer J. P., Bates D. M., "Quantifying Sonochemistry: Casting Some Light on a Black Art," *Ultrasonics*, 30, 40-42, 1992.

Mason, T. J., Lorimer J. P., Bates, D. M., Zhao, Y., "Dosimetry in Sonochemistry: The Use of Aqueous Terephthalate Ion as a Fluorescence Monitor," *Ultrasonics Sonochemistry* 1, 91-95, 1994.

Mason, T. J., Cordemans de Meulenaer, E., "Ultrasonic Intensification of Chemical Processing and Related Operations: A Review," *Chemical Engineering Research and Design*, 74, 511-516, 1996.

Mason, T. J., Cordemans de Meulenaer, E., "Practical Consideration for Process Optimization,"in Luche J.L. (Eds.), *Synthetic Organic Sonochemistry*, 301-331, Plenum Press, New York, 1998.

Mason, T. J., *Sonochemistry*, Oxford University Press Inc., New York, 1999.

Microbics Co., *Microtox Manual*, Carlsbad, CA., 1992.

Motulski, J. H., Analyzing Data with GraphPad Prism®, GraphPad Software, Inc.San Diego C.A., 1999.

Naffrechoux, E., Chanoux, S., Pétrier, C., Suptil, J., "Sonochemical and Photochemical Oxidation of Organic Matter," *Ultrasonics Sonochemistry*, 7, 255-259, 2000.

Namboodri, C. G., Walsh, W. K., "Decolorizing Spent Dyebath with Hot Peroxide," *American Dyestuff Report*, 9, 86-95, 1995.

Namboodri, C. G., Walsh, W. K., "Ultraviolet Light/Hydrogen Peroxide System for Decolorizing Spent Reactive Dyebath Waste Water," *American Dyestuff Report*, 85, 15-25, 1996.

Nappolian, B., Choi H. C., Sakthivel S, Arabindoo B., Murugesan V., "Solar Light Induced and TiO_2 Assisted Degradation of Textile Dye Reactive Blue 4," *Chemosphere*, 46, 1173-1181, 2002.

Negishi, K., "Experimental Studies on Sonoluminescence and Ultrasonic Cavitation," *Journal of the Physical Society of Japan*, 16, 1450-1465, 1961.

Nemerow, N. L., "*Industrial Water Pollution: Origins, Characteristics, and Treatment*," Addison-Wesley Publishing Company, Inc., 1978.

Neppiras, E. A., "Acoustic Cavitation," *Physical Reports*, 61, 159-251, 1980.

Noltingk, B. E., Neppiras, E. A., "Cavitation Produced by Ultrasonics," *Proceedings of Physical Society*, B63, 674-685, 1950.

Oakes, J., Gratton, P., "Kinetic Investigations of Azo Dye Oxidation in Aqueous Media," *Journal of the Chemical Society- Perkin Transactions* 2, 1857-1864, 1998.

Olson, T. M., Barbier, P. F., "Oxidation Kinetics of Natural Organic Matter by Sonolysis and Ozonation," *Water Research*, 28, 1383-1391, 1994.

Özen, A. S., Aviyente, V., Klein. R. A., "Modeling the Oxidative Degradation of Azo Dyes : A Density Functional Theory Study," *Journal of Physical Chemistry A*, 107, 4898-4907, 2003.

Pétrier, C., Micolle, M., Merlin, G., Luche, J. L., Reverdy, G., "Characteristics of Pentachlorophenate Degradation in Aqueous Solution by means of Ultrasound," *Environmental Science and Technology*, 26, 1639-1642, 1992.

Pétrier, C., Lamy, M. F., Francony, A., Benahcene, A., David, B., Renaudin, V., Gondrexon, N., "Sonochemical Degradation of Phenol in Dilute Aqueous Solutions:Comparison of the Reaction Rates at 20 kHz and 487 kHz," *Journal of Physical Chemistry*, 98, 10514-10520, 1994.

Pétrier, C., Francony, A., "Ultrasonic Waste-Water Treatment: Incidence of Ultrasonic Frequency on the Rate of Phenol and Carbon Tetrachloride Degradation," *Ultrasonics Sonochemistry*, 4, 295-300, 1997.

Pétrier, C., Naffrechoux, E., Gimeno, C. H., El Hachemi, M. E., "Combined Process Ultrasound/Ozone and Ultrasound/UV for Liquid Waste Treatment," *TU Hamburg-Harburg Reports on Sanitary Engineering, 35*, 2002.

PISA Textile Corp. Istanbul, 2000-2002, private communication.

Ravikumar, J. X., Gürol, M. D., "Chemical Oxidation of Chlorinated Organics by Hydrogen Peroxide in the Presence of Sand," *Environmental Science and Technology*, 28, 394-400, 1994.

Rayleigh, O. M., "On the pressure Developed in a Liquid during the Collapse of a Spherical Cavity," *Philosophical Magazine Series*, 34, 94-98, 1917.

Reife, A., Freeman, S., "*Environmental Chemistry of Dyes and Pigments*," John Wiley & Sons, Inc., Canada, 1996.

Reisse, J., *Proceedings of the 15th International Congress on Acoustics*, Trondheim, Norway, 409, 1995.

Riesz, P., Kondo, T., Krishna, C. M., "Sonochemistry of Volatile and Nonvolatile Solutes in Aqueous Solutions." *Ultrasonics*, 28, 295-303, 1990.

Riesz, P., Mason, T. J. (Ed.), *Advances in Sonochemistry*, Vol. 2, JAI Press, London 1991.

Robinson, T., McMullan, G., Marchant R., Nigam, P., "Remediation of Dyes in Textile Effluent: A Critical Review on Current Treatment Technologies with a Proposed Alternative," *Bioresource Technology*, 77, 247-255, 2001.

Ruppert, G., Bauer, R., and Heisler, G., "The Photo-Fenton Reaction-An Effective Photochemical Wastewater Treatment Process" *Journal of Photochemistry and Photobiology A-Chemistry*, 73, 75-78, 1993.

Ryes, P., Zollinger, H., *Fundamentals of the Chemistry and Application of Dyes*, Wiley-Interscience, New York, 1992.

Sehgal, C., Yu, T. J., Sutherland, R. G., Verrall, R., "Use of 2,2-Diphenyl-1-Picrylhydrazyl to Investigate the Chemical Behavior of Free Radicals Induced by Ultrasonic Cavitation," *Journal of Physical Chemistry*, 68, 2982-2986, 1982.

Serpone, N., Terzian, R., Hidaka, H., Pelizetti, E., "Ultrasonic Induced Dehalogenation and Oxidation of 2-Chlorophenol, 3-Chlorophenol, and 4-Chlorophenol in Air-Equilibrated Aqueous MediaSimilarities with Irradiated Semiconductor Particulates," *Journal of Physical Chemistry*, 98, 2634-2640, 1994.

Shu, Y. H., Huang, C. R., Chang, M. C., "Decolorization of Mono-Azo Dyes in Wastewater by Advanced Oxidation Process: A Case Study of Acid Red 1 and Acid Yellow 23" *Chemosphere*, 29, 12, 2597-2607, 1994.

Silverstein, R.M.C., Bassler, G.C., Morrill, T.C., *Spectrophotometric Identification of Organic Compounds.* Wiley, NewYork, 1991.

Snider, E. H., Porter, J. J., "Ozone Treatment of Dye Waste," *Journal of Water Pollution Control Federation*, 46, 886-894, 1974.

Soares, G. M. B, Costa-Ferreira, M., Pessoa de Amorim, M. T., "Decolorization of an Anthraquinone Type Dye Using a Laccase Formulation." *Bioresource Technology*, 79, 171-177, 2001.

Staehelin, J., and Hoigné, J., "Decomposition of Ozone in Water: Rate of Initiation by Hydroxide Ions and Hydrogen Peroxide." *Environmental Science and Technology*, 16, 676-681, 1982.

Stock, N. L., Peller, J., Vinodgopal, K., Kamat, P. V., "Combinative Sonolysis and Photocatalysis for Textile Dye Degradation," *Environmental Science and Technology*, 34, 1747-1750, 2000.

Stockinger, H., Kut, Ö. M., Heinzle, E., "Ozonation of Wastewater Containing N-Methylmorpholine-N-Oxide," *Water Research*, 30, 1745-1748, 1996.

Suslick, K. S., "Sonochemistry," *Science*, 247, 1439-1445, 1990.

Suslick, K. S., Doktycz, S. J., Flint, E. B., "On the Origin of Sonoluminescence and Sonochemistry," *Ultrasonics*, 28, 280-290, 1990.

Suslick, K. S., "The Chemistry of Ultrasound", 1994, http://www.scs.uiuc.edu//~suslick/britannica.html

Tauber, A., Schuchmann H. P., von Sonntag C., "Sonolysis of Aqueous 4-Nitrophenol at Low and High pH," *Ultrasonics Sonochemistry*, 7, 45-52, 2000.

Tchobanoglous, G., Burton, F. L., "*Wastewater Engineering. Treatment Disposal and Reuse*," McGraw-Hill, Inc., New York, 1991.

Tezcanli, G., "Reuse of Textile Dyebaths by Treatment with Advanced Oxidation," M.S. Thesis, Bogazici University, 1998.

Tezcanli-Guyer, Ince N. H., "Structure Related Degradability of Textile Dyestuff by Acoustic Cavitation: A Study with Dyebath Effluents," *Proceedings of 9th International Conference on Dyes and Pigments, ColorChem 02*, P5, May 12-16, 2002.

Tezcanli-Guyer, G., Ince, N. H., "Degradation and Toxicity Reduction of Textile Dyestuff by Ultrasound," *Ultrasonics Sonochemistry*, 10, 235-240, 2003.

Tezcanli-Guyer, G., Alaton, I. A., Ince, N. H., "Sonochemical Destruction of Textile Dyestuff in Wasted Dyebaths." *Coloration Technology*, 119,292-296, 2003.

Tezcanli-Guyer G., Ince, N. H., "Ultrasound in Advanced Oxidation Processes: A Case Study with Acid Orange 7," *Ultrasonics International 03, UI03 Meeting*, Granada, Spain, July 2003.

Thoma, G., Gleason, M., Popov, V., "Sonochemical Treatment of Benzene/Toluene Contaminated Wastewater," *Environmental Progress*, 17, 154-160, 1998.

Verrall, R. E., Sehgal, C., Suslick, K. S. (Ed.), *Sonochemistry: Its Chemical, Physical and Biological Effects*, VCH, New York, 1988.

Vinodgopal, K., Peller, J., Makagon, O., Kamat, P. V. "Ultrasonic Mineralization of a Reactive Textile Azo Dye. Remazol Black B," *Water Research*, 32. 3646-3650,1998.

Vinodgopal K, Kamat P. V. "Hydroxyl-Radical-Mediated Oxidation: A Common Pathway in the Photocatalytic, Radiolytic, and Sonolytic Degradation of Textile Dyes" in Cooper W. J., Curry R. D., O'Shea, E. (Eds), *Environmental Applications of Ionizing Radiation*, John Wiley&Sons, Inc., New York, 1998.

Wakeford, C. A., "Effect of Ionic Strength on the Acoustic Generation of Nitrite, Nitrate and Hydrogen Peroxide," *Ultrasonics Sonochemistry*, 6, 141-148, 1998.

Walling, C., "Fenton's Reagent Revisited," *Acoustical Chemical Research*, 8, 125-131, 1975.

Weast, R. C., Astle, M. J., *CRC Handbook of Chemistry and Physics*, 63rd, CRC press, Inc., Florida, 1983.

Weavers, L. K., Ling, F. H., Hoffmann, M. R., "Aromatic Compound Degradation in Water Using a Combination of Sonolysis and Ozonolysis," *Environmental Science and Technology*, 32, 2727-2733, 1998.

Weavers, L. K., Hoffmann, M. R., "Sonolytic Decomposition of Ozone in Aqueous Solution: Mass Transfer Effects," *Environmental Science and Technology*, 32, 3941, 1998.

Weissler, A., Cooper, H. W., Snyder, S., *J. Am. Chem. Soc.*, 72, 1769, 1950.

Wu, J., Eiteman, M. A., Law, S. E., "Evaluation of Membrane Filtration and Ozonation Processes for Treatment of Reactive-Dye Wastewater," *Journal of Environmental Engineering*, 124, 272-277, 1998.

Wu, J., Wang, T., "Ozonation of Aqueous Dye in a Semi-batch Reactor," *Water Research*, 35, 1093-1099, 2001.

Young, F.R., *Cavitation*, McGraw-Hill, New York, 1989.

APPENDIX A

A.1. H_2O_2 Determination by the I_3^- Method and Calibration Curve

H_2O_2 determination for the System I, II, and III was carried out according to the procedure described by Klassen *et al.*, (1994). This method is based on the reaction of (I^-) with H_2O_2 to form the triiodide ion (I_3^-), which has a strong absorbance 351 nm. The analysis of H_2O_2 at concentrations as low as 1 μM is conveniently done by determining the yield of I_3^- formed when H_2O_2 reacts with KI in a buffered solution containing ammonium molybdate tetrahydrate as a catalyst.

Solutions A and B for the I_3^- method were prepared according to the recipe given by Kalssen *et al.*, (1994). Solution A consisted of 33 g of KI, 1 g of NaOH, and 0.1 g of ammonium molybdate tetrahydrate diluted to 500 ml with deionized water. The solution was stirred for ~1 h to dissolve the molybdate. Solution A was kept in dark to inhibit the oxidation of I^-. Solution B, an aqueous buffer, contained 10 g of KHP per 500 ml. Various concentrations of H_2O_2 was prepared from reagent grade H_2O_2 (35%), Merck. 2.5 mL of solution A, 2.5 mL of solution B, 1 mL of sample were mixed and diluted to 10 mL by deionized water, and the absorbance at 351 nm was recorded. Blank sample was prepared in the absence of sample. Various concentrations of H_2O_2 and the corresponding absorbance values at 351 nm are recorded for calibration curve, and given in Table A.1. Plot of H_2O_2 concentration versus the corresponding absorbance of the solution, and the calibration curve for H_2O_2 analysis in sonicated samples is given in Figure A.1.

Table A.1. H_2O_2 concentration versus absorbance at 351 nm data used for calibration curve preparation

H_2O_2 concentration (mgL^{-1})	H_2O_2 concentration (μM)	Absorbance at 351 nm
0.3955	11.63	0.037
0.7907	23.25	0.070
1.1866	34.90	0.090
1.5821	46.53	0.121
1.9776	58.16	0.158
2.3732	69.92	0.188

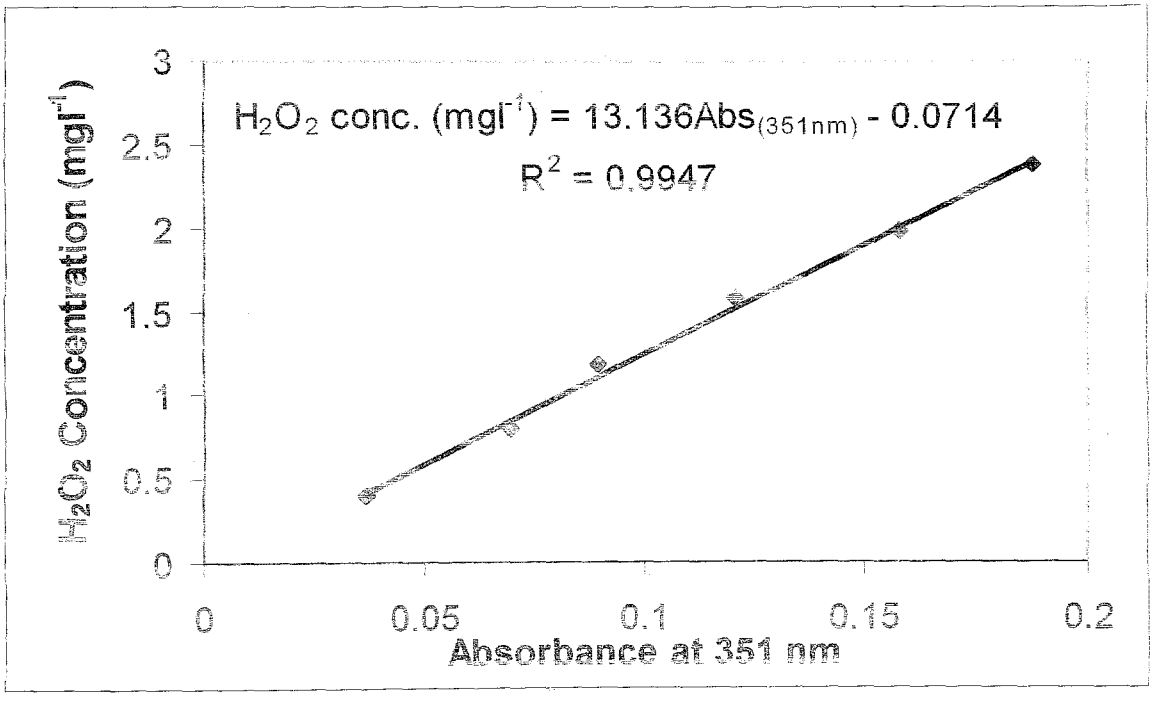

Figure A.1. H_2O_2 calibration curve.

A.1.1. H_2O_2 Production during Sonication in System I, II, and III

1 mL of sample was taken for 10 min intervals during 1 h sonication of deionized water, and mixed with 2.5 mL solution A and solution B, and then diluted to 10 mL with deionized water. The absorbance at 351 nm was recorded for each sample, and then substituted into H_2O_2 calibration curve equation given in Figure A.1.1. Table A.2. shows

the results obtained for H_2O_2 production during sonication of pre-aerated deionized water in System I, II, and III by I_3^- Method.

Table A.2. H_2O_2 production during sonication of deionized water in System I, II, and III

Time (min)	SYSTEM (I)		SYSTEM (II)		SYSTEM (III)	
	$A_{351\ nm}$	H_2O_2 (μM)	$A_{351\ nm}$	H_2O_2 (μM)	$A_{351\ nm}$	H_2O_2 (μM)
0	0	0	0	0	0	0
10	0.147	55	0.080	29	0.107	39
20	0.284	108	0.182	68	0.262	99
30	0.419	160	0.278	106	0.432	165
40	0.554	212	0.359	137	0.647	248
50	0.691	265	0.482	184	0.842	323
60	0.825	317	0.610	234	0.988	380

APPENDIX B

B. 1. Determination of the Ozone Concentration in System III

Ozone concentration in solution in System III was carried out according to the indigo colorimetric method described in Standard Methods for the Examination of Water and Wastewater (APHA, 1989). This method is quantitative, selective, and simple; it replaces methods based on the measurement of total oxidant. The method is based on the decolorization of indigo by ozone in acidic solution. The decrease in absorbance is linear with increasing ozone concentration.

For the preparation of indigo stock solution, 770 mg potassium indigo trisulfonate ($C_{16}H_7N_2O_{11}S_3K_3$) and 1 ml conc. phosphoric acid was added to a volumetric flask and filled to 1 L with deionized water. The stock solution is stable for about 4 months when stored in the dark, and should be discarded when absorbance at 600 nm of a 1:100 dilution falls below 0.16/cm. For the preparation of indigo reagent, 100 mL indigo stock solution, 10 g sodium dihydrogen phosphate (NaH_2PO_4), and 7 mL conc. phosphoric acid were added to a volumetric flask and filled to 1 L with deionized water. Then 10 ml indigo reagent and 5 mL sample were mixed and diluted to 100 mL with deionized water. Blank sample was prepared in the absence of sample. The absorbances of both solutions were measured at 600 nm and the ozone concentration was prepared by the following equation:

$$\text{mg } O_3 / L = \frac{100 \times \Delta A}{0.42 \times b \times V}$$

where ΔA is the difference in absorbance (600 nm) between blank and sample, b is the pathlength of cell, cm (1 cm), V is the volume of the sample, ml, and the proportionality constant at 600 nm is 0.42 ± 0.01/cm/mg/L ($\Delta \epsilon$ = 20 000/M. cm) compared to the ultraviolet absorption of pure ozone of ϵ = 2950/M. cm at 258 nm).

The absorbance values at 600 nm were recorded for each set of experiments (described in Chapter 11, Section 11.3.1.1.3.) and samples taken within short intervals, and

given in Table B.1. The ozone concentration for each sample was calculated by substuting the absorbance value at 600 nm into the above equation.

Table B.1. Results for the ozonation experiments conducted at different experimental conditions

	Experiment							
	A		B		C		D	
Time (min)	A_{600}	O_3 (mgL^{-1})	A_{600}	O_3 (mgL^{-1})	A_{600}	O_3 (mgL^{-1})	A_{600}	O_3 (mgL^{-1})
0	0.000	0.000	0.000	0.000	0.000	0.000	0.000	0.000
1	0.161	0.047	0.152	0.476	0.161	0.047	0.152	0.476
2	0.156	0.285	0.149	0.619	0.161	0.047	0.152	0.476
3	0.154	0.381	0.147	0.714	0.157	0.238	0.152	0.476
5	0.152	0.476	0.143	0.904	0.154	0.380	0.153	0.428
7	0.149	0.619	0.143	0.904	0.151	0.523	0.149	0.619
10	0.145	0.809	0.14	1.047	0.153	0.428	0.148	0.666
12	0.142	0.952	0.139	1.095	0.152	0.476	0.15	0.571
15	0.142	0.952	0.139	1.095	0.15	0.571	0.152	0.476
17	0.142	0.952	0.14	1.047	0.151	0.523	0.151	0.523
20	0.141	1.000	0.139	1.095	0.15	0.571	0.151	0.619

APPENDIX C

C. 1. Determination of the Light Intensity of UV-C Lamps in System III

The applied UV dose in System III was measured by peroxidisulphate/ tert butanol chemical actinometer which included an aqueous solution containing potassium peroxidisulfate (0.01 M) and tert-butanol (0.1 M) (Mark *et al.*, 1990). Upon photolysis of solution with three mercury low pressure UV lamps (108W, and emitting at 254 nm) resulted in a sulphuric acid (H^+) formation. The concentration of hydrogen ions was followed with a WTW-100 pH meter and the drop in pH as a function of irradiation time (400 sec) was recorded and converted into $[H^+]$ (pH = -log$[H^+]$). Plot of $[H^+]$ concentration versus irradiation time is given in Figure C.1.

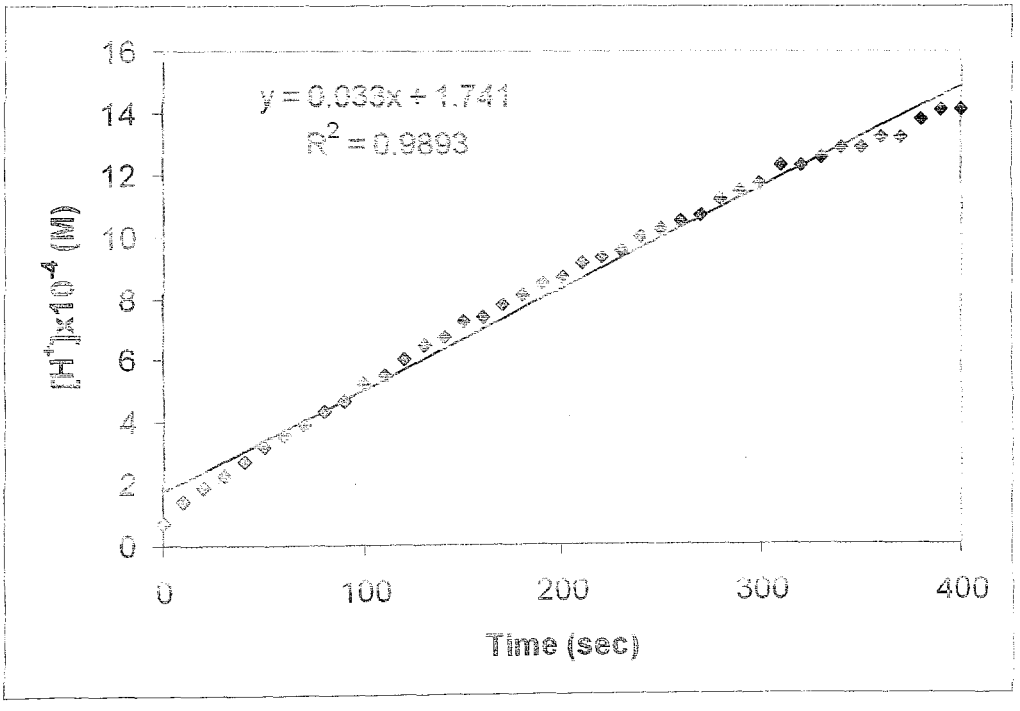

Figure C.1. Increase in the hydrogen ion concentration in an actinometer solution irradiated with UV light in System III as a function of irradiation time.

($[H^+]$)/t) value was obtained from the slope of $[H^+]$ versus t plot data given in Figure C.1.1. Then, the quantum yield of H^+ formation (the ratio of the number of H^+ ions formed to the number of photons absorbed) (ϕ (H^+)) was calculated according to the following equation:

$$\phi(H^+) = \frac{[H^+] \times N_L \times V_{tot} \times 10}{t \times I_{abs} \times M}$$

where V_{tot} denotes the total volume of the solution (cm^3), M is the irradiated surface area of the solution (cm^2), t is the irradiation time (sec), I_{abs}/N_L (N_L, Avogadro number) is the absorbed fluence rate in terms of Einsteins m^{-2} s^{-1}, ϕ (H^+) is a reference value of 1.8, and $[H^+]/t$ is 3.3×10^{-6} mol L^{-1} s^{-1}(from Figure C.1.1.). Each UV light sources were transmitted by quartz windows with 5 cm width, and 14 cm height, therefore the surface area (M) was 3x70 cm^2. The absorbed fluence rate was then calculated as:

$$\frac{I_{abs}}{N_L} = \frac{3.3 \times 10^{-6} \times 1200 \times 10}{1.8 \times 210} = 1.05 \times 10^{-4} \text{ Einstein m}^{-2} \text{ s}^{-1}$$

$$= (49.56 \text{ W m}^{-2}) \text{ (1 Einstein=4.72x10}^5 \text{ J)}$$

Incident photon influence rate (I_0) was calculated by:

$I_{abs} = I_0 (1 - 10^{-(\varepsilon x C x l)})$

where ε is the molar extinction coefficient of potassium peroxidisulfate (20 dm^3 mol^{-1} cm^{-1}), C is the concentration of the potassium peroxidisulfate (0.01 M), and pathlength of the cell that UV light is transmitted (in our case 3 x 0.5 cm).

$$I_0 = \frac{1.05 \times 10^{-4}}{1 - 10^{-(20 \times 0.01 \times 1.5)}} = 2.1 \times 10^{-4} \text{ Einstein m}^{-2} \text{ s}^{-1} (99.12 \text{ W m}^{-2})$$

As a result, fifty per cent of the incident fluent rate was found to be absorbed in actinometer solution.